Design Optimization of Active Magnetic Thrust Bearing Systems Using Multi-Objective Genetic Algorithms

A Thesis submitted
in partial fulfillment of the requirements
for the Degree of

Doctor of Philosophy

by

Jagu Srinivasa Rao
(04610307)

DEPARTMENT OF MECHANICAL ENGINEERING
Indian Institute of Technology Guwahati
Guwahati
December, 2009

CERTIFICATE

It is certified that the work contained in this thesis entitled **Design Optimization of Active Magnetic Thrust Bearing Systems Using Multi-Objective Genetic Algorithms** by **Mr. Jagu Srinivasa Rao (Roll no. 04610307)** has been carried out under my supervision and that the work has not been submitted elsewhere for a degree.

Dr. Rajiv Tiwari
Professor
Department of Mechanical Engineering
Indian Institute of Technology Guwahati
Guwahati - 781 039, INDIA

Dedicated to

My **Lord Jesus Christ**

who died on the Cross

and rose again on the third day

Acknowledgements

I am deeply indebted to my supervisor Prof. Rajiv Tiwari for his perseverance and never quitting attitude who tolerated with me all these years, supported and allowed me to shape up into what is important (a character). His integrity, humbleness and learning nature is a model to follow. I am thankful to him for introducing me to an exciting multi disciplinary and emerging area of research. His enduring, practical and friendly guidance in the research helped me move forward in understanding the subject as well as the surroundings in depth. I am also thankful to the other members of my doctoral committee, Prof. Santosha Kumar Dwivedy, Prof. Debabrata Chakraborty, and Dr. Harshal B. Nemade for their rational and insightful suggestions, comments, discussions, and corrections which helped me to enhance my research into connecting areas. I am also thankful to Prof. C. Sujatha (IIT Madras) for her rational evaluation.

I would like to thank all the faculty of the department of Mechanical Engineering (especially Dr. K. S. R. K. Murthy, Prof. Anoop Kumar Das, and Dr. U. K. Saha) who were always ready to help by giving valuable suggestions which boosted my confidence in pursuing the research. I am also thankful to Mr. Dhruba Jyoti Bordoloi for his assistance in vibration laboratory and Mr. Amal Kalita for his assistance in CAD laboratory. I am thankful to the faculty and staff of computer centre, library, student affairs, academic affairs, research and development, establishment and other administrative departments of the institute who are directly or indirectly involved in completion of my research.

My special thanks go to Mr. Sachin Kumar Singh (my successor from M Tech) and Mr. A. V. Dhanunjaya Reddy (M. Tech-2nd year) whose mutual sharing with me is a blessed

time of learning. I am also thankful to all of my other friends, colleagues, juniors, and seniors with whom I spent heartfelt moments and learned lot in practical life.

I am deeply indebted to my parents whose constant love and prayers are a blessing. I am also thankful to my siblings and in-laws for their well-wishes and support during this research. Finally I am thankful to my wife, Lokeswari who is a source of encouragement, enduring the gap of distance and time between us without whose love, cooperation and prayers I would not be able to come to this end. I am also thankful to my church members for their prayers about my research.

Last but most importantly, if there was nothing eternal there would be nothing temporary. If there is no permanent source of intelligence, knowledge, wisdom, character and capability, there would be no such quality seen in the world. Science is the study of character and creativity of God, and engineering is the imitation of the work of His hands. I am in adoration of my Lord who is praise worthy for all His power and knowledge and wisdom poured in this universe. He is the source of all character. He came down to earth, died on the cross for my sin and rose again from the dead with a promise that he will rise whoever believes him as the genuine one. He is my strength in doing great things and enduring hardships of life.

Jagu Srinivasa Rao

Abstract

In the present work, an optimum design and analyses of *active magnetic thrust bearings* (AMTB) and *hybrid magnetic thrust bearings* (HMTB) have been carried out. The active magnetic bearing contains only electromagnets, whereas, the hybrid contains both the electro-magnets and permanent magnets. Initially, the optimization has been carried out using *single-objective genetic algorithms* (SOGA). Two objectives, namely the power-loss and overall weight of the bearing, are considered one at a time. Different constraints considered are the maximum current density flow in the coil, the maximum flux density flow in the stator iron, the maximum power-loss allowed, and the maximum space occupied by the bearing. Two objectives considered are found to be conflicting. This led to the attempt of optimization by using *multi-objective genetic algorithms* (MOGA) by considering two objectives simultaneously namely, the power-loss and overall weight of the bearing. The effect of load on the Pareto frontier has been studied, and the load is found out to be an objective in addition to the weight and the power-loss.

A complex system of *double-acting hybrid magnetic thrust bearings* (DAHMTB) with a centralized controller as an integrated system has been optimized by using MOGA. Five objectives are considered with three for the actuator and two for the controller. Additional constraints considered are stability conditions of the controller.

Though power amplifiers can be designed with respect to designed controller requirements, sometimes it is not possible to have the required power amplifiers as a standard one, and one has to design the controller by taking the constraints of the power amplifier available at hand. Though centralization of controller requires less number of

power amplifiers, but needs some complex winding scheme and control strategies. To go for a simpler winding and control strategies one may have to go for a decentralized actuator, controller and power amplifier in double acting magnetic bearing systems. Hence, the design optimization methodology is extended to the DAHMTB with decentralized controller systems by taking consideration of constraints of the power amplifier, namely the maximum power rating, and the voltage of the power amplifier.

The overall exercise of the optimization gives rise to a novel methodology of analysis of Pareto optimal systems called *Pareto optimal design analysis* by which one can predict the behavior of different designs in the Pareto front with respect to each other. It has also lead to a general *integrated design optimization methodology* by which one can optimize magnetic bearing systems with the actuator, controller, and amplifier as an integrated system by using the SOGA or the MOGA. The behavior of different parameters with respect to tradeoffs has been explored in detail.

Contents

List of Figures

List of Tables

Nomenclature

A_c	Cross sectional area of the coil winding
A_g	The area of the air gap at poles
A_m	Pole face area of permanent magnet
A_w	Cross sectional area of coil wire
B_g	Flux density
B_m	Magnetic flux flowing in the permanent magnet
B_r	Remnant magnetic flux of the permanent magnet
C_e	Equivalent damping coefficient
F	Resultant force of the both the actuators at operating position
F_c	Controlling force
F_m	Force purely due to permanent magnets at operating position
F_{xi}	Force at minimum position of rotor disc
F_{xo}	Force at maximum position of rotor disc
H	Magnetic field intensity
J	Coil current density
J_{sat}	Saturation current density
K_a	Actuator loss factor
K_e	Equivalent stiffness
K_f	Flux leakage factor
K_i	Coil MMF loss factor
L	Inductance of the coil
P	Total power-loss of both the actuators at operating position
$P_{\max}$	Maximum power-loss
P_{xi}	Power-loss at minimum position of rotor disc
P_{xo}	Power-loss at maximum position of rotor disc
T_{cr}	Critical operating temperature of the bearing
T_∞	Temperature of the cooling medium

V_c	Volume of the coil
W	Overall weight of the bearing
h_c	height of the coil
h_t	Height of bearing
h_{tub}	maximum height of bearing
i	Current in the coil
i_b	Bias current
i_c	Control current
k_D	Derivative gain
k_P	Proportionality gain
k_i	Current stiffness
k_x	Displacement stiffness
l_g	Air gap length, air gap allowed
l_{g0}	Operating gap
$l_{g\max}$	Maximum gap allowed
$l_{g\min}$	Minimum gap allowed
l_m	Thickness of bias magnets
m	Mass of the rotor
n	Number of turns of the coil winding
ni	Magneto-motence
$ni_{\max}$	Maximum magneto-motence
$ni_{\min}$	Minimum magneto-motence
p	Power rating of the power amplifier
p_c	Probability of crossover
p_m	Probability of mutation
r	Radius, electric resistance
r_{ci}	Inner radius of the coil
r_{co}	Outer radius of the coil
r_i	Inner radius of bearing

r_o	Outer radius of the bearing
r_{oub}	Maximum outer radius of the bearing
r_s	Radius of shaft
t_b	The back wall thickness of the bearing
t_c	Thickness of the coil
t_i	The inner wall thickness of the bearing
t_o	The outer wall thickness of the bearing
t_s	Settling time
t_s, t_f	The settling time
x_c	Displacement of the rotor to be controlled
x_0	Initial displacement
x_{ci}	Nearest position of the rotor from the bearing
x_{co}	Farthest position of the rotor from the bearing
$x_{\max}$	maximum displacement of the rotor that is allowed from the operating position
x_s	Settling tolerance
v	Voltage supplied by the power amplifier, velocity of the rotor
v_0	Initial velocity

Greek Symbols

Λ	Coefficient of thermal conduction
α	Iron saturation factor
γ	Specific gravity of the material
γ_c	Specific gravity of the copper
γ_m	Specific gravity of the Nb-Fe-B
γ_s	Specific gravity of the stator-iron
η	Coil packing factor
η_c	Crossover distribution index
η_m	Mutation distribution index
ρ	Electric resistivity of the coil wire
τ	Sampling time
μ_0	Permeability of the vacuum
ϑ	Magneto-motence
υ_f	Variation in the load
υ_x	Variation in the air-gap
ϕ_g	Magnetic flux
χ_d	Dynamic performance index
χ_o	Output performance index
χ_i	Input performance index

Subscripts

a	Active or due to electro magnet
b	Bias, back-wall
c	Control, coil
i	Nearest position of the rotor from the bearing, inner radius
lb	Lower bound
m	Permanent magnet
max	Maximum
min	Minimum
o	Farthest position of the rotor from the bearing, outer radius
ub	Upper bound
0	Initial perturbation, operating point

Superscripts

lb	Lower bearing
ub	Upper bearing
xi	Nearest position of the rotor from the bearing
xo	Farthest position of the rotor from the bearing

Abbreviations

AMB	Active Magnetic Bearing
AMTB	Active Magnetic Thrust Bearing
DAHMTB	Double Acting Hybrid Magnetic Thrust Bearing
GA	Genetic Algorithm
HMB	Hybrid Magnetic Bearing
HMTB	Hybrid Magnetic Thrust Bearing
MOGA	Multi Objective Genetic Algorithms
MTB	Magnetic Thrust Bearing
SBX	Simulated Binary Crossover
SOGA	Single Objective Genetic Algorithms
Pμ	Polynomial Mutation

Part - I
Background

Chapter 1
Introduction and Literature Survey

1.1 Introduction

A force is the factor by which the objects of the universe interact with each other starting from a nuclear particle to a celestial object. According to quantum physics there are four kinds of fundamental forces which cause interaction between any two particles of the physical world. These four fundamental interactions are namely the gravity, strong nuclear interaction, weak nuclear interaction, and electro-magnetism. The gravity is sensed by objects of mass of any small quantity even at large distances but weakest of all interactions. The strong nuclear interaction is that which keeps the nucleons together overcoming the repulsion due to charges of same polarity and is the strongest of all kinds of interactions. The weak nuclear interaction is the powerful nuclear interaction which causes nuclear decay in radioactive elements. The electromagnetic interaction acts between charged particles. The word *strong* is used for strong force since the strong interaction is the "strongest" of the four fundamental forces; its typical field strength is 100 times the strength of the electromagnetic force, some 10^5 times as great as that of the weak force, and about 10^{39} times that of the gravitation.

The two important facts about electricity and magnetism observed by ancient world are loadstone (also known as magnetite) attracting iron and amber attracted small objects when rubbed with fur. The first definite statement is by Thales of Miletus (about 585B.C.) who said '*loadstone attracts iron*' (Fowler, 1997). In his treatise of the year 1600 *De Magnete*, the English physician William Gilbert coined the new Latin term *electricus*, to refer to this property of attracting small objects after being rubbed (Baigrie, 2006). The term *electricity* is derived from the Latin *ēlectrum*, which came from the Greek word ήλεκτρον (*ēlektron*) for amber. The term magnet is believed to be formulated from the place called magnesia where magnet ore (i.e., the load stone) is found plenty.

Thales in the 6th century B.C. is said by later writers to have been the first to mention the attractive property of amber. An Indian philosopher and surgeon of the same century, Susruta is credited with having made use of the magnet for surgical purposes (Vowles, 1932). Vowles mentions that references to the attractive properties of either amber or loadstone or both are to be found in a number of classical Greek and Roman works, as for example the works of Plato, Aristotle, Theophrastus, Pliny, Dioscorides, Lucretius, and others.

For a long time electricity and magnetism were assumed to be different forces. However while preparing for an evening lecture in 1820, Hans Christian Oersted developed an experiment that provided surprising evidence that by switching off and on of electric current, the conductor deflected a magnetic needle nearby. Consequently Michael Faraday showed in 1831 that a changing magnetic field can induce a current in a circuit. Conclusively from the works of Oersted, Faraday and others, James Clerk Maxwell predicted that a changing electric field has an associated magnetic field and consequently he unified them as Maxwell's equations of electromagnetism in 1864. According to the theory of

electromagnetism, when charged particles are at rest they interact by electric forces, but when in motion the charged particles will be acted upon both by electric and magnetic forces called electro-magnetic interaction.

Before electromagnets were invented the permanent magnets were used in different engineering and medical applications. Susruta made use of the magnet for surgical purposes. Navigation compass is another application of permanent magnets that the early world used in the dark ages of history which is believed to have originated in China. There are claims that it had been known for centuries there, and that there were "south pointing carts" presumably with built-in compasses, thousands of years earlier. Unfortunately, in 200 B.C. or so the emperor destroyed all books and killed the scholars, so that earlier tales wouldn't detract from his own greatness (Fowler, 1997). Fowler also mentions that the permanent magnetic spheres had been used by Otto von Guericke of 17th century A. D. in his invention of the first generator of static electricity. The conversion of electrical energy into mechanical energy by electromagnetic means was demonstrated by the British scientist Michael Faraday in 1821. In 1827, Hungarian Anyos Jedlik started experimenting with electromagnetic rotating devices which he called electromagnetic self-rotors. In the years of 1831-1832 Michael Faraday discovered the operating principle of electromagnetic generators. The Dynamo was the first electrical generator capable of delivering power for industry. The dynamo uses electromagnetic principles to convert mechanical rotation into a pulsing direct electric current through the use of a commutator. The first dynamo was built by Hippolyte Pixii in 1832.

Apart from the applications to motors and generators the permanent magnets were tried to be utilized in hovering an object without contact. However, the passive systems involving all permanent magnets faced problems in rotor positioning and stability. This problem in

practice was proved by Earnshaw in 1842, as a theorem named after him, that it is not possible to hover a body in all six degrees of freedom in a three axis passive environment (Earnshaw, 1842). Earnshaw's theorem indicates the necessity of stabilizing the object by an alternative non-passive means.

Taking the restrictions of Earnshaw's theorem into consideration there were methods developed by means of electro-magnetic levitation. Filatov and Maslen (2001) summarized some of these well known methods of electromagnetic levitation of an object including using non-superconducting diamagnetic materials, conducting objects with time varying magnetic fields, gyroscopic torques, diamagnetism of superconducting materials and electro-magnets with feedback control systems. Among these methods non-superconducting diamagnetic materials are still not practically implemented due to small forces developed. The gyroscopic torques method has very few applications such as levitron (Berry, 1996; Romero, 2003). Conductors when put on a rotor in a permanent magnetic field develop currents in the conductor and a repulsive force against the magnetic field in which it rotates are under development stage (Filatov and Maslen, 2001). Superconductors have increased applications in maglev systems and magnetic bearings with developments in cryogenics and high temperature superconductors (Bray, 2009). However the superconductors are costly due to generation of cryogenic temperatures in their production and maintenance. Bray provides also the information on the properties and different applications of superconductors. The most commercially and technically implemented method is active magnetic levitation which needs active control systems to adjust the current to bring the system into stable operation. In this category magnetic bearings have found ample applications in the present industrial world (Dussaux, 1990; Kasarda, 2000). The working

principle of active magnetic bearings, classification, advantages and applications, limitations and research areas are provided in the following subheadings.

1.2 Basic components of an AMB

A *magnetic bearing* (MB) system supports a rotating element on air without any physical contact. It suspends the rotor on air with the electrically controlled or/and permanent magnetic forces. A simple AMB system consists of a rotor, actuator, sensor, controller, and power amplifier (Figure 1.1). Hence, an AMB is a complex interdisciplinary product where mechanical, electrical, electronics, control, and computer fields of engineering are involved. The magnetic actuator coil is supplied with an electric current which converts into the magnetic flux in the stator-iron and attracts the rotor (radially or axially) due to the magnetic force generated. The actuator supports the rotor to be positioned at a gap from the actuator pole called the operating air-gap.

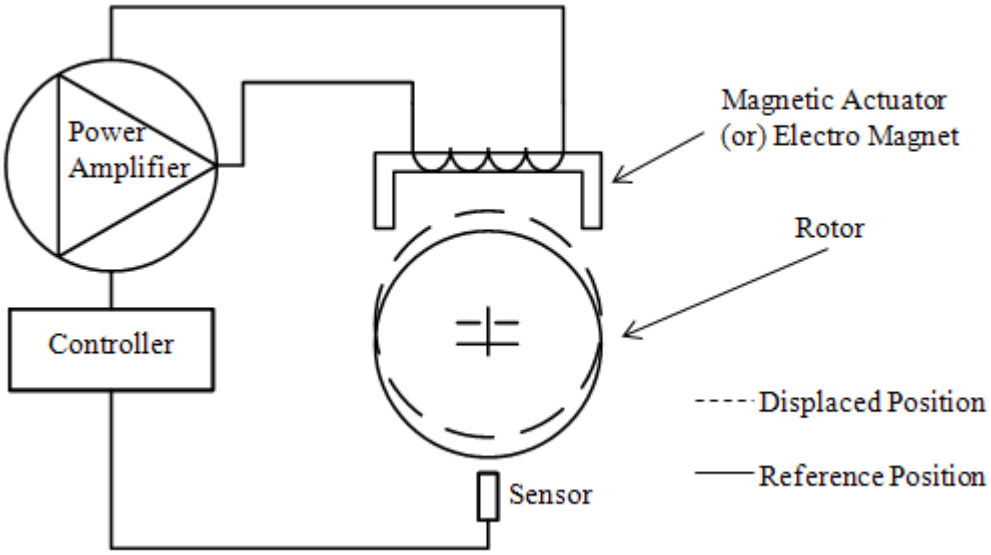

Figure 1.1 The working principle of AMB systems

There are mainly two types of loads acting on the rotor namely, the static and the dynamic. The static load include the load due to the weight of the rotor, external static loads on the rotor due to interconnectivity to other machine elements such as springs, preloads, etc. Dynamic loads include the mass imbalance of the rotor due to eccentricity, external disturbances due to base vibrations, applied load variations on the system, impact forces due to touch down bearings, etc. A current called the bias current is supplied to cancel out the static load acting on the rotor or a set of permanent magnets are used to support the static load. But due to the negative stiffness owing to the magnetic force a small disturbance would move the rotor away from the operating position. Hence, the rotor should be brought back to the operating position by using control methods. In this regard the rotor position is sensed by a sensor and the sensor signal is given to the controller, which sends the signal to the power amplifier based on the difference of the sensor signal from the reference signal. To bring back the rotor to its original position, the actuator is supplied with an additional current demanded by the controller through the power amplifier.

1.3 Classification of magnetic bearings

MBs are classified based on many factors. There is good number of classification of MBs available in literature. One such classification involving unification of complicated issues in MBs has been provided by Bleuler (1992). Salajer et al. (2000) gave classification of bearing-less motors based on different factors such as type of motor (synchronous PM, homo-polar, synchronous reluctance, switched reluctance); Stator winding configuration (4-pole motor & 2-pole radial force, 2-pole motor & 4-pole radial force, 2-pole motor & 4-pole radial force, Split winding, Concentrated winding, Single phase drive, 2-phase radial force); and mechanical structure of the rotor or motor (Slice motor, Disk type rotor, Outer rotor,

Ring type rotor). It also provides some types of motors on test machines (Induction, PM, reluctance), and applications (Blood pump, Computer spindle, Canned pump, Bio-pump). On the other hand Chiba et al. (2005) provided classification of different bearing-less motors. After observing the literature available an alternative diverse classification for magnetic bearing systems based on different factors has been provided in this section (refer Table 1.1). MBs can be classified according to

- Control action
  - *Active*: MBs operated by purely electrically controlled magnets are called *active magnetic bearings* (AMB). These require continuous power supply and computation of the control current.
  - *Passive*: MBs operated by purely permanent magnets are called *passive magnetic bearings* (PMB). These do not require any additional power supply. However they need some special conditions to achieve stability (Moser et al., 2006).
  - *Hybrid*: AMBs that involve also permanent magnets are called *hybrid magnetic bearings* (HMB) (Groom et al., 2000). These combine advantages of both the active and passive magnetic bearings. One constraint with HMB is that the control flux should not flow through the permanent magnet. Different configurations were proposed to make this constraint met as follows.
    - Permanent magnet on the stator (Kenny and Palazzolo, 2003; Schmidt, 2008)
    - Permanent magnet on the rotor (Yanliang et al., 2006)

Table 1.1 Classification of magnetic bearings

Main classification	Sub-classification
Control Action	• Active (Bornstein, 1991) • Passive (Paden et al., 2003) • Hybrid (Lee et al., 1994)
Forcing action	• Repulsive (Ohji et al., 2004) • Attractive (Robertson, 2003) • Gyroscopic torques (Berry, 1996)
Sensing action	• Sensor-sensing (Maslen, 2000) • Self-sensing (Maslen, 2006)
Load Action	• Axial (Banerjee and Rao, 1995) • Radial (Park and Chung, 1998) • Tangential (Chiba et al., 2005) • Combined axial and radial (Imoberdorf et al., 2007) • Combined radial and tangential(Chiba et al., 1993) • Combined axial and tangential (Ueno and Okada, 2000) • Combined axial, radial and tangential (Han et al., 2002)
Magnetic effect	• Electro-magnetic or reluctance force (Bleuler, 1992) • Electro-dynamic or Lorenz force (Salazar et al., 2000) • Super-conduction or Meissner effect (Bray, 2009) • Conductors in variable magnetic flux (Filatov and Maslen, 2001) • Non-Meissner Diamagnetic effect (No practical application; Bleuler, 1992)
Flux path	• Homo polar: flux flow radial and axial (Na, 2004) • Hetero polar: flux flow radial and circumferential (Kim et al., 2000)
Number of poles	• Two pole (Schweitzer et al., 1994) • Three pole (Chen and Hsu, 2002) • Four pole (Maslen, 2000) • Six pole (Maslen, 2000) • Eight pole (Maslen, 2000) • Sixteen pole (Kasarda, 2000)
Number of air gaps	• Single air gap (Cavarec et al., 2001) • Teeth pole (Cavarec et al., 2001)
Number of layers	• Monolithic (Moser et al., 2006) • Layered (Moser et al., 2006)
Winding scheme	• Centralized (Schweitzer et al., 1994) • Decentralized (Fan and Lee, 1995)

Motion generated or constrained	• Linear: levitation and propulsion (Boldea and Nasar, 1999)
	  ○ Flat
	  ○ Tubular
	• Rotary: levitation and torque (Shimada et al., 2000)

Objective of the application	• Precision flotors (Lee and Gweon, 2000) • Levitated rotors (Shimada et al., 2000) • Linear bearing motors (Cavarec et al., 2001) • Bearing-less motors (Chiba et al., 2005) • Contactless gears (Yao et al. , 1996) • Magnetic conveyors (Ohjia et al., 2004) • Noncontact springs and dampers (Robertson, 2003)

- Forcing action
  - *Repulsive*: When poles of same polarity used on rotor and stator (Hussien et al., 2005).
  - *Attractive*: When poles of opposite polarity used on rotor and stator.
  - *Gyro-torque*: Though Earnshaw's theorem affirms the impossibility of hovering an object purely by passive means, some special cases such as levitron disobey this theorem. When the speed of the rotor is more than a critical value, the rotor is observed to be in equilibrium even when the rotor is under passive levitation (Xu and Kian, 2008). This lead Earnshaw's theorem to be extended from the static equilibrium to the dynamic equilibrium.
- Sensing action
  - *Sensor sensing*: We need additional sensor probes to sense the position of the rotor. Generally, active magnetic bearings are of this category.
  - *Self sensing*: Based on Lenz's law the change of current flow in the bearing coil and back-emf generated due to the change of position of the rotor can be identified directly without the use of an external sensor. This technology has been developed to the level of commercial application. An overview of the technology is provided by Maslen (2006)
- Load action
  - *Axial or Thrust*: To support axial loads. The thrust action can be achieved by the radial or axial bearings
    - *Single acting*: A single rotor disc for a single actuator.
    - *Double acting*: A single rotor disc for two actuators on both sides of the disc.

- *Radial or Journal*: Used for supporting radial forces.
  - *Homo polar*: The magnetic flux flows through poles of the same magnet to close the magnetic circuit, i.e. radially and axially to the rotor disc.
  - *Hetero polar*: The magnetic flux flows through poles of different magnets to close the magnetic circuit, i.e. radially and circumferentially to the rotor disc.
- *Tangential or Torque*: This force is used for motoring action or rotating action. This is a simple motor. The same is also used in magnetic gears.
- *Combined axial and radial loading:* The loading can be a combination of above three types of loading
  - *Conical bearing*: used for combined loading of axial and radial (Mohamed and Emad, 1992)
  - *Teeth pole bearing*: radial or axial bearing are used to support both the axial and radial displacement controls (Kim and Lee, 2006)
- *Combined radial and tangential loading*: This is used in bearing-less motor with a radial bearing (Chiba et al., 2005)
- *Combined axial and tangential loading*: This is used in a bearing-less motor with an axial bearing (Ueno and Okada, 2000)
- *Combined axial, radial and tangential loading*: This concept is used in most of the linear systems such as MAGLEV systems and newer class of bearing-less motors (Imoberdorf et al., 2007)

❖ Calculation of force

- *Electro-magnetic effect*: This is due to the reluctance force and these results in magnetic bearings.

- *Electro-dynamic effect*: This is due the Lorentz force and these are called bearing-less motors.
  - Radial bearing motors
  - Axial bearing motors
  - Linear bearing motors

❖ Magnetic effect

- Ferro Magnetic effect
  - Attractive
  - Repulsive
- Dia-magnetic effect
  - *Diamagnetic materials at room temperature:* Forces are very small , however, still investigations are continuing.
  - *Meissner or super conducting effect*: This action comes when the magnet is working as a superconductor; an image of same polarity is induced in the rotor which generates repulsive forces of considerable strength. Super conductors are found increasing application in the area of magnetic bearings, bearing-less motors as well as linear bearing motors
    - High temperature superconductors
    - Low temperature superconductors

❖ Flux path: This falls under the radial magnetic bearing category

- Homo polar: Flux flows radially and axially
- Hetero polar: Flux flows radially and circumferentially

- Number of poles: The number of poles affect the winding scheme, control strategy, linearity etc. These are mainly subclass of magnetic radial bearings of hetero polar category.
  - Two pole
  - Three pole
  - Four pole
  - Six pole
  - Eight pole
  - Sixteen pole
- Number of air gaps: Analogical to number of poles. Tooth pole bearings have special advantage of generating axial force in combination with radial force. The different sub categories have been given in Cavarec et al. (2001).
  - Single air gap
  - Tooth-pole
- Number of layers: Analogical to number of teeth or poles. This class falls under permanent magnet radial bearings with hall batch arrays. (Moser et al., 2006)
  - Monolithic
  - Layered
- Winding Scheme: The winding scheme with respect to other electro magnets determines the control system strategy.
  - Centralized: The supplied control current supplied to one controller linearly dependant on the other magnet's control current.
  - Decentralized: Magnets are independently supplied with control current.

- ❖ Motion generated or constrained (Boldea and Nasar, 1999)
  - – Linear: These devices use both levitation and/or propulsion (Molenaar, 2000)
    - Flat
    - Tubular
  - – Rotary: These devices use levitation and/or torque
    - Axial
      - Single acting
      - Double acting
    - Radial
      - Homo polar
      - Hetero polar
    - Tangential
    - Combinational
      - Axial and radial
        - Conical: analogues to axial bearings
          - Single cone
          - Double cone
        - Tooth pole
      - Axial and tangential: bidirectional axial gap bearing motor (Ueno and Okada, 2000).
      - Radial and tangential: These are general bearing-less motors.
      - Axial, radial and tangential: these are used in conical bearing-less motors, tooth pole bearing-less motors and in bevel gear systems.
- ❖ Objective of the application: Based on the purpose of application
  - – *Motion to be constrained*: Bearings and Precision stages: used for positioning the stage or rotor at a particular position with high precision, indexing tables, machine tool tables, etc.
  - – *Motion to be generated in one direction while controlled in other directions*: Bearing-less motors and linear bearing motors: Motion in one axis and

control in other axes. These are used for rotary drives such as transportation systems like magnetic trains, elevators, IU-modules etc.

- *Motion to be transmitted:* Magnetic gears and conveyers to control the transmission of torque.
- *Energy to be absorbed:* Magnetic springs and dampers: To absorb/dissipate energy.

A number of configurations of magnetic bearing systems can be developed by combining different kinds of the above bearing classifications.

1.4 Advantages and applications of magnetic bearings

Any technology exists due to its advantages to certain applications. Hence, these advantages can be tracked out from where it is applied. In this section some of the advantages of magnetic bearings mentioned in literature have been summarized along with their applications.

Kimura and Nigshi (1990) applied magnetic bearings in a vacuum chamber where a gear train for the speed reduction is used in the production of Titanium powder. The different advantages mentioned are (i) AMBs can be applied in vacuum without any problem of lubrication pressure and vapours generation, (ii) oil free and no contamination, (iii) increase of natural frequency due to double end free axis, (iv) increase allowable unbalance due to non-contact support, and (v) rotation of the rotor around the principle axis of inertia by automatically balancing the system. The above advantages also led Ota et al., (1990) of Seiko Seiki Co., Ltd., of Japan to implement Maglev systems as a semiconductor wafer

transporter, which is carried in ultra-high-vacuum chambers where the particle generators such as ball bearings cannot be used. The goals of the process are horizontal translation, a pick and place motion in the vertical plane and restriction of rolling of the transporter rod. High precision is another advantage with which a magnetically suspended (MS-type) stepping motor was developed for ulta-high vacuum environments with high-precision of the rotor (Higuchi et al., 1990).

Magnetic bearings are implemented in the flywheel energy storage system where energylosses should be minimal. AMB systems show very low frictional losses and extemely long expected operating life times (Zmood et al., 1990). In magnetically levitated supports, the stiffness and damping parameters can be varied actively during the operation; hence it is possible to avoid different critical speeds actively during the coast-up or coast-down of rotors. Crossing different critical speeds by active methods is another advantage for AMBs to be implemented in high speed rotors (Zhang and Kobayashi, 2006). AMBs are applied in machining operation for they are superior to the mechanical one in terms of high speed, low friction, vibration damping, and diameter of the rotational axis which gives high precision. Therefore, AMB has the advantage that the stiffness of the machine which is attached to the tools can be high, and the high precision and stable cutting process can be obtained for a long time. AMBs are also superior to the air bearing for the high-speed spindle in terms of suspension stiffness, load volume, and bearing clearance. It is a promising tool for creating the micro- and nano-precision manufacturing (Shimada et al., 2000).

Identification of parameters by using AMBs has applications in condition monitoring of rotating machines. They allow for the adjustment of the damping, system monitoring and fault detection (Lösch and Bühler, 2000). There are literature available on the fault detection

including unbalance, run out, crack on the rotor shaft etc. (Aenis and Nordmann, 1998). Ventricular assistance devices for artificial blood pumps are being developed using the AMB technology in biomedical engineering. Conventional rolling element bearings or ball bearings use the processing fluid (i.e., blood) as lubricating fluid which results in damage of blood cells and clotting problems (Song et al., 2001). As there is no lubrication needed AMBs are effectively implemented in these devices (Wearden et al., 2006).

The interdisciplinary nature made AMBs expensive as well as posing challenging problems in the area of control and sensing. However, it has immense power of generating novel technologies, for example, extremely high-speed spindles, energy storage flywheels, high precision planar moving tables, indexing tables, etc (Junga and Leeb, 2009). Due to its highly nonlinear characteristic between the force and the current, now-a-days the AMB has become a standard object of testing by any new control methods (Schweitzer et al., 1994).

Dussaux (1990) gave some industrial applications of AMBs in the aerospace, machine tool, light industry and heavy industry. Kasarda (2000) discussed some advantages with commercial applications and research applications of the magnetic bearing technology. Okada and Nonami, (2003) gave a review of research topics in the magnetic bearing technology based on the 8th International Symposium on Magnetic Bearings (ISMB-8). Elaborated advantages and applications of the AMB technology have been explored by Schweitzer et al. (1994), Chiba et al. (2005), and Schweitzer and Maslen (2009). Some of the applications based on the advantages suitable to different fields of engineering are provided in Table 1.2.

Table 1.2 Advantages and specific applications of magnetic bearings

Field of application	Advantage	Specific applications
Semiconductor industry	No contamination, no lubrication, active control.	Electron beam choppers, turbo molecular pumps, molecular beam choppers, contact free linear guides (Kim et al., 2009).
Bio-medical engineering	No contamination, no contact, no lubrication, no distortion of the processing fluid.	Pediatric blood pumps, axial flow blood pumps, centrifugal blood pumps.
Vacuum technology	High speeds, no contact, no lubrication, and no contamination.	Turbo molecular pumps.
Structural isolation	Active and passive damping.	Springs and dampers for railway wagons, bases for building to absorb earth quake vibration.
Rotor dynamics	Active damping, no lubrication, and high speeds.	Crossing critical speeds (Zhang and Kobayashi, 2006), system identification and diagnosis. (Lösch and Bühler, 2000)
Transportation	No contact, high speed.	Maglev, conveyors. (Ohjia et al., 2004)
Precision engineering	Robustness to external disturbances, reliability, active control.	Precision position tables, indexing tables, measurement balance (Ren and Stephens, 2005) (Hussien, et al., 2005).
Energy storage	High speeds.	Energy storage flywheels.
Aerospace	Reliability, no lubrication maintenance, no lubrication pressure required.	Smart aero engines, jet engines.
Turbo power	No contact, no lubrication, bearing life independent of speed, and less power losses.	High speed gas turbines, generators, motors.
Material processing	No contamination, and high speeds.	Epitaxy centrifuges, sewage pumps.
Manufacturing	High speeds, active control, and precision.	Spindles for grinding, milling, gears, contact free linear guides, test rig for high speed tires.
Novel technology	No contact, friction free, and active control.	Novel technologies(Kim et al., 2009), new control methods, testing of control methods

1.5 Limitations of magnetic bearings and research areas

There is theory and practice with any subject and the same is true with magnetic bearing technology. What we expect in theory may not be reflected in practice due to assumptions made in the development of the theory. These limitations sometimes will be stumbling blocks for the technology to be realized into products of utility and commerce. The objective of a research is to overcome these stumbling blocks by elimination of the drawback or overriding through other means. Eliminating or overriding the drawback will be resulted either by perfecting the same system or by adding another new technology into the system. For an example a passive magnetic system cannot create a stable system. This draw back can be overridden by using a control system which is an additional technology. However, if this additional technology is eliminated from the system operation and if one creates a stable system without control system then the conventional technology is perfected.

Though there are many advantages as mentioned above the magnetic bearing technology has certain limitations which drive the further research for better solutions and applications. Kasarda (2000) gave some limitations and research topics in magnetic bearings. Some practical limitations of magnetic bearings were given by Schweitzer (2002). A summary of disadvantages with some of the drawbacks of active magnetic bearing technology mentioned in the literature and how they are overridden over years will be seen in this section. The different issues of magnetic bearing technology lie in the areas of magnetic materials such as permanent magnets and superconductors, control system technology, sensing technology, and power electronics.

One of the drawbacks with passive levitation is its inability to generate static stable equilibrium unassisted (Earnshaw, 1842). This drawback was a major stumbling block till the active control systems were realized in 1930s (Schweitzer, 1994; Kasarda, 2000). In 1937, Beams published an article on rotating steel balls spinning in air by different methods and finally by electromagnetic means. Holmes and Beams (1937) worked on magnetic axial suspension systems and Kemper (1937) applied for a patent of magnetically levitated vehicle systems, MAGLEVs.

One disadvantage with active magnetic bearings is that a continuous power supply to the system is required to support a static continuous load. This load could be supported by a permanent magnet to reduce the power consumption; however, the non-availability of permanent magnetic materials which can support a moderate load within an affordable size became a drawback. The property used for the load bearing capability within a size for permanent magnetic materials is energy density $BH_{\max}$. AlNiCo was the material known from 1932, however, it needs large volumes. Rare earth cobalt alloys are later developed. Later at some point of time samarium-cobalt (SmCo5) was the best permanent magnet material which resulted in substantial increase in weight efficiency (Studer, 1977). However, magnetic materials with higher energy density and mechanical strength Neodymium-Iron-Boron (NdFeB) alloys are available now (Schweitzer, 1994). Working with the optimization of the topology is another way of reduction of size (Dyck and Lowther, 1996).

The other reason of power consumption in AMB systems according to the linear control theory is that they should work in linear range of operation. For this purpose a high bias current should be supplied to the system at an operating position and small control currents should be used to regulate the position of the rotor. However, virtually zero power (VZP)

control techniques which were developed later, made it feasible to operate AMBs with all static loads being supported by permanent magnets (Studer, 1977). Developments in optimal control methods led to further reduction in power consumption (Maslen, et al., 1996; Betschon and Knospe, 2001).

The power consumption also is a result of operating air-gap maintained between the rotor disc and the electromagnet. Now nonlinear control methods further reduce the operating air-gap to a few microns. Using complete passive magnetic levitation is another way of eliminating the power-loss. There are cases observed where the dynamic stable equilibrium is possible above a critical speed of rotors with the passive levitation (Berry, 1996; Xu and Kian, 2008). Another case of passive levitation which is inherently stable in theroy during rotation was presented by Post and Ryutov (1998) in which an array of permanent magnets on the stator and a wire on the rotor to produce eddy currents was used.

The load bearing capacity is low in the case of AMB as compared to conventional mechanical bearings. The specific load capacity of magnetic bearings is in the order of 40:1 which is very less when compared to conventional mechanical bearings. Different aspects of reduction in the load capacity are the space available for the stator-iron, the saturation magnetic-density of the stator iron, the saturation current-density of the coil, the fringing and leakage losses, and eddy current losses. There are attempts to reduce these losses and improve the load carrying capacity of AMB. Ferro magentic material used for the stator with the higher saturation flux-density will increase the load carrying capacity. Efficient usage of the space available by the stator iron and coil (Kasarda, 2000), using the stator iron efficiently by the flux path by split flux method (Maslen, 2000), incorporating permanent magnets into AMB (studer, 1977; sortore et al., 1990) varying the air-gap and flux path in series and parallel (Khoo et al., 2005) are different ways of improving the specific load

capacity of AMBs. A specific load capacity of 108:1 for active systems and 450:1 for passive systems was observed by Khoo et al. (2005).

A high investiment is involved in the procurement of control system, sensors, and power amplifiers. Cost involved and space occupied with additional equipment in the control system is another drawback. Now a days self sensing bearings are investigated seriously to eliminate additional sensor probes (Maslen, 2006). Generally, equipment costs of AMBs will be in decreasing trend. However the procurement cost of AMBs is far higher than mechanical bearings. This requires a special analysis including maintainance, long life, application advantage such as the semiconductor industry and biomedical appications, to justify the cost involved (Kasarda, 2000). However, the special applications where the conventional mechanical bearings cannot be fitted justify the cost involved in it. Gray et al., (1990) performed such analysis for the implementation of AMB technology in power plant engineering.

In any dynamic system there are two issues to be dealt, the first is with internal nonlinearities, and the second is with external uncertainties. AMBs are highly nonlinear internally and subjected to sudden changes in loads frequently. As shown in Figure 1.2, in control system technology these two issues are dealt with namely as the adaptive control and the robust control, respectively. To meet these requirements control algorithms were treated as a different part of the AMB system technology (Burrows, 1987). Initially linear control methods were developed to make the system in dynamic stability by levitation using high bias currents. Later the adaptive and robust methods were developed (Johnson et al., 1998; Knospe and Tamer, 1997). Nonlinearities in magnetic bearings are very high when they are operating at critical conditions such as near the saturation of magnetic flux density, low bias or zero bias current operation, or very large operating air-gaps. Nonlinear control

methods are other class of methods being used in the magnetic bearing control to deal with these critical operating issues. Levine et al., (1996) attempted a uni-mode nonlinear control method for AMBs. They also provided different linear, adaptive and robust methods along with references of prior work namely the linear control including the transfer function or the state space approach, self-tuning methods, H_2- method, H^{∞}-method, μ-synthesis, sliding modes, and fuzzy control methods.

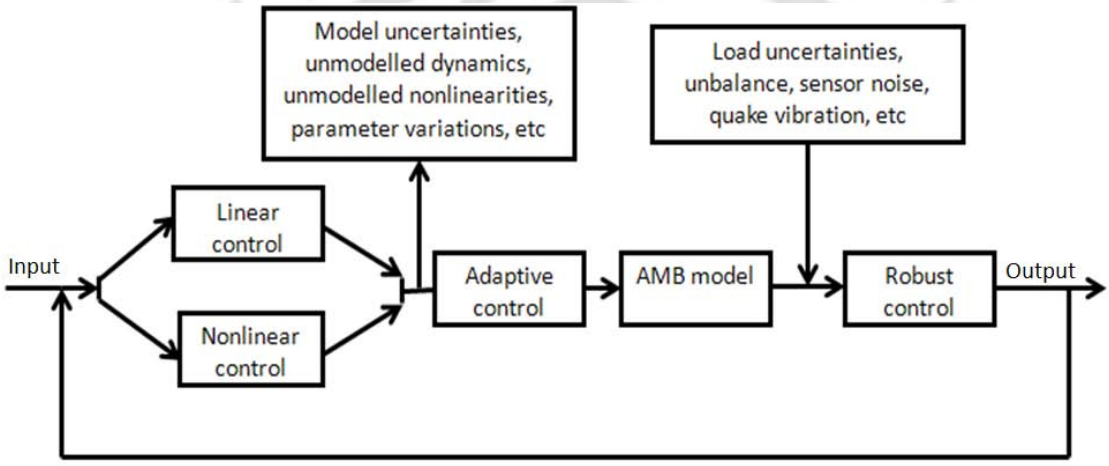

Figure 1.2 The classification of control system technology

A sudden failure of some of power amplifiers or coils due to powercut or damage results in the instability of the AMB system. The term used to deal with this problem is the fault-tolerance and is a reliability aspect of AMBs. Fault tolerant control seeks to provide continued operation of bearing even when some of the power amplifiers or coils suddenly fail. The solution for this task is to generate compensative currents that keep the system stable in remaining coils when some other coils fails (Na and Palazzolo, 2000). Much work is done to make the AMB control system that will be able to generate a stable operation (Maslen and Meeker, 1995; Na, 2004). The worst case is that the whole control system is distablilized due to the failure of all power amplifiers and coils or due to overloading

beyond capability of the system. In that case mechanical bearings or permanent magnetic bearings are used as backup bearings (Schweitzer et al., 1994; Schweitzer and Nordmann, 2009). Moreover, the rotor rests on these backup bearings when it is not rotating. These bearing are also called as touchdown or retainer or auxiliary bearings. Using AMB as a backup bearing is another idea being explored which would help in the fault tolerance (Cade et al., 2009).

Till now we have described brief introduction of AMBs including the background, working principle, classification, advantages with applications, and some drawbacks and how they have been overcome by the years. The state of the art of different fields of AMBs and the motivation of the present work and organization of thesis will be described in the following section.

1.6 Literature review

The idea of letting a body hover without any contact by using magnetic forces is an old dream of mankind. Earnshaw (1842) showed that permanent magnets alone are unable to keep a ferromagnetic body in a free and stable hovering position in all six degrees of freedom. In 1939, when there was already real interest in technical applications of magnetic bearings, Braunbek gave further physical insights. Only materials with diamagnetic properties would allow suitable configuration of permanent magnets with magnetic field distributions for stable hovering. The diamagnetically produced magnetic forces are too small to be of technical interest. High-temperature superconductors with diamagnetic properties could be of high engineering value.

To make use of the large forces achievable by ferromagnets for a stable free hovering, the magnetic field has to be adjusted continuously to the hovering state of the body. Kemper (1937, 1938) suggested the application of this idea in transportation and physics. The first description of a totally active magnetic suspension system was only issued in 1957 as a French patent assigned to the Hispano-Suiza Company (Habermann and Liard, 1980). In the middle of 1970s, a primitive electromagnet with stator windings having pole numbers of p and (p+2) was proposed by Hermann (1973, 1974). This electromagnet was proposed as a motor, which had a radial magnetic bearing function. A split-winding motor was proposed by Meinke and Flachenecker (1976).

Since an electromagnet can only produce attractive force, magnetic bearings are inherently unstable and require closed-loop control for a stable operation. The development was limited in the early days since there was little knowledge of inverters, digital signal processors, and field-oriented control theories at that time. A stepping motor, which was magnetically combined with a magnetic bearing, was proposed by Higuchi (1984). Allaire et al. (1989) presented the design of a prototype of thrust magnetic bearing for a high load-to-weight ratio. A design method was described for magnetic devices, with the topology and the material optimization by Dyck and Lowther (1996). Zeisberger et al. (2001) studied the optimization of levitation forces for an ideal super-conductive magnetic bearing. The classical design of magnetic bearings depends on the ideal magnetic circuit theory, which deviates drastically from experiments due to different losses such as leakage, fringing, and eddy current effects (Maslen, 2000; Schweitzer et al., 1994; Chiba et al. 2005; Schweitzer and Maslen, 2009).

Magnetic suspensions and subsequently magnetic bearings have been studied and developed in the laboratory environment as early as the mid 1930s. Economics associated

with their complexity kept them in the laboratory until the 1970s. By then, advancements in the microprocessor and solid-state amplifier technologies began to make the economics attractive in certain industrial applications. Original attempts at active control consisted of analog systems, which implemented a series of filters and a control loop. Further refinements resulted in a hybrid system that implemented the control algorithm in analog circuits and digitized the result to increase switching efficiency. A fully digital system was first implemented using a multiple processor per axis configuration to produce an all digital system (Bear, 1994). Some designs took the advantage of increased processing speeds to integrate all control loops into a single processor (Keith, 1988; Fedigan 1993).

Some of the preliminary works in the areas of permanent magnets, electromagnets and magnetic suspension have been provided in the above paragraphs. The design methodologies, configurations of magnetic bearings, works on magnetic thrust bearings, control system technology, and genetic algorithms in the area of magnetic bearings will be reviewed in following subsections.

1.6.1 Design methodologies

A design methodology is a systematic procedure in the development of a system for a unique situation. Figure 1.3 shows different aspects involved in the design and production of any system based on which a methodology could be deduced. These are modelling, design, analysis, procedure, and production. These different aspects are described in the following sub-headings.

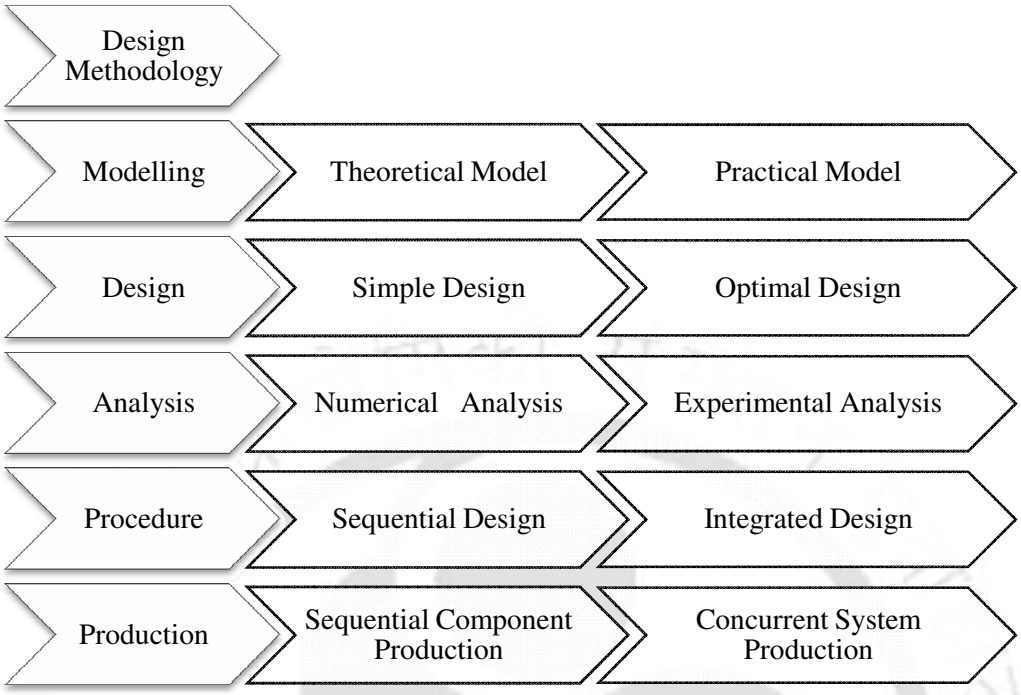

Figure 1.3 Different areas to be considered in a design methodology

Modelling: There are two aspects of the modelling, namely the theoretical and the practical, where the first one deals with the modelling simplicity (developing a hypothetical model) and the second one deals with modelling complexity or accuracy (bringing the model nearer to the reality in the practice). In magnetic bearings, modeling is done through a magnetic circuit of one-dimension or by using FEM in 2D or 3D. However 3D analysis by FEM is a costly effort due the manual mesh generation involved. The magnetic circuit model is simple one-dimensional and most commonly used in many applications (Schweitzer et al., 1994; Meeker et al., 1996; Na and Palazzolo, 2000).

There is simplified magnetic circuit model used for the analysis of magnetic bearings which is well established (Banerjee and Rao, 1995). Correction factors are added to this model including the eddy current, fringing, and leakage factors by Meeker et al. (1996). However, the analysis of eddy currents is available since 1970s (Stoll, 1974). Groom and Bloodgood, (2000) proposed a method for finding loss factors from 3D FEM analysis and

1D magnetic circuit analysis to bring the magnetic circuit analysis near to FEM predictions. Subsequently, this method was applied to a hybrid thrust magnetic bearing by Bloodgood et al. (2000). Kenny et al. (2002) proposed a method of using one-dimensional magnetic circuit model initially for design then, using 3D FEM analysis for getting more accurate results. It had benefits of both the magnetic circuit model and the FEM. The research on considering eddy current effects on other system parameters such as dynamic stiffness (Sun et al., 2009) is still continuing.

Design: In developing a new technology, the primary stage involves the development of a simple design procedure, and subsequently the evolution of optimal design procedures. A simple design methodology targets to make the system feasible or sustainable to some specified conditions which the system should undergo. An optimal design methodology targets to optimize a *specified objective or some objectives* while sustaining *specified conditions*, which the system should undergo. From this concept we can deduce the difference between a constraint and an objective. A constraint is the function whose feasibility is enough and can attain any value in the feasible range, while an objective is the function and it is our primary aim to attain its best value. Now the trend is to go for optimal designs in almost all fields of engineering.

Various approaches have been developed to aid the design of magnetic bearings. Simple design procedures are followed by many and vast literature is available for determining static load capacities or dynamic load capacities. Bornstein (1991) presented a simple design procedure for determining bearing force and dynamic load bearing capacity of an AMB with pure electromagnets. Design formulas for PMB are provided by Paden et al. (2003). Many configurations of HMB were given simple design formulas (Zhilichev, 2000).

Parametric and systematic approaches have been developed to optimize the power to weight ratio of magnetic bearings (Malone, 1993) and to achieve minimum power (Klesen, et al., 1999). These approaches are useful in developing design strategies. A direct minimum power optimization method was developed in 1998 (Bloodgood, 1998; Groom and Bloodgood, 2000).

Analysis: The design optimization involves two kinds of analyses, namely the numerical and the experimental. In the numerical analysis, the optimization of different tradeoffs are studied by using mathematical models available, while in the experimental one, tradeoffs are studied by conducting experiments on real test setups. However, the latter involves a lot of investment in terms of money and skilled-human hours in developing each prototype. Moreover, the experimental optimization cannot be done in a continuum due to the impracticality and the cost involved in manufacturing and conducting experiments. On the other hand, the numerical optimization needs accurate models; otherwise the numerical optimum may end up at a distance from the actual one. Hence, the practice is to use an available model and perform the numerical optimization to reach a solution nearer to the actual one. Then conduct experiments on real setups to check the model accuracy. Based on these observations, update the new numerical model. Hence, the numerical and experimental optimizations could be concluded as an iterative process.

There are mainly two kinds of numerical optimization, i.e. the deterministic and the stochastic. In the deterministic approach a single solution is analyzed and search is carried for the next best solution analytically by using mostly the calculus. In stochastic methods a population is generated in random and the best solution is traced out by analyzing each solution. Many numerical optimization procedures were provided for different configurations of AMBs with different objectives in literature (Khoo et al., 2007). However,

very little work is done on the experimental design optimization due to cost involved in developing set ups. Samanta and Hirani (2008) made one such attempt of theoretical and experimental study of various radial configurations, including hydrodynamic lubrication to enhance the radial load and radial stiffness, and reduced the axial thrust to improve dynamic performance of a permanent magnetic bearing.

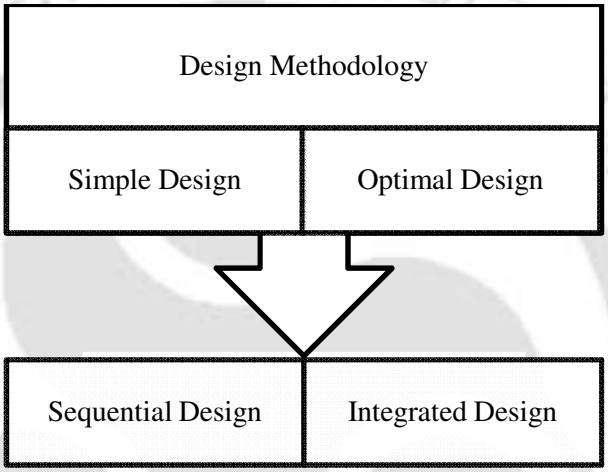

Figure 1.4 Levels of design methodology

Procedure: For systems which have more than one component, the design can be proceeded sequentially component-by-component or simultaneously as an integrated single system. Figure 1.4 shows various levels of design methodologies. There are two levels in the classification; a simple design and an optimal design come under the first level. A sequential design and an integrated design fall under the next level. In a sequential design optimization procedure initially one component is designed and optimized with corresponding objectives. Then a next component is designed to meet requirements of previous component and optimized for its corresponding objectives. On the other hand, an integrated design optimization necessitates the optimization of a system by simultaneous consideration of overall objectives and constraints corresponding to different components of the unified system.

A quote from Zmood et al. (1997) is given here in regard of magnetic bearing system optimization.

> *In the design of magnetic bearings the two key elements, which need to be considered, are the magnetic bearing actuator and its control system. The design process, which is highly complex, involves many engineering trade-offs. The performance measure of AMBs could be the load, size, stiffness, temperature, precision, speed, power losses and dynamics. One aspect of considerable importance is the influence of the bearing control system. Little emphasis was focused on this issue until 1990s (Schweitzer, et al. 1994) although experience showed that a holistic approach to their design was necessary to ensure a successful design outcome.*

Zmood et al. described a sequential design methodology for magnetic bearing systems, which was applied to the design of magnetic bearings for a 50 Wh open core flywheel and was used to illustrate the concepts developed as part of the methodology. The methodology was successful in providing feasible systems. However, by this sequential way the overall system may not be optimal in the overall system conditions and objectives. The integrated design methodology is in practice in other areas of mechatronic systems such as aero-space applications (Hale et al., 1985), robotics (Park and Asada, 1994), and servo-motor control (Yan and Yan, 2009). Other terminologies used for the *integrated design* are *simultaneous design* (Ravichandran et al., 2006)*, unified design, or concurrent design* (Park and Asada, 1994), etc.

Production: The major disadvantage with the sequential design optimization is the time involved in procuring individual components after the design. The various stages of the time

involved are namely the ordering time, the manufacturing time, and the procuring time. If multiple components of a system are sequentially procured, then the time will be the summation of the time of ordering, production and procuring of individual components. On the other hand if all components are simultaneously ordered, the time involved will be the maximum of summation of the times of ordering, production, and procuring of the individual components.

1.6.2 Configurations of magnetic bearings

In Section 1.3, has been given a variety of classification of magnetic bearing technology based on literatures available. A number of configurations can be developed by the combination of different classification type. Some of the configurations of magnetic bearings mentioned in literature have been provided in this section. For mechanical systems applicable for industry mainly the reluctance forces are used, in most situations, two opposing electromagnet poles allow control forces in two directions. This is beneficial for the position control since AMBs are unstable. Even for such simple classes of AMBs there are many different design principles, e.g. the homo polar and hetero polar pole arrangements, bearings with and without bias magnetic flux (i.e., when the bias magnetic flux originates from a bias current), bearings using permanent magnets for bias magnetic flux, the coplanar and non-coplanar arrangements of the bias and the control magnetic flux (Molenaar *et al*., 1997), etc.

Usually *permanent magnets* are used to save energy (zero current control) and reduce the number of power amplifiers or to minimize the size of the bearing (Lee *et al*., 1994), especially when combining the radial and axial bearings (McMullen *et al*., 2000). However,

the permanent magnet influences the negative stiffness and the inductivity, which both are most important for the achievable control quality. Ehmann et al. (2004) investigated the design of active magnetic bearings with permanent magnets to create the bias magnetic flux, and others with a purely electric bias and control flux generation. Criterions of comparison were the negative stiffness, the coupling between the two radial force directions, the force/volume ratio and the number and complexity of necessary parts. For the evaluation of performance characteristics three main parameters were considered, namely: the load capacity, stiffness, and damping. The latter two are related to designing the control algorithm. They suggested that in the main-body design, the specification of load capacity must be considered. The so-called main-body refers to a permanent/electro-magnetic magnetic bearing with the controller excluded.

Many researchers have attempted to develop a *variety of AMBs* that are compact and simple-structured, yet maintaining desirable performance. The single axis controlled repulsive type magnetic bearing system has been studied, where it has the feature of reduction of peripheral devices and displacement sensors for the active control. It also has a soft and constant stiffness to the passive control axes. Many applications were proposed employing this system, such as turbomolecular pumps, conveyor systems, and high-speed polygon scanner motors (Mukhopadhyay et al., 2000; Ohji et al., 2001). A single cone-shaped magnetic bearing can simultaneously produce the axial and radial forces (Mohamed and Emad, 1992; Lee and Jeong, 1996), but in turn, its control becomes complicated due to the coupled dynamics between the axial and radial directions.

Hybrid AMB incorporates with permanent magnets, leading to a simple composition as well as low power consumption (Sortore et al., 1990; Maslen et al., 1996; Fukata, 1998). A millimeter-sized, miniaturized AMB with solid cores and rotor was tested for high-speed

operations (Closs et al., 1998; Komori and Yamane, 2000; Kim and Lee, 2000). The eddy current induced on a non-laminated rotor generates a braking force that is one of the factors influencing the rotational power loss. Kim and Lee (2000) proposed an eddy current model accounting for the arrangement of poles and the size of pitch, and developed a hybrid-type AMB that was able to reduce the eddy current loss.

The integrated motor-bearing or self-bearing motor, which is a functional combination of motor and AMB, was developed using lamination cores and a rotor (Han et al., 2000; Okada et al., 2000; Kim et al., 2000 and 2002). These integrated motor-bearings use the Lorentz force for levitation and motoring of rotor. Han et al. (2000) developed a Lorentz-type integrated motor-bearing system with a disc-shape rotor. Okada et al. (2000) and Kim et al. (2000, 2002) introduced another disc-type integrated motor-bearing system and a cylindrical one, using the Lorentz force. Kim and Lee (2006) introduced a five-axes AMB with solid cores and rotor, which consisted of four permanent magnets, four U-shaped cores, and 16 control coils. It featured that the radial and axial magnetic bearing units was integrated for a compact design and that the homo-polar type configuration of poles with optimized pitch length was adopted to minimize the eddy current induced braking force. The homo-polar AMB system was levitated by the Lorentz-type axial as well as Maxwell-type radial forces. Based on the magnetic flux distribution analysis, the control algorithm was designed to account for the coupled effect between the radial and axial control magnetic fluxes. Experiments were carried out with a prototype AMB system to validate the design concept.

1.6.3 Magnetic thrust bearings

Magnetic thrust bearings (MTB) have not been discussed as much in the literature as magnetic radial bearings. However, in recent years there has been a lot of research published on thrust magnetic bearing. Some of the works on magnetic thrust bearings and applications in the literature is presented in the present section.

Simple design procedures for MTB are well established (Banerjee and Rao, 1995). Allaire et al. (1985) described a single-pole electromagnetic support system to verify the concept and compare it to some theoretical calculations. Humphris *et al.* (1986) investigated effects of control algorithms on magnetic support systems. Some early work on magnetic thrust bearings was reported (Shimizu and Taniguchi, 1968; Shimizu and Taniguchi, 1971), which considered the control system required for operating the bearing. Some information on the design of commercially available thrust bearings, was given by Haberman and Liard (1980), and Haberman and Brunet (1984). A description of a combination radial and thrust bearing was given by Haberman and Brunet (1984).

Allaire et al. (1989) designed a single-acting magnetic thrust bearing and tested it for a canned pump. They used a theoretical model to design and then modified the load capacity by using a fringing factor. Miki et al. (1990) developed an axial magnetic bearing for a high-speed rotor using a mechanical damper for a radial support. Banerjee and Rao (1995) carried out a simple design and analysis procedure of AMTB. A double-acting AMTB was designed and the detailed analysis considered the dynamic force capabilities and slew rate limits for a 60,000 rpm machine.

DeWeese et al. (1998) performed an experimental analysis for different *configurations* of magnetic thrust bearings and compared the results with FEM analysis. Different configurations considered are based on the shape of the laminated stack namely, washer-shaped laminate stack (WL), tape-wound laminate stack (TL), U-shaped laminate stack (UL), and solid metal (S). These are four ways a stator or rotor of a magnetic thrust bearing can be manufactured by laminations. A solid metal is without lamination which has high losses due to eddy currents. Over hanging of the shaft is taken into consideration for fringing effects. Jang et al. (2008) designed an AMTB and experimentally tested the designed set up. A 3-dimensional FEM was used in the nonlinear analysis of the bearing. Many control methods have been applied and tested on magnetic thrust bearings for it is easy to implemnt. Chen (2008) proposed an adaptive genetic algorithm (AGA) approach for multi-objective optimization of a PID controller for a HMTB with a vertical shaft.

Structural and functional integration:

Generating axial control with a radial bearing: Matsumura et al. (1987) attempted to integrate the radial and thrust controls by using active radial beaings. Canders and Lee (1997) introduced a teeth-pole model of the radial bearing with combined axial action. Subsequently, Lee et al. (2000) proposed new approaches for axial control. Hijikata et al. (2008) studied the characteristics of a magnetic thrust bearing with a cylindrical rotor core.

Generating rotation with an axial gap bearing: Ueno and Okada (2000) developed a bidirectional axial gap type bearing-less motor which works as a thrust bearing as well. Song et al., (2001) implemented the bidirectional axial gap bearing-less motor to a brushless direct current (BLDC) blood pump.

Generating radial control with axial gap magnetic thrust bearing: This effect is studied by Kenny and Palazzolo (2002) with a toroid axial gap double-acting bearing.

Generating radial control as well as rotation with axial gap bearing: An axial gap type bearing-less motor with hollow rotor which controls all the levitation in the radial and axial directions along with rotation of the rotor was studied by Schneeberger and Kolar (2006). The other advantage with this kind of bearing configuration is the rotor tilt also could be controlled.

Applications of magnetic thrust bearings were reported for pipeline compressors (Foster et al., 1986; Hustak, 1986). Operation of AMBs in the industrial environment has been quite successful. Work on an unusual magnetic bearing design was reported (Walowit and Pinkus, 1982; Albrecht et al., 1982), in which the bearing was designed to be active axially but passive radially. Lewis and Allaire (1987) investigated the potential use of magnetic thrust bearings for control of transmitted forces. The magnetic bearing was used in conjunction with an oil thrust bearing. Fairly extensive work has been reported on applications of AMB for the satellite attitude control and the energy storage flywheel. A three-axis magnetic suspension system was described by Eisenhaure *et al*. (1984), which employed high-energy samarium-cobalt permanent magnets. Anand *et al.* (1986) described a flywheel magnetic bearing of combined active and permanent magnet design.

Optimal Design: Groom and Bloodgood (2000) proposed a model by adding the loss and leakage factors to ideal models, with and without bias permanent magnets. Subsequently, Bloodgood et al. (2000) applied the theory for the deterministic optimal design of a magnetic thrust bearing with bias permanent magnets. The magnetic bearing design included the determination of geometries of the bearing and the current supplied to carry a

specified load for a specified gap. Optimal design was carried out in two steps, including modeling the magnetic circuit, which determines the accuracy of achieving the requirement, and optimization of the design, which determines the efficiency of achieving the requirement (Bloodgood et al., 2000).

Various approaches have been developed to aid the design of magnetic bearings. Parametric and systematic approaches have been developed to optimize the power-to-weight ratio of magnetic bearings (Malone, 1993) and to achieve minimum power (Klesen, et al., 1999). These approaches are useful in developing design strategies. A direct minimum power optimization method was developed by Bloodgood (1998), and Groom and Bloodgood (2000). It optimized an ideal model without considering the magnetic flux leakage or MMF losses.

1.6.4 Control system technology in magnetic bearings

The major research related to the design of AMB system is focused on the controller part. In the design of controllers, various control laws have been applied to magnetic bearings from the classical proportional-derivative (PD) controller (Humphris et al., 1986) to even robust and nonlinear ones (Ide et al., 1996; Smith and Weldon, 1995). Park and Chung (1998, 1999) performed optimum designs for the radial and axial magnetic bearings with a minimum volume to endure a required bearing load carrying capacity and the stiffness. Yeh and Toumi (1994) analysed performance of the one-axis and five-axis magnetic bearing systems using the bond-graph modeling method, the dimensional analysis technique, and the LRT controller; and proposed the design and control integration for magnetic bearing systems. Lee and Hsiao (1994) performed the optimum design of the rotor structure, the control

system, and the magnetic bearing, simultaneously, over a three-disc rotor-bearing system. Their design objectives were to minimize the rotor response and the control current.

When using MBs as force actuators, a large amount of bias current is commonly provided to coils of electromagnets (EMs) to retain the linearity between bearing forces and the coil control current. However, this approach unavoidably consumes a large amount of electric power. An alternative approach to solve this problem involves using permanent magnets (PMs) to provide the required bias magnetic flux field at the expense of a more precise alignment. Lee *et al*. (1994) and Amiss et al. (1988) proposed a rotor supported by the permanent/electromagnetic magnetic bearing (PEMB) to operate well under the control of four simple analog PD controllers. In the study by Hua, *et al*. (1997), the design considerations of PEMBs and the method for analyzing the complete rotor-bearing system were presented. Also, a decentralized output feedback control algorithm was used to simplify the controller design and implementation.

1.6.5 Genetic Algorithms in magnetic bearing design optimization

Among the optimization techniques applied to the design of other types of bearings (Choi et al., 2001; Chakraborthy et al., 2003; Rao and Tiwari, 2006; Gupta et al., 2006) genetic algorithms (GAs) (Goldberg, 1989) are popular and promising ones, in that they overcame the problem of the local optima. One of the advantages of GAs is that they explore different areas of the search space in parallel and have no presumptions with regard to the search space. Chen and Hsu (2002) studied the optimal design of a three pole magnetic bearing. Optimal design by using GAs of radial active magnetic bearings integrated with their control was studied by Chang and Chung (2002). Many techniques of multi-objective

genetic algorithms (MOGAs) are developed in recent years (Fonseca and Fleming, 1995; Gao et al., 2000; Coello, 2000) among which Non-dominated Sorting Genetic Algorithm-II (NSGA-II) (Deb et al., 2002) is one of the widely used techniques (Bui et al., 2005; Hu et al., 2003), successfully implemented to different problems such as the optimization of brag gratings (Manos and Poladian, 2005).

The optimization of bearing locations of rotor systems with magnetic bearings was performed by Srinivasan et al. (1997). The single- and multi- objective optimizations for a flexible rotor system with magnetic bearings were performed by Shiau et al. (1997). Carlson et al. (1999) suggested the optimization procedure of the actuator of a magnetic bearing. Bloodgood et al. (2000) used the sequential quadratic programming (SQP) method to optimize the design of a thrust magnetic bearing with bias permanent magnets for the deterministic optimum design.

Optimization of radial active magnetic bearings was investigated by Stumberger et al. (2000). The finite element technique was used to calculate forces and the stiffness, and an evolutionary algorithm called the differential evolution was used with a single objective and penalizing the constraints. The same method was considered by Polajzer (2003) to optimize the radial magnetic bearing. Zeisberger et al. (2001) studied the optimisation of levitation forces for an ideal super-conductive magnetic bearing. The optimization of radial magnetic bearings integrated with the control was carried out by Chang and Chung (2002), by considering a single-objective optimization. Kim et al. (2002) studied the optimization of the power-loss of hetero polar magnetic bearings by using single-objective genetic algorithms. Hu et al. (2004) studied the reduction of power-loss by optimizing the bias current.

Hu et al. (2005) proposed a design methodology that dealt with the constraints on the rotor displacements. Onuma et al. (2005) proposed a magnetically levitated centrifugal blood pump with hybrid magnetic bearings. Glauser et al. (2006) performed a design optimization of an axial flow left ventricular assist device with combination of the active and passive magnetic bearings for minimizing the size and the power-loss. Optimization of a PID controller for a magnetic bearing was performed by Chen and Chang (2006). Single objective optimization of magnetic force of electromagnetic micro-power generator was carried out by Buren and Troster (2007). Noh et al. (2008) proposed a methodology to design and optimize in a unit level and a system level, with application to a blood pump magnetically supported using permanent magnets for the radial support and active electromagnets for the axial support.

1.7 Books, conferences, and journals

Schweitzer et al. (1994) was the first to write a book on active magnetic bearings, which covered basics of the magnetic bearing technology and introduced certain applications. The book composed different characteristics of magnetic bearings and their applications and explained basic methods of control of magnetic bearings. The control of the rigid and flexible rotors by using magnetic bearings was dealt in detail. Maslen (2000) presented a concise work on the design and analysis of magnetic bearings of both the axial and radial magnetic bearings. The structure of different elements of active magnetic bearing systems such as power amplifiers, position sensors, and controllers were also discussed. Control of different structures by using magnetic bearings was also presented.

Chiba et al. (2005) summarized different doctoral works and introduced different kinds of bearing-less motors. In this type of motors, the levitation force is supplied by the motor winding, which also supplies the torque, instead of a separate magnetic bearing to support the rotor. This makes it unifying magnetic bearing and motor in the same unit. They presented two kinds of such motors namely, the induction and permanent magnet types. The fundamental of electro-magnetism and controls were covered. The structure and characteristics of different kinds of bearing-less motors was also explained. Schweitzer and Maslen (2009) compiled an expertise of nine pioneers of the field of magnetic bearings for rotating machinery. The book starts with an overview of the technology and a survey of the range of applications. The different component technologies have been explained along with a state-of-the-art exposition. At the end of the book, some special concepts and systems, including micro-scale bearings, self-bearing motors, and self-sensing bearings are put forth as promising directions for a new research and development.

International symposium on magnetic bearings and international symposium on magnetic suspension technology are the two conferences dedicated specially for AMB technology. Many other conferences such as IFToMM, IMechE, MoViC, etc have been presented with articles and posters related to AMBs. The main sources of journal articles for AMB are IEEE Transactions on Magnetics, ASME/IEEE Transactions on Mechatronics, IEEE Transactions on Dynamics and Control, ASME Transactions on Gas Turbine and Power, ASME Transactions on Dynamic Systems Vibration and Control, etc. Elsevier Mechatronics, Magnetics, Precision Engineering, Control Engineering Practice etc. to mention a few where frequent articles are seen. Similarly, the other journals like Transactions of JSME, Transactions of KSME and some Chinese Journals are emerging with good amount of knowledge base in this area of magnetic bearing technology.

1.8 Aim and objective of the present work

As discussed in section 1.6.3, *magnetic thrust bearings* (MTB) have not been discussed as much in the literature as magnetic radial bearings. Though some investigations on MTBs have been looked at as given in section 1.6.3, however, the area of optimization is not explored much in their optimal design. In the present section, the general challenges involved in the design of magnetic bearings and the motivation for the design optimization will be discussed.

1.8.1 General Challenges in the Design of AMBs

The basic challenge of such a mechatronic system is to design components compatible to each other to meet requirements within given constraints. The rotor should be designed to support the load applied, which involves the stress-strain and rotor dynamic analyses. The magnetic actuator design includes two issues namely, the magnetic circuit design and the coil design. The actuator should be designed to generate the magnetic flux required to support the load acting on the system. Moreover, the magnetic flux-density is a constraint of the stator material, which is called the saturation magnetic flux-density. Beyond the saturation flux-density the actuator cannot support the additional flux requirement. One can increase the load capacity (i.e., the maximum load that can be supported by the bearing) by increasing the area of magnetic flux flow of stator-iron; however, this increases the weight of the bearing. To reduce the weight, smaller coil volumes can be implemented within constraints of the saturation current density. However, this leads to larger copper losses (i.e., losses due to electric resistance of the coil material) due to less volume available for the flow of current.

The operating temperature of the bearing is another important issue, and after certain limit the coil insulation spoils. The heat is generated mainly due to electric resistance of the coil and is constrained by the critical temperature of the insulation material and the heat absorption capacity of the cooling system used. In conventional mechanical bearings some of the power of the rotor is lost due to the friction (i.e., damping). As there is no mechanical friction in AMB there should be a zero power-loss ideally. However, copper losses due to electric resistance, iron losses due to eddy currents, and the magnetic hysteresis contribute to the losses in AMB. The designer's aim would be to reduce these losses to a minimum level.

The other challenge is the compatibility between the actuator and control systems. To have a linear control, a high bias current is implemented with small variations in control currents and the air-gap. However, this leads to high power-loss due to high bias current. Hence, to reduce these losses one has to maintain a lesser air-gap and a low (or zero) bias current. However, nonlinearities of the force with the current and/or the displacement increase with such a low bias current (or air-gap), which may lead to the control saturation or the singularity.

The compatibility of the power amplifier and the controller is another task in the design of magnetic bearing systems. Though power amplifiers can be designed with respect to designed controller requirements, sometimes it is not possible to have the required power amplifiers as a standard one, and one has to design the controller by taking constraints of the power amplifier available at hand. Though centralization of controller requires less number of power amplifiers, it needs some complex winding and control strategies. To go for simpler winding and control strategies one may have to go for a decentralized actuator, controller and power amplifier.

The integrated design is another task in AMB systems where interdisciplinary components are simultaneously involved. For such a case, a serial design methodology was mentioned by Zmood et al. (1997). As per their design methodology each individual component is sequentially designed and checked for compatibility. However, the integrated design methodology implemented in the present work considers all components simultaneously to optimally design and analyze. The genetic algorithm provides a tool to implement this kind of integrated design methodology.

The above discussions are valid for both the radial and thrust AMBs; however, our main focus of the present works in on the thrust AMB without and with bias magnets.

1.8.2 Objectives of the Design Optimization and its Importance

As discussed in section 1.6.3, *magnetic thrust bearings* (MTB) have not been discussed as much in the literature as magnetic radial bearings, especially in their optimal design. As discussed in section 1.6.1, in developing a new technology, the primary stage involves the development of a simple design procedure and subsequently the evolution of optimal design procedures. Now the trend is to go for optimal designs in almost all fields of engineering. As much work is well established in simple designs and still continuing further, the present work is targeted to implement optimal design for MTBs.

There are two aspects of design, namely the theoretical and the practical, where the first one deals with the modeling simplicity (developing a hypothetical model) and the second one deals with modeling accuracy (bringing the model nearer to reality in the practice). In

the present work, we adapt a practical model which takes the different loss-factors and constraints of nonlinearities into consideration.

Similarly, from section 1.6.1, the design optimization involves two kinds of analyses, namely the numerical and the experimental. The latter involves a lot of investment in terms of money and skilled-human hours in developing each prototype. Moreover, the experimental optimization cannot be done in a continuum due to the impracticality and the cost involved in manufacturing and conducting experiments. On the other hand, the numerical optimization needs accurate models; otherwise the numerical optimum may end up at a distance from the actual one. Hence, the practice is to use an available model and perform the numerical optimization to reach a solution nearer to the actual one. Then conduct experiments on real setups to check the model accuracy. Based on these observations, update the new numerical model. Hence, the numerical optimization and experimental optimization can be concluded as an iterative process. In the present work we attempt a numerical optimization and analysis.

The design optimization can be done in the component level and/or in the system level. Researchers have attempted the design of AMB at the component level (i.e., actuators, sensors, controllers, or power amplifiers) as well as the system level (i.e., the integration of all components). Most of the research in the design optimization of AMB systems was performed by the single-objective optimization especially of the controller unit. Very few attempts were made on multi-objective optimization, that to on a component level. On the other hand the multi-objective optimization tools such as genetic algorithms were also under intensive research (Fonseca and Fleming, 1995; Coello, 1999; Coello, 2000; Raghuwanshi and Kakde, 2004).

Hence, in the present work a multi-objective optimization of AMTBs and HMTBs in component level and system level has been attempted. Varieties of configurations of components have been optimized and the performance has been evaluated with number of AMB/HMB parameters. Moreover, a novel design analysis methodology is adopted to study the parameters of the Pareto front of the multi-objective optimization. This method will be explained with AMTB and HMTB configurations.

In the system level an integrated optimization methodology has been adapted for double-acting hybrid magnetic bearings (DAHMTBs) with controller as a single unit. Initially, the controller is designed without taking the power amplifier constraints. A centralized controller is implemented.

A power amplifier has limitations of voltage supply and bandwidth, and the controller should be designed to be compatible with the power amplifier. Hence, the constraints of the power amplifier have also been included in the integrated design optimization model. A centralized controller is simple to implement but needs some complex winding schemes of the coil. Hence, a decentralized centralized controller is assumed.

1.9 Organization of the thesis

In the present thesis, *Chapter 1* gives an introduction to the magnetic bearing technology, advantages, applications and drawbacks in the first part. A literature review and motivation for the present problem are given in remaining part.

Chapter 2 gives the formulation of the problem. Different relations and the optimization problem formulation for the magnetic actuator of an *active magnetic thrust bearing* (AMTB)

(i.e., without bias magnets) and a *hybrid magnetic thrust bearing* (HMTB) (i.e., with bias magnets) are presented. The descriptions of objective functions, design vector and constraints as an optimization problem of the magnetic actuator will be given. At the end the influence of different parameters on objectives and constraints are provided.

Chapter 3 gives the introduction to genetic algorithms. In this chapter, different tools available for optimization, genetic algorithms as the choice of optimization tool for solving the present problem, and some of the basic aspects of genetic algorithms implemented in the present work have been discussed.

In *Chapter 4*, the design optimization of actuators of an AMTB and a HMTB by using single-objective genetic algorithms (SOGA) has been presented. Single-objective genetic algorithms have been implemented for the optimization (minimization) of the power-loss in the coil and the weight of the actuator, one at a time. Apart from the comparison of objective functions in the tabular form, geometries of optimized magnetic bearings are compared in the form of diagrams.

Chapter 5 gives a multi-objective design optimization methodology and a novel analysis implemented to AMTB. The multi-objective optimization is carried to actuators of AMTB using *multi-objective genetic algorithms* (MOGAs). The trade-offs namely the minimization power-loss and the weight of the actuator will be studied together. The comparison of performance parameters are presented in the form of plots, tables, and line diagrams. A design analysis of Pareto optimal solutions has been introduced to study the behavior of different parameters of the Pareto optimal designs in the final population.

In *Chapter 6,* the optimization of HMTB will be carried by the methodology presented in Chapter 5. Two objective functions, namely the minimization of power-loss and the minimization of weight, are considered for the case of HMTB and the results are compared with AMTB. Inclusion of permanent magnets leads to remodeling of the problem as compared to the pure electro-magnetic bearings.

In *Chapter 7,* the analysis on the final population introduced in this work is studied at various loads in the optimal design of actuators of AMTB and HMTB. The Pareto optimal fronts obtained at different loads from a minimum to a maximum feasible load and the behavior of other parameters are detailed. The effectiveness of the method of analysis will be clearly seen at the end of the chapter.

Chapter 8 deals with the design optimization of an actuator-controller integrated system of a *double-acting hybrid magnetic bearing* (DAHMTB) by using the MOGA. This chapter takes the analysis from a component optimization to an integrated system optimization. The performance tradeoffs of the actuator and the controller, when they are optimized independently might not be the optimum when considered as a unified system. Hence, in the present work, an optimal design methodology of *double-acting hybrid active magnetic thrust bearings* (DAHMTB) has been proposed. Double-acting actuators and centralized controller are optimized as a unified system. Three objectives namely the power-loss, the weight of bearing and the load capacity have been considered for the actuator. Whereas, two objectives namely the input performance index and the dynamic performance index have been considered for the controller. The design considers the ten geometric, two electrical, and two control design parameters. Constraints are classified into three categories, namely the geometric, electrical, and control constraints. The convergence and Pareto-front spaces are studied by using different population sizes and run for different generations. Some of the

convergence criterions have been observed for actuator controller systems. Designs which are nearest to the utopia point in Pareto-front fronts are compared. Performance parameters of double-acting actuators and the controller of the magnetic bearing for different choices have been presented.

Chapter 9 deals with the design optimization of an actuator-controller-power amplifier system of a DAHMTB by using MOGA including power amplifier constraints. Without considering voltage limits on the power amplifier, the controller may choose its gains in such a way that it demand a very large voltage from the power amplifier. Hence, the main purpose in the present chapter is to study how constraints of the power amplifier affect the integrated design optimization of the actuator, controller and power amplifier system. A decentralized controller amplifier system is considered for the optimization.

The conclusions of the overall thesis and the future scope of the work are given in *Chapter 10*. The *references* are included at the end of the thesis.

Chapter 2
Formulations of Optimization Problems of Magnetic Bearings

2.1 Introduction

The previous chapter summarized the background of magnetic bearings, working principles, classifications, advantages and limitations. A literature survey on areas of the design of magnetic bearing actuator, control, and amplifier was also presented including different methodologies, configurations of magnetic bearings, magnetic thrust bearings, control system technology, optimization and genetic algorithms implemented in the design optimization of magnetic bearing technology. The general challenges involved in the design of magnetic bearings and the motivation for the design optimization have been discussed at the end of Chapter 1.

In the present chapter, fundamental relations of the thrust magnetic bearing (actuator) geometry and the magnetic-circuit are presented. The optimization problem formulations are presented for the magnetic actuator of *active magnetic thrust bearings* (AMTBs) and *hybrid magnetic thrust bearings* (HMTBs). Descriptions of objective functions, the design vector and constraints as an optimization problem of the magnetic actuator are provided in detail. The influence of different input, design, and dependent parameters on objectives and

constraints are provided. Expressions of fundamental relations namely the tradeoffs and constraints are summarised for the HMTB. For AMTB these fundamental relations can be obtained by eliminating terms corresponding to permanent magnets.

2.2 Geometry of Magnetic Bearings and Fundamental Relations

To have an idea of active magnetic bearing (AMB) systems some photographs and 3D solid models are provided in this section. Photographs of AMTBs produced by Synchrony, Inc. and SKF are shown in Figure 2.1 and Figure 2.2 respectively. Radial magnetic bearings configured with four poles, six poles, and eight poles have been shown in Figure 2.3. Solid models (3D) of rotors have been shown in Figure 2.4 and Figure 2.5 respectively. A 3D solid model of rotor with one radial magnetic bearing and a double acting magnetic thrust bearing has been shown in Figure 2.4. A 3D solid model of rotor with two radial magnetic bearings and one double acting magnetic thrust bearing has been shown in Figure 2.5. A 2D model of rotor-AMB system with two radial magnetic bearings and two single-acting magnetic thrust bearing is shown in Figure 2.6. A 2D model of rotor-AMB system with two radial magnetic bearings and one double-acting active magnetic thrust bearing is shown in Figure 2.7. The macro-geometry of an actuator of an AMTB and a HMTB are shown in Figure 2.8 and Figure 2.9, respectively. An AMTB actuator consists of an iron-core which is a stator, an iron-disc which is fixed to the rotor. The rotor gets disturbances from external thrust loads through machine element like gears, blades, fans, etc. The stator-iron core is provided with a space to accommodate a copper-coil winding. In HMTB of the present configuration considered as shown in Figure 2.9, permanent magnets are also fixed to the

stator-iron core in addition to the components of AMTB. The geometric and magnetic circuit relations are explained in the following subsections.

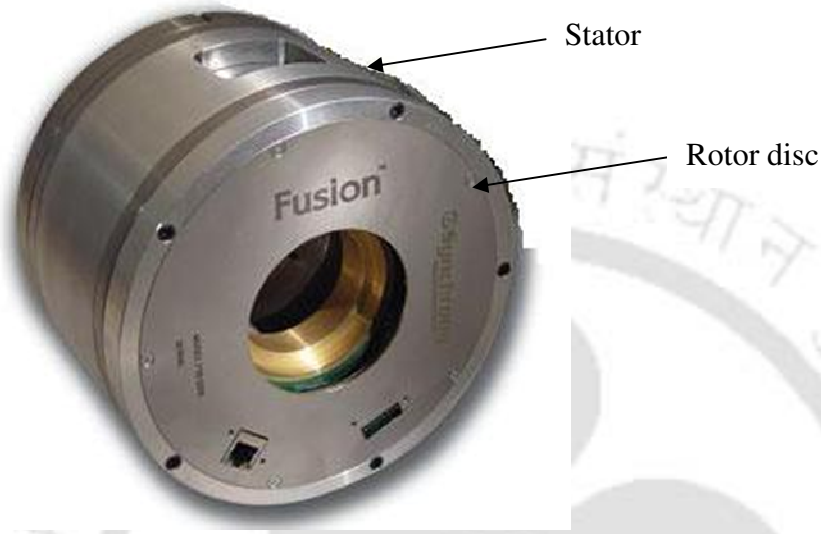

Figure 2.1 A magentic thrust bearing *with integrated control electronics* supporting a 250-hp industrial motor (courtesy: Synchrony, Inc., 2009)

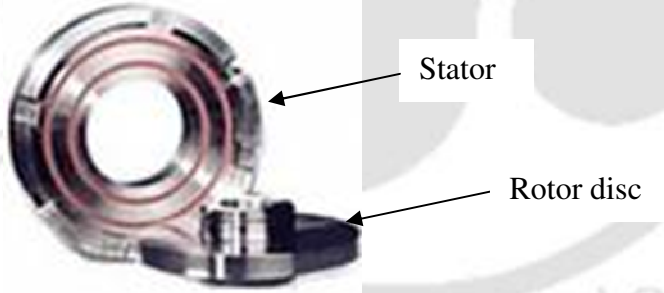

Figure 2.2 A magnetic thrust bearing with 17,000 N capacity for a 12,000 rpm turbocompressor with a 120 mm shaft. (courtesy: SKF, 2009)

Figure 2.3 Different configurations of radial magnetic bearings (source: world wide web)
(left) four pole (middle) six pole (right) eight pole

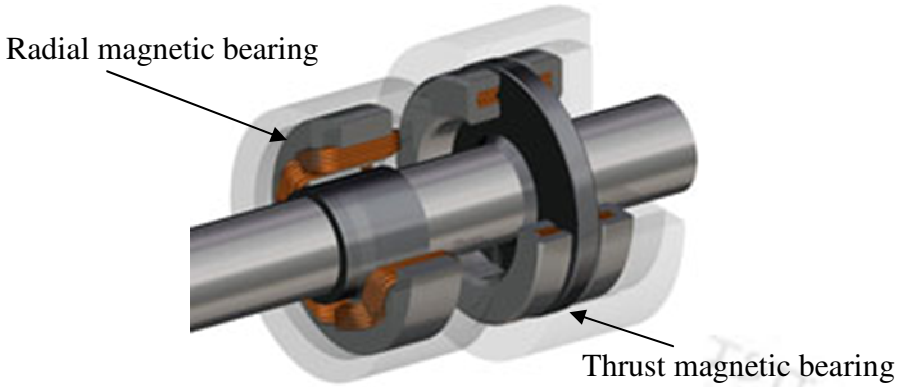

Figure 2.4 A 3D solid model of rotor with one radial and a double acting magnetic thrust bearings (Courtesy: S2M)

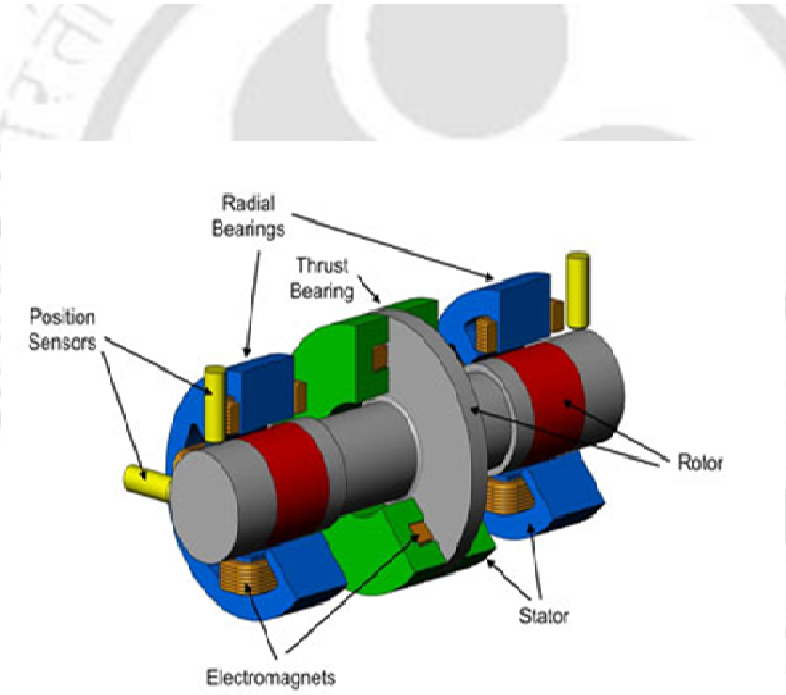

Figure 2.5 A 3D solid model of a rotor system with two radial magnetic bearings and one double acting magnetic thrust bearing (Courtesy: Synchrony, Inc.)

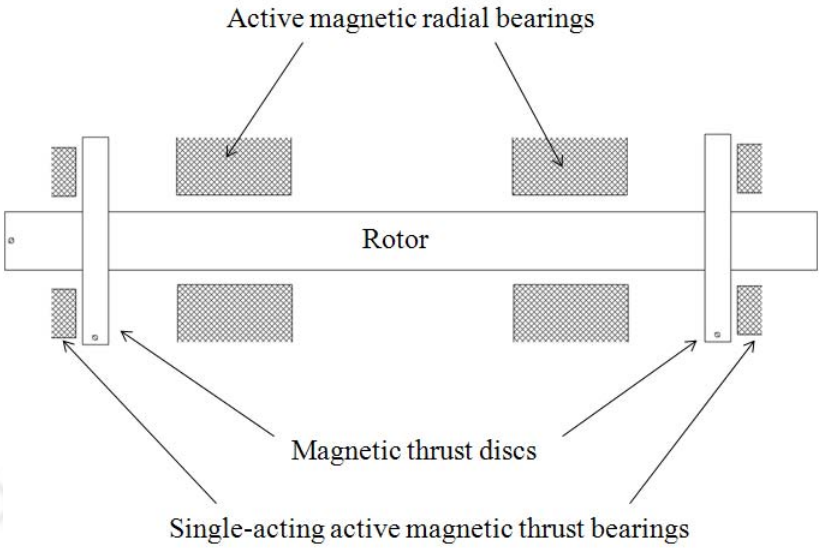

Figure 2.6 A rotor AMB system with two radial and two single acting thrust magnetic bearings

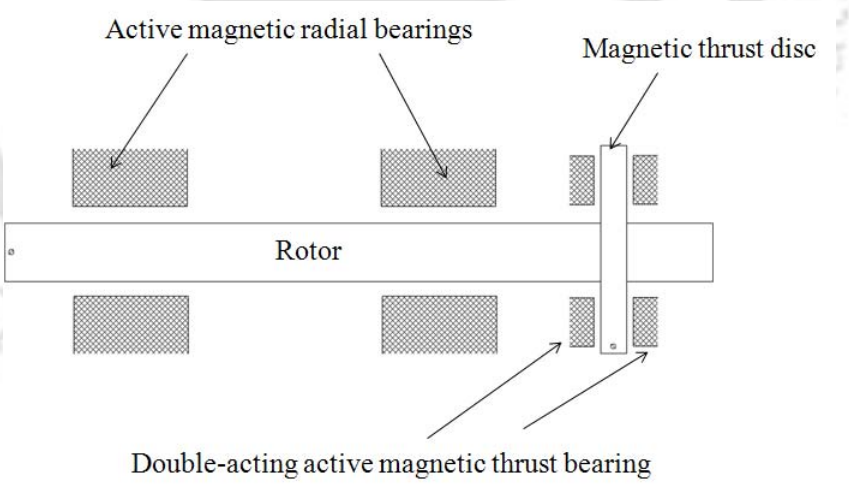

Figure 2.7 A rotor-AMB system with two radial and one double acting magnetic thrust bearings

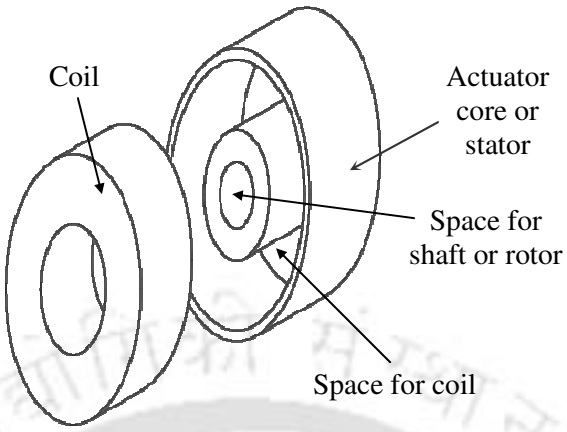

Figure 2.8 Parts of the actuator of an active magnetic thrust bearing

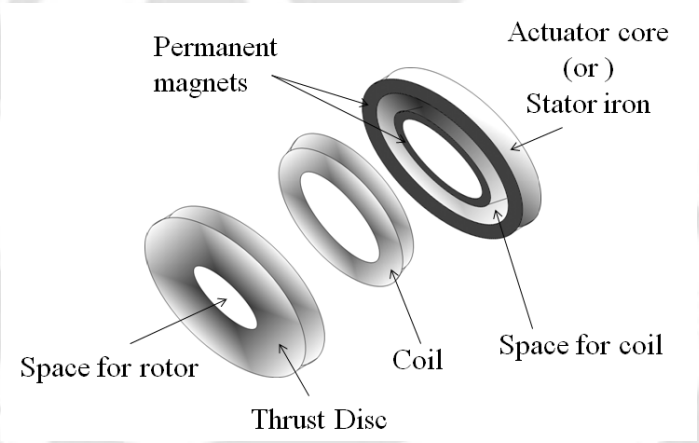

Figure 2.9 Parts of actuator of a hybrid magnetic thrust bearing

2.2.1 Geometrical Relations

Various design parameters of the AMTB are shown in Figure 2.10 and that of the HMTB are shown in Figure 2.11. Design parameters are defined in Nomenclatures. The rotor is generally of a specified radius. A clearance is provided in the stator-iron core so that the rotor shaft rotates freely in it. Thicknesses are provided in the inner-wall, back-wall, and outer-wall of the actuator to support the magnetic-flux flow in the stator-iron. The coil

winding is of the form of a hollow cylinder of a specified volume with an inner radius, an outer radius and a height. The permanent magnets in the case of HMTB actuator will be fixed to the inner and outer walls of the iron-core to their thickness and a length as shown in Figure 2.11. An air-gap is provided between the rotor disc and the stator to avoid any physical contact.

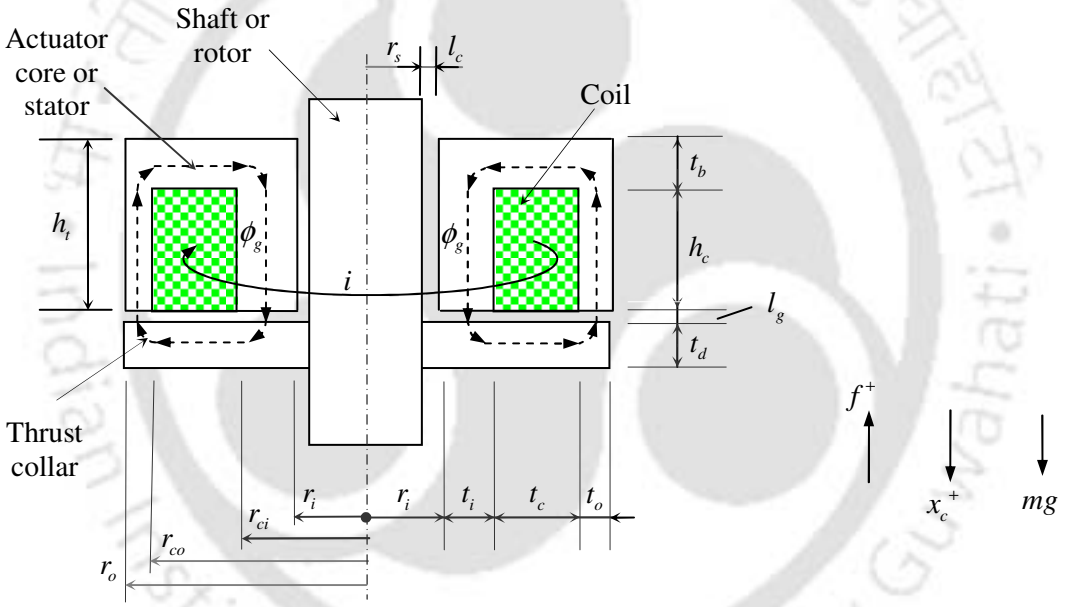

Figure 2.10 The geometry of an AMTB actuator

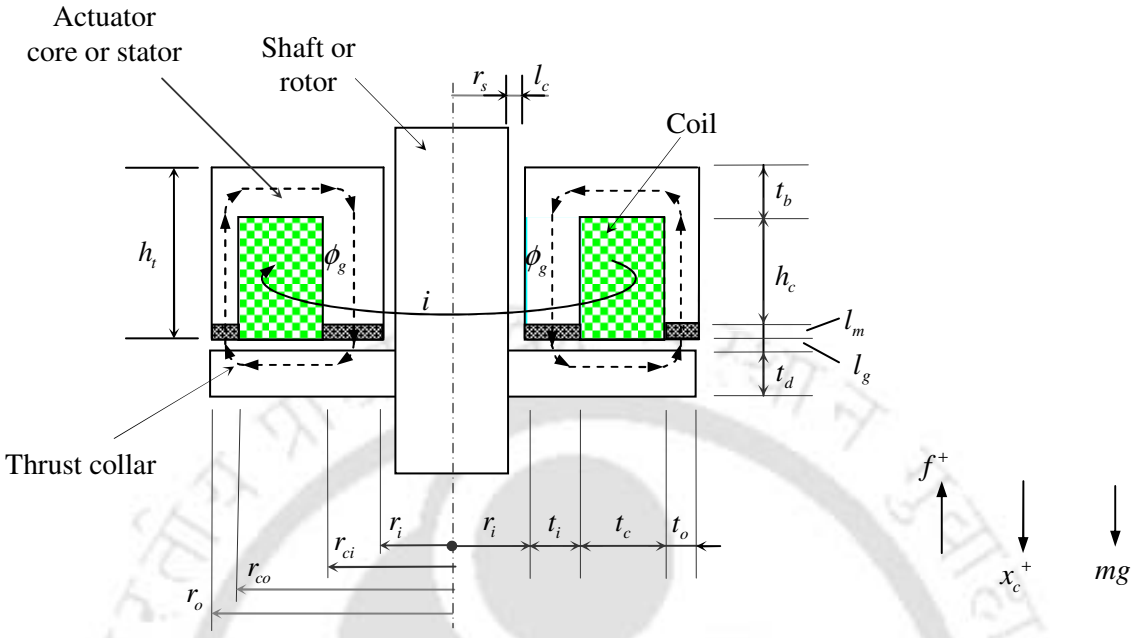

Figure 2.11 Geometries of a HMTB actuator

The radius of the shaft r_s, the clearance between the shaft and the inner radius of the magnetic bearing l_c, the inner radius of the bearing actuator r_i, the outer radius of the bearing r_o, the inner radius of the coil r_{ci}, the outer radius of the coil r_{co}, the height of the coil h_c, the thickness of the coil t_c, the inner-wall thickness of the bearing t_i, the outer-wall thickness of the bearing t_o, the back-wall thickness of the bearing t_b, the length of permanent magnet l_m, and the air-gap length l_g. From Figure 2.11, it can be observed that the inner radius of the bearing can be expressed as

$$r_i = r_s + l_c \tag{2.1}$$

From Figure 2.11, r_o and h_t are expressed as

$$r_o = r_i + t_i + t_c + t_o; \qquad h_t = l_m + h_c + t_b \tag{2.2}$$

From Figure 2.11, t_i, t_c and t_o can be expressed in terms of r_i, r_{ci}, r_{co} and r_o, as

$$t_i = r_{ci} - r_i; \qquad t_c = r_{co} - r_{ci}; \qquad t_o = r_o - r_{co} \tag{2.3}$$

where r_o and t_b are related to coil dimensions according to

$$A_g = \pi\left(r_{ci}^{\,2} - r_i^2\right) = 2\pi r_{ci} t_b = \pi\left(r_o^{\,2} - r_{co}^2\right) \tag{2.4}$$

where A_g is the pole-face area of the air-gap at poles, which is assumed to be maintained constant throughout the cross-section of the stator-iron and the collar through which magnetic-flux flows (Maslen, 2000). Different relations mainly between geometrical parameters have been presented in this section. Some fundamental relations regarding the magnetic bearing according to the magnetic-circuit theory are presented in the next section.

2.2.2 Magnetic Circuit Theory

In this section, we present the method of analysis used for magnetic bearing actuators. The analysis can be carried by using finite element methods (FEM) or by equivalent one-dimensional circuital equations analogous to electric circuits. The theory is called the magnetic circuit theory. Some of the terminology related to magnetism and magnetic circuits are introduced below.

Electro-magnet: An iron-core wound by a coil which gets magnetised due the flow of the electric current in the coil is called the *electro-magnet.*

Permanent-magnet: A magnet, whose magnetism is permanently retained, is called the *permanent-magnet*.

Magnetic field: When an electric charge in motion, it is surrounded by a distortion in its electric field called magnetic field.

Magnetic field intensity: The *magnitude or strength of the magnetic field* at any point in the vicinity of the moving electric charge is called the magnetic field intensity. It is symbolized by H.

Magnetic flux: When a magnetic material is brought into a magnetic field, the electro-dynamic relativistic effect will spread through the magnetic material, which is called the *magnetic flux,* φ.

Magnetic-flux density: The *magnetic flux* across a unit area is called as *magnetic-flux density*. It is symbolized by B. The magnetic-flux density in a material is the summation of effect of aligned dipole field in the material and the external field applied on the material.

Remnant flux: The magnetic flux retained in the material of the magnet after removal of magnetizing source is called the *remnant flux*. It is symbolized by B_r.

Magneto-motive force (*MMF*): The force which drives the spread of magnetic flux in the magnetic circuit is called the *magneto-motive force*.

Reluctance: Each material has a resistance to the spread of magnetic flux in it and this resistance is called the *reluctance* of the material.

The magnetic flux is generally three-dimensional in nature. However, the magnetic actuator analysis can be simplified by considering the magnetic-flux flow in one dimension. The one-dimensional path of magnetic-flux flow in a closed loop is called as the *magnetic circuit*. Analogous to electric circuits, magnetic actuators could be analyzed by magnetic circuits.

The magnetic circuits corresponding to an AMTB and a HMTB are shown in Figure 2.12 and Figure 2.13, respectively. Their corresponding electrical analogies have been given in Figure 2.14. Due to the electric current flow in the coil, a magnetic flux flows in the magnetic circuit. The coil winding and permanent magnets generate the magnetic flux in the magnetic circuit. Hence coil winding and permanent magnets act as sources of *magneto-motive force*. The generated magnetic flux spreads through the stator-iron core, permanent magnets, the air-gap, and the thrust-collar (or the rotor-disc) to close the magnetic flux path. The main reluctance to the spread of magnetic flux occurs in permanent magnets and the air-gap.

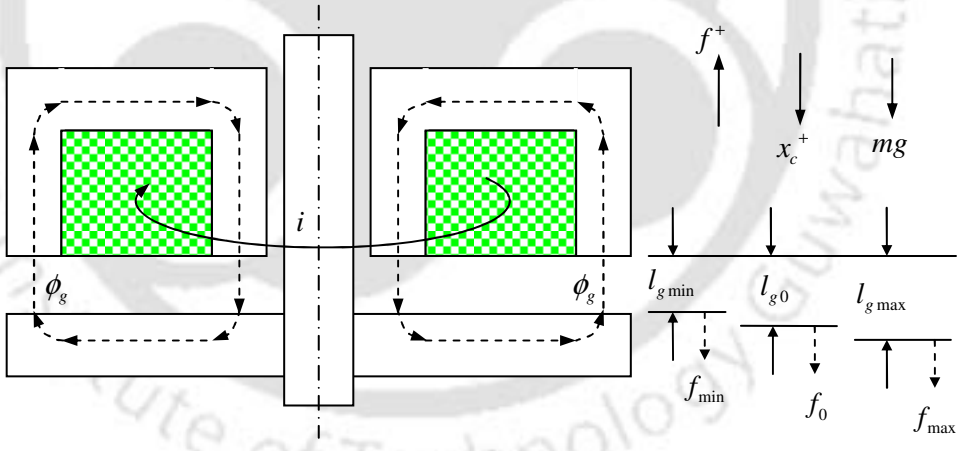

Figure 2.12 The magnetic circuit and limits of air-gap in a single acting AMTB

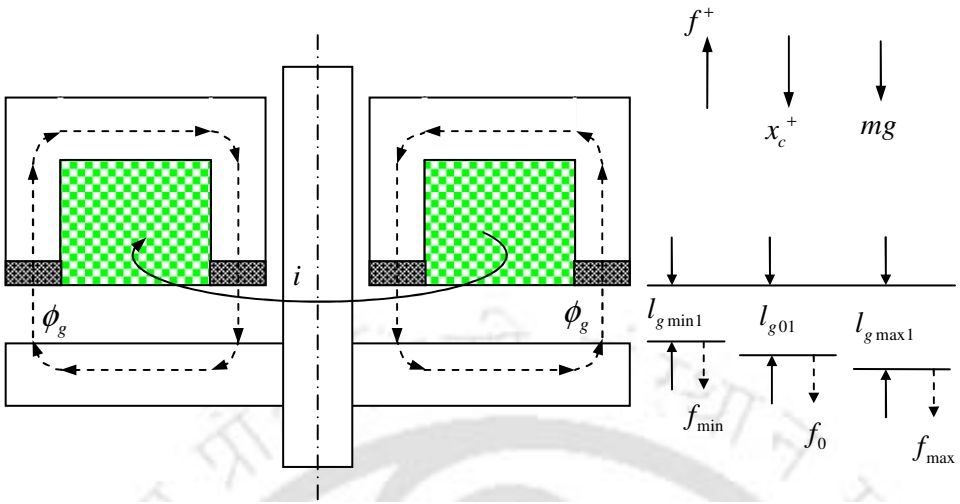

Figure 2.13 The magnetic circuit and limits of the air-gap in a single acting HMTB

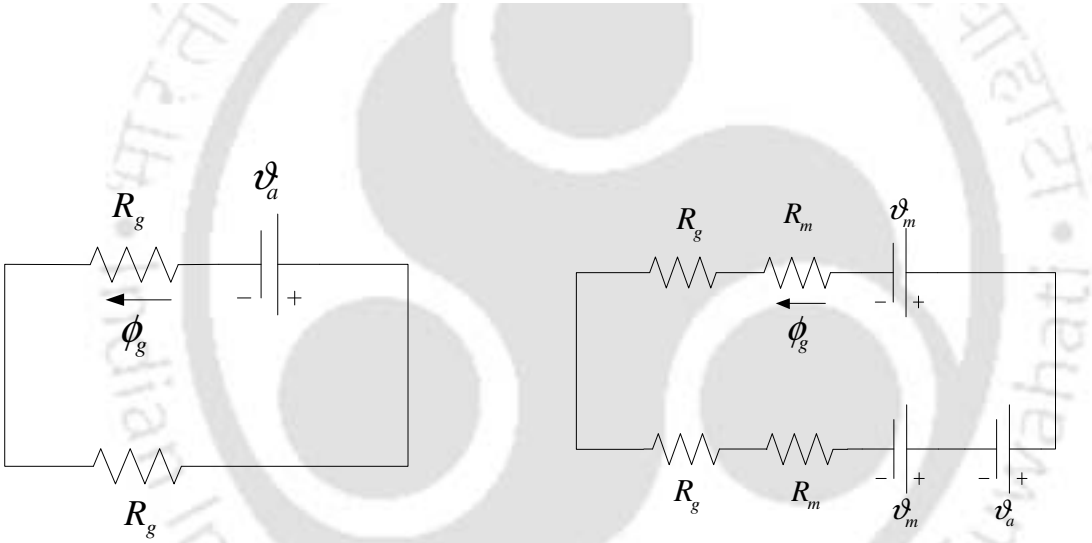

Figure 2.14 The magnetic circuit (left) AMTB configuration (right) HMTB configuration

Equation (2.4) is obtained by assuming the magnetic flux, ϕ_g, and the magnetic flux-density, B_g, flowing in the whole magnetic circuit as shown in Figure 2.13, to be constant and they are related as

$$B_g = \frac{\phi_g}{A_g} \tag{2.5}$$

From the magnetic circuit theory (Bloodgood et al., 2000), by observing Figure 2.13, the following expression can be written

$$2H_g l_g + 2H_m l_m + H_s l_s + H_d l_d = ni \tag{2.6}$$

where H is the magnetic field intensity, l is the length of path of the magnetic flux, with suffixes: g, m, s, and d representing the air-gap, the permanent-magnet, the stator-iron, and the thrust-collar, respectively; and ni is the magneto-motence. By neglecting the reluctance of the stator-iron and the thrust-collar, the flux flowing in the magnetic circuit is expressed as

$$B_g = \frac{\mu_0 \left(\vartheta_a + 2\vartheta_m\right)}{2\left(l_g + l_m\right)} \quad \text{with} \quad \vartheta_a = ni \quad \text{and} \quad \vartheta_m = B_r l_m / \mu_0 \tag{2.7}$$

where ϑ_a and ϑ_m are magneto-motenses due to the electro and permanent magnets, respectively; μ_0 is the permeability of the vacuum, and B_r is the remnant flux of bias magnets. Equation (2.7) can also be written in terms of reluctance as

$$\phi_g = \frac{\left(\vartheta_a + 2\vartheta_m\right)}{2\left(\rho_g + \rho_m\right)} \quad \text{with} \quad \rho_g = \frac{l_g}{\mu_0 A_g} \quad \text{and} \quad \rho_m = \frac{l_m}{\mu_m A_m} \tag{2.8}$$

where ρ_g and ρ_m are reluctances of the air-gap and the permanent magnet, respectively. The classical design of magnetic bearings depends on the ideal magnetic circuit theory, which deviates drastically from experiments (Maslen, 2000; Schweitzer et al., 2003; and Chiba et al., 2005). Groom and Bloodgood (2000) implemented a model by adding the loss and leakage factors to ideal models. By the application of loss factors, equation (2.7) can be rewritten as

$$B_g = \frac{\mu_0 \left(K_i \vartheta_a + 2\vartheta_m \right)}{2\left(K_a l_g + K_f l_m \right)} \tag{2.9}$$

where K_i is the coil MMF loss factor, K_a is the actuator loss factor, and K_f is the flux leakage factor. Permanent magnets are designed such that the current supplied is zero in equation (2.9). Hence, the thickness of bias magnets can be determined by using

$$l_m = \frac{K_a l_g B_g}{B_r - K_f B_g} \tag{2.10}$$

The magnetic force generated can be derived from the principle of virtual work as (Schweitzer et al., 2003)

$$F = \frac{B_g{}^2 A_g}{\mu_0} = \frac{\phi_g{}^2}{\mu_0 A_g} \qquad \text{with} \qquad \phi_g = B_g A_g \tag{2.11}$$

In magnetic bearings, the electrical energy transforms into the magnetic energy which transforms into the mechanical energy. Hence, during analysis the magnetic flux is determined from the magneto-motense using equation (2.9), and the magnetic force is determined from the magnetic flux using equation (2.11). Conversely, during the design of actuator, the magnetic-flux required is determined from the force required to be supported by using equation (2.11); and the magneto-motense required is determined from the magnetic-flux that should flow in the circuit using equation (2.9). The standard form of expression of the power-loss in the coil is given as

$$P = i^2 R \tag{2.12}$$

where P is the power-loss, i is the current flow in the coil, and R is the resistance of the coil to the current flow.

Coil winding is made of an electrically conductive material such as the copper in the form of a wire with a specified cross-section. The coil-wire is wound on a core of a given shape in terms of number of turns. The volume occupied by the coil depends upon two factors namely the shape of the coil cross-section and the winding efficiency. The shape of the coil cross-section defines a maximum volume that can be occupied by the wire in a particular space provided. The ratio of maximum volume that can be occupied by the coil-winding in a cylinder to the volume of the cylinder is called *the shape factor,* η_s. Due to gaps left between different turns, while the coil is wound, the space actually occupied by the coil will be less than the maximum volume that can be occupied. The ratio of the actual volume occupied and the maximum volume that can be occupied is called *the winding efficiency,* η_w. The ratio of the actual volume occupied by the coil-winding in a cylinder to the volume of the cylinder is called *the coil packing factor,* η. Moreover, from the definitions provided above the coil packing factor is the product of shape factor and winding efficiency. The corresponding expressions have been provided as follows

$$\text{Shape factor, } \eta_s = \frac{\text{Maximum possible volume occupied by the wire}}{\text{Cylinder volume}}$$

$$\text{Winding efficiency, } \eta_w = \frac{\text{Actual volume occupied after winding}}{\text{Maximum possible volume occupied}}$$

$$\text{Packing factor, } \eta = \frac{\text{Actual volume occupied after winding}}{\text{Cylinder volume}}$$

$$\text{Packing factor } (\eta) = \text{Shape factor } (\eta_s) \times \text{ Winding efficiency } (\eta_w)$$

The *current-density* (i.e., the flow of electric current across a unit area of the cross-section of the coil-wire) in the coil wire, J , is related as

$$J = \vartheta_a / \eta A_c \tag{2.13}$$

where J is the current-density in the coil, η is the coil packing factor, and A_c is the cross sectional area of the coil. Using equation (2.13), equation (2.12) can be rewritten as (Schweitzer et al., 2003, Groom and Bloodgood, 2000)

$$P = \rho \eta J^2 A_c l / n \tag{2.14}$$

where n is the number of turns, and l is the total length of coil. The different turns of the coil may have different lengths; however, l/n could be taken as the average length of the coil per turn.

2.3 Optimization Model for the Design of Actuators of Magnetic Bearings

The magnetic actuator optimization is one of the important issues to be carried in the design of magnetic bearings. The designer has to identify performance parameters of the system

that are important to be optimized. These performance parameters are called the objective or fitness functions.

Unconstrained optimization problem: An optimization problem consists of finding out a design vector that optimizes an objective function within a given design space without any constraints defined is called as *unconstrained optimization* problem. Depending on the number of objectives to be optimized optimization problems are classified as single and multiple objective optimization problems. In a single objective optimization problem, a single objective is considered to be optimized. If two or more objective functions are to be optimized simultaneously, then it is called as multi-objective optimization problem. General models of the single and multiple objective optimization problems have been shown in Table 2.1 and Table 2.2, respectively.

Table 2.1 A model of constrained single objective optimization problem

Minimize $f(\mathbf{x})$
where $\mathbf{x}=\{x_1, x_2,..., x_n\}$; $x_p^L \le x_p \le x_p^U$ $p=1,2,...,n$
Subject to $g_j(\mathbf{x}) \ge 0$ $j=1,2,\ldots,q$; and $h_k(\mathbf{x})=0$ $k=1,2,...,r$;

Table 2.2 A model of the constrained multi-objective optimization problem

Minimize $f_i(\mathbf{x})$ with $i=1,2,...,m$
where $\mathbf{x}=\{x_1, x_2,..., x_n\}$; $x_p^L \le x_p \le x_p^U$ $p=1,2,...,n$
Subject to $g_j(\mathbf{x}) \ge 0$ $j=1,2,\ldots,q$; and $h_k(\mathbf{x})=0$; $k=1,2,...,r$

Constrained optimization problem If there are *constraints* which are to be satisfied by the design vector in an optimization problem, it is called as *constrained optimization problem*; Constraints involved may be the equality and/or inequality types. Inequality constraints consist of mathematical operators of types of greater-than or less-than. A greater than type constraint can be transformed into a corresponding less than type by multiplying the equation with a negative sign throughout the equation. An equality constraint can be converted as two inequality constraints with small tolerance of error in satisfying the equality. An equality constraint can also be satisfied exactly by determining some dependent variables from it rather than satisfying with a tolerance.

Objective functions in MBs are those which account for the most of the cost involved in productions, installations, transportations, and stable operations. These objectives may be at times conflicting to each other and the designer has to take a decision based on priorities of the objectives or other tradeoffs of an application. The multi-objective optimization problems of the AMBs considered in the present work are constrained optimization problems involving single-objective or multi-objectives. Design variables of the problems aim to optimize the objective functions while satisfying certain constraints in the process of optimization.

The different objective functions identified for the actuator of AMB systems will be presented in following subsections. Expressions are presented of objective functions for the design of thrust magnetic bearings with bias magnets (i.e., HMTB). Expressions for the case of without biased-magnets can be obtained by eliminating terms involving parameters of bias magnets.

2.3.1 Objective functions of actuators

Different costs involved in an AMB usage are the initial (or purchasing/acquisition) cost, the carrying (or transportation) cost, the erection cost, and the running (or operating) cost. Moreover, the power-loss represents the *running cost* of an AMB, while the weight represents both the *initial* and *carrying costs* of an AMB. In the present case for the design optimization of actuators, the weight and the power-loss of the bearing have been considered at a fixed operating load. The weight of the bearing includes weights of the stator and rotor cores, coils, and permanent magnets. The power-loss includes mainly copper-losses in the coil-winding. Moreover, the power-loss is determined at the operating point (or at the stable state) of the bearing.

The initial and carrying costs of the bearing decrease with the decrease in the size of the bearing. However, the running cost of the bearing increases with the decrease in the size of the bearing, since the copper-volume reduces with the reduced bearing size, which results in more power-loss. The reduced power-loss means the reduction of running costs of the bearing, which results in the implementation of the smaller and economical power amplifiers, and reduced load on the cooling system considered.

In bio-medical applications, such as ventricular-assisted devices, used for heart patients (Wearden et al., 2006) the weight and the volume are design objectives of significant importance in addition to power requirements. In aviation applications, the weight adds also to the carrying cost in addition to issues of the space occupied, strengths and dynamic stabilities of structures. In the production machinery (such as lathes, drill mills, etc.) and the turbo-machinery, the weight of the AMB adds the load to the supporting base in addition to

fluctuating loads; hence it needs stronger foundations with greater weights. With weight densities of materials of the magnetic bearing fixed, the weight also represents the space occupied by the bearing. The running costs are of more importance in ground applications. The carrying and running costs are of more importance in the aviation and space applications. While applications, such as the space based systems and small pumps for biomedical applications, have the most to gain by reducing power requirements; other typical commercial systems could also be significantly improved.

Table 2.3 Influence of different objectives in terms of costs for various applications

Application	Objectives	
	Power-loss	Weight
Ground	Running cost; acquisition costs of controller, power amplifier, cooling system; cooling costs of the coil.	Purchasing, space occupied, foundation strength
Aviation		Purchasing, transportation, space occupied, foundation strength, dynamic stability of the structure

The contributions of individual objectives to different costs in various applications have been summarized in Table 2.3. From the above discussion both the weight and the power-loss have significant importance in both the ground and aviation applications. Thus both the power-loss and the weight get important roles in the magnetic bearing actuator design and are chosen as objective functions for the single and multi-objective optimizations. Consequently, in the present thesis an attempt is made to analyze the multi-objective design optimization of AMTBs and HMTBs with the power-loss and the weight as objectives, and their relevant expressions are briefly provided in the following subsections.

2.3.1.1 Power-loss

The power-loss in the magnetic-coil of a thrust magnetic bearing from equation (2.14) is expressed as

$$P = \rho \eta J^2 V_c \tag{2.15}$$

where V_c is the volume of the coil. From the geometry of the thrust magnetic bearing in Figure 2.10, the cross-sectional area and the volume of the coil are expressed as

$$A_c = (r_{co} - r_{ci}) h_c \quad \text{and} \quad V_c = \pi (r_{co}^{\,2} - r_{ci}^{\,2}) h_c \tag{2.16}$$

where A_c is the cross-sectional area of the magnetic-coil. By simple observations from equations (2.4) and (2.9) to (2.11), the power-loss for supporting a specified load in the present case could be concluded as a function of coil dimensions only, i.e. $[r_{ci}, r_{co}, h_c]$.

2.3.1.2 Weight of the bearing

The overall weight of the bearing, W , can be expressed as

$$W = W_c + W_s + W_m \tag{2.17}$$

where W_k represents the weight of a component of the bearing with subscripts c, s and m representing the coil, the stator-iron, and the biased (or permanent) magnet; respectively. The minimization of the weight causes the reduction in the volume of the bearing for a designed load. With reference to Figure 2.11, components of the weight of the bearing can be expressed as

$$W_c = \gamma_c \pi \left(r_{co}^2 - r_{ci}^2 \right) h_c \tag{2.18}$$

$$W_s = \gamma_s \pi \left[\left(r_{ci}^2 - r_i^2 \right) h_c + \left(r_o^2 - r_{co}^2 \right) h_c + \left(r_o^2 - r_i^2 \right) t_b \right] \tag{2.19}$$

$$W_m = \gamma_m \pi \left[\left(r_{ci}^2 - r_i^2 \right) + \left(r_o^2 - r_{co}^2 \right) \right] l_m \tag{2.20}$$

where $\gamma_k \left(k = c, s, m \right)$ is the weight density of the respective material. As materials of the magnetic bearing are selected according to their properties required, hence weight densities are specified; and final weights of components depend only on volumes. From equations (2.17) to (2.20), we can observe that the weight of the bearing is a function of the coil and stator-iron dimensions. Among the dimensions of the stator-iron, the radius of the rotor shaft and the shaft clearance are as expressed in equation (2.1), which specifies the inner radius of bearing. The outer radius and the back-wall thickness of the bearing could be expressed in terms of coil dimensions and the inner radius of the bearing according to equation (2.4). It can also be concluded from equation (2.10), that the dimensions of bias magnets can be determined in terms of coil dimensions. Hence, it can be concluded that the weight of the bearing for the present case is a function of coil dimensions only.

Different objective functions have been provided in the present section. The design vector which influences these objective functions will be provided in the next subsection.

2.3.2 The design vector of Actuators

In summary, from Subsections 2.3.1.1 and 2.3.1.2, it is concluded that both the power-loss in the coil and the weight of the bearing could be related as functions of coil dimensions. By simple observations from equations (2.4) and (2.9)-(2.11), the power-loss for supporting a

specified load has been concluded as a function of coil dimensions only, i.e., $[r_{ci}, r_{co}, h_c]$. Similarly, from equations (2.4), (2.10), and (2.17) to (2.20), it has been concluded that the weight of the bearing is a function of coil dimensions only. Moreover, it has been concluded from equations (2.4) and (2.10), that other dimensions of the stator-iron and biased-magnets could be determined in terms of coil dimensions. Hence, the design vector for the present optimization problem is chosen as $[r_{ci}, r_{co}, h_c]$, and dependent parameters are $[r_o, t_b, l_m]$.

2.3.3 Design constraints of Actuators

Main operating requirements and practical limitations, which serve as constraints for the optimization problem, are explained in this section. The load to be supported by the bearing is a main operating requirement. Any sets of values chosen for design parameters might not provide the required load. Providing a constraint based on the load to be supported eliminates these sets of design variables. The coil can sustain a limited maximum current-density, since the resistance offered by the coil generates the heat, which might even cause burn out of the insulation of the coil. Using proper cooling system, it could increase the allowable current-density, which forms the second constraint. The magnetic flux-density that flows in the stator-iron core is also limited. Beyond this there won't be any response of the actuator and it is called the saturation magnetic flux-density, which forms the third constraint. The space available for the bearing is limited and is specified in terms of maximum limits of design variables, which forms the rest of constraints. These constraints need to be taken into consideration while designing thrust magnetic bearings and are now described in more detail.

2.3.3.1 Load to be supported

The actuator of the magnetic bearing should be able to support the specified operating load. The permanent magnet is designed according to equation (2.10) by making the current flow in the actuator to be equal to zero at the minimum air-gap, which is called *the permanent magnet design point*. The force exerted by the permanent-magnet decreases with the increase in the air-gap, and vice-versa. The maximum current flow in the coil is at the maximum air-gap and the minimum (zero) current is at the minimum air-gap. The maximum and minimum forces exerted by the bearing, respectively $F_{\max}$ and $F_{\min}$, are specified a priori and are expressed as constraints by equation (2.11) as

$$\frac{\mu_0 A_g}{4}\left(\frac{K_i \vartheta_{a\max} + 2\vartheta_m}{K_a l_{g\max} + K_f l_m}\right)^2 = F_{\max} \quad \text{and} \quad \frac{\mu_0 A_g}{4}\left(\frac{K_i \vartheta_{a\min} + 2\vartheta_m}{K_a l_{g\min} + K_f l_m}\right)^2 = F_{\min} \qquad (2.21)$$

where $\vartheta_{a\max}$ and $\vartheta_{a\min}$ are, respectively, the maximum and minimum magneto-motenses due to electro-magnets; $l_{g\max}(=l_{g0}+x_{\max})$ is the maximum gap allowed, $l_{g\min}(=l_{g0}-x_{\max})$ is the minimum gap allowed, and $x_{\max}$ is the maximum displacement of the rotor that is allowed from the operating position and that can be expressed as a percentage of the operating gap l_{g0}.

The load to be supported influences the magneto-motense and the magnetic flux-density according to equations (2.9) and (2.11) for a particular area of the air-gap at poles. The thickness of permanent magnets can be determined from equation (2.10). The magneto motense due to permanent magnets can be determined from equation (2.7). Hence, the

maximum and minimum magneto-motenses due to electro-magnets, $ni_{\max}$ and $ni_{\min}$ could be determined, respectively, using equation (2.21). From equation (2.4), the area of the air-gap at poles depends on the inner radii of the bearing and the coil. The inner radius of bearing is specified and hence the inner radius of coil influences the area of air-gap at poles. As the magneto-motense influences the current-density corresponding to the cross-sectional area of coil, the outer radius of the coil, and the height of the coil are influenced.

2.3.3.2 Current density supplied in the coil

For a particular temperature the coil material can sustain a maximum current density that is called *the saturation current* density. Below a particular temperature, the coil material acts as a super-conductor that can carry large amounts of currents without restriction. From equation (2.21), the maximum and minimum magneto-motenses required can be found. Then current-densities that are required to be supplied in the coil can be determined as (Schweitzer, et al., 2003)

$$ni_{\max} = \eta J_{\max} A_c \quad \text{and} \quad ni_{\min} = \eta J_{\min} A_c \tag{2.22}$$

where $J_{\max}$ and $J_{\min}$ are the maximum and minimum current densities to be supplied in the coil, respectively. From equations (2.21) and (2.22), we get

$$J_{\max,\min} = \sqrt{\frac{4F_{\max,\min}}{\mu_0 A_g}\left(\frac{K_a l_{g\max,\min} + K_f l_m}{K_i \eta A_c}\right)} - \frac{2B_r l_m}{\mu_0 K_i \eta A_c} \tag{2.23}$$

Hence, the constraint becomes

$$J_{sat} \geq J_{\max} \quad \text{and} \quad J_{\min} \geq 0 \tag{2.24}$$

where J_{sat} is *the saturation current-density* that the coil can sustain at the operating temperature.

From equation (2.15), it can be observed that this constraint directly influences the maximum power-loss that can be allowed. From equation (2.15) for a fixed power-loss, as the volume of the coil increases the required current-density decreases. Thus, by choosing maximum possible volume for the coil, equation (2.24) can be satisfied. From equation (2.22), it can be observed that $J_{\max}$ is influenced by A_c, which is turn depends upon the inner and outer radii of the coil and the height of the coil. As explained in Section 3.2.1, the area of air-gap at poles specifies the inner radius of the coil; hence the coil current-density influences the outer radius of the coil and the height of the coil in the design vector.

2.3.3.3 Magnetic flux-density in the stator-iron

The flux-density in the stator-iron should not be more than *the saturation flux-density*, B_{sat}, beyond this the actuator will not respond to the increase in current. From equation (2.11), the maximum and minimum flux densities that are required to support the maximum and minimum loads, respectively; are expressed as

$$B = \sqrt{\frac{\mu_0 F}{A_g}} \quad \text{and} \quad B_{\max,\min} = \sqrt{\frac{\mu_0 F_{\max,\min}}{A_g}} \tag{2.25}$$

From equation (2.25), it can be observed that for a fixed maximum force, as the area of air-gap increases, the maximum flux-density required in the stator-iron reduces. But as the space available is finite, the area of air-gap cannot be increased indefinitely.

From equations (2.9) and (2.22), it can be observed that the stator magnetic flux-density is proportional to the coil current-density supplied and vice versa. As the stator magnetic flux-density is inversely proportional to the pole-face area of the air-gap, we can conclude that the pole-face area of the air-gap also has an effect on the power-loss. According to equation (2.9), when the optimization is only for the minimization of power-loss, the magnetic flux-density won't be at the maximum possible. Hence, it does not take the minimum possible the pole-face area of the air-gap. However, while minimizing for the weight, the magnetic flux-density would be at the maximum possible value as it takes the minimum pole-face area of the air-gap at poles, which reduces the weight.

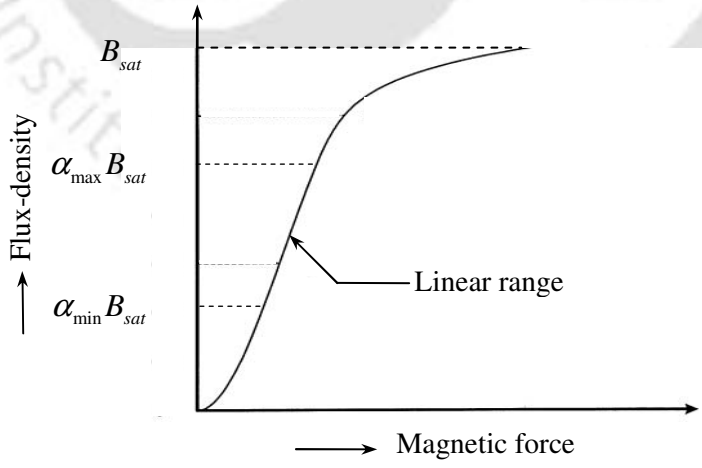

Figure 2.15 A magnetization curve with a linear range

For a linear range of operation (Kim et al., 2002), the actuator can be designed to have the flux-density between two limits. In the present work, a factor named as *the iron*

saturation factor, α, is used to express the linear range as a percentage of the saturation flux. Limits of the linear range are shown in Figure 2.15, and it is assumed that the magnetic hysteresis of the stator-iron is negligible while setting the linear range. According to equation (2.9), the linear range limits, can be expressed as

$$\alpha_{\max} B_{sat} \geq \frac{\mu_0 \left(K_i \vartheta_{a\max} + 2\vartheta_m \right)}{2\left(K_a l_{g\max} + K_f l_m \right)} \quad \text{and} \quad \frac{\mu_0 \left(K_i \vartheta_{a\min} + 2\vartheta_m \right)}{2\left(K_a l_{g\min} + K_f l_m \right)} \geq \alpha_{\min} B_{sat} \tag{2.26}$$

Though equations (2.21) and (2.24) are satisfied, equation (2.26) constrains the choice of $\vartheta_{a\max}$ and l_m. The choice of $\vartheta_{a\max}$ influences the cross sectional area of the coil. It in turn influences the selection of the thickness and height of the coil. As the thickness of coil increases, the available thickness of the iron-core decreases, this in turn increases the flux-density for supporting a fixed load. Thus equation (2.26) influences the choice of design parameters, i.e., the inner-radius of the coil and the outer-radius of the coil.

2.3.3.4 Maximum power-loss allowed in the coil

The insulation of the coil can sustain only a finite temperature, which is called *the critical operating temperature of the coil*, and beyond this temperature the coil will be damaged. The maximum power-loss, $P_{\max}$, that can be allowed is specified by the capacity of the cooling system being used. The maximum power-loss allowed is expressed from the steady-state heat transfer equation (Schweitzer et al., 2003) as

$$P_{\max} = \Lambda (T_{cr} - T_{\infty}) \tag{2.27}$$

where Λ is the coefficient of thermal conduction, T_{cr} is the critical operating temperature of the bearing, and T_{∞} is the temperature of the cooling medium. From equation (2.27), it can be observed that the capacity of the cooling system could be increased in two ways; first by increasing the critical operating temperature of bearing which depends on the coil insulation material, and second by decreasing the temperature of the cooling medium. For a fixed cooling system, the increase in the power-loss would result in the increase of the operating temperature. If the power-loss is high, the operating temperature would be increased beyond the critical temperature. Hence, the temperature of the cooling medium should be reduced to increase the capacity of the cooling system without altering the critical operating temperature of the coil. For every operating temperature of the coil, the saturation current density of coil material is specified. Hence, by rearranging equation (2.15), the maximum volume of the coil that is available can be determined as

$$V_{\max} = \frac{P_{\max}}{\rho \eta J_{sat}^2} \tag{2.28}$$

The constraint can be expressed as

$$V_{\max} \geq \pi \left(r_{co}^{\ 2} - r_{ci}^{\ 2} \right) h_c \tag{2.29}$$

where $V_{\max}$ is the maximum allowable volume of the coil. For a fixed load to be supported, the volume of the coil depends on the power-loss that is allowable, and the saturation current-density as expressed by equation (2.28). For each set of design variables selected, the magnetic bearing has a maximum load that can be supported at the coil saturation current-density; however, for a specified load the coil current-density might not be saturated

for all the designs. Hence, it is better to use the maximum allowable power-loss as constraint instead of the maximum allowable volume of the coil. This gives a constraint, as

$$P_{\max} \geq P \tag{2.30}$$

The advantage of using equation (2.30) as constraint over equation (2.29) is that the coil is freely allowed to take a volume within the available space that minimizes the power-loss or the weight. The volume of the coil influences the outer radius of coil and the height of the coil in the design vector.

2.3.3.5 Space available for the bearing

In many applications, the space available for the bearing is limited. The space available for the whole bearing can be specified by the maximum outer diameter, r_{oub}; and the maximum height, h_{tub}, available. The corresponding constraints can be expressed as

$$r_{oub} \geq r_o \quad \text{and} \quad h_{tub} \geq l_m + t_b + h_c \tag{2.31}$$

The trade-offs among objective functions are optimised within the space available for the bearing. By specifying the volume available for the bearing, it is possible to take any dimensions of the stator and the coil within the available volume of the bearing that minimize the overall weight of the bearing and/or the power-loss. Since the back-wall thickness of the bearing is specified by the pole-face area of the air-gap, hence, the upper bound of height of the bearing constrains the maximum available height of the coil. The

upper bound of outer radius of the bearing constrains the inner and outer radii of coil that can be attained at most.

In summary, equations (2.24), (2.26), (2.29), (2.30) and (2.31) are inequality constraints, while equation (2.21) is an equality constraint. For a given h_{tub}, by satisfying constraints mentioned in equations (2.21) and (2.23), a minimum r_{oub} below which there will not be a feasible solution that can be determined, and the specified r_{oub} should be more than this value so that the optimization of the bearing geometry can be performed.

Table 2.4 The multi-objective optimization formulation of the magnetic thrust bearing

Minimize $f_1(\mathbf{x}) = P$
$f_2(\mathbf{x}) = W$
where $\mathbf{x} = \{r_{ci}, r_{co}, h_c\}$; $x_p^L \le x_p \le x_p^U$ $p = 1,2,3$
Subject to $g_j(\mathbf{x}) \ge 0$ $j = 1,2,\ldots,8$; and $h_k(\mathbf{x}) = 0$ $k = 1,2$

Table 2.5 Objective functions and constraints for the magnetic thrust bearing

Objective	Equation	Constraint	Equation	Constraint	Equation
$f_1(\mathbf{x}) = P$	(2.15)	$g_1(\mathbf{x}) = J_{\text{sat}} - \max\left(J_{\max}^{ub}, J_{\max}^{lb}\right)$	(2.24)	$g_6(\mathbf{x}) = r_{oub} - \max\left(r_o^{ub}, r_o^{lb}\right)$	(2.31)
$f_2(\mathbf{x}) = W$	(2.17)	$g_2(\mathbf{x}) = \min\left(J_{\min}^{ub}, J_{\min}^{lb}\right)$	(2.24)	$g_7(\mathbf{x}) = h_{tub} - \max\left(h_t^{ub}, h_t^{lb}\right)$	(2.31)
		$g_3(\mathbf{x}) = \alpha_{\max} B_{\text{sat}} - \max\left(B_{\max}^{ub}, B_{\max}^{lb}\right)$	(2.26)	$h_1(\mathbf{x}) = F_{\max} - F\left(l_{g\max}, i_{\max}\right)$	(2.21)
		$g_4(\mathbf{x}) = \min\left(B_{\min}^{ub}, B_{\min}^{lb}\right) - \alpha_{\min} B_{\text{sat}}$	(2.26)	$h_2(\mathbf{x}) = F_{\min} - F\left(l_{g\min}, i_{\min}\right)$	(2.21)
		$g_5(\mathbf{x}) = P_{\max} - \max\left(P_{\max}^{lb}, P_{\max}^{ub}\right)$	(2.30)		

The multi-objective optimization problem is summarized in Table 2.4 and the corresponding objective functions and constraints are summarized in Table 2.5. If the individual objectives are used one at a time in Table 2.4, the multi-objective optimization problem will be converted to two single-objective optimization problems. The influence of

different input, design and dependent parameters on objectives and constraints will be discussed in the next section.

2.3.4 Influence of different parameters on objectives and constraints

There are three different categories of parameters involved in the design of a system, namely the input, design, and dependant parameters. Apart from these parameters there are objective functions and constraint violations to be determined. The flow of information of calculations of different parameters, objectives and constraints involved in the optimum design of a system are shown Figure 2.16.

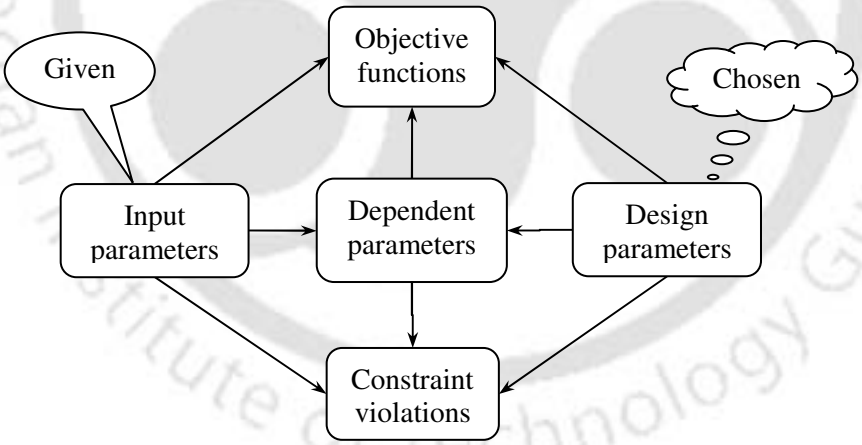

Figure 2.16 The flow of information for the optimization

The input parameters are given for the system and design parameters can be chosen any value within the design search space provided. Dependent parameters will be determined from the input and design parameter values. While objective functions and constraint violations will be determined from the input and design parameters, they may also require

the information of dependent parameters. Moreover, dependent parameters are useful in analyzing the system properties with respect to different objectives. The influence of different parameters is studied while optimization problem formulation in Section 2.3.

Table 2.6 The influence of different constraints on different design parameters

Constraint	Design parameters*					Constraint	Design parameters				
	r_{ci}	r_{co}	h_c	t_b	r_o		r_{ci}	r_{co}	h_c	t_b	r_o
Load to be supported	✓	✓	✓	✓	✓	Maximum power-loss allowed	×	✓	✓	×	×
Magnetic flux-density	✓	×	×	✓	✓	Available volume of the coil	×	✓	✓	×	×
Current-density	×	✓	✓	×	×	Available space of the bearing	✓	✓	✓	✓	✓

* ✓ → Influences; × → Does not influence;

Table 2.7 The influence of the design and input variables on various objective functions

Parameters		*Dependant parameters*			*Objective functions*		*Constraint violations*					
		l_m	r_o	h_t	W	P	$F_{\max}$	$B_{\max}$	$J_{\max}$	T_{cr}	$r_{o\max}$	$h_{t\max}$
Input	r_i	×	✓	×	✓	×	×	×	×	×	✓	×
	l_g	✓	✓	✓	✓	✓	✓	×	×	×	✓	✓
	F	✓	✓	✓	✓	✓	✓	✓	✓	✓	✓	✓
	B_r	✓	×	✓	✓	×	×	✓	×	×	×	✓
Design	r_{ci}	✓	✓	✓	✓	✓	✓	✓	✓	✓	✓	×
	r_{co}	×	✓	×	✓	✓	✓	×	✓	✓	✓	×
	h_c	×	×	✓	✓	✓	✓	×	✓	✓	×	✓
Dependant	l_m	–	×	✓	✓	×	✓	✓	×	×	×	✓
	r_o	×	–	×	✓	✓	✓	✓	✓	✓	✓	✓
	h_t	✓	×	–	✓	✓	✓	✓	✓	✓	✓	✓

* ✓ → Influences; × → Does not influence; – →Not applicable

Based on the discussions of Section 2.3, the inter-dependency of different constraints on design parameters has been summarized in Table 2.6. The influence of different input, design and dependant parameters on the different objectives and constraints have been presented in Table 2.7.

2.4 Conclusion

In this chapter, the general challenges involved in the design of magnetic bearings have been discussed. The objectives of the optimization and the importance of design optimization of magnetic bearing actuators have been discussed. Geometries of actuators of AMTB and HMTB have been described. Geometrical relations of actuators have been provided. The magnetic circuit and corresponding relations have been explained. Expressions for the single and multiple objective optimization problems for magnetic actuators have been provided. Objective functions, the design vector, and design constraints have been described and presented. Relations of different variables, objectives and constraints have been presented. In the next chapter, the information on optimization tools used for optimization processes will be provided.

Chapter 3
Single- and Multi-Objective Genetic Algorithms

3.1 Introduction

The design optimization tool is one of the key elements in achieving a desired solution of the problem. The choice of optimization tool depends on many factors such nature of the objective function(s), simplicity of implementation, reliability of the solutions obtained by a tool, ability to find a global optimum, etc.

In the last chapter, the design optimization problem for the actuator of magnetic bearings has been detailed. Geometrical relations and electromagnetic relations have been established. Different requirements of magnetic bearing design and objectives of optimization have been discussed. The single and multi objective optimization problem for magnetic thrust actuators has been detailed including objective functions, design vector and

corresponding constraints. In the present chapter, different tools available for optimization including the deterministic and stochastic methods will be discussed. Genetic algorithms (GAs) as the choice of optimization tool for solving the present problem will be discussed. The process of genetic algorithm will be explained with a flow chart. Some of the basic aspects of genetic algorithms implemented in the present work including evaluation, selection, crossover, mutation, etc. and the corresponding operators implemented will be described. Finally, some of the key issues of convergence of GA will be discussed.

3.2 The Choice of the optimization tool

There are two spaces while dealing with optimization, namely the design space and the objective space. Based on the number of dimensions (i.e., design variables) in the design-space, it is classified as *the one-dimensional or the multi-dimensional* optimization. This classification also termed as *single variable* or *multi-variable* optimization. Based on the number of objectives in the objective space, it is classified as *the single-objective or the multi-objective* (Rao, 1996). There are two kinds of optima, namely the minimum and the maximum of the objective function. The minimum of a function $f(\mathbf{a})$ can be written as the maximum of $[-f(\mathbf{a})]$. Based on the vicinity considered around a point in the design space, the optimum can be classified as the *local or global optimum*. There are basically two kinds of optimization tools available, namely the deterministic and the stochastic that is based on the number of solutions used in the method. In deterministic methods again there are gradient based methods and non-gradient based methods. Whereas, in stochastic methods there are two broad classes namely, local search and population based search stochastic methods (Onwubolu and Babu, 2004). These are described in more detail subsequently.

3.2.1 Deterministic optimization methods

There are enumerable literatures available for deterministic optimization and their applications in book form (Rao, 1996; Deb, 1995; Taha, 2005; and Ravindran et al., 2006). There are necessary and sufficient conditions that must be satisfied for a solution point to be either the maximum, or the minimum or the point of inflection. The necessary condition is that the first derivative at that solution point must be zero, which decides that the point is a stationary point. But the first derivative does not indicate the exact status of the point, whether it is a maximum or a minimum. The condition that conveys the exact status of the solution point is called the sufficient condition. The sufficient condition will be decided by the least non-zero n^{th} derivative with all other lower-order derivatives to be zero at that solution point. If the least non-zero n^{th} derivative (n is even) is greater than zero, the solution point is minimum, if it is less than zero the solution point is maximum, and if n is odd then it is neither a minimum nor a maximum and this point is called as the point of inflection. Figure 3.1 shows different points on a curve representing an objective function. In Figure 3.1, point A is a local maximum, point B is a global minimum, point C is a global maximum, point D is a local minimum and point E is a point of inflection.

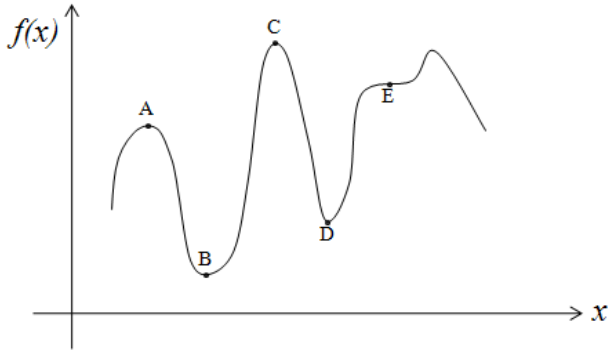

Figure 3.1 Different stationary points

One-dimensional methods such as bisection, golden section, and secant methods (Deb, 1995) do not need gradient information. The steepest descent method searches for the best direction. The Newton's method requires the information of the zero, first and second derivatives of the objective function at all points in the design space. Secant method follows an approximate of Newton's method without the use of second derivatives hence it is a quasi-Newton method.

In the multi-dimensional design space, there are many kinds of optimization problems occur. The different problems include

- Based on the nature of the problem they are classified as linear programming problems, quadratic programming problems, and non-linear problems
- Based on the constraints on the design space they are classified as unconstrained optimization, constrained optimization problems with equality constraints, and constrained optimization problems with both equality and inequality constraints.

Different combinations of problems can be arrived at from the two classes mentioned above. Some of the solution methods are given in the following paragraphs.

Linear programming problems with linear constraints can be solved by the Simplex method. Among multi-dimensional unconstrained methods the Newton's method is used. The necessary condition for the Newton's method is the gradient vector of the objective function with respect to the design vector must be zero. The sufficient condition is that the Hessian-matrix must be positive definite for the minimum, and negative definite for the maximum. If all Eigen values of a matrix are positive then it is called the positive definite.

If all Eigen values are negative then it is called the negative definite. If some of Eigen values are positive and some are negative then it is called the indefinite.

For unconstrained nonlinear multi-dimensional problems the Newton and Quasi-Newton methods are used. The quasi-Newton method is a generalization of secant method for nonlinear unconstrained multi-dimensional problems. The Newton method requires the determination of inverse of Hessian matrix. The computation of inverse of Hessian is very difficult in many cases. Consequently, quasi-Newton methods which are also known as variable-metric methods, have been developed in which the inverse of Hessian matrix is updated with an approximation (Davidon, 1959). Quasi-Newton methods use the advantage of the Newton's method while eliminating the computation of the Hessian matrix and/or its inverse. Two of the popular methods are DFP (Davidon-Fletcher-Powell) and BFGS (Broyden-Fletcher-Goldfarb-Shanno) methods (Rao, 1996). Broyden's method uses a combination of BFGS and DFP update (Wei et al., 2006).

For constrained nonlinear multi-dimensional problems with equality constraints the Lagrange multiplier technique is used. A general objective function called the Lagrange-function is defined with each equality constraint multiplied with a corresponding weighting variable called the *Lagrange-multiplier* and added to the objective function. Now a generalized design vector is defined for the Lagrange function which includes the design vector of the objective function and the Lagrange-multiplier vector. Similar necessary and sufficient conditions as of the Newton's method are applied to solve the problem. For inequality constraints in nonlinear multi-dimensional problems, Karush-Kuhn-Tucker (KKT) conditions (Kuhn and Tucker, 1951) are applied for the generalized Lagrange function.

A sequential quadratic programming method is an iterative method. It assumes that the nonlinear objective behaves as a quadratic function and the constraints are linearized in the vicinity of any solution point. This is one of the popular methods for solving nonlinear problems with equality and inequality constraints. A quadratic program allows the objective to be quadratic and constraints to be a linear. Hence, any nonlinear problem with nonlinear constraints can be reduced to a quadratic sub-problem within the vicinity of a point. The next update of the solution is found based on the solution obtained by a quadratic sub-problem. Hence, this is called the sequential quadratic programming method (Gruver and Sachs, 1980).

However, gradient based methods have a higher probability of landing on local optima. In the above mentioned deterministic methods one needs to find the next update of the solution with a Hessian matrix update. Moreover, the matrices are to be positive definite, and they do not always give a guarantee of convergence. It depends on the initial solution assumed, and one has to try number of trials to get the right initial solution to be assumed. To avoid the above mentioned drawbacks of deterministic methods, the stochastic algorithms have been developed. The following sub-section gives introduction to stochastic optimization methods.

3.2.2 Stochastic optimization methods

Onwubolu and Babu (2004) classifies the stochastic methods into two broad categories namely, the local search and populaton based search methods. In local search methods a current solution is maintained and its neighbouring space is explored for better solutions. In population based methods a population of solutions is maintained and its members are

reproduced for better solution by recombination and/or mutations. Some of the stochastic local search methods are Stochastic Hill Climbing (HC), Tabu Search (TS), and Simulated Annealing (SA) (Deb, 2001). Some of the population based methods are Genetic Algorithms (GA) (Goldberg, 1989), Evolution Strategies (ES) (Deb, 2001), Differential Evolution (DE) (Storn and Price, 1995), Particle Swarm Optimisation (PSO) (Kennedy and Eberhart, 1995), Ant Colony Optimization (ACO) (Dorigo, 1992), and Artificial Bee Colony approach (ABC) (Karaboga, 2005), etc. In the present study, genetic algorithms have been applied and are described in following subsections.

3.2.3 Genetic algorithms as the optimization tool

For the optimization problem formulated in the previous chapter, we have two objectives with three design variables and ten constraints. The present problem is a multi-dimensional in the design-space, and single-objective and multi-objective in the objective-space. The single-objective is considered in the present chapter and multi-objective problems are attempted in subsequent chapters. Moreover, it is a constrained optimization problem. Objective functions (i.e., weight of the bearing and power-loss in the coil winding) and constraints are also nonlinear functions of design variables. Hence, derivatives of objectives and constraints with respect to design variables are not easy to find.

Due to complexities involved in the optimization problem mentioned in the above paragraph, obtaining a closed form formula for the solution is very difficult; and one has to opt for a numerical optimization. Population (stochastic) based methods such as genetic algorithms have proven to land on the global optimum within the provided search space with a higher probability in contrast to classical gradient (deterministic) based methods.

Though there are different stochastic optimization tools available some are under development stage and some are in advanced stage. Genetic algorithms have been developed to a fairly advanced level and are implemented in the present problem of the design optimization of magnetic-thrust bearings in the component as well in the system level. The component design optimization of actuators of MTBs has been presented in Chapters 3 to 6. Whereas, the system level optimization is dealt in Chapters 7 and 8.

Different procedures and operators involved in GAs have been briefly described in the following section.

3.3 Details of Genetic Algorithms Implemented

GAs involve the population initialization, the calculation of fitness and constraints, the crossover and the mutation for generating the child population, the ranking of individuals, and the selection of population for the next generation. The flowchart of a typical algorithm implemented in the present work has been provided in Figure 3.2.

In this section, the different terminology is defined followed by the general description of GA. The detailed explanation of the different operations involved in the GA namely, population initialization, evaluation, assigning fitness, and sorting, will be given. Then follows the details of reproduction operations namely the selection, crossover, mutation. The key issues of convergence and decision making are discussed at the end.

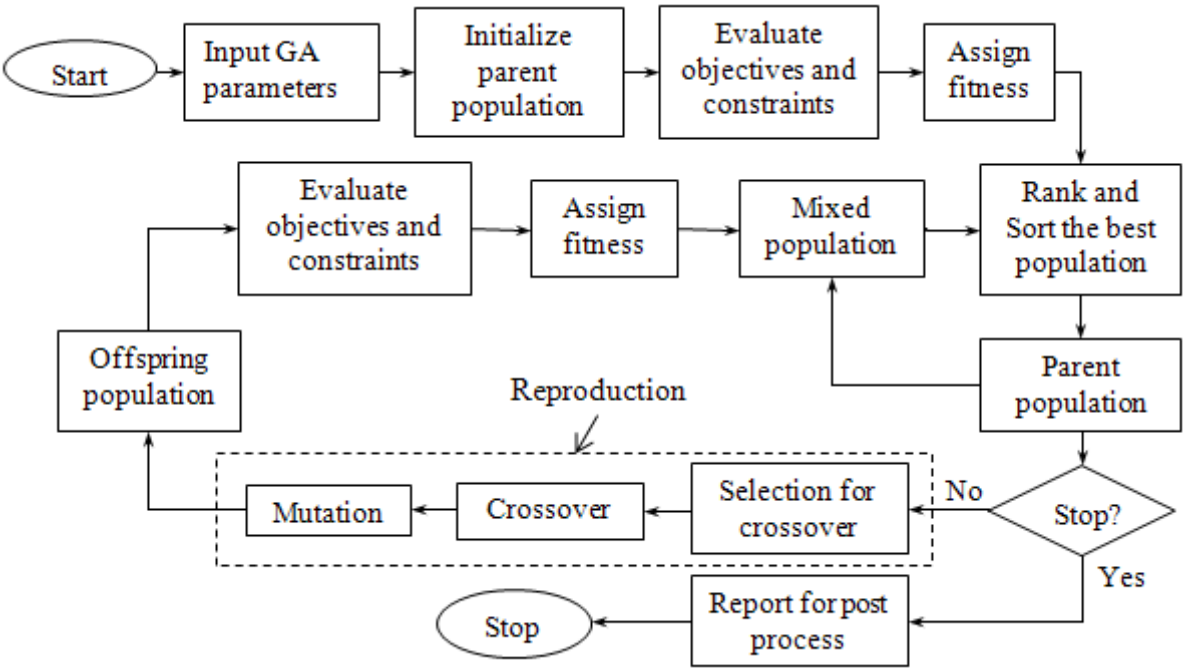

Figure 3.2 A flowchart of a genetic algorithm implimented in the present work

The different terminology involved in the implementation of GA are given as follows

Chromosome: The design vector or a solution is represented in a binary-coded form or a real-coded form or a combination and that is called as *chromosome*.

Binary code: A chromosome has design variables of different nature (real, integer, Boolean, etc) and can be represented as a string of 'zeros' and 'ones' with a specified length depending on the accuracy needed and this process is called the *binary coding*. Real numbers can be binary-coded to a specified accuracy while the integer and Boolean numbers can be binary-coded exactly. Logical operators can also be given proper integer values and can be binary-coded exactly.

Real code: If real-values are directly used in operations of GA then it is called as a *real-coded* form.

Individual: A design vector or a solution (i.e., the chromosome) along with corresponding values of objectives, constraints, fitness, rank, etc is called as an *individual*.

Random number generator: An algorithm which generates a series of random numbers, corresponding to an initial random number given, is called as *random number generator*.

Seed: To have consistent results, a specific series of random numbers are to be generated from the beginning to the end of the run of a computer programme, the random number generator is provided with an initial random number and it is called the *seed*.

Population: A group of solutions of design vector and corresponding evaluated objectives and constraints, fitness, rank, etc called as *population*.

Initial population: The population used in the initial iteration is called the *initial population*. Chromosomes of the *initial population* are generated by the use of a random generator.

Final population: The population captured, at the end of the prescribed number of generations or when other convergence criteria are met, is called the *final population*.

Parent population: The population, on which the crossover and mutation operations are carried successively, is called as the *parent population*.

Offspring population: The population resulted after the crossover and mutation operations are carried on the parent population, is called as the *offspring or child population*.

Mixed population: The union of parent and offspring populations is called as the *mixed population*.

Fitness value of an individual: A value assigned to the individual based on the corresponding values of objective functions and constraint violations is called as the *fitness value* of that individual

Dominance: The relative position of an individual between two individuals based on their fitness values is called as the *dominance*.

Dominance Rank: The number of individuals in a population that an individual dominate is called its *dominance rank*.

Dominance count: The number of individuals of a population that dominate an individual is called as *dominance count*. It can be observed that the dominance rank and dominance count are opposite values of dominance corresponding to an individual. For an individual the sum of the dominance rank and dominance count equals to the size of the population.

Dominance depth: Based on objective values and constraint violations the different individuals of a population can be classified into different groups called a front. The distance of the front from a reference worst or best point is called as the *dominance depth*.

Sorting of a population: The process of arranging individuals of a population in a sequence based on a criterion is called the *sorting*. In GA the sorting criterion may be the dominance rank, or the dominance count or the dominance depth or their combination.

3.3.1 The general description of GA procedure

The working principle of a GA is outlined in a flowchart as given in Figure 3.2. In the GA procedure initially different input parameters are given such as the seed, population sizes for

the parent population, the child population, and the mixed population. Then the parent population is initialized in the first generation. Objective functions and constraint violations of individuals of the population are calculated. Fitness values are assigned and the sorting of the population is carried based on the rank of the individuals in the population. Now there will be a criterion used to check whether the algorithm is to be terminated such as maximum number of generations, convergence of the population such as the mean and the standard deviation of the population fitness.

Once the convergence criterion is not met then the algorithm goes for the reproduction where the parent population is copied to a temporary population which undergoes three basic operations to form the offspring population. First the different individuals are formed as groups to undergo the crossover. After the crossover operation the offspring individuals are formed. Then the offspring individuals after the crossover undergo the mutation operator. All the offspring individuals that undergo the mutation operator form the offspring population.

Then individuals of offspring population are assigned fitness, and a mixed population is formed using the parent and offspring population. The mixed population is then ranked and sorted for the best population. This completes one generation. This cycle of reproduction of offspring from the parent population and extracting the best population from the mixed populations are repeated until the convergence criterion is met. Once the convergence criterion is met the parent population is reported for the post-processing of results before stopping the algorithm.

The details of different operations involved in GAs are explained in following subsections.

3.3.2 Chromosome (Representation of a solution)

The chromosome is the representation of a solution of design variables. For a binary-coded form a length of string is provided. The integer and Boolean variables are represented exactly while real-coded variables need to be provided with a tolerance of accuracy. The total string length of all the variables represents the chromosome. However, when real-coded operators are used the real variables are directly used as the chromosome without any binary-coded representation.

Real coded operators: Design variables are generally coded in binary form and different operations of GA are carried on these coded variables. However, for calculations of objective functions, it needs to decode them as real numbers again. These steps are called *binary-coded genetic algorithms* (BCGA). Instead of coding the real variables into binary form, the operations could be carried directly in the real form with the same search capability as that of the binary-coded GA and these algorithms are called *real-coded genetic algorithms* (RCGA). The recent trend is to use the RCGA more in real world applications (Kumar and Tiwari, 2008).

The *design vector* presented in the previous chapter has been chosen as the *chromosome*. All design variables in the present problem are real in nature. Hence, the present single-objective optimization problem has been implemented by real-coded genetic algorithms on the basis of non-dominated sorting strategy.

3.3.3 Generating the initial population

The generation of the initial population involves generating the chromosome of all individuals in the population. Before generating the initial population different GA input parameters should be given to the algorithm. Different GA input parameters are summarized in Table 3.1.

Table 3.1 Input parameters to the population

Parameter	Symbol
Seed	s
Lower bound on the i^{th} variable	x_i^l
Upper bound on the i^{th} variable	x_i^u
Probability of crossover,	p_c
Probability of mutation,	p_m
Crossover distribution index,	η_c
Mutation distribution index,	η_m
Population size	n
Number of runs	N

For a binary coded form the chromosome can be generated as follows. Generate a random number u_i between 0 and 1. For the i^{th} digit z_i in the string will be assigned a value by the following criterion.

$$z_i = \begin{cases} 0 & \text{if } u_i \le 0.5 \\ 1 & \text{if } u_i > 0.5 \end{cases} \tag{3.1}$$

A binary solution can be represented as shown in Figure 3.3.

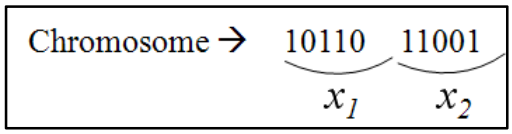

Figure 3.3 representation of a binary coded solution

For a real-coded chromosome each design variable, x_i, can be initialized by the following criterion

$$x_i = (1-u_i)\,x_i^l + u_i x_i^u \tag{3.2}$$

where u_i is a random number between 0 and 1. Once the chromosomes of all individuals are generated then the population is ready for evaluation and assigning the fitness for different individuals.

3.3.4 Evaluation of objectives and assigning the fitness

For a binary-coded variable the string should be decoded to real or integer value. The value of the i^{th} design variable, x_i, can be obtained by using the following decoding formula

$$x_i = x_i^l + \frac{x_i^u - x_i^l}{2^{l_i} - 1} \tag{3.3}$$

where l_i is the length of the string of the i^{th} design variable. Once the decoding is over the design variables will be used to determine objectives and constraint violations of the design vector. For a real-coded variable no decoding is needed and the design variable is directly used for calculation of design objectives and constraint violations.

The fitness value of an individual is a function of values of the objective function and corresponding constraint violations. In a penalty method, the fitness is given with a maximum penalization on an individual of the population which violates the constraints so that the individual is eliminated in subsequent generations. If there is no constraint violation then the fitness is simply the objective function value which can be used directly in ranking and sorting of individuals in the population.

$$F_i = f_i + \beta \sum c_i \tag{3.4}$$

where F_i is the fitness value, f_i is the objective function value, c_i is the constraint violation of the i^{th} individual and β is the penalty parameter of multiplication. One has to choose the penalty parameter suitably that it scales the constraint violations above maximum feasible objective values. Else an infeasible solution will be reflected as a better solution than a feasible solution.

To eliminate the penalty parameter a parameter-less approach is used to handle constraints. In parameter-less approach of the fitness assignment, the objective function value and the constraint violation will be treated separately.

$$F_i^f = f_i; \quad \text{and} \quad F_i^c = \sum c_i \tag{3.5}$$

where F_i^f is the fitness value corresponding to objective function, and F_i^c is the fitness value corresponding to constraint violation. While ranking of the individuals in the population, more preference will be given to one with zero constraint violation and then the objective function value will be taken into consideration.

3.3.5 Ranking and sorting of the population

The sorting of population is done by the dominance check. The different sorting strategies available are based on the dominance count, the dominance rank, the dominance depth, or a combination of above.

The dominance is checked by the parameter-less approach to handle constraints. In a conventional penalty method a huge penalty is applied on the individuals who violate constraints. But in the parameter-less approach three cases of the dominance occur. Case 1, between two infeasible individuals the one with lesser constraint violation dominates the other. Case 2, between an infeasible and a feasible one the feasible one dominates the other. Case 3, between two feasible individuals the one with better objective dominates the other. In a non-dominating sorting strategy used here the individuals are sorted based on the front at which an individual falls.

3.3.6 The selection operator

The selection operator is the first process of the reproduction. The selection operator makes the subgroups called mating pools for carrying the crossover operator on them. The main criterion for the selection operator is to make sure that the best solutions of the population are selected into the mating pool while maintaining the population size unchanged. There are several kinds of selection operators developed namely, the tournament selection, the ranking selection, and the proportional selection. The combination of these three methods will give rise to number of variants in selection operators.

In the tournament selection a tournament scheme is used with a number of sub-tournaments that produce a specified size of population into the mating pool. In a tournament selection operator there are two stages involved namely, (a) forming into subgroups for sub-tournaments (b) bringing out one individual as the winner from each subgroup by a criterion of tournament. One such scheme is to produce the mating pool equal to the size of parent population. Sub-tournaments have two players in each subgroup resulting in a single winner that goes to the mating pool out of each sub-tournament.

The other kind of selection is the proportionate selection or the stochastic selection and it is also called as *the roulette-wheel selection*. In this case a simulated roulette-wheel is run by giving each individual a probability of getting selected into the mating pool proportional to a criterion. The simulated roulette-wheel is run for a specified number of times equal to the size of the mating pool. Each run of the roulette-wheel is done by generating a random number. The problem with this kind of selection is that when a single or few members only get very high fitness value over the others then all other members are ignored by the process.

Hence, we need to properly scale the fitness values of different members. This is taken care of by the ranked selection method.

In the ranking selection method solutions are sorted according to their fitness and a new fitness is given, which is called the ranked fitness. The ranked fitness of a member is one for the worst ranked fitness, and the best ranked fitness equal the size of the population. Finally, the proportional selection operator is applied based on the ranked fitness.

Hence in the selection operation there are three issues to be dealt with

- Best solutions are to be given better chance to enter into the mating pool and this is taken care of by the tournament selection
- Best solutions are to be given chances proportionate to their fitness values. This is taken care of by the proportionate selection or the stochastic selection
- All the chances given to members should be scaled properly. This is taken care of by the ranking selection.

The different combinations of the above three factors will give rise to variations in the selection process. There are different variations of the roulette-wheel selection namely, simple roulette-wheel selection (RWS) also known as the stochastic selection, the stochastic remainder roulette-wheel selection (SRRWS) also known as the remainder stochastic sampling, the rank based roulette-wheel selection (RRWS) also known as the stochastic ranking selection (SRS), the stochastic universal sampling (SUS), the stochastic tournament selection (STS), and the stochastic ranking tournament selection (SRTS) (Goldberg, 1989; Raghuwanshi and Kakde, 2004).

3.3.7 The crossover operator

The crossover operator is applied after the selection of the mating pool is completed. The mating pool will be subdivided into pairs of chromosomes chosen as parents for the crossover. Before applying the crossover operator one has to decide whether the operator should be carried out on a pair of individuals. This is done by using a parameter called probability of crossover (p_c). The crossover operation is shown in Figure 3.4. For binary-coded variables the crossover is carried by generating a number of random crossover sites and the alternative parts of strings of both the parent chromosomes involved in crossover are interchanged. The number of crossover sites can also be chosen conveniently up to the maximum half of the length of the string.

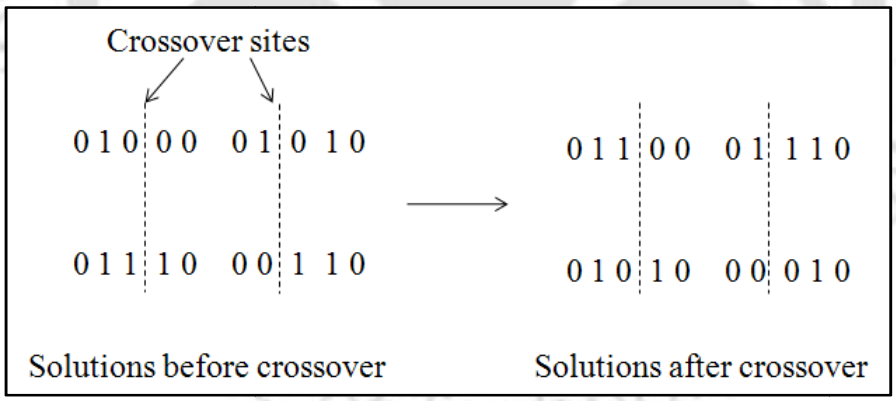

Figure 3.4 Multi-point crossover operator

For real-coded operators the crossover operation can be applied with more flexibility and variety. There are different crossover strategies that are implemented in GA and these are the linear crossover (LX), blend crossover (BLX), fuzzy recombination operator (FR), uni-modal normally distributed crossover (UNDX), simplex crossover (SPX), simulated binary crossover (SBX), parent centric crossover (PCX), etc. There are mainly two kinds of

crossovers namely, the mean-centric recombination and the parent-centric recombination. Crossovers LX, BLX, UNDX, SPX, and FR are mean-centric recombination operators, while SBX and PCX are parent centric recombination operators (Deb, 2001; Raghuwanshi and Kakde, 2004).

3.3.7.1 Simulated binary crossover (SBX)

In the present case the *simulated binary crossover* (SBX) and the *polynomial mutation* have been implemented for real-coded variables. The offspring set $\left(x_i^{(1,t+1)}, x_i^{(2,t+1)}\right)$ obtained from a parent set $\left(x_i^{(1,t)}, x_i^{(2,t)}\right)$ by using the SBX operator (Deb and Agarwal, 1995) is expressed as

$$x_i^{(q,t+1)} = 0.5\left[a \pm \beta_i b\right] \quad q = 1, 2 \tag{3.6}$$

where a is the sum of parent solutions and b is the difference of parent solutions. The parameter β_i is expressed as

$$\beta_i = \begin{cases} \left(2u_i\right)^{1/(\eta_c+1)}, & \text{if } u_i \le 0.5; \\ \left(\dfrac{1}{2\left(1-u_i\right)}\right)^{1/(\eta_c+1)}, & \text{otherwise.} \end{cases} \tag{3.7}$$

where u_i is a random real between 0 and 1, and η_c is the crossover distribution index. A large value of η_c gives a high probability of creating offspring nearer to the parent set.

3.3.8 The mutation operator

The *mutation operator* is carried after the *crossover operator* is applied. Similar to the application of the crossover operator, before the mutation operator is carried on an individual it should checked whether the mutation operator should be carried out to the chosen individual. This is decided by the probability of mutation by the following criterion

$$\text{If } u_i < p_m \text{ carry on the mutation else copy the individual} \tag{3.8}$$

If the mutation is to be carried then the digit to be mutated will be chosen by generating another random number. For a binary-coded variable the mutation is carried by replacing a 0 digit with 1, and vice versa. The mutation can be done by bit-by-bit. Then a random number is generated for each bit and is checked with the probability of mutation. The mechanism of single point mutation is shown Figure 3.5.

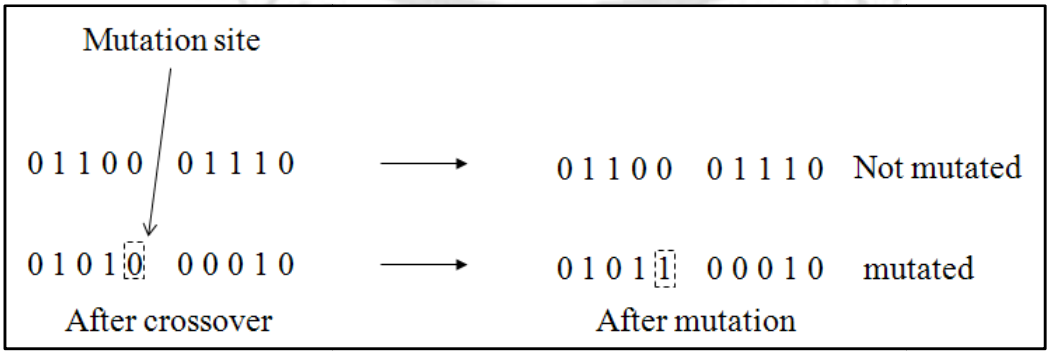

Figure 3.5 Mechanism of mutation of operator

For real-coded variables there are different mutation operators available and these are the random mutation (Rμ), the non-uniform mutation (NUμ), the normally distributed mutation (NDμ), and the polynomial mutation (Pμ).

It involves generating a random solution within a predefined range in the vicinity of solution to be mutated. A mutated solution z_i from a solution x_i by using the *polynomial mutation* (Deb, 2003) is expressed as

$$z_i^{t+1} = x_i^{t+1} + \left(x_i^U - x_i^L\right)\delta_i \tag{3.9}$$

where δ is determined by

$$\delta_i = \begin{cases} \left(2u_i\right)^{\frac{1}{\eta_m+1}} - 1, & \text{if } u_i \le 0.5, \\ 1 - \left[2\left(1-u_i\right)\right]^{\frac{1}{\eta_m+1}} & \text{otherwise.} \end{cases} \tag{3.10}$$

where u_i is a random real number between 0 and 1, and η_m is *the mutation distribution index* of the polynomial function. The chromosome of the GA is the design vector presented in Section 2.3.2 of Chapter 2 and comprises of all real variables. The crossover and mutation operators are applied on members of the population with a probability. In general, the crossover operator is applied with a higher probability, i.e. between 0.6 to 1, while the mutation is applied with a probability of $\frac{1}{n}$, where 'n' is the number of variables in the design vector.

3.3.9 Elitism operator

The elitism operator has the basic steps of (a) mixing the parent and the offspring population (b) Sorting the mixed population based on a criterion (c) copying the best (elite) individuals to the parent population. Other ways of implementing elitism scheme are (a) maintain a separate elite population (b) modify few members of this elite population with the better ones in each generation (c) replace a few individuals of the parent population with some percentage of the members of elite population to involve in the reproduction and (d) update elite population in each generation (Deb, 2001).

3.3.10 Key issues of convergence in SOGA

Constraint handling: There are two types of constraint handling, i.e., the hard and the soft. In the case of hard, the violation of the constraint is not tolerated; while in the case of soft constraint the violation of the constraint is tolerated to a specified degree. Generally equality constraints are taken care of by making the two equivalent inequality constraints with inaccuracies of small tolerance.

Convergence criterion: The convergence criterion is a set condition where the algorithm shall be terminated. The criterion of convergence could be chosen from either the design space or objective space depending on the problem. In the present case, the mean and optimum values of objective functions for the parent population have been chosen as a convergence criterion. The algorithm is run for sufficient number of generations such that the convergence criterion is ensured. As genetic algorithms are stochastic in nature, the converged solutions and the number of generations taken to converge depend on several

parameters for a particular problem such as the seed, the population size, GA operators used in the algorithm, probability of crossover, probability of mutation etc.

Population size: In an SOGA, a high population size increases the computational complexity of calculation consequently it takes long time per generation. A low population size involves less complexity of calculations hence it is faster in completing a generation. But the low population size has drawback of poor distribution of the individuals search space, hence it takes large number of generations to land on the global optimum. Moreover, the low population size has a poor predictability of optimal values (Deb, 2001).

Decision making: The making of design choice is treated as the *decision making*. For a SOGA the best choice will be the single best solution generated in the final population. For a multi-modal problem the number of solutions can be identified in the final population and can be captured as solutions. If no feasible solution is obtained the solution with least constraint violation can be chosen as best.

3.4 Conclusion

In the present chapter different methods of the single objective optimization both in deterministic and stochastic approaches have been introduced. The reasons for the choice of genetic algorithms as an optimization tool for the present work have been provided. A general working principle of GAs with the flowchart has been explained. The different terminology used in a simple GA has been introduced. The details of operators involved in GA namely, the selection, the crossover, the mutation, and the elitism have been explained. At the end some key issues of the convergence, the decision making and the population size related to SOGA have been discussed.

Numerical results of the implementation of SOGA to the design optimization of actuators of AMTB and HMTB will be provided in the next chapter. The problem of design optimization of actuators of AMTB and HMTB using MOGA will be provided in Chapters 5 to 7. The implementation of MOGAs to the design optimization of integrated systems of double acting hybrid actuators, controllers, and power amplifiers will be provided in Chapters 8 and 9.

Part - II
Optimal Design of Actuators

Chapter 4
Design Optimization of Magnetic Thrust Bearing Actuators Using Single Objective Genetic Algorithms

4.1 Introduction

The design optimization problem of actuators of magnetic thrust bearings and the genetic algorithm as the optimization tool have been detailed in Chapters 2 and 3, wherein, geometries of the magnetic thrust bearing actuator, different objectives to be traded-off, the design vector and constraints have been explained (see Sections 2.2 and 2.3). The optimization problem, different objectives and constraints has been presented in a standard form with detailed equations (see Tables 2.4 and 2.5). Working principle of genetic algorithms has been described (see Section 3.3).

In the present chapter, the single objective optimization problem of an optimal design of *magnetic thrust bearing* (MTB) *actuators* has been worked out using *single objective genetic algorithms* (SOGAs). The optimization is carried on two objective functions one at a time namely, the minimization of power loss in the actuator winding and the minimization of weight of the actuator. Two configurations of actuators namely, the *active magnetic*

thrust bearing (AMTB) and the *hybrid magnetic thrust bearing* (HMTB) have been considered. The coil dimensions namely, the inner radius, the outer radius, and the height of the coil have been proposed as design variables. The force required to be supported, the maximum flux-density that is allowed in the stator iron (i.e. the flux-density at the saturation), the maximum current-density that can be supplied in the coil, and the maximum space available are the different design requirements chosen as constraints. A factor called the iron-saturation factor is used to define the linear range of the magnetization curve. Apart from the comparison of objective functions in the tabular form, geometries of optimized magnetic bearings are compared in the form of diagrams. The above mentioned design optimization problems are illustrated through numerical simulations and results are interpreted in following sections.

4.2 Numerical Simulations

The design includes determining the geometric dimensions of the magnetic-coil, the bias-magnet and the stator-iron, the current-density in the coil for a particular load, the radius of the shaft clearance, and the air gap. As explained in Section 2.3.4 (see Figure 2.9) in an actuator analysis a specified input data and design space is provided to the program, while dependent variables, the objective function and constraint violations are determined during the analysis. Design variables will be chosen from the design space by GA operators. The input data will be provided in two parts respectively for the GA and for the actuator. The design space is provided as input to the GA.

Details of different input parameters assumed corresponding to the actuator and the GA, and the interaction between the GA, and the flow chart of the actuator analysis implementation have been presented in following subsections.

4.2.1 Input Variables

Design variables for the optimization of the actuator in a magnetic thrust bearing include dimensions of the coil as discussed in Section 2.3.2. Main constraints include the maximum allowable current density to be supplied in the coil corresponding to a given load, the inner radius of the bearing, and the air-gap.

Actuator input parameters: In the present work, the inner radius of the bearing is 25 mm, and the operating gap is 4 mm with the operating load of 2025 N. It is assumed that the gap and the load vary 5% and 10% of their respective operating quantities. The saturation flux-density of the iron core and the remnant flux-density of bias magnets are assumed to be 1T and 1.2T, respectively. Iron saturation factors, $\alpha_{\min}$ and $\alpha_{\max}$, are chosen to be 0 and 0.8, respectively..

Correction factors K_i, K_a and K_f, which are suggested to increase the model accuracy of the magnetic circuit, are chosen as 1.394, 1.072 and 0.840, respectively (Groom and Bloodgood, 2000). A packing factor of the coil η is assumed to be 0.85. Specific gravities of the iron and the copper are assumed as 7.77 g/cm^3 and 8.91 g/cm^3, respectively; and the specific gravity of the permanent magnet material neodymium-iron-baron is assumed to be 7.5 g/cm^3. Different input variables corresponding to the actuator design have been summarized in Table 4.1 (Bloodgood et al., 2000).

Table 4.1 Input parameters assumed for the design of the actuator of magnetic thrust bearing

Parameter	Value	Parameter	Value
Inner radius of the bearing, r_i	25.00 mm	Specific gravity of the stator-iron, γ_s	7.77 g/cm^3
Operating air-gap, l_g	4.00 mm	Specific gravity of the copper, γ_c	8.91 g/cm^3
Operating load, F	2025 N	Coil mmf loss-factor, K_i	1.394
Variation in the air-gap, υ_x	±5%	Actuator loss-factor, K_a	1.072
Variation in the load, υ_f	±10%	Maximum allowable coil volume, $V_{\max}$	820 mm^3
Saturation flux-density of iron, B_{sat}	1.00 T	Maximum outer radius of bearing, r_{oub}	120 mm
Saturation current-density of coil, J_{sat}	4.0 A/mm^2	Maximum height of bearing, h_{tub}	70 mm
Coil packing factor, η	0.85	Iron saturation factors, ($\alpha_{\min}$, $\alpha_{\max}$)	(0, 0.8)

Typical input parameters to be supplied by the user for particular applications would be $[r_i, l_g, F, B_{sat}, \alpha_{\max}, \alpha_{\min}, J_{sat}, \eta, \gamma_s, \gamma_c, K_i, K_a, r_{o\max}, h_{i\max}, V_{\max}, P_{\max}]$. Correction factors K_i and K_a are considered to increase the model accuracy of the magnetic circuit (Groom et al., 2000). Table 4.1 lists different input parameters chosen (Groom and Bloodgood, 2000) for the optimal design of thrust magnetic bearings in the present work.

Bounds on design variables: From Table 4.1, it can be observed that the inner radius of bearing is 25.00mm, the maximum allowed outer radius of bearing is 120.00mm, and the maximum allowed height of the coil is 70.00mm. Hence, bounds of design variables are chosen as r_{ci} (25.00, 120.00), r_{co} (25.00, 120.00), h_c (0.00, 70.00); where all dimensions are in mm. These bounds are obtained simply by taking the inner radius of the bearing as the lower bound, and the outer radius of the bearing as the upper bound for both the inner radius and outer radii of the coil. The height cannot be negative and it cannot be more than the maximum allowed height of the coil. These bounds on design variables are summarized in Table 4.2.

Table 4.2 Bounds of the design variables chosen

Design variables	r_{ci} (mm)	r_{co} (mm)	h_c (mm)
Lower limit	25.00	25.00	0.00
Upper limit	120.00	120.00	70.00

GA input parameters: The computer code developed by Kanpur Genetic Algorithm Laboratory (KanGAL), IIT Kanpur is implemented to the present single-objective optimization problem. The algorithm involves the single point crossover and bitwise mutation for binary variables; the simulated binary crossover (SBX) and polynomial mutation (Pμ) for real coded variables (explained in Sections 3.3.7 and 3.3.8, respectively) and the parameter-less approach (it is detailed in section 3.3.5) is used to handle constraints.

As discussed in Section 3.3.10, the choice of GA parameters affects the convergence rate and reaching the global optimum, etc. For this purpose one has to try the solution of the problem by using different sets of GA input parameters. For the optimization, input parameters of the GA namely, the probability of the crossover p_c, the probability of the mutation p_m, the crossover distribution index η_c, and the mutation distribution index η_m, are suggested (Deb, 2003; and Manos and Poladian, 2005) to be 0.9, 1/3, 5, and 10, respectively; for a population size of 100 populations with 1000 generations. However, in the present implementation, respective SBX parameters assumed to be 0.8, 0.005, 5, and 10 for a population size of 1000 with 100 generations. As the number of design variables are 3 only, the probability of mutation is assumed to be small (i.e., 0.005). The whole algorithm is allowed for 10 runs and the best of the feasible solutions obtained in terms of optimization of the objective are presented.

Table 4.3 The GA parameters assumed for the implementation of SOGA

Parameter	Value
Probability of crossover, p_c	0.8
Probability of mutation, p_m	0.005
Crossover distribution index, η_c	5
Mutation distribution index, η_m	10
Population size	1000
Number of runs	10

The different GA parameters assumed for implementation of SOGA have been summarized in Table 4.3. By trial and error the different parameters have been chosen of Table 4.3. When the number of design variables is less the convergence is slow with the high mutation probability. However, the high mutation probability helps in coming out of the local minimum. However, the crossover probability has been suggested between 0.6 and 1 to increase the convergence rate (Deb, 2003). Objective functions are optimized at the operating point (Schweitzer et al., 2003) of magnetic bearings.

4.2.2 Implementation of the algorithm

Interactions of genetic algorithms and actuator analysis: When the problem is implemented into the computer program, and the program can be observed as of two modules, the first is the genetic algorithm (GA) module and the second is the actuator analysis (AA) module. While the GA module targets on finding out the best solutions of the population, the AA module involves in evaluating the individual. In this process the GA module supplies the design vector to the AA module, while the AA module evaluates and supplies values of objective functions and constraint violations to the GA module. This process of interaction

and interconnection is shown in Figure 4.1 and is implemented with a separate function in the computer program.

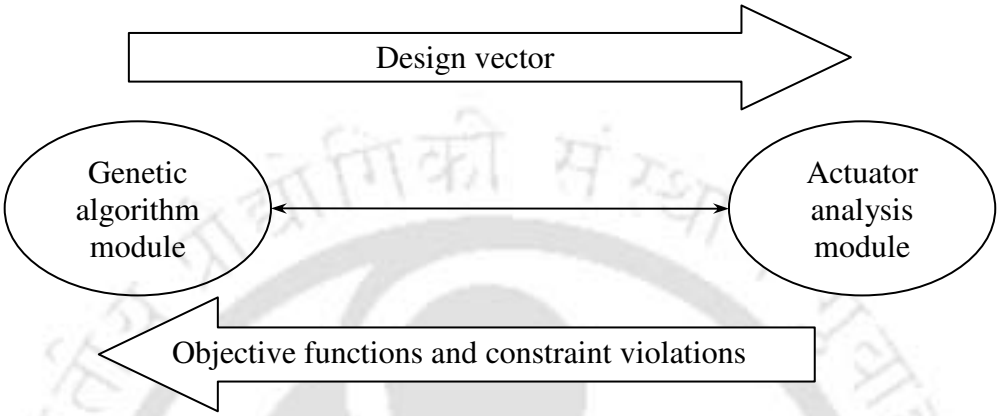

Figure 4.1 The flow of information between the genetic algorithm module and the actuator analysis module in the comuputer program

The flowchart of the optimization: A flowchart of the actuator analysis module in the GA implementation has been presented in Figure 4.2 and briefly described here. According to Figure 4.2, before going into the problem formulation different design requirements of the actuator, such as the load to be supported, maximum power-loss allowed, maximum current-density allowed, and maximum flux-density allowed, are identified. Then the design vector is chosen (i.e., coil dimensions namely, the inner radius, the outer radius and the height of the coil) and the actuator input is given to the actuator analysis module.

Next GA generates an initial population and each individual of the population is evaluated by the actuator analysis module. As shown in Figure 4.2, in the actuator analysis module, initially the pole face area of the air-gap, the volume of the coil and cross sectional area of coil are given by using input parameters and design variables as shown in Figure 2.11. Then, for the case of the HMTB determine the thickness of bias magnets corresponding to operating load and air-gap.

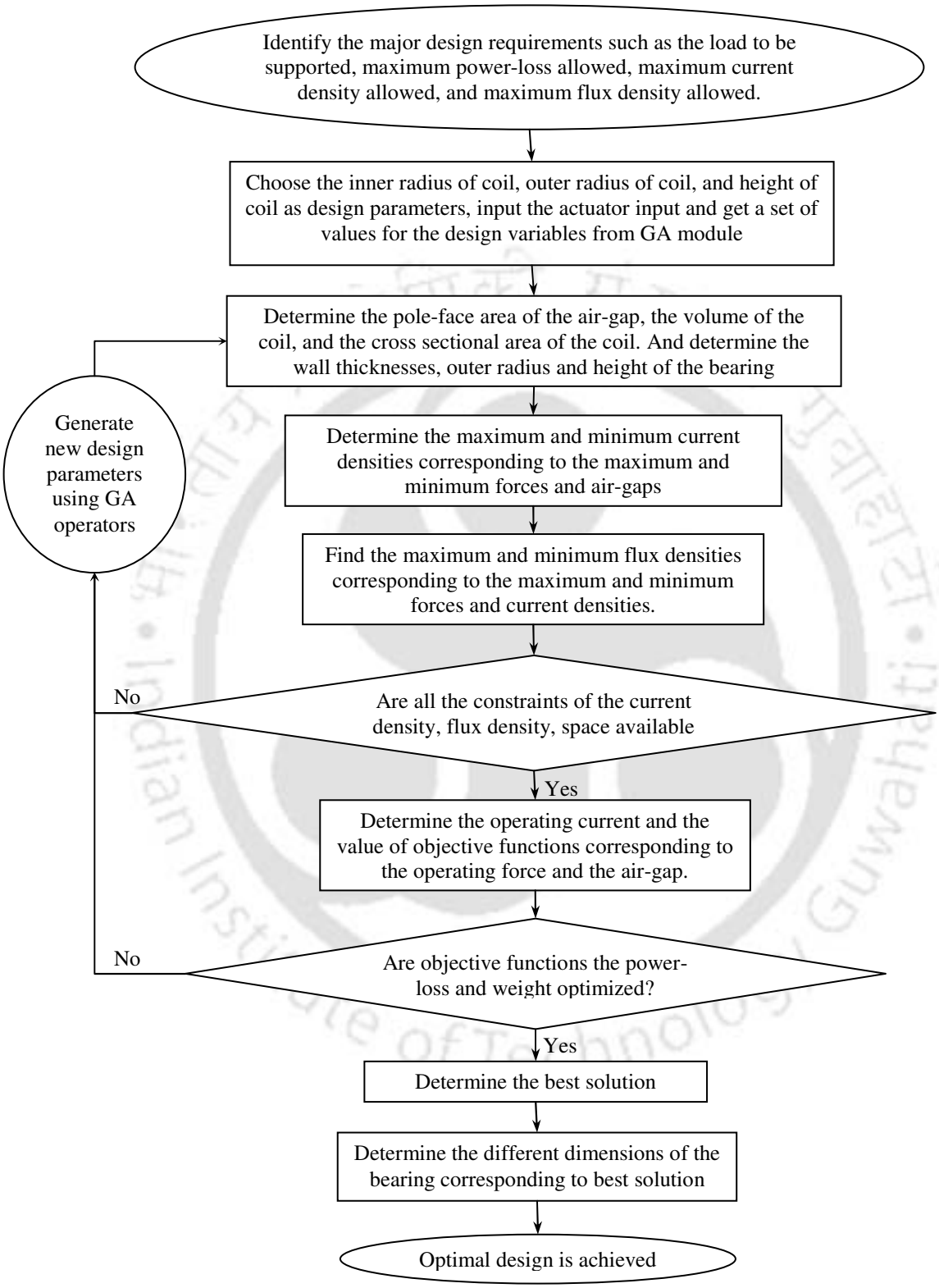

Figure 4.2 A flowchart of the implementation of actuator analysis in the genetic algorithm

Next constraints of the maximum current-density in the coil and the maximum flux-density in the stator iron are calculated corresponding to the maximum force and the air-gap specified as the input for the actuator analysis. Then, the outer radius and height of the bearing are determined, and the constraint values are checked for violations. If these constraints are not violated then the current and the power-loss (i.e., objective function) corresponding to the operating load and the air-gap are determined. Now objective function values are checked for the optimization. If the objective function has been optimized, then the best solution is obtained from the final population. Finally, different dimensions and other parameters of the bearing corresponding to best solution are determined from the post-processing of the obtained results.

4.2.3 Optimized Geometries of the Bearing

Two types of magnetic bearings are considered, i.e. one without bias magnets (AMTB) and the other with bias magnets (HMTB). Two objective functions are considered one at a time for the optimum design of a magnetic bearing, namely, the minimization of the power-loss, P, which is given by equation

$$P = \rho \eta J^2 V_c \tag{4.1}$$

and the minimization of the weight W, which is given by equation

$$W = W_c + W_s + W_m \tag{4.2}$$

Different quantities involved in equations (4.1) and (4.2) have been detailed in Sections 2.3.1.1 and 2.3.1.2, respectively. Convergence issues and comparison of results will be discussed in the following subsections.

4.2.3.1 Convergence issues

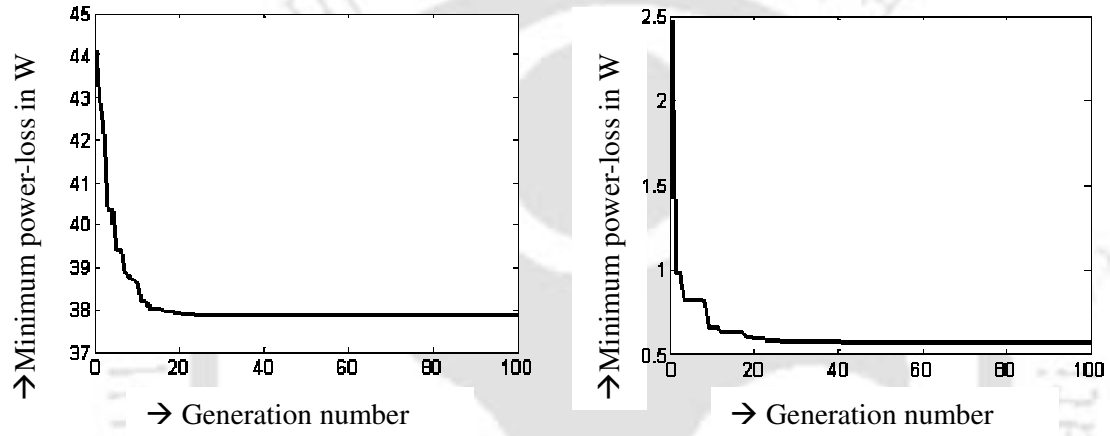

Figure 4.3 The convergence of the minimum powerloss at load 2025 N

(left) without bias magnets(AMTB) (right) with bias magnets(HMTB)

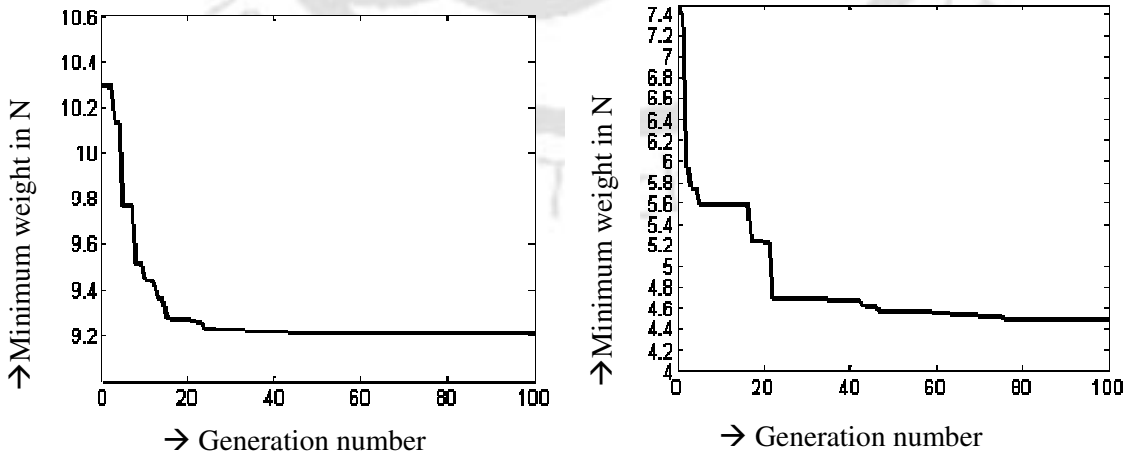

Figure 4.4 The convergence of the minimum weight at load 2025 N

(left) without bias magnets(AMTB) (right) with bias magnets(HMTB)

The convergence trends of objective functions, i.e. respectively the minimization of power-loss and minimization of weight are shown in Figure 4.3 and Figure 4.4. Convergence plots are given for the best feasible solution in the whole population in each generation. It can be observed from Figure 4.3 and Figure 4.4 that in all the cases there is at least one feasible solution in the initial population and the best values of objectives reduced in subsequent generations. The best values of objectives are constant for all the cases after some number of generations. Generations taken for the convergence in each case have been observed to be different. Generations taken for the convergence and best values of the convergence have been summarized in Table 4.4.

Table 4.4 Number of generations and obective best values of convergence

Objective functions	No. of generations taken for convergence	Best values of objectives converged
minimum weight (AMTB)	42	9.21(N)
minimum weight (HMTB)	79	4.48(N)
Minimum power-loss (AMTB)	23	37.85(W)
Minimum power-loss (HMTB)	40	0.566(W)

4.2.3.2 Comparison of results

Geometries of optimized magnetic bearings are given in Table 4.5 and different volumes and operating parameters are shown in Table 4.6. Magnetic bearing geometries showing optimized dimensions for the cases of minimum weight and minimum power-loss (with and without bias magnets) are shown in Figure 4.5 and Figure 4.6, respectively.

Table 4.5 Optimized actuator input, design and dependant parameters

Objective functions	Input parameters				Design parameters			Dependant parameters			
	r_i (mm)	l_g (mm)	F (N)	B_r (T)	r_{ci} (mm)	r_{co} (mm)	h_c (mm)	l_m (mm)	t_b (mm)	r_o (mm)	h_t (mm)
minimum weight (AMTB)	25.00	4.00	2025	–	44.91	75.45	39.60	–	15.50	84.17	55.10
minimum weight (HMTB)	25.00	4.00	2025	1.2	45.87	65.03	16.35	4.67	16.12	75.56	37.14
Minimum power-loss (AMTB)	25.00	4.00	2025	–	69.13	100.0	50.00	–	30.04	119.0	80.04
Minimum power-loss (HMTB)	25.00	4.00	2025	1.2	66.76	98.39	49.92	2.13	28.70	116.2	80.75

Table 4.6 Optimized actuator performance parameters

Objective functions	Volumes			Performance parameters at the operating point			
	V_c (cm^3)	V_s (cm^3)	V_m (cm^3)	J (A/mm^2)	B (T)	P (W)	W (N)
minimum weight (AMTB)	457.36	661.00	–	3.63	0.762	102.58	9.21
minimum weight (HMTB)	109.15	409.67	43.44	2.01	0.740	7.50	4.48
Minimum power-loss (AMTB)	820.00	2582.4	–	1.65	0.441	37.85	27.37
Minimum power-loss (HMTB)	819.20	2363.4	51.3	0.20	0.460	0.566	26.05

The first rows of Table 4.5 and Table 4.6 show the parameter values correspond to the minimization weight as the objective for the case of AMTB and second rows refer to the minimization of weight as objective for the HMTB, third rows refer to the minimization of power-loss for the AMTB and fourth rows refer to the minimization of power-loss for HMTB. From rows 1 and 2 of Table 4.5 and Table 4.6, it can be observed that the minimization of weight chooses the minimum feasible dimensions, and this causes the copper volume to be reduced; resulting in the increased power-loss in the coil. Similarly, from rows 3 and 4 of Table 4.5 and Table 4.6, it can be observed that with the minimization

of the power-loss as the objective, the maximum allowable coil volumes are chosen to reduce the resistance effect in the coil and this increases the actuator dimensions causing increase in the weight of the actuator.

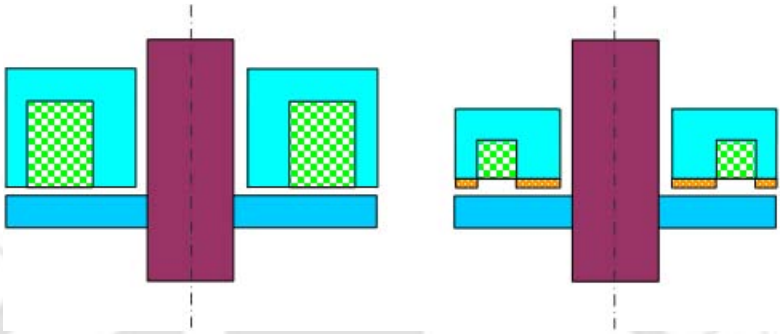

Figure 4.5 Optimized magnetic bearing geometries for the objective function as the minimum weight

(left) without bias magnets (right) with bias magnets (dimensions can be referred in Table 4.5)

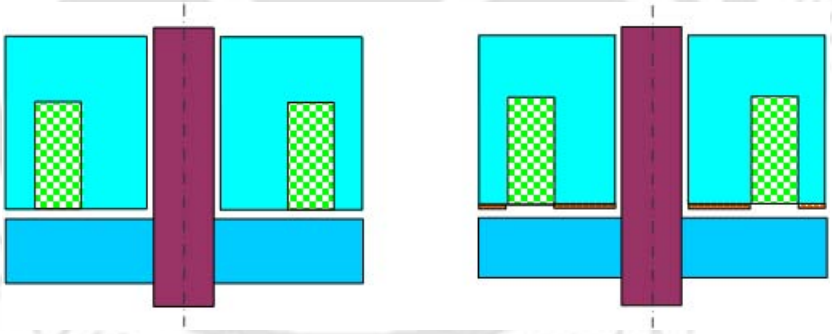

Figure 4.6 Optimized magnetic bearing geometries for the objective function as the minimum power-loss

(left) without bias magnets (right) with bias magnets (dimensions can be referred inTable 4.5)

Now comparisons are double-folded, and are expressed as the comparison of configurations with the same objective and the comparison of objectives with the same configuration.

Comparison of configurations with the same objective: Differences in the geometry and performance parameters for the comparison of configurations with the same objective have been summarized in Table 4.7 and Table 4.8, respectively. The first row of Table 4.7 shows the differences in values for the AMTB and for the HMTB in rows 1 and 2 of Table 4.5 for the case of minimizing the weight. The second row of Table 4.7 shows the differences in values for the AMTB and for the HMTB in rows 3 and 4 of Table 4.5 for the case of minimizing the power-loss. Similarly, the first row of Table 4.8 shows the differences in values for the AMTB and HMTB in rows 1 and 2 of Table 4.6 for the case of minimizing the weight. The second row of Table 4.8 shows the differences in values for the AMTB and HMTB in rows 3 and 4 of Table 4.6 for the case of minimizing the power-loss.

Table 4.7 Comparison of configurations with same objectives (differences in the geometry)

Objective functions	Design parameters			Dependant parameters			
	r_{ci} (mm)	r_{co} (mm)	h_c (mm)	l_m (mm)	t_b (mm)	r_o (mm)	h_t (mm)
minimum weight (AMTB) - (HMTB) Table 4.5 (row 1 – row 2)	0.96 (less)	10.42 (more)	23.25 (more)	4.67 (less)	0.63 (less)	8.61 (more)	17.96 (more)
Minimum power-loss (AMTB) - (HMTB) Table 4.5 (row 3 – row 4)	2.37 (more)	1.61 (more)	0.08 (more)	2.13 (less)	1.34 (more)	2.80 (more)	0.71 (less)

From Table 4.5 and Table 4.7 for minimizing the overall weight of the bearing as objective (i.e., the first row of Table 4.7), it can be observed that as compared to the case of without bias-magnets (AMTB), dimensions of the actuator are drastically reduced (except negligible quantities of increase in the inner radius of the coil and the back-wall thickness of the stator-iron) in the case of using bias magnets (HMTB) for the same conditions. In the case of minimizing power-loss (i.e., the second row of Table 4.7), there is not much

difference in dimensions in the case of using bias magnets as compared to no bias-magnets (comparing rows 1 and 2 of Table 4.7).

The effect of dimensions in the first row of Table 4.6 can be observed in the first row of Table 4.8 that the volumes of coil and stator iron, the power-loss and weight are reduced significantly for the HMTB as compared to the AMTB for the minimization of the weight as the objective function. From the second row of Table 4.8, there is a negligible difference in coil volume. Moreover, rows 3 and 4 of Table 4.6 show that it is the maximum volume of the coil chosen for the minimization of power-loss. Both the power-loss and the weight are more in the case of without bias-magnets as compared to the case of using bias-magnets, since the bias-magnets share considerable amount of magnetic flux-density to support the operating load.

Table 4.8 Comparison of configurations with same objectives (differences in volumes and performacne parameters)

Objective functions	Volumes			Performance parameters at the operating point			
	V_c (cm^3)	V_s (cm^3)	V_m (cm^3)	J (A/mm^2)	B (T)	P (W)	W (kg)
minimum weight (AMTB) - (HMTB) Table 4.6 (row 1 – row 2)	348.21 (more)	251.33 (more)	43.44 (less)	1.62 (more)	0.022 (more)	95.08 (more)	4.73 (more)
Minimum power-loss (AMTB) - (HMTB) Table 4.6 (row 3 – row 4)	0.80 (more)	219.00 (more)	51.30 (less)	1.45 (more)	0.019 (less)	37.284 (more)	1.31 (more)

Comparison of objectives with the same configuration: From Table 4.9 and Table 4.10, it can be observed that all dimensions and volumes are more for the objective as the minimization of power-loss than those of the minimization of weight. Moreover, from rows of Table 4.10, the power-loss is less and the weight is more when the objective is the minimization of power-loss as compared to the objective as the minimization of weight.

This is due to the fact that the minimization of power-loss chooses maximum available dimensions to reduce the resistance effect, while to the minimize weight the maximum allowable current-density is chosen by the algorithm to support the specified load within the least space in both the cases of AMTB and HMTB. Hence, it can be concluded that the power-loss and the weight are two conflicting quantities; characterizing a decrement in one objective causes an equivalent increase in the other (i.e., the reduction in weight causes the increase in power-loss, and vice-a-versa) and to have a better design characteristic multi-objective optimization is suggested.

Table 4.9 Comparison of objectives with same configurations (differences in the geometry)

Objective functions	Design parameters			Dependant parameters			
	r_{ci} (mm)	r_{co} (mm)	h_c (mm)	l_m (mm)	t_b (mm)	r_o (mm)	h_t (mm)
(AMTB) (Power-loss) – (weight) Table 4.5(row 3 – row 1)	24.22 (more)	24.55 (more)	10.40 (more)	–	14.54 (more)	34.83 (more)	24.94 (more)
(HMTB) (Power-loss) – (weight) Table 4.5 (row 4 – row 2)	20.89 (more)	33.36 (more)	33.57 (more)	2.54 (less)	12.58 (more)	40.64 (more)	43.61 (more)

Table 4.10 Comparison of objectives with same configurations (differences in volumes and performacne parameters)

Objective functions	Volumes			Performance parameters at the operating point			
	V_c (cm^3)	V_s (cm^3)	V_m (cm^3)	J (A/mm^2)	B (T)	P (W)	W (kg/kg)
(AMTB) (Power-loss) – (weight) Table 4.6 (row 3 – row 1)	362.64 (more)	1921.4 (more)	–	1.98 (less)	0.321 (less)	64.73 (less)	14.16 (more)
(HMTB) (Power-loss) – (weight) Table 4.6 (row 4 – row 2)	710.05 (more)	1953.73 (more)	7.86 (more)	1.81 (less)	0.280 (less)	6.934 (less)	21.57 (more)

4.3 Conclusions

In the present chapter, the optimal design of a thrust magnetic bearing using SOGAs has been performed. Two types of bearing actuator configurations, i.e. without and with bias magnets have been taken into consideration. Two objectives have been considered one at a time, namely minimizing the power loss and minimizing the overall weight of the actuator. The method of implementation for the problem considered has been described in the flowchart. Input parameters corresponding to SOGA and the actuator analysis have been presented.

Convergence plots of objective functions with the generation have been shown. The number of generations taken for the convergence is observed to be different for different cases. The best geometries of different cases have been compared in tables and figures. From results, it is observed that the size of the bearing actuator with bias magnets is considerably reduced as compared to the case of without bias-magnets for the same conditions for the objective function as the maximization of load-to-weight ratio. Similarly, current densities reduce drastically with biased magnets when the objective function is chosen as the minimization of the power-loss.

Comparison has been done in two fold and it is specified as the comparison of objectives with the same configuration and the comparison of configuration with the same objective. It is also observed that objectives chosen, namely the power-loss and the weight are two conflicting quantities characterizing a decrement in one objective causes an equivalent increase in the other (i.e., reduction in the weight causes increase in the power-loss, and vice-a-versa) and to have a better design characteristic the multi-objective optimization is

suggested. This will be taken up in the subsequent chapters for the actuators of AMTB and HMTB separately. Multi-objective optimization of AMTB actuators will be dealt in Chapter 5 and that of HMTB will be dealt in Chapter 6.

Chapter 5
Optimum Design & Analysis of Magnetic Thrust Bearings Using Multi-Objective Genetic Algorithms

5.1 Introduction

The optimization problem formulation has been given in Chapter 2, and fundamentals on optimization tools used namely genetic algorithms have been explained in Chapter 3. In Chapter 4, the optimization of the actuator has been performed by using the SOGA, and it is concluded therein that the two trade-offs namely the power-loss in the coil and the overall weight of the actuator are mutually conflicting quantities. Hence, for a better optimization characteristic the multi-objective optimization has been suggested.

Based on the background provided in previous chapters, in the present chapter, the design optimization is extended to the multi-objective optimization of actuators in *active magnetic thrust bearings* (AMTB) (i.e., without permanent magnets) by using *multi-objective genetic algorithms* (MOGAs). The trade-offs namely, the power-loss and the weight of the actuator which have been considered independently using SOGA in the

previous chapter, will be now considered together in the multi-objective optimization of actuators of AMTB in the present chapter. For present case, constraints remain the same as described for the case of single-objective optimization in the previous chapter, namely, the maximum available space for the actuator, the maximum current-density that can be supplied in the coil, the maximum magnetic flux-density that is allowed in the stator-iron (i.e., the magnetic flux-density at the saturation), and the load required to be supported. The inner radius, the outer radius, and the height of the coil have been considered as design variables. Apart from the comparison of performance parameters in the form of figures and tables, designs are also compared through line diagrams. The post-processing has been done on the final optimized population by studying the variation of different parameters with respect to objective functions. A novel analysis methodology on Pareto optimal designs of the final population has been introduced and is titled as *Pareto optimal design analysis methodology*. According to this analysis a post-process is done on the final population to study how different parameters of the designs of the final population relatively behave with respect to other parameters.

Geometries of the thrust magnetic bearing and the optimization model have been discussed in Section 2.3 of Chapter 2. The optimization problem is defined in Table 2.4, and different objectives and constraints have been summarized in Table 2.5. Different formulations provided in Chapter 2 are corresponding to a HMTB. However, one can obtain formulations corresponding to an AMTB by simply eliminating terms of permanent magnets (e.g. the thickness and remnant flux density of the bias magnets) in formulations of HMTB. Hence, the detailed discussion of the formulations is same as provided in Chapter 2, and hence it is not repeated here.

Different aspects of genetic algorithms have been discussed in Section 3.3 of Chapter 3. Some terminologies related to the multi-objective optimization such as the objective space, the design space, the dominance, the Pareto optimal front are provided, followed by discussions of results, and conclusions are detailed in following sections.

5.2 Pareto optimal front

As shown in Figure 5.1, in a multi-objective optimization problem there are two spaces namely, the design space and the objective space (Deb, 2001). Each point in the design space can be represented by a corresponding unique point in the objective space as shown in Figure 5.1. The concept of dominance for the multi-objective optimization problem is shown in Figure 5.2. The dominance of a point 'A' can be determined with respect to any other point in the four quadrants of the two dimensional space with respect to point 'A'. Any point 'B' in Quadrant I is dominated by point 'A'. Hence, it is a dominated quadrant by point 'A'. Any point 'C' in quadrant III dominates point 'A', hence quadrant III is a dominating quadrant to point 'A'. Points 'D' and 'E' in quadrants II and IV, respectively, neither dominating nor dominated by point 'A', hence quadrants II and IV are non-inferior with respect to point A.

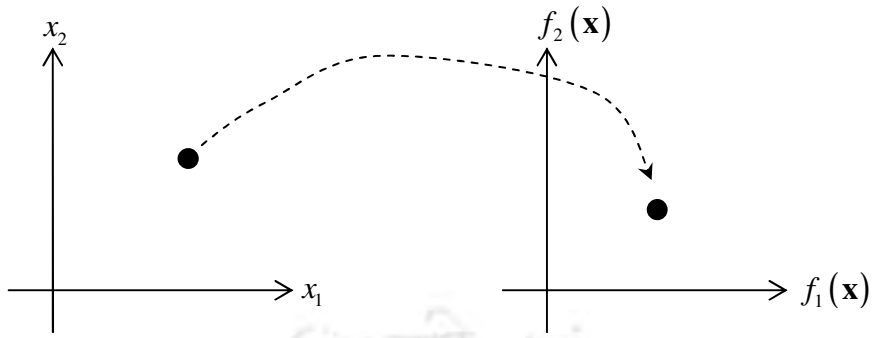

(a) Design space (b) Objective space

Figure 5.1 Representation of the design space and the objective space of an MOOP

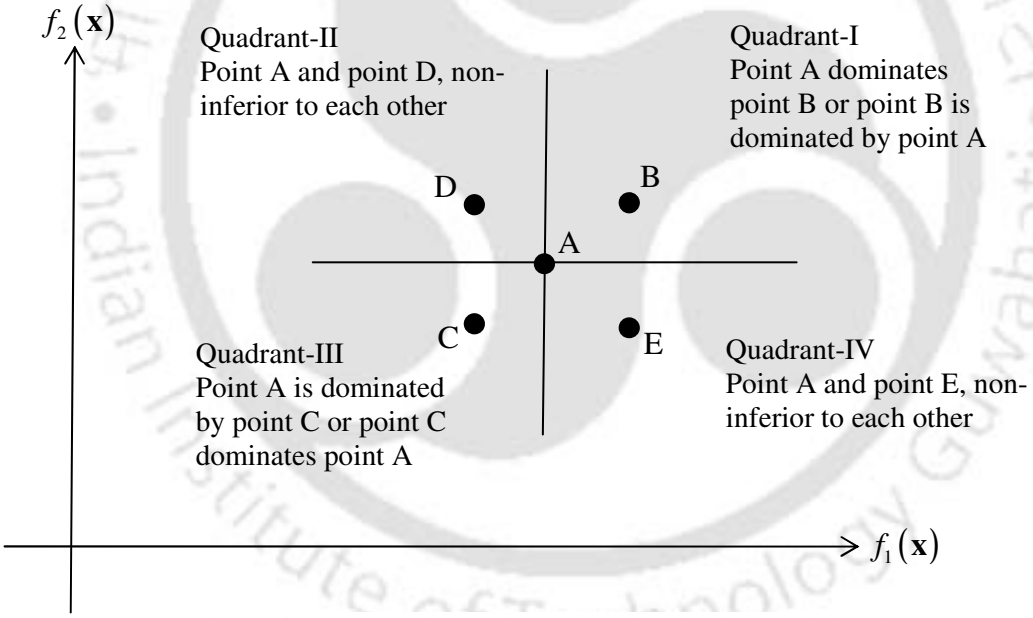

Figure 5.2 The dominance in the multi-objective optimization

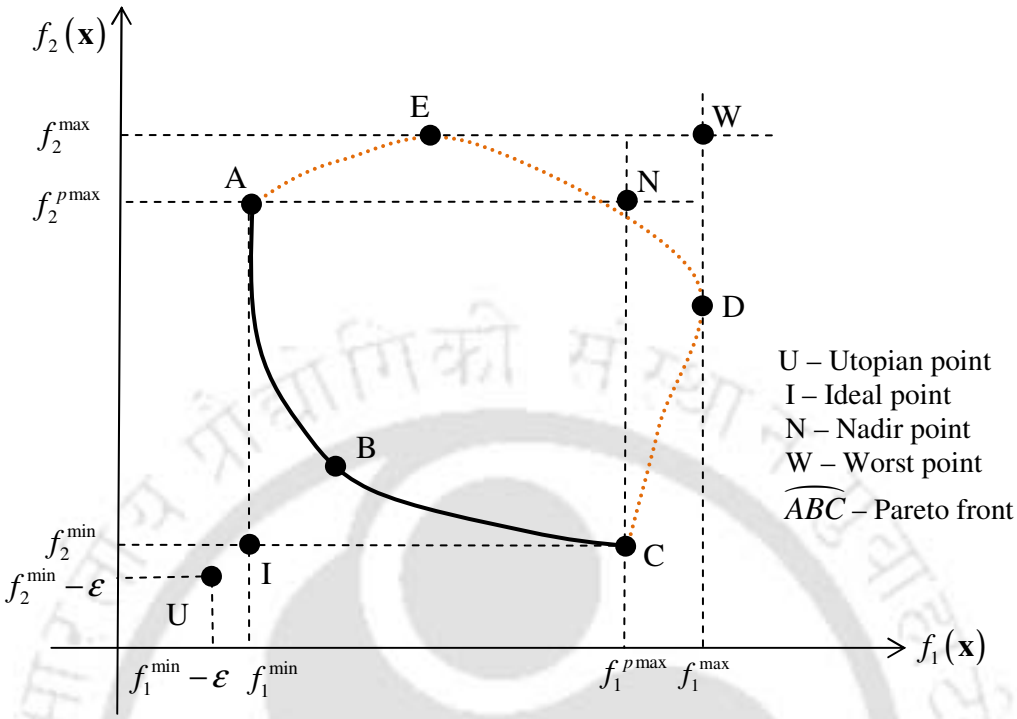

Figure 5.3 The Pareto optimal front and different objective vectors

The Pareto optimal solution of a minimization problem is the design vector, which has no other feasible solution that decreases an objective function without causing at least one of the other objective functions (Coello, 2000). The Pareto optimum gives a set of solutions; in general, these are called as the non-dominated set of solutions. The Pareto front is the locus of different non-dominated solutions in the multi-objective space. Pareto optimal solutions optimize objective functions to different degrees and each is the best in their own sense.

The Pareto optimal front and different points in the objective space corresponding to the Pareto front have been shown in Figure 5.3. It includes a space with boundary ABCDEA and points namely U, I, N, and W. The space inside the closed loop curve ABCDEA represents the feasible space in the objective space of a MOOP. The curve ABC represents

the Pareto optimal front of the minimization problem in both objective functions. Point 'I' (where minimum values of the curve ABC intersect) is called the *ideal solution or ideal point*. Point 'U' (with objective values less by small quantities (ε) than those of ideal point 'I'), is called as the *utopian point*. Point 'N' (where maximum values of the Pareto front ABC intersect) is called the *Nadir point*. Point 'W' which involves the intersection of maximum (or the worst) feasible solutions in both objective functions in a minimization problem is called the *worst point*.

Different concepts related to *Pareto optimal front* have been explained in previous sections and now in the next section, the design optimization of the actuator of an *active magnetic thrust bearing* (AMTB) has been carried for multi-objective functions. A set of inputs required from the user for a particular application has been mentioned in Table 4.1 of Chapter 4 for the single objective optimization and the same is utilized in the present chapter. Optimised bearing objective function values have been provided in the form of Pareto front. For a typical comparison, results of individual objective functions have also been included. The sensitivity analysis has been performed of design variables on objective functions at a particular chosen design. The variation of different design parameters on the final optimized population is studied in order to have an understanding of the relationship of the design parameters on different values of objective functions, and constraint parameters in the final population.

5.3 Multi-objective optimization problem formulation for AMTB

Geometries of the thrust magnetic bearing and the optimization model have been discussed in Section 2.3. The optimization problem is defined in Table 2.4, and different objectives and constraints have been summarized in Table 2.5. Different formulations provided in Chapter 2 are corresponding to a HMTB. However, one can obtain formulations corresponding to an AMTB by simply eliminating terms of permanent magnets (e.g. the thickness and remnant flux of bias magnets) in formulations of HMTB. For convenience and completeness, formulations corresponding to AMTB are provided in the following section. However, the detailed discussion about formulations is same as provided in Chapter 2, and hence it is not again repeated here.

5.3.1 Fundamental relations

Different dimensional parameters of the actuator of an AMTB are shown in Figure 2.5 of chapter 2. From Figure 2.5, it can be observed that the inner radius of the bearing can be expressed as

$$r_i = r_s + l_c \tag{5.1}$$

From Figure 2.5, t_i, t_c and t_o can be expressed in terms of r_i, r_{ci}, r_{co} and r_o, as

$$t_i = r_{ci} - r_i; \qquad t_c = r_{co} - r_{ci}; \qquad t_o = r_o - r_{co} \tag{5.2}$$

where r_o and t_b are related to coil dimensions according to

$$A_g = \pi\left(r_{ci}^{\ 2} - r_i^2\right) = 2\pi r_{ci} t_b = \pi\left(r_o^{\ 2} - r_{co}^2\right) \tag{5.3}$$

where A_g is the pole face area of the air-gap at poles, which is assumed to be maintained constant throughout the cross section of the stator-iron and the collar through which the magnetic flux flows (Maslen, 2000). Equation (5.3) is obtained by assuming the magnetic flux, ϕ, and the magnetic flux density, B, flowing in the whole magnetic circuit as shown in Figures 2.7 and 2.9 of Chapter 2, as constant and they are related as

$$B = \frac{\phi}{A_g} \tag{5.4}$$

The magnetic flux density, by neglecting losses, is expressed as

$$B_g = \frac{\mu_0 ni}{2l_g} \tag{5.5}$$

Equation (2.7) gives the flux density in terms of the coil current, where ni is the magneto motence and μ_0 is the permeability of the vacuum. The classical design of magnetic bearings depends on the ideal magnetic circuit theory, which deviates drastically from experiments (Maslen, 2000; Schweitzer et al., 2003; and Chiba et al., 2005). Groom and Bloodgood (2000) proposed a model by adding the loss and leakage factors to ideal models. By the application of loss factors, equation (2.7) takes the following form

$$B_g = \frac{\mu_0 K_i ni}{2K_a l_g} \tag{5.6}$$

where K_i is the coil mmf loss-factor and K_a is the actuator loss-factor. The magnetic force exerted by the actuator could be expressed as

$$F = \frac{B_g{}^2 A_g}{\mu_0} = \frac{\phi_g{}^2}{\mu_0 A_g} \qquad \text{with} \qquad \phi_g = B_g A_g \tag{5.7}$$

In the magnetic bearing design, the magnetic flux is determined from the required force to be supported and the magneto-motense is determined from the magnetic flux that should flow in the magnetic circuit. The standard form of expression of the power-loss in the coil is given as

$$P = i^2 R \tag{5.8}$$

where P is the power-loss, i is the current flow in the coil, and R is the resistance of the coil to the current flow. Equation (5.8) can be rewritten as (Schweitzer et al., 2003, Groom and Bloodgood, 2000).

$$P = \rho \eta J^2 A_c l / n \tag{5.9}$$

where J is the current-density in the coil, n is the number of turns, η is the coil packing factor, A_c is the cross-sectional area of the coil, and l is the total length of coil. The different turns of the coil may have different lengths; however, l/n could be taken as the average length of the coil per turn.

In this section, expressions for objective functions and constraints are presented for the design of active magnetic thrust bearings AMTB.

5.3.2 Objective Functions

The power-loss expressed as

$$P = \rho \eta J^2 V_c \tag{5.10}$$

where V_c is the volume of the coil. From the geometry of the thrust magnetic bearing in Figure 2.5 of Chapter 2, the cross sectional area and the volume of the coil are expressed as

$$A_c = (r_{co} - r_{ci}) h_c \quad \text{and} \quad V_c = \pi (r_{co}^2 - r_{ci}^2) h_c \tag{5.11}$$

The overall weight of the magnetic bearing, W , could be expressed as

$$W = W_c + W_s \tag{5.12}$$

where W_k are weights of components of the bearing with subscript k: c and s represent the coil and the stator-iron, respectively. The components of the weight of the bearing could be expressed as

$$W_c = \gamma_c \pi (r_{co}^2 - r_{ci}^2) h_c \tag{5.13}$$

And

$$W_s = \gamma_s \pi \left[\left(r_{ci}^2 - r_i^2 \right) h_c + \left(r_o^2 - r_{co}^2 \right) h_c + \left(r_o^2 - r_i^2 \right) t_b \right] \tag{5.14}$$

where γ is the weight density of the corresponding material.

5.3.3 Choice of the Design Vector

In Chapter 4 the design vector chosen is for individual objectives and for SOGA. However, for a multi-objective optimization problem the union of all the design variables of different individual objectives will be taken as the design vector. For the present problem, as explained from Subsections 2.3.1.1 and 2.3.1.2, it is concluded that both the power-loss in the coil and the weight of the bearing could be related as functions of coil dimensions. It is also shown that for the present case other dimensions of the stator-iron could be determined from the coil dimensions. Hence, the design vector for multi objective optimization is chosen as $[r_{ci}, r_{co}, h_c]$ and dependent parameters for the actuator of AMTB are $[r_o, t_b]$ which can be determined from equation (5.3).

5.3.4 Constraints

The maximum and minimum forces exerted by the bearing, $F_{\max}$ and $F_{\min}$, are determined

$$\frac{\mu_0 A_g}{4} \left(\frac{K_i n i_{\max}}{K_a l_{g\max}} \right)^2 = F_{\max} \tag{5.15}$$

and

$$\frac{\mu_0 A_g}{4}\left(\frac{K_i n i_{\min}}{K_a l_{g\min}}\right)^2 = F_{\min} \tag{5.16}$$

then current densities required to be supplied in the coil is determined as

$$ni_{\max} = \eta J_{\max} A_c \tag{5.17}$$

and

$$ni_{\min} = \eta J_{\min} A_c \tag{5.18}$$

From equations (2.21), (5.16), (2.22) and (5.18), we get

$$J_{\max,\min} = \sqrt{\frac{4F_{\max,\min}}{\mu_0 A_g}}\left(\frac{K_a l_{g\max,\min}}{K_i \eta A_c}\right) \tag{5.19}$$

The constraints becomes

$$J_{sat} \geq J_{\max} \tag{5.20}$$

and

$$J_{\min} \geq 0 \tag{5.21}$$

the maximum and minimum magnetic flux densities of the stator that are required to support the maximum and minimum loads are expressed as

$$B_{\max,\min} = \sqrt{\frac{\mu_0 F_{\max,\min}}{A_g}} \tag{5.22}$$

According to equation (2.9), the linear range limits of flux density could be expressed as

$$\frac{\mu_0 K_i n i_{\min}}{2K_a l_{g\min}} \geq \alpha_{\min} B_{sat} \tag{5.23}$$

and

$$\alpha_{\max} B_{sat} \geq \frac{\mu_0 K_i n i_{\max}}{2K_a l_{g\max}} \tag{5.24}$$

The maximum power-loss allowed is determined from the steady state heat transfer equation (Schweitzer et al., 2003) as

$$P_{\max} = \Lambda(T_{cr} - T_{\infty}) \tag{5.25}$$

The maximum allowable volume of the coil, $V_{\max}$, could be determined as

$$V_{\max} = \frac{P_{\max}}{\rho \eta J_{sat}^2} \tag{5.26}$$

Thus, from equations (2.16) and (2.28) the maximum space occupied by the coil could be expressed as a constraint (Bloodgood et al., 2000)

$$V_{\max} \geq \pi\left(r_{co}^{\,2} - r_{ci}^{\,2}\right) h_c \tag{5.27}$$

$$P_{\max} \geq P \tag{5.28}$$

The space available for the whole bearing could be specified by the maximum outer diameter, r_{oub}, and the maximum height, h_{tub}, which is available. Corresponding constraints could be expressed as

$$r_{oub} \geq r_o \tag{5.29}$$

and

$$h_{tub} \geq t_b + h_c \tag{5.30}$$

For a predefined load, the multi-objective optimization problem presented in the previous chapter has multiple optimum solutions, which are non-dominated called the Pareto-frontier. Most of deterministic techniques give a single solution. For the whole Pareto frontier to be generated, one has to run the same algorithm for several times. A multi-objective problem can be solved by single-objective genetic algorithms (SOGAs) by converting multiple objectives into a single one using a criterion such as the weighted-sum approach, but it also produces a single solution. Multi-objective genetic algorithms (MOGAs) attempt to generate the whole Pareto frontier in a single run. Hence the present problem is attempted to solve by MOGAs.

5.3.5 Multi-objective optimization tool

Classical multi-objective optimizing methods are mainly classified based on the knowledge and usage of the priority of objectives as *generating* and *preference-based* methods (Cohon, 1985). Generating methods generate a set of solutions for a particular problem, however, not the whole Pareto-frontier, while the preference based methods give out a single solution. *Generating* methods are further classified as the *no-preference* and *a-posteriori* methods.

The *no-preference* method uses a heuristic while the *a-posteriori* method uses a weighting vector. The *preference-based* methods are subdivided as the *a-priori* and *interactive* methods. The *a-priori* method uses preferential information of objectives, which do not change during the optimization process, where as the *interactive* method changes the priority of objectives during the optimization process based on results at the end of each iteration. However, all classical methods attempt to get a single solution or a few set solutions of the Pareto frontier and not the whole Pareto front in a single run.

Stochastic or population based methods such as multi objective genetic algorithms (MOGA) generate the Pareto frontier solutions in a single run. There are different MOGA tools available such as vector evaluated genetic algorithm (VEGA) (Schaffer, 1985), strength Pareto evolutionary algorithm (SPEA) (Zitzler and Thiele, 1999), non-dominated sorting genetic algorithm (NSGA) (Srinivas and Deb, 1993), Pareto archived evolutionary strategy (PAES) (Knowles and Corne, 2004), etc. Among these the non-dominated sorted genetic algorithm - II (NSGA-II) (Deb et al., 2002) a successor of NSGA is one of the widely used tools applied for many problems. It gives a group of solutions, which are classified based on the depth of the front to which a solution belongs. Final solutions optimize objective functions to different degrees maintaining diversity of solutions on the Pareto front (Raghuwanshi and Kakde, 2004).

5.3.6 Crowding selection operator

There are two goals in an MOGA to be met, (1) solutions converging to the Pareto-front and (2) a uniform distribution of solutions along the Pareto-front. The first goal is achieved by checking the dominance, and the second goal is achieved by checking the diversity of

individuals. NSGA-II takes both these goals into consideration, the first goal is achieved by grading individuals according to the non-domination rank, and the second goal is achieved by using a crowding distance for each individual.

Hence to check the dominance between two individuals (or solutions), the tournament selection operator for multi-objective optimization should take three issues into consideration namely the feasibility, the Pareto optimality, and the diversity. Between two solutions the feasible solution dominates the infeasible. Among two feasible solutions the one belonging to the front nearer to the Pareto front will dominate the other. Between two solutions belonging to the same front the one with higher crowding distance dominates the other.

All other operators namely the crossover, the mutation, and the elitism are same as explained for the single-objective genetic algorithm in Chapter 3.

5.4 Numerical simulations

As explained in the end of section 2.3 of Chapter 2, in the present case, the equality constraint of load to be supported is satisfied by determining the required current-densities and flux-densities. All other constraints are greater than or equal to type, and all constraints are treated to be hard (refer section 3.3.10 of chapter 3).

In the present section for a particular application, the design of the magnetic bearing has been optimised for multi-objective functions. A set of inputs required from the user for a particular application have been mentioned. Optimised bearing objective functions have been given in the form of Pareto front. For a typical comparison, results of the individual

objective functions have also been included. The sensitivity analysis has been performed of design variables on objective functions. The variation of different design parameters on the final optimized population is studied in order to have an understanding of the relationship of the optimized design parameters on different optimized values of objective functions.

5.4.1 Input Variables

The input should be given two parts namely the actuator input parameters and the GA input parameters. These input parameters are given in the following subsections.

Actuator input parameters: As explained in Section 2.3.2, design variables for the optimization of different elements of the actuator of AMTB include dimensions of the coil. Main constraints include the maximum allowable current-density to be supplied in the coil corresponding to a given load, the inner-radius of the bearing, and the air-gap.

Typical input parameters to be supplied by the user for particular application of the actuator of AMTB would be $[r_i, l_g, F, B_{sat}, \alpha_{\max}, \alpha_{\min}, J_{sat}, \eta, \gamma_s, \gamma_c, K_i, K_a, r_{o\max}, h_{i\max}, V_{\max}, P_{\max}]$. Correction factors K_i and K_a are considered to increase the model accuracy of the magnetic circuit (Groom et al., 2000). Table 4.1 (in Chapter 4) lists different input parameters chosen for the optimal design of actuator of AMTB in the present work.

GA input parameters: For the optimisation, SBX parameters namely the probability of the crossover p_c, the probability of the mutation p_m, the crossover distribution index η_c, and the mutation distribution index η_m are assumed to be 0.9, $1/n$, 5, and 10, respectively (Manos and Poladian, 2005); where n is the number of real variables, and $n = 3$ for the present problem. To have better understanding of behaviour of design variables with

respective to objective functions in the final optimized population, a population of 1000 is taken with 100 generations. GA parameters assumed for MOGA are given in Table 5.1. Objective functions are optimized at the operating point (Schweitzer et al., 2003) of the AMTB. Bounds on design variables chosen are given in Table 5.2.

Table 5.1 GA parameters assumed for the implementation of MOGA

Parameter	Value
Probability of crossover, p_c	0.9
Probability of mutation, p_m	1/3
Crossover distribution index, η_c	5
Mutation distribution index, η_m	10
Population size	1000

Table 5.2 Initial bounds on design variables

Design variables	r_{ci} (mm)	r_{co} (mm)	h_c (mm)
Lower limit	25.00	25.00	0.00
Upper limit	120.00	120.00	70.00

5.4.2 Optimized Geometries of the Bearing

Non-dominated sorting genetic algorithm - II (NSGA-II) developed by KanGAL (Kanpur Genetic Algorithms Laboratory) has been adapted in the present work. However the present work is carried using

- Object oriented programming concept using C++ language.
- C++ Classes have been used instead of structures used in C.
- The modular concept has been used for carrying out calculations of different functions and interactions between GA, actuator, controller and amplifier.

- Required additional functions have been developed for the post processing of the final population.
- MATLAB has been used for plotting the graphs.

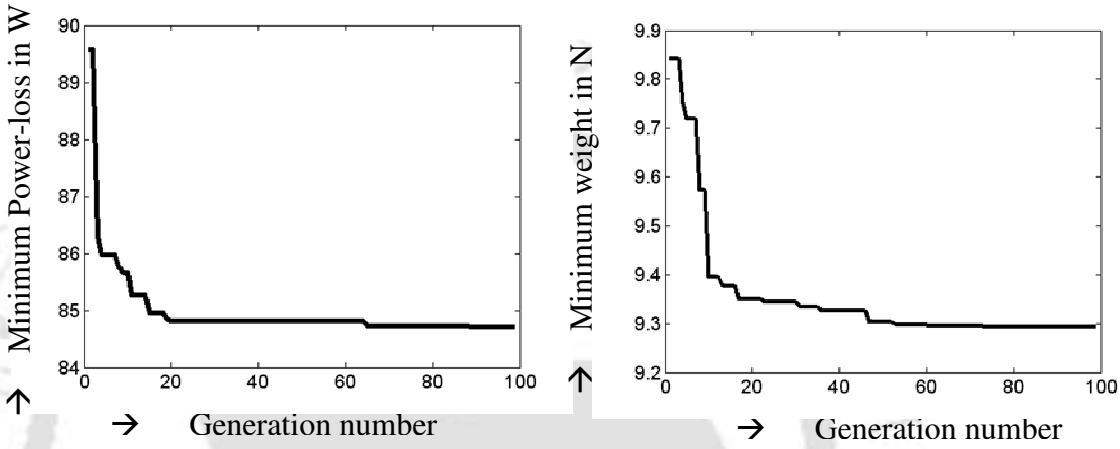

Figure 5.4 Convergence graphs of power-loss and weight

Two objective functions are considered for the optimum design of a magnetic bearing, namely, the minimization of the power-loss, P, which is given by equation (2.15), and the minimization of the weight W, which is given by equation (2.17). Convergence of the minimum weight and the minimum power-loss with the generation are plotted in Figure 5.4.

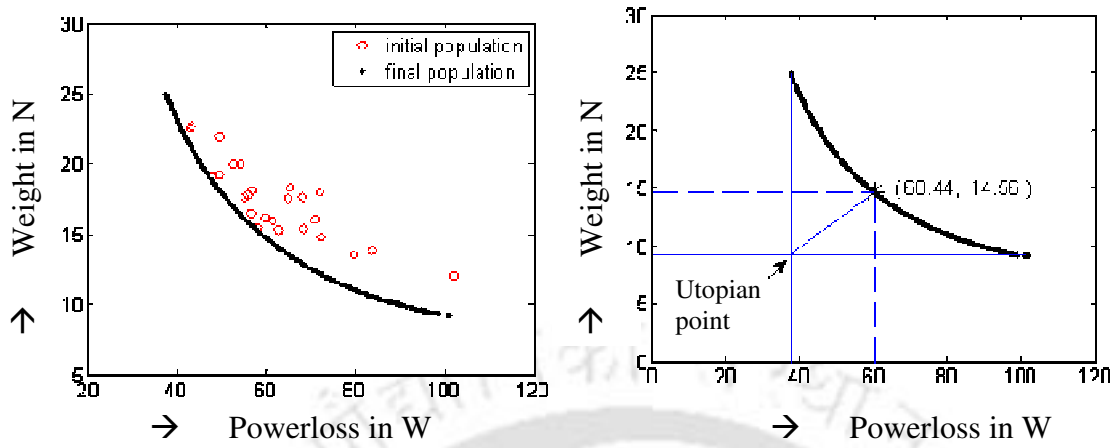

Figure 5.5 (a) The Pareto front of multi-objective optimization for the initial and final populations after 100 generations (b) A procedure to select an optimized bearing geometry from the Pareto front

The Pareto front of the present multi-objective optimization (i.e., the weight versus the power-loss) of the magnetic bearing for the initial and final populations after 100 generations is shown in Figure 5.5(a). The minimum and maximum values of the design vector in the final optimized solution and the theoretical feasible bounds on the design vector are given in Table 5.3. It could be noted that bounds obtained by GAs are within the range of theoretical bounds. Moreover, from Table 5.3, it could be observed that the optimum ranges (in the final population after 100 generations) on the inner radius, outer radius and height of the coil are 37.34%, 87.23% and 40.68% of feasible ranges, respectively. The optimum ranges of the inner and outer radii of the coil are near the lower limit of the feasible range and that of the height of the coil is near the upper limit.

Table 5.3 Bounds of the design variables

Design variables	Optimum bounds of design variables obtained*			Feasible bounds of design variables		
	r_{ci} (mm)	r_{co} (mm)	h_c (mm)	r_{ci} (mm)	r_{co} (mm)	h_c (mm)
Lower limit	44.9137	67.2439	39.0924	44.9137	66.0488	16.6610
Upper limit	57.2567	109.1159	54.4848	77.9671	114.0518	54.5013

*In the final population after 100 generations.

The decision making could be done on the basis of '*a priori*' or '*a posteriori*' approach (Rachmawati and Srinivasan 2006, Carlyle, et al., 2001). In an '*a priori*' or '*interactive*' approach one needs the prior knowledge of trade-offs for taking a decision. Hence the designer can directly end up with the specified design choice by guiding or navigating the search direction. Instead in an '*a posteriori*' approach the designer need not have a prior knowledge of trade-offs for taking a decision. Different designs are generated as a Pareto-frontier and the designer can take a decision of choice depending on different trade-offs generated. In the present paper '*a posteriori*' approach is used for making a choice and is explained as follows.

It should be noted that the final population gives the best minimum bearing weights corresponding to different values of the power-loss and vice versa, thus each design is a best one in its own sense. The utopia point (Gurnani, et al., 2005) is the point corresponding to the minimum values of the individual objective functions on the Pareto frontier space as shown in Figure 5.5(b). For a comparison of optimized geometries of the magnetic bearing, a typical choice of the solution is taken as the nearest normalized distant member from the utopia point in the Pareto front of the final optimised population as shown in Figure 5.5(b). The minimum normalized weighted distance from the utopia point is expressed as

$$\zeta = \sqrt{\left(\varepsilon_1 \frac{P - P_{\min}}{P_{\max} - P_{\min}}\right)^2 + \left(\varepsilon_2 \frac{W - W_{\min}}{W_{\max} - W_{\min}}\right)^2} \tag{5.31}$$

where ε_1 and ε_2 are multiplicative constants of objective functions considered while calculating the minimum distant member. P and W are values of objective functions (i.e., the power-loss and the weight, respectively) of a member in the final population, considered for calculating the distance. $P_{\min}$ and $W_{\min}$ are minimum values of individual objective functions corresponding to the utopia point in the final population from which the distance

is calculated for each member. P_{max} and W_{max} are maximum feasible values of individual objective functions in the final population. With $\varepsilon_1 = 0$, the minimum weight of the bearing will be resulted, and for $\varepsilon_2 = 0$ the minimum power-loss will be resulted; whereas $\varepsilon_1 = \varepsilon_2$ gives equal weights for both objective functions. With $\varepsilon_1 = \varepsilon_2$ the selected design, which is shown in Figure 5.5(b), has a power-loss of 60.44 W with a weight of 14.556 N. Geometries of different designs chosen from the best population are summarized and compared in Table 5.4.

For the case of minimum weight (i.e., row 1 of Table 5.4), which is obtained by using $\varepsilon_1 = 0$, from the final population the minimum pole-face area of the air-gap and the cross sectional area of the coil is achieved. In the case of minimum power-loss (i.e., row 2 of Table 5.4), which is obtained by using $\varepsilon_2 = 0$, the maximum available thickness and height of the coil are chosen and the maximum available cross sectional area of the coil is achieved. The maximum available dimension of the height and outer radius of the bearing are achieved. As compared to the case of the minimum weight there is an increase in the inner-wall thickness and the pole-face area of the air-gap. The magnetic flux-density also decreases for the same reason according to equation (2.11). Dimensions of the coil are chosen according to the pole-face area of air-gap and the cross-sectional area of the coil that minimize of the power-loss.

Table 5.4 Optimized bearing geometries in the final optimized population through the multi-objective optimization

Objective functions*	Input variables			Design variables			Dependant variables						Cross sectional areas		Volumes		Performance parameters at the operating point			
	r_i (mm)	l_g (mm)	F (N)	r_{ci} (mm)	r_{co} (mm)	h_c (mm)	r_o (mm)	t_i (mm)	t_c (mm)	t_o (mm)	t_b (mm)	h_t (mm)	A_g (mm^2)	A_c (mm^2)	V_c (cm^3)	V_s (cm^3)	J (A/mm^2)	B (T)	P (W)	W (N)
1	25.00	4.00	2025	44.93	75.87	39.09	84.56	19.93	30.94	8.69	15.51	54.60	4380.7	1209.5	459.06	660.64	3.63	0.762	102.80	9.22
2	25.00	4.00	2025	57.74	109.0	47.73	119.9	30.74	53.34	10.83	22.26	69.99	7797.8	2545.9	1318.28	1706.5	1.29	0.571	37.42	25.00
3	25.00	4.00	2025	48.14	83.34	52.40	92.94	23.14	35.19	9.60	17.58	69.98	5318.3	1844.0	761.69	999.90	2.16	0.691	60.44	14.55
4	25.00	4.00	2025	44.91	–	–	–	19.91	–	–	15.50	–	4373.7	1209.3	–	–	3.63	0.762	–	–

*1→ Minimum weight, 2→ Minimum power-loss, 3→ Minimum normalized weighted distance from least values of both the objective functions, 4→ Theoretical minimum values required supporting the given load with given constraints of the flux and current densities as explained in section 4.4

Table 5.5 Optimized bearing geometries through single objective optimization

Objective functions*	Input variables			Design variables			Dependant variables						Cross sectional areas		Volumes		Performance parameters at the operating point			
	r_i (mm)	l_g (mm)	F (N)	r_{ci} (mm)	r_{co} (mm)	h_c (mm)	r_o (mm)	t_i (mm)	t_c (mm)	t_o (mm)	t_b (mm)	h_t (mm)	A_g (mm^2)	A_c (mm^2)	V_c (cm^3)	V_s (cm^3)	J (A/mm^2)	B (T)	P (W)	W (N)
1	25.00	4.00	2025	44.91	75.45	39.60	84.17	19.91	30.54	8.72	15.50	55.10	4372	1209.3	457.29	660.8	3.63	0.76	102.60	9.21
2	25.00	4.00	2025	69.13	100.00	50.00	118.97	44.13	30.87	18.97	30.04	80.04	13050	1543.5	820.00	2582.4	1.65	0.44	37.85	27.37

*1→ Minimum weight, 2→ Minimum power-loss

5.4.2.1 Comparison of Results from MOGAs and SOGAs

Results obtained by using the single-objective genetic algorithm, for the same application, are reproduced in Table 5.5 for comparison. On comparing corresponding first rows (i.e., for the minimum weight) and second rows (i.e., for the minimum power-loss) of Table 5.4 and Table 5.5, it can be observed that results obtained by the multi-objective optimization and the single-objective optimization are very close. A slight domination of SOGA results over MOGA could be observed in the minimum weight case, while results of the MOGA dominated that of the SOGA in the minimum power-loss case. These variations (though small) can be perceived because of the variation between the MOGA and the SOGA in the sorting process (i.e., the non-domination is defined for the present case by two objectives in the MOGA while in the SOGA, it is the single objective), and the selection for the crossover and the mutation. By these, the search direction could change to a better or inferior solution. The MOGA takes the effect of both the objectives and may lose the Pareto optimum solutions to maintain a good spread, while the SOGA takes the account of only one objective ignoring the effect of other and has more probability of ending up in a local optima (Hisao et al., 2006, Tsutomu et al., 2006, Martorell et al., 2004). Based on these characteristics modified hybrid algorithms involving combination of the SOGA and the MOGA was suggested by Hisao et al. (2006).

5.4.2.2 A Typical Choice of an Optimum Design

A typical choice of an optimum design nearest to the utopia point in the Pareto front of the final population is shown in the third row of Table 5.4 for a comparison. Optimized magnetic bearing dimensions for objective functions are shown in Figure 5.6. It could be

observed that dimensions lie in between the minimum power-loss and the minimum weight cases. From Figure 5.5(a) and Figure 5.5(b), it could be observed that the power-loss and the weight are two conflicting quantities, characterizing a decrease in the power-loss causes an equivalent increase of the weight of bearing.

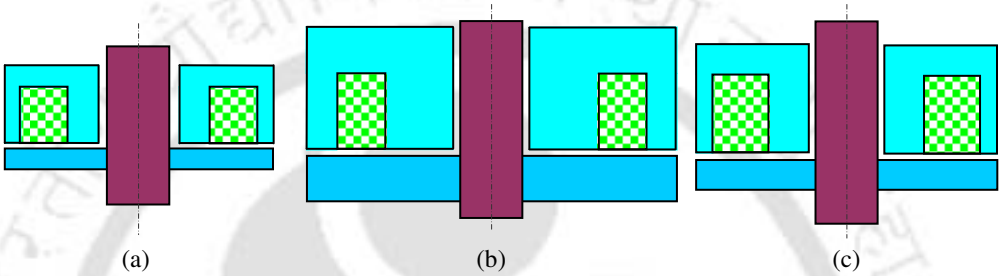

Figure 5.6 Optimized magnetic bearing geometries for the objective function as (a) Minimization of overall weight (b) Minimization of power-loss (c) Minimum normalized weighted distance of the objective functions namely the minimization of power-loss and the minimization of weight

When observed the typical multi-objective function optimum design of the minimum normalized distant member (e.g., the third row of Table 5.4) an increase of 35.92 percent in the power-loss generated a decrease of 64.34 percent in the weight, where the percentage of change is determined according to the following formula

$$\text{Percent of change of the quantity considered} = \frac{x - x_{\min}}{x_{\max} - x_{\min}} 100 \qquad (5.32)$$

where x represents the quantity (i.e., the power-loss or weight) considered. $x_{\max}$ and $x_{\min}$ are the maximum and minimum values of corresponding quantities in the cases of minimum weight (i.e., the first row of Table 5.4) and minimum power-loss (i.e., the second row of Table 5.4).

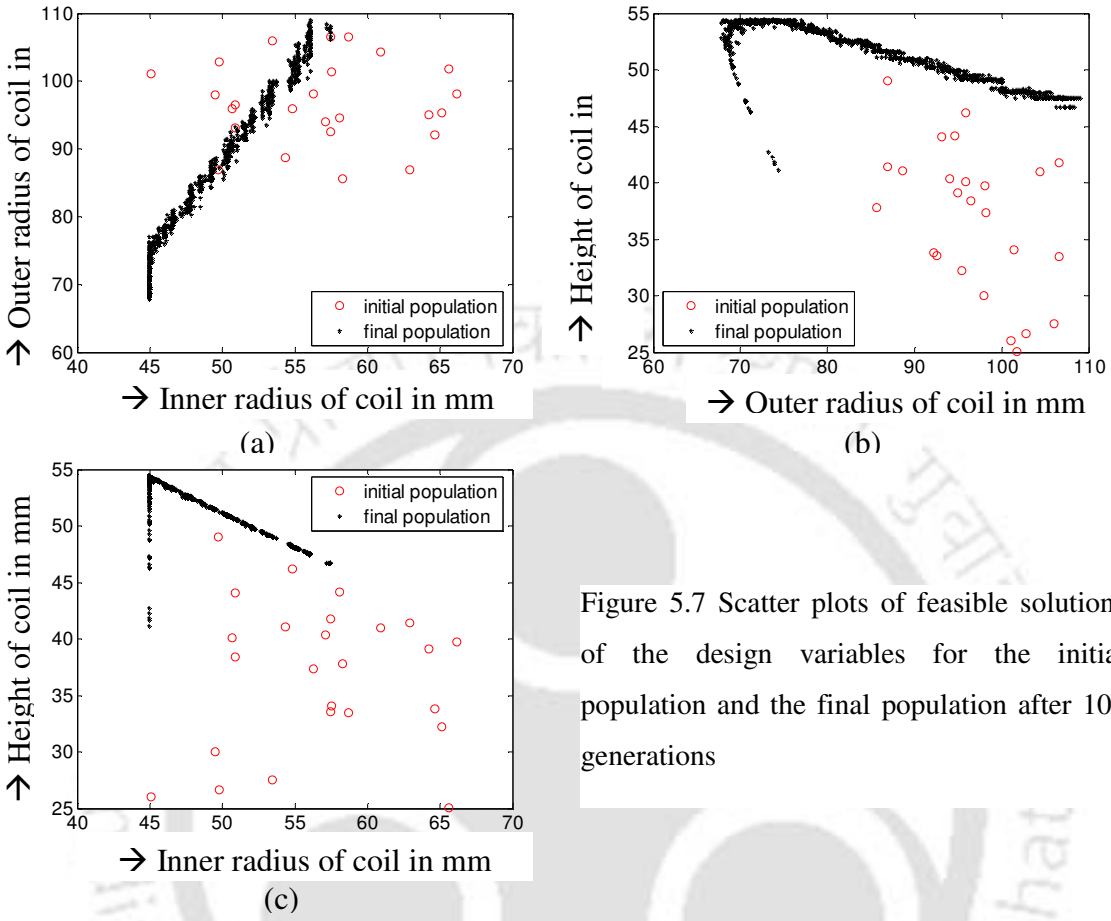

Figure 5.7 Scatter plots of feasible solutions of the design variables for the initial population and the final population after 100 generations

Figure 5.7(a, b, and c) show the scatter plots of design variables in pairs that are feasible in the initial and final (i.e., after 100 generations) populations. The convergence of design variables from the choice of initial population to the final population, which represent the optimum edges of the design variable space, could be observed.

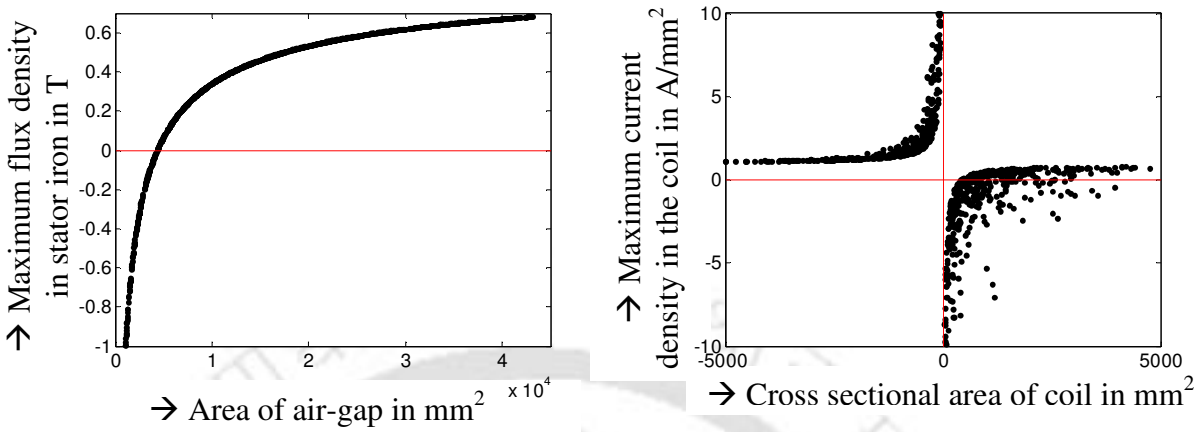

Figure 5.8 Constraint violation plots of the initial population at designed load.
(a) Maximum flux density versus area of air-gap
(b) Maximum current density versus cross-sectional area of coil

Figure 5.8(a) and (b) show the constraint violation of the magnetic flux-density in the stator iron and the current-density in the coil, respectively. Constraints considered are implemented as greater than or equal to zero type. Hence, all points that lie on negative side are violating constraints. From the fourth row of Table 5.4 and Figure 5.8(a), it can be observed that the pole-face area of air-gap cannot be feasible below 4373.7 mm^2 as the design fails to satisfy the constraint of the magnetic flux-density for supporting the given load (i.e. the maximum magnetic flux-density in the stator-iron is more than the allowable flux-density). This is due to the fact that the flux density in the stator-iron required to support a specified load is a function of only pole-face area of the air-gap as in equation (2.25). Moreover, the pole-face area of air-gap is a function of only the inner radius of the coil as in equation (5.3). In Figure 5.8(b) the constraint violation could be observed in two ways. The first violation is due to the higher value of the inner radius of coil than its outer radius (i.e., area of coil becomes negative). The second violation is due to the maximum current-density is more than the allowable current-density in the coil.

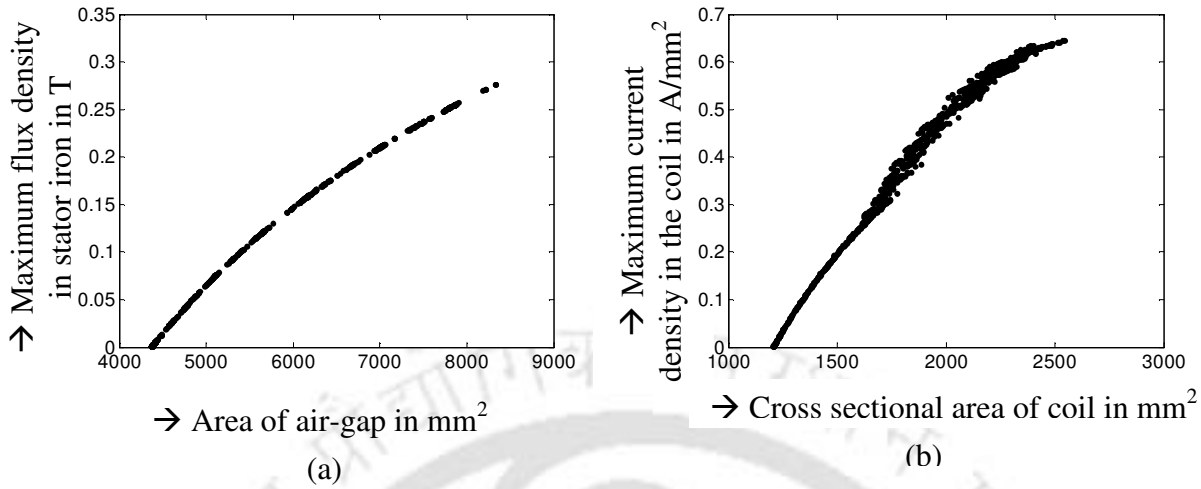

Figure 5.9 Constraint violation plots of the final population after 100 generations at designed load.
(a) Maximum flux density versus area of air-gap
(b) Maximum current density versus cross sectional area of coil

Constraint violation plots in the final population (i.e., after 100 generations) are shown in Figure 5.9. Constraints used are greater than or equal to type, and as all the values are above zero in the vertical-axis all the solutions are feasible solutions. The vertical-axis shows the saturation of flux-density in the stator-iron or coil current-density.

5.5 Sensitivity Analysis

A change in value of objective functions and dependant variables has been studied with respect to a small change in values of different optimised design variables. Table 5.6 shows sensitivities of objective functions and dependant variables with respect to perturbation of 1% in design variables. The sensitivity of any function $f(z)$ can be derived from Taylor's series as

$$\frac{f(z+\Delta z)-f(z)}{f(z)}=\frac{f'(z)\Delta z}{f(z)} \tag{5.33}$$

The perturbation is done on the optimized design obtained by choosing $\varepsilon_1 = \varepsilon_2$ in equation (5.31). Orders of percentages of deviations of different dependant variables, cross-sectional areas, the magnetic flux and current densities, and objective functions with perturbations on individual design variables and their combination are shown in Table 5.6. The third row of Table 5 gives design values about which perturbations are applied. Cases 1 to 3 show percentages of deviation for the perturbation on individual design variables. Cases 4 to 6 show percentages of deviation for the perturbation on combination of two design variables. Case 7 shows the percentage of deviations with the perturbation on all three design variables, simultaneously.

It can be observed from cases 1 to 3 of Table 5.6 that all three design variables influence both objective functions but the effect of the outer radius of coil on objective functions is nearly double that of the inner radius of coil or height of the coil. Case 6 shows the combination of inner radius of coil and height of coil is less than that of other two cases 4 and 5, which shows the effect of perturbation of the outer radius of coil on the objective functions is dominant than the other two.

Though these results do not convey any qualitative information, these results can be utilized when tradeoffs between different parameters are considered the designer can work with the design variables namely the height, inner radius and outer radius of the coil. The analysis is useful in critical conditions (i.e., at the boundaries of constraints) where a small variation is a major issue. When small tolerances are considered by the designer, these tradeoffs can be taken into consideration. However when the actuator does not work in critical conditions (i.e., at the boundaries of constraints) the results show that there will not be major changes in performance with changes of small tolerances.

Table 5.6 Sensitivity analysis of optimized bearing geometries of a chosen design*

% deviations on design variables			% deviations on dependant variables					% deviations on cross sectional areas		% deviations on flux and current densities at the operating point		% deviations on objective functions at the operating point	
r_{ci}	r_{co}	h_c	r_o	t_i	t_c	t_o	t_b	A_g	A_c	J	B	P	W
1.000	0.000	0.000	0.269	2.080	-1.368	2.606	1.735	2.752	-1.368	0.020	-1.348	-0.967	0.899
0.000	1.000	0.000	0.805	0.000	2.368	-0.889	0.000	0.000	2.368	-2.313	0.000	-1.694	1.818
0.000	0.000	1.000	0.000	0.000	0.000	0.000	0.000	0.000	1.000	-0.990	0.000	-0.990	0.764
1.000	1.000	0.000	1.072	2.080	1.000	1.697	1.735	2.752	1.000	-2.325	-1.348	-2.678	2.724
0.000	1.000	1.000	0.805	0.000	2.368	-0.889	0.000	0.000	3.392	-3.280	0.000	-2.667	2.596
1.000	0.000	1.000	0.269	2.080	-1.368	2.606	1.735	2.752	-0.382	-0.970	-1.348	-1.948	1.666
1.000	1.000	1.000	1.072	2.080	1.000	1.697	1.735	2.752	2.010	-3.292	-1.348	-3.642	3.506

* Taken from the third row of Table 5.4 with 1% perturbation on individual design variable

Table 5.7 The influence of design variables on different dependant parameters

Design variables	Dependant variables					Areas		Volumes		Densities		Objectives	
	r_o	t_i	t_c	t_o	t_b	A_g	A_c	V_s	V_c	J	B	P	W
r_{ci}	✓	✓	✓	✓	✓	✓	✓	✓	✓	✓	✓	✓	✓
r_{co}	✓	×	✓	✓	×	×	✓	×	✓	✓	×	✓	✓
h_c	×	×	×	×	×	×	✓	✓	✓	✓	×	✓	✓

From case 2 of Table 5.6, it can be observed that the outer radius of the coil has no effect on the inner-wall thickness, the back-wall thickness, and the pole-face area of the air-gap; it is because they are function of the inner radius of the bearing and the inner radius of the coil. It can be observed from case 3 of Table 5.6 that the height of the coil has no effect on dependant variables but it depends only on the cross-sectional area of the coil. The only effect of the height of the coil on objective functions is due to the change in the cross-sectional area of the coil. From cases 1, 4, 6 and 7 of Table 5.6; the magnetic flux-density could be observed to be the function of only the inner radius of the coil. Cases 2, 3 and 5 of Table 5.6 show that the outer radius and height of coil do not affect the magnetic flux-density. This is due to the fact that the magnetic flux-density is a function of only the load and the pole-face area of the air-gap. Moreover, it is observed that sensitivities are dependent on the point of design space at which sensitivities are determined. The influence of different variables of design vector on different parameters is summarized in Table 5.7.

5.6 Pareto Optimal Design Analysis on the Final Population

The final optimized population is a set of the best solutions, each in their own sense. The variation of different design parameters of the final optimized population with respect to the corresponding power-loss and weight has been studied in this section. Plots are generated for different design variables versus the power-loss or the weight of the final population. Generally large population size in GA necessitates high complexity in carrying GA operators. But in the present case we can find an advantage of using a large population. We do not have closed form solutions for how the optimised population behaves in respect of

different performance parameters of Pareto optimal systems. Hence, these performance parameters could be studied by using large population sizes. Different quantities could be plotted discretely and observe how the Pareto optimal system behaves in respect of different performance parameters. This allows us to fit behaviours of different parameters of the Pareto optimal systems and based on the pattern we can even take proper design choices. The analysis is explained in following paragraphs.

Plots of the variation of different performance parameters in the final population with respect to the power-loss have been provided in Figure 5.10 and Figure 5.11. From Figure 5.10 and Figure 5.11, it could be observed that there are two distinct points namely, the point of saturation of the magnetic flux-density (i.e., point A in Figure 5.10 and Figure 5.11) and the point of saturation of the coil current-density (i.e., point B in Figure 5.10 and Figure 5.11). Hence, the whole analysis of optimized results can be separated into three zones, i.e., prior to A, between A and B, and beyond B. From Figure 5.10(a) and (b), it is observed that prior to the saturation of the magnetic flux-density of the iron, the coil current-density and the magnetic flux-density are chosen in a range (i.e., the number of choices are more) such that they optimize the power-loss and the weight. Once the magnetic flux-density is saturated (i.e., point A) as shown in Figure 5.10(a), the magnetic flux-density is constant with the increase in the power-loss. From Figure 5.10(b) after point A, the increase in the power-loss is accompanied by the increase in the current-density, which linearly increases up to its saturation limit (i.e., point B of Figure 5.10(b)). Beyond point B, the current-density is constant with the increase in the power-loss.

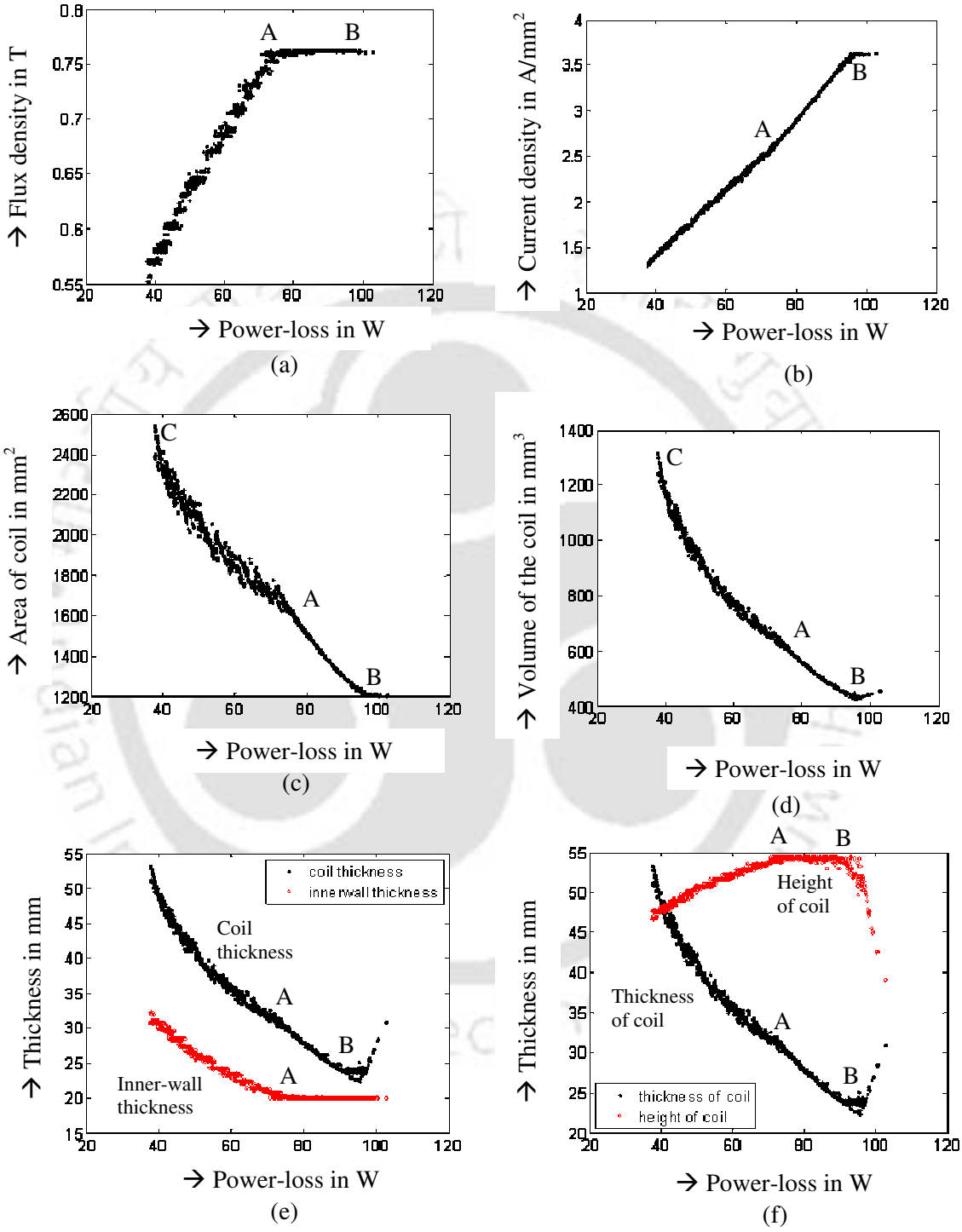

Figure 5.10 The variation of different quantities in the optimized final population at the designed load

(a) Flux density versus power-loss
(b) Current density versus power-loss
(c) Area of coil versus power-loss
(d) Volume of coil versus power-loss
(e) Thickness versus power-loss
(f) Thickness versus power-loss

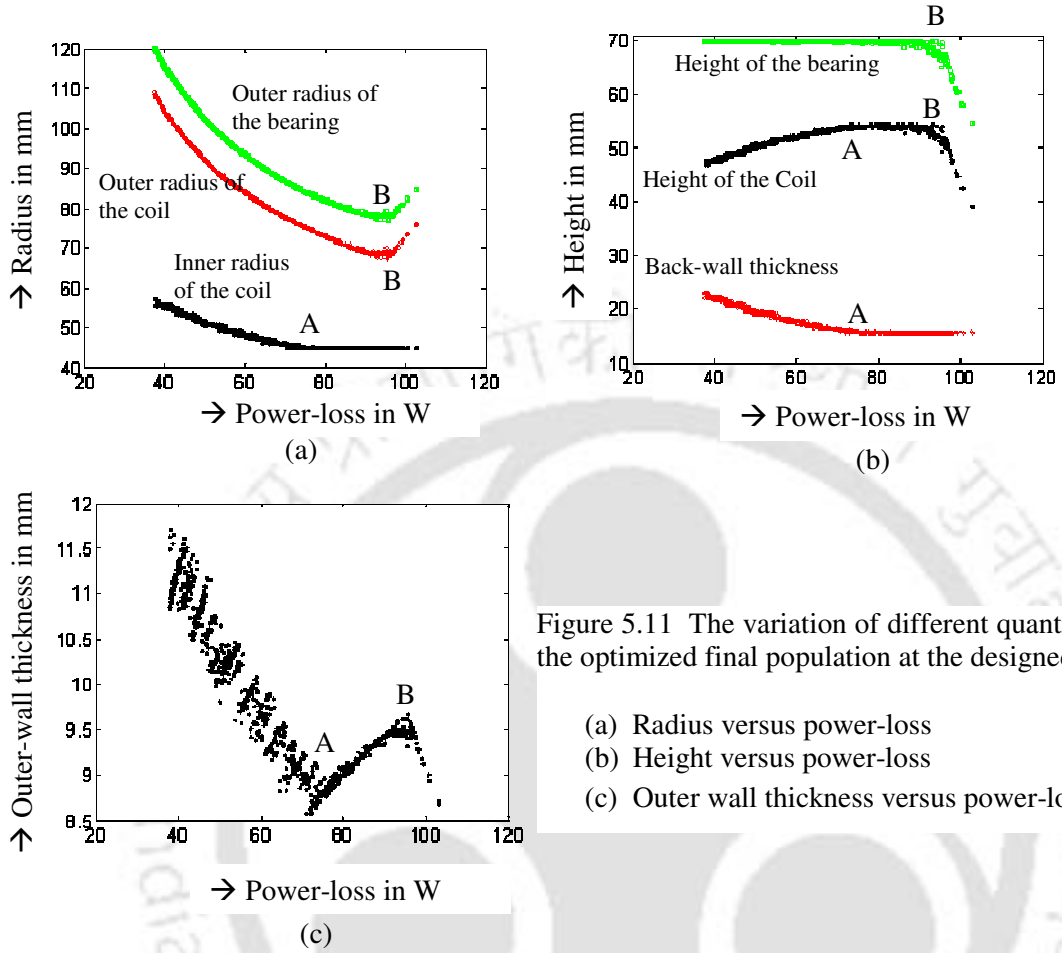

Figure 5.11 The variation of different quantities in the optimized final population at the designed load.

(a) Radius versus power-loss
(b) Height versus power-loss
(c) Outer wall thickness versus power-loss

As shown in Figure 5.10(c and d), the cross-sectional area and the volume of the coil decreases with the power-loss to a minimum limit, i.e., till the saturation limit of the current density is reached. Between points C and A of Figure 5.10(c), solution points are more scattered than between points A and B. Beyond point B the area of the coil becomes constant with the increase in the power-loss as the current-density in the coil becomes saturated. The volume of the coil as shown in Figure 5.10(d), shows similar trends as the area of cross-section before point B, but after point B the volume increases with the increase in the power-loss. This could be justified from equation (2.15), that at a constant current-density the increase in the power-loss is solely due to the increase in the volume of the coil.

Graphs of the coil thickness and the inner-wall thickness versus the power-loss are shown in Figure 5.10(e). The inner-wall thickness decreases with the increase in the power-loss till the saturation of magnetic flux-density at the power-loss corresponding to point A occurs as in Figure 5.10(e) and then remains constant. The constant inner-wall thickness corresponds to the minimum pole-face area of air-gap required for the magnetic saturation flux-density to support the designed load, which could be observed from equation (2.25). The coil thickness decreases till point B, which corresponds to the power-loss of the saturation of coil current-density. After point B the coil thickness increases with increase in the power-loss.

Graphs of the height of the coil and the thickness of coil versus the power-loss are shown in Figure 5.10(f). The height of coil increases till the saturation of flux-density occurs (i.e., point A). This constant value is the maximum available height of coil by subtracting the back-wall thickness from the maximum total height according to equation (5.30). Once the magnetic flux-density is saturated, as the height of the coil is constant and the thickness of coil reduces further to a minimum value till the coil current-density is saturated (i.e., Point B). After point B the height of the coil decreases while the thickness of coil increases with further increase in the power-loss as in Figure 5.10(f). Reasons of this effect could be explained as follows. When the magnetic flux-density reaches the saturation value, the pole-face area of air-gap becomes constant (which is the minimum feasible) and the area of the coil reduces till the current-density reaches the saturation value, with the increase in the power-loss. It can also be observed from equation (2.15) that with the constant current-density, the power-loss increases with the increase in the volume of the coil. Moreover, as the volume increases with the power-loss also increases on keeping the area of the coil constant at the minimum. This is the minimum required area of the coil below which it

cannot be taken for supporting a given load and a saturation current-density. The only way of increasing the volume is by keeping the area of the coil constant, while increasing the thickness of the coil and decreasing the height of coil. Thus the thickness of the coil increases while the height of the coil decreases (proportionately to maintain the area constant), which results in increase in the volume after the saturation of current-density, and it is observed form Figure 5.10(f).

In the whole process, the power-loss increases with the decrease in the weight. Thus the volume of the coil decreases with the increase in the power-loss. But after point B, as the volume of the coil increases with the volume of the stator-iron decreases, which causes a decrease in weight of the bearing and increase in the power-loss. However, percentages of changes are more for the power-loss than that of the weight.

From Figure 5.11(a), it can be observed that once the magnetic flux-density saturation occurs, the pole-face area of air-gap remains constant but the coil thickness decreases thus the outer radius of the coil decreases with the increase in the power-loss. Hence, the outer-wall thickness increases to maintain the area of air-gap at the outer-pole to be equal to the constant minimum pole-face area of air-gap. Once the saturation of current-density occurs, the inner radius of coil increases and the thickness of the outer-wall decreases proportionately, to maintain the pole-face area of the air-gap at the outer pole to be constant.

From Figure 5.11(b), it could be observed that the height of the bearing is always equal to the maximum allowable height of the bearing till the saturation of the current-density occurs. Till saturation of the magnetic flux-density occurs (i.e., point A), the back-wall thickness decreases with the power-loss and the height of the coil increases to a maximum value during the same region as in Figure 5.11(b). From equation(5.3), the back-wall

thickness depends only on the pole-face area of air-gap. Hence, we can conclude that once the back-wall thickness is found, the height of the coil is chosen such that, the maximum allowable height of the bearing is achieved. Thus, till the saturation of the magnetic flux-density occurs (i.e., point A), the back-wall thickness decreases with the power-loss. As the pole-face area of air-gap decreases the power-loss increases till the saturation of the magnetic flux-density occurs. Consequently, the height of the coil increases proportionately till the saturation of the magnetic flux-density occurs.

Once the saturation of the magnetic flux density occurs the pole-face area of air-gap becomes constant and the back-wall thickness, and thus the height of the coil become constant till the saturation of the current-density occurs. As the cross-sectional area of the coil decreases, with the power-loss the thickness of the coil decreases continuously and thus the outer radius of the coil decreases. If we observe the variation of outer-wall thickness with respect to the power-loss shown in Figure 5.11(c), till the saturation of the magnetic flux-density occurs, the outer-wall thickness decreases as the pole-face area of air-gap decreases.

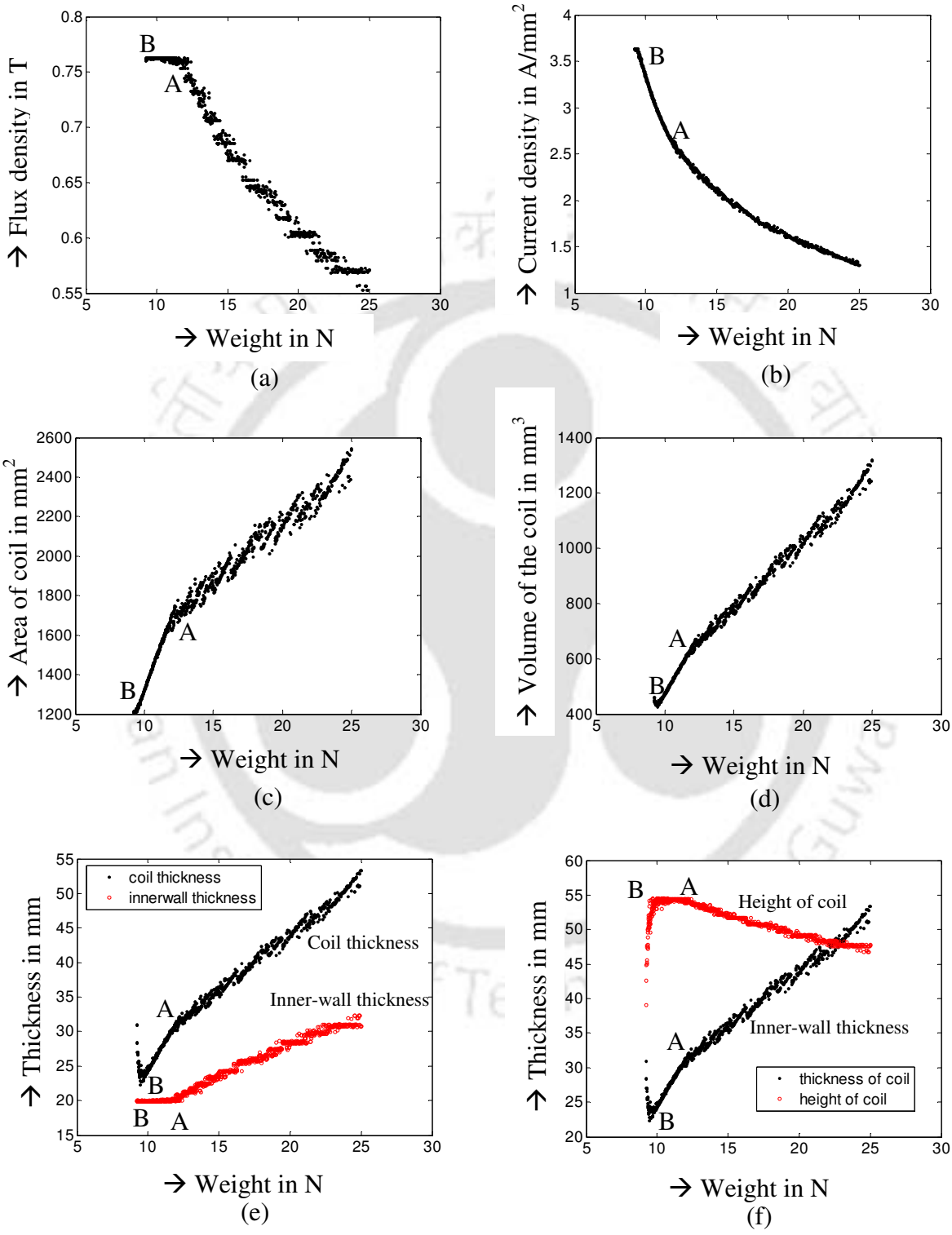

Figure 5.12 The variation of different quantities in the optimized final population at the designed load.

(a) Flux density versus weight (b) Current density versus weight
(c) Area of coil versus weight (d) Volume of coil versus weight
(e) Thickness versus weight (f) Thickness versus weight

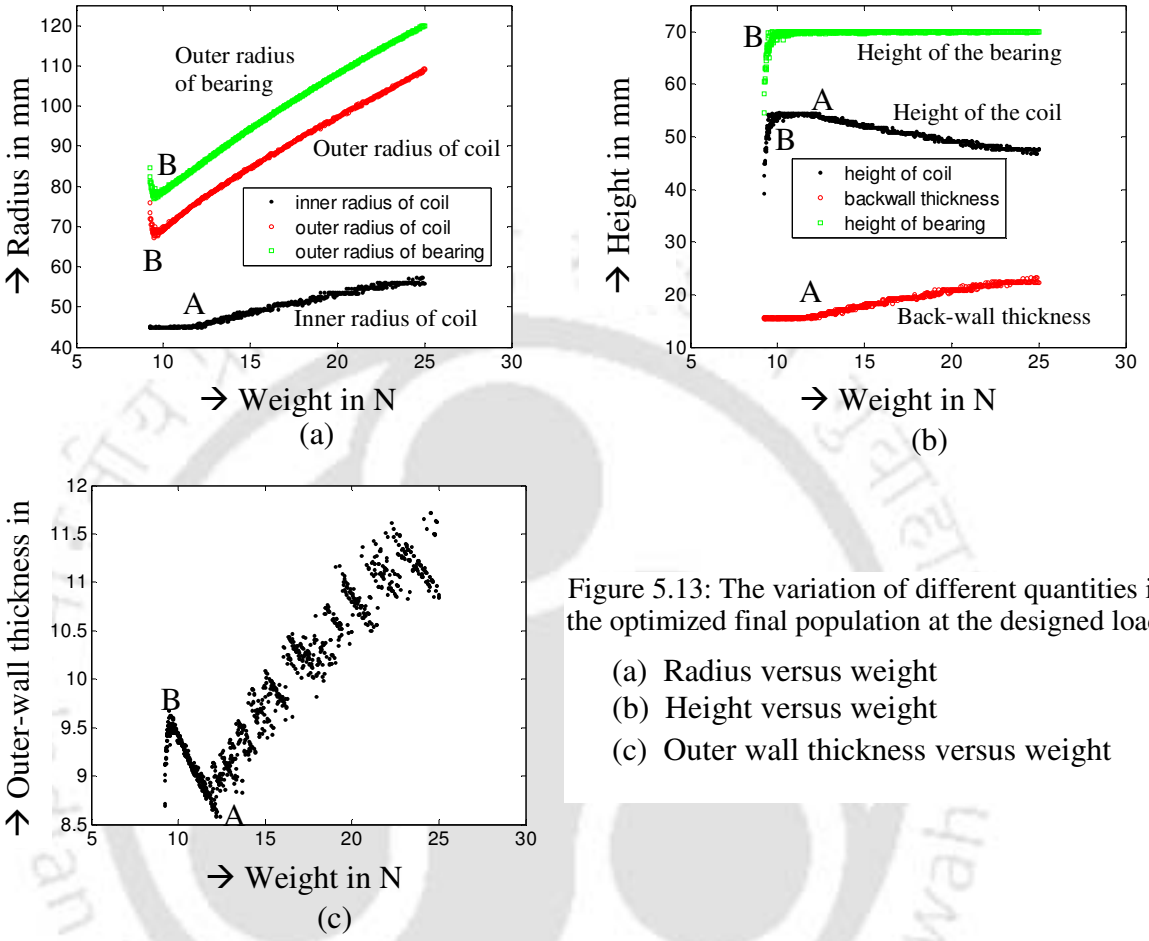

Figure 5.13: The variation of different quantities in the optimized final population at the designed load.

(a) Radius versus weight
(b) Height versus weight
(c) Outer wall thickness versus weight

Similar to Figure 5.10 and Figure 5.11, which are plotted with respect to the power-loss, the corresponding plots with respect to the weight of the bearing are shown in Figures 14 and 15. It could be observed that Figure 5.12 and Figure 5.13 are nearly mirror images of plots in Figure 5.10 and Figure 5.11, respectively. This is due to the fact that the weight and the power-loss are mutually inversely related quantities, which is observed from the Pareto front in Figure 5.5.

5.7 Conclusions

In the present chapter, the optimal design of actuators of AMTB using MOGAs has been carried out. Mathematical models of objective functions and associated constraints have been presented and discussed. Two objectives have been considered, namely, the minimizing the power loss and minimizing the weight of the bearing. The inner and outer radii of the coil, and the height of the coil have been proposed as design variables based on their dependency on objective functions. The method of implementation of the multi-objective genetic algorithm for the problem considered has been described. Geometries of designs with optimal individual objectives and a chosen design from the optimal Pareto front based on the minimum normalized distance criterion are compared in drawings and tables. The sensitivity analysis is carried out with respect to a small perturbation of dimensions of design variables. It is observed that the effect of outer radius of coil is nearly double than the other two design variables. However, overall objective functions were insensitive for small perturbations.

A novel Pareto optimal design analysis has been introduced to study the behavior of final optimized population designs of AMTB actuator systems by using large population size. By the analysis on the final population, the saturation of magnetic flux-density and coil current-density are observed to be the salient points, where the major changes occur in the behavior of different design parameters in the final population. On the whole, the present work gives a direction to choose the proper design options for different applications based on the a-posteriori knowledge provided by the final population. The methodology could be implemented to the optimal design of different types of magnetic bearings with permanent magnets and with integration of differential control as well and will be implemented in the subsequent chapters.

Chapter 6
Optimum Design & Analysis of Hybrid Magnetic Thrust Bearings Using Multi-Objective Genetic Algorithms

6.1 Introduction

The design optimization of the actuator of a *hybrid magnetic thrust bearings* (HMTB) is carried out using multi-objective evolutionary algorithms (MOGAs) and compared with the case of *active magnetic thrust bearings* (AMTB). Different aspects of MOGA implementations have been discussed in Chapter 5. In Chapter 4 we used single-objective genetic algorithms (SOGA), for the optimization of power-loss and overall weight (one at a time) of the actuator for AMTB and HMTB, respectively. Subsequently, in Chapter 5 we implemented multi-objective genetic algorithms (MOGAs) for the multi-objective optimization of AMTB with the power-loss and the weight as the minimization type of

objective functions, simultaneously. However permanent magnets were not included in the study. At this point, it would be interesting to analyze, the optimal design of the HMTB (with permanent magnets) in comparison with the AMTB (with pure electro-magnets) while optimized by using MOGAs.

In the present chapter using MOGAs, the optimization of *hybrid magnetic thrust bearings* (HMTB) for supporting axial loads has been carried out. Two objective functions, namely the minimization of power-loss and the minimization of weight, are considered for the case of HMTB and compared with the AMTB. Inclusion of permanent magnets leads to remodeling of the problem as compared to the pure electro-magnetic bearings. Geometries of the thrust magnetic bearing are provided in Section 2.2 of Chapter 2. An optimization mathematical model of objective functions and constraints common for both AMTB and HMTB has been presented in section 2.3 of Chapter 2, and the implementation algorithm has been detailed in Chapters 3 and 4. A standard form of the multi-objective optimization problem of the present work and corresponding objective functions and constraints involved are summarized in Tables 2.4 and 2.5, respectively. Hence, discussion of results and conclusions of the present design optimizations are detailed in following sections.

6.2 Results and discussions

Different elements of the magnetic bearing (namely the coil, the bias magnet, and the stator-iron) are to be optimized for the tradeoffs namely the power-loss and weight of the actuator. The current-density to be supplied in the coil for a given load depends on the inner radius of the bearing and the air gap. The weight density of copper is higher than that of iron or permanent magnets, so it tries to take lesser space for the copper to minimize the weight of

the bearing. However, as the reduction in the volume of copper increases the power-loss, hence the optimum volume for the copper is chosen.

6.2.1 Input Variables

The input is given in two modules namely the actuator analysis module of HMTB and the genetic algorithm module. These parameters are detailed in following paragraphs.

Actuator input parameters: As explained in Section 5.6.1, the input to the algorithm includes the constraints on quantities such as the load, the inner radius of bearing, etc. and material properties such as the saturated magnetic flux-density, the saturated current-density, etc. As discussed in Section 2.3.2, the design vector for the optimization of actuator of the HMTB includes dimensions of the coil. Main constraints include the maximum allowable current-density to be supplied in the coil corresponding to a given load, the inner radius of the bearing and the air-gap.

Typical input parameters to be supplied by the user for particular applications would be $[r_i, l_g, F, B_{sat}, \alpha_{\max}, \alpha_{\min}, J_{sat}, \eta, \gamma_s, \gamma_c, \gamma_m, K_i, K_a, K_f, r_{o\max}, h_{t\max}, l_{m\max}, V_{\max}, P_{\max}]$. Correction factors K_i, K_a and K_f are considered to increase the model accuracy of the magnetic circuit (Groom et al., 2000). Table 3 lists different input parameters chosen (Groom and Bloodgood, 2000) for the optimal design of thrust magnetic bearings in the present work. Different input parameters assumed for the actuator have been given in Table 4.1 of Chapter 4.

GA input parameters: GA input parameters assumed for the MOGA include bounds on design variables, constants of the crossover and mutation operators, the population size, the number of generations, etc. For the optimization, parameters of the crossover and the mutation; namely the probability of the crossover p_c, the probability of the mutation p_m, the crossover distribution index η_c, and the mutation distribution index η_m are empirically assumed to be 0.9, $1/n$, 5, and 10, respectively, where n is the number of real variables, and n = 3 for the present problem. To have a clear study of different operating parameters with tradeoffs, a population of 1000 is taken with 100 generations. These parameters are summarized in Table 5.1 of Chapter 5. Bounds on design variables are given in Table 5.2. For a comparison the GA input parameters are chosen to be same for both the cases of AMTB and HMTB.

A computer code with two modules using classes and OOP (object oriented programming) concept in C++, the first for the GA and the second for analysis of the actuator, has been developed with the interconnection between the GA and actuator analysis modules. Objective functions are optimized at the operating point of magnetic bearings. As explained in Section 4.2.2, while evaluating an individual the GA module gives the design vector to actuator analysis module, while the actuator analysis module gives back values of objective functions and constraint violations to the GA module.

Computations have been carried on a Pentium 4(R), 2.4 GHz machine with 1.25 GB of RAM using VISUAL C++ 6.0. The maximum computational time of the optimization algorithm, for the present case of 1000 population and 100 generations, is observed to be 8.438 sec.

6.2.2 Optimized Geometries of the Bearing

Two objective functions at the operating load of the actuator of a HMTB are optimized simultaneously as a multi-objective optimization of the present problem. Two objective functions are the minimization of the power-loss, P, which is given by

$$P = \rho \eta J^2 V_c \tag{6.1}$$

and the minimization of the weight W, which is given by equation

$$W = W_c + W_s + W_m \tag{6.2}$$

The different quantities involved in equations (4.1) and (4.2) have been detailed in Sections 2.3.1.1 and 2.3.1.2, respectively. The convergence issues and comparison of results will be discussed in the following subsections.

6.2.3 Convergence

The convergence of the minimum weight and the minimum power-loss versus the generation number are shown in Figure 6.1(a) and (b), respectively. It could be observed that the minimum power-loss converged in 95 generations to a value 0.623W, while the minimum weight takes 73 generations to converge to a value 4.33kg. Maximum values of the final population are observed to be 7.55W and 24.16N.

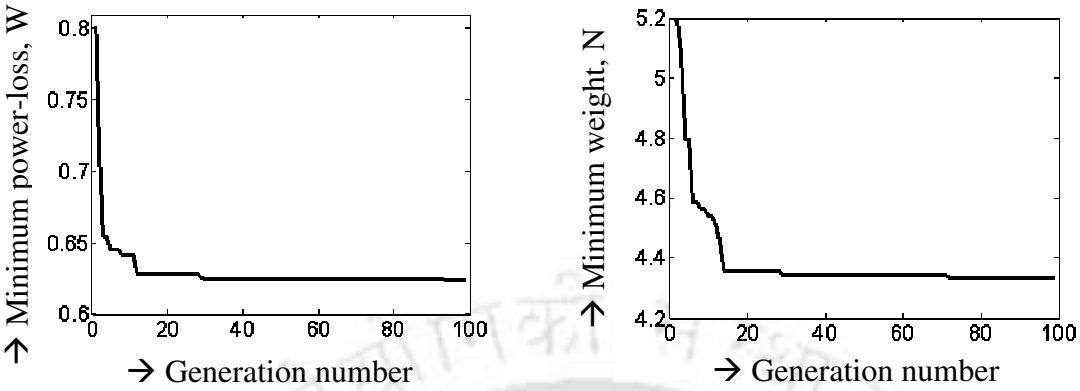

(a) Minimum power-loss vs. generation (b) Minimum weight vs. generation

Figure 6.1 Convergence of fitness functions

6.2.4 Pareto optimal front

Pareto optimal fronts of the initial and final populations for the cases of without and with bias magnets are shown in Figure 6.2(a) and (b), respectively. It could be observed that the optimal front with bias magnets is more asymptotic as compared to without bias magnets. This is due to the fact that the major part of the magnetic flux supplied to support the static loading is given by permanent magnets, and a small part of the magnetic flux is to support the dynamic loading, which is given by electromagnets. However, in the case of not using bias magnets the whole magnetic flux is supplied by electromagnets by the supplying electric current.

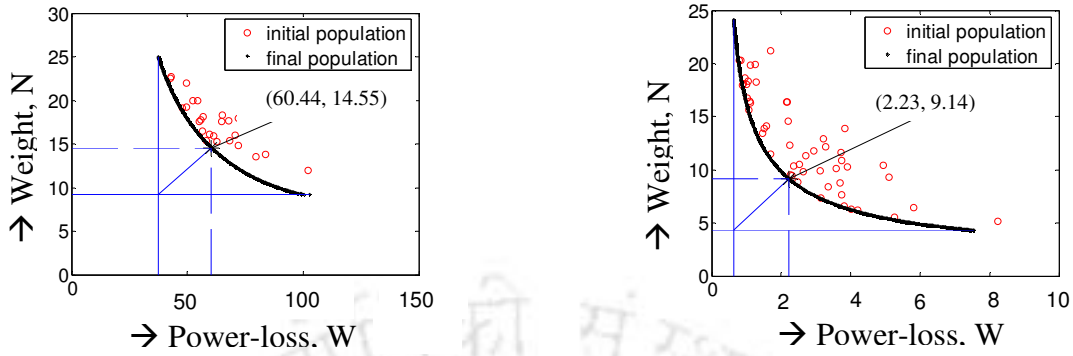

(a) Without bias magnets (AMTB) (b) With bias magnets (HMTB)

Figure 6.2 The variation of weight versus power-loss for the best optimized population and a procedure to select the optimized bearing geometry from the best population

6.2.5 Scatter plots

A design variable in any population are scattered in the feasible design space and can be represented in a plot called a scatter plot. Scatter plots of feasible design variables for the initial and final populations after 100 generations for the case with bias magnets and for the case without bias magnets are shown in Figure 6.3(a – c) and (d – f), respectively. On comparing Figure 6.3(a) and Figure 6.3(d), it could be concluded that the inner and outer radii of the coil show similar trend for both the cases with and without bias magnets (i.e., the outer radius of coil increases initially at minimum inner radius of the coil, and then increases with the increase in the inner radius of coil). On comparison of Figure 6.3(b) and Figure 6.3(e), it can be observed that the maximum height of the coil is constant for a range of the outer radius of the coil and then reduces in the case of without bias magnets. While in the case with bias magnets after reaching the maximum height of the coil, it reduces immediately. On comparing Figure 6.3(c) and Figure 6.3(f), it could be observed that the height of the coil increases at the minimum inner radius of coil then drops in the case of

without bias magnets, while in the case of with bias magnets initially it increases to the minimum inner radius of coil, then increases to a maximum quantity with increase in the inner radius of coil, and subsequently drops with further increase in the inner radius of coil.

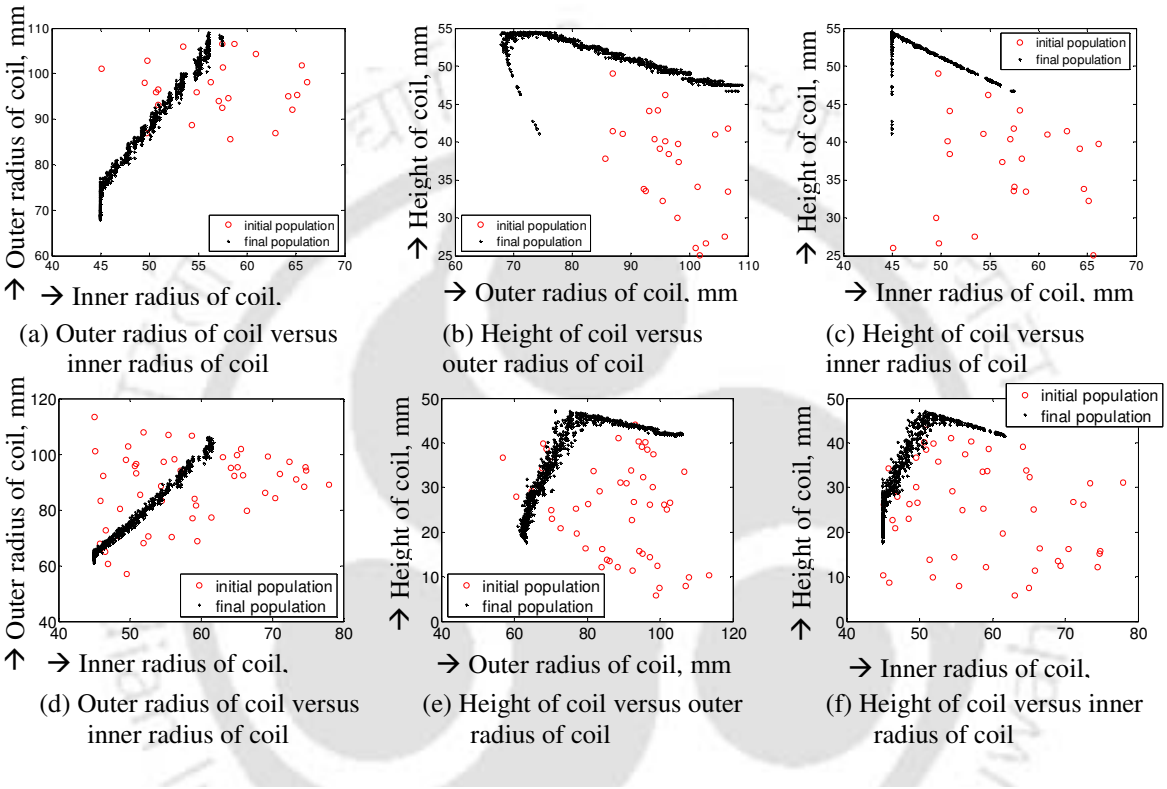

Figure 6.3: Scatter plots of feasible solutions of design variables for the initial and final populations after 100 generations
(a – c) AMTB (Chapter 5) (d – f) HMTB (present Chapter)

6.2.6 A typical design choice

In Chapter 5, the minimum normalized weighted distance from the utopia point has been used as an '*a posteriori*' criterion to make a design choice in equation (5.3) for two objective functions. A generalized form of this criterion for '*p*' objectives can be expressed as

$$\zeta = \sqrt{\sum_{i=1}^{p} \left(\varepsilon_i \frac{f_i - f_{i\min}}{f_{i\max} - f_{i\min}} \right)^2} \tag{6.3}$$

where ζ is the normalized distance from the utopia point, p is the number of objectives, ε_i is the multiplicative constant correspond to i^{th} objective, f_i is the value of i^{th} objective, $f_{i\min}$ and $f_{i\max}$ respectively are the minimum and maximum values of i^{th} objective in the population. However, in the present case, p = 2; and i = 1, 2 correspond to the power-loss and the weight, respectively. The discussion on different choices is carried in following paragraphs.

Different choices of designs for the case of with bias magnets from the final population after 100 generations, chosen according to equation (5.31), are given in Table 6.1(rows 1–3). For comparison results of without bias magnets are given in Table 6.1(rows 4 – 6) and results of SOGA are given in Table 6.1(rows 7, 8). These results are discussed in following paragraphs.

Magnetic bearing geometries showing optimized dimensions for different objective functions, which are considered with and without bias magnets, are shown in Figure 6.4. As compared to the case of without bias magnets as given in Table 6.1(row 4), it is observed that in the case of minimum weight as the objective function, the power-loss and the weight are very low for the case of using bias magnets (row 1). This is due to the reason that in the case of using bias magnets around 92.1% magnetic flux is supplied by permanent magnets whereas in the case of without bias magnets the whole magnetic flux is supplied by the electric current.

For the same reason in the case of the minimum power-loss as the objective function, weights of bearings in both cases of with and without bias magnets have converged to the maximum available dimensions to reduce the resistance effect of the coil (Table 6.1: rows 2 and 5). But the power-loss with bias magnets is much lesser than that of without bias magnets. The power-loss for the case with bias magnets (with respect to the case without bias magnets) for optimum designs corresponding to the minimum weight alone (i.e., $\varepsilon_2 = 0$), the minimum power-loss alone (i.e., $\varepsilon_1 = 0$), and the minimum distant member from utopia point (Table 6.1: rows: 3 and 6 for $\varepsilon_1 = 0.5, \varepsilon_2 = 0.5$) are 7.3%, 1.66%, 3.86%, respectively. Moreover, corresponding weights for the case of with bias magnets (with respect to the case of without bias magnets) are observed to be 46.96%, 96.64%, 62.82%; respectively. The inner radius of coil and the total bias flux supplied to support the same load in rows 1 and 4 of Table 6.1 could be observed to be the same as it is the choice of minimum weight condition. However, the variation occurs in the outer radius of coil and the height of coil, which causes a large difference in the power-loss.

For minimum normalized distant members (i.e., rows 3 and 6 of Table 6.1), it could be observed that an increase of 23.23% in the power-loss causes a decrease of 75.74% in the weight for the case of using bias magnets. Whereas an increase of 35.92% in the power-loss generated a decrease of 64.34% in the weight. The percentage of change is determined with the maximum and minimum values of corresponding quantities in cases of minimum weight (i.e., rows 1 and 4 of Table 6.1) and the minimum power-loss (i.e., rows 2 and 5 of Table 6.1).

Table 6.1 Final bearing geometries of results for different cases

Objective functions*	Design variables			Dependant variables							Cross sectional areas		Volumes			Performance parameters at the operating point					
	r_{ci} (mm)	r_{co} (mm)	h_c (mm)	l_m (mm)	r_o (mm)	t_i (mm)	t_c (mm)	t_o (mm)	t_b (mm)	h_t (mm)	A_g (mm^2)	A_c (mm^2)	V_c (cm^3)	V_s (cm^3)	V_m (cm^3)	J (A/mm^2)	B_m (T)	B_j (T)	B (T)	P (W)	W (N)
HMTB - MOGA (rows 1 – 3) (present Chapter)																					
1	44.93	63.39	17.70	4.97	73.57	19.93	18.46	10.18	15.51	38.18	4379.2	326.70	111.18	388.32	43.54	2.00	0.70	0.06	0.76	7.55	4.33
2	61.18	106.12	42.03	2.48	119.9	36.18	44.94	13.79	25.48	70.00	9794.6	1889.0	992.86	1924.4	48.61	0.19	0.47	0.04	0.51	0.62	24.16
3	48.35	71.06	38.62	4.08	82.23	23.35	22.71	11.17	17.71	60.40	5380.2	877.05	329.02	757.00	43.87	0.63	0.64	0.05	0.69	2.23	9.14
AMTB - MOGA (rows 4 – 6) (Chapter 5)																					
4	44.93	75.87	39.09	—	84.56	19.93	30.94	8.69	15.51	54.60	4380.7	1209.5	459.06	660.64	—	3.63	—	0.762	0.762	102.8	9.22
5	57.74	109.0	47.73	—	119.9	30.74	53.34	10.83	22.26	69.99	7797.8	2545.9	1318.28	1706.5	—	1.29	—	0.571	0.571	37.42	25.00
6	48.14	83.34	52.40	—	92.94	23.14	35.19	9.60	17.58	69.98	5318.3	1844.0	761.69	999.90	—	2.16	—	0.691	0.691	60.44	14.55
HMTB - SOGA (rows 7, 8) (Chapter 4)																					
7	45.87	65.03	16.35	4.69	75.55	20.87	19.16	10.52	16.12	37.16	4646.5	313.27	109.14	409.39	43.55	2.01	0.68	0.06	0.74	7.50	4.48
8	66.76	98.39	49.92	2.13	116.2	41.76	31.63	17.85	28.70	80.75	12038	1578.9	819.22	2363.8	51.32	0.20	0.42	0.04	0.46	0.57	26.05

*1, 4, 7→ Minimum weight; 2, 5, 8→ Minimum power-loss; 3, 6→ Minimum normalized weighted distance from utopia point

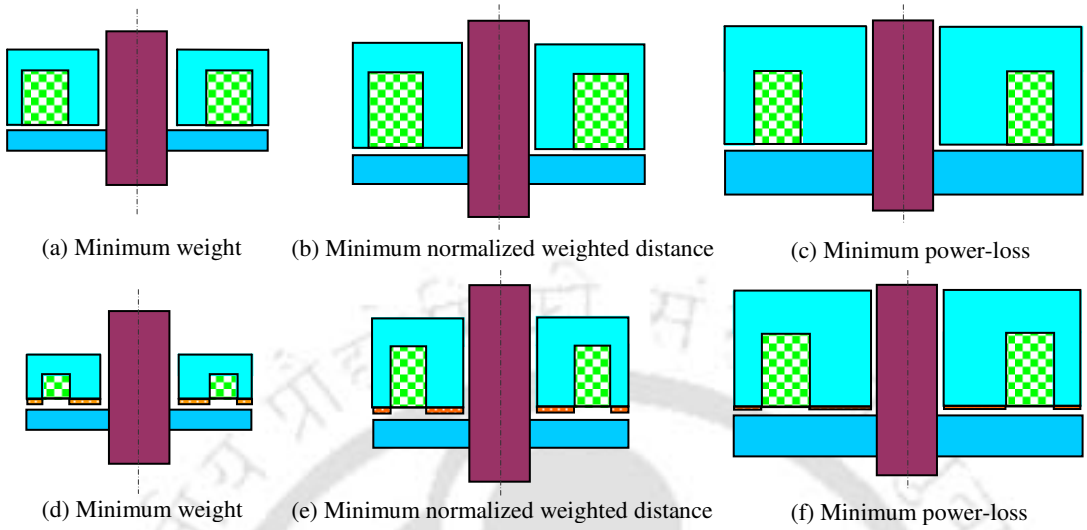

Figure 6.4 Final actuator geometries
(Dimensions can be referred to Table 6.1 and Figures 2.5 and 2.6)
(a – c) AMTB (Chapter 5) (d – f) HMTB (present Chapter)

6.2.7 Comparison of results of MOGAs with SOGAs

In the case of HMTB, both results of Pareto frontiers by using the MOGA (rows 1 and 2 of Table 6.1) and by using the SOGA (rows 7 and 8 of Table 6.1) are produced in Table 6.2. It can be observed from Table 6.2 that the MOGA and SOGA results are non-inferior to each other. While in the case of without bias magnets, the SOGA dominated the MOGA in the case minimum weight and the MOGA dominated the SOGA in the case minimum power-loss. This result shows that the search direction depends on the type of GA criterion used and either SOGA or MOGA can produce a better result. Based on such results combination of criterions of the MOGA and SOGA operators is suggested as hybrid algorithms (Hisao et al., 2006).

Table 6.2 A comparision of the MOGA and SOGA results for HMTB

Type of GA	Power-loss (W)	Weight (kg)	Comment
MOGA	7.55	4.33	SOGA dominates in the power-loss and MOGA dominates in the weight
SOGA	7.50	4.48	
MOGA	0.62	24.16	SOGA dominates in the power-loss and MOGA dominates in the weight
SOGA	0.57	26.05	

6.2.8 Sensitivity analysis of the chosen optimum design

Sensitivities of objective functions and dependant variables has been studied with respect to a small change in values of different optimized design variables, which may occur due to manufacturing limitations. Sensitivities are determined by using Taylor's series (Kreyszig, 2006).

For illustrations, 1% perturbation is given to design variables (individually or in combinations) of optimized design obtained by choosing $\varepsilon_1 = \varepsilon_2$ in equation (5.31). Corresponding percentages of deviations of different dependant variables, cross-sectional areas, the magnetic flux and current densities, and objective functions are shown in Table 4 for the case of with bias magnets. First three rows of Table 6.3 represent deviations corresponding to perturbation on one variable while keeping the two variables constant, rows 4 to 6 of Table 6.3 represents deviations corresponding to deviations of design

variables while keeping the third design variable constant. Row 7 of Table 6.3 represents deviations corresponding to perturbation in all the design variables simultaneously.

From Table 6.3, the increase in the inner radius of the coil increases the inner wall thickness and the area of air gap; hence the thickness of bias magnets and the magnetic flux-density in the stator-iron are reduced. The increase in the inner radius of coil keeping all the other design variables constant reduces the thickness of coil as well as the cross-sectional area of coil and reduces the power-loss. Overall the increase in the inner radius of coil increases the weight of the bearing.

Form Table 6.3, the increase in the outer radius of coil does not affect the inner wall thickness. The area of air-gap, hence, the thickness of bias magnets and the magnetic flux-density in the stator iron are unaltered for supporting a fixed load. Moreover, it increases the coil-thickness and the cross-sectional area of coil, and hence the coil current-density is reduced. Overall the increase in the outer radius of coil reduces the power-loss and increases the weight of the bearing.

From Table 6.3, the increase in the height of coil does not alter any geometric quantities except in increasing the height of the bearing and the area of the coil. Hence, the coil current-density and the power-loss are reduced, and the weight of the bearing is increased.

From the last two columns (i.e. bearing tradeoffs) of Table 6.3, it can be observed that the effect of outer radius of the bearing on objective functions is more than that of the other two design variables, and followed by the inner radius of coil. The height of coil affects objective functions least, among three design variables. Moreover, effects of the outer radius, inner radius and height of the coil on both objective functions could be observed to

be approximately in the ratio 2.5:1.6:1, respectively. These effects on objective functions are correspondingly reflected in their deviations in combinations (Table 6.3: rows 4 – 7). For the comparison the sensitivity for the case of without bias magnets is presented in Table 6.4. Moreover, the effect of the outer radius of the coil on objective functions is approximately double of other two design variables in the case of without bias magnets. This is due to the fact that in the case of using bias magnets most of the magnetic flux is supplied by permanent magnets, and only small portion of the magnetic flux is supplied by the electric current to support the dynamic loading on the bearing in the case of with bias magnets. Moreover, an increase in the inner radius of coil decreases the thickness of bias magnets, while the changes in the other two dimensions namely the outer radius of coil and the height of coil do not affect bias magnets. The corresponding affect due to bias magnets is observed in the tradeoffs of power-loss and weight of the actuator of HMTB in Table 6.3.

Table 6.3 Sensitivity of optimized bearing geometries of a chosen design with bias magnets * (results of the present chapter)

% deviations on design variables			% deviations on dependant variables							% deviations on cross sectional areas		% deviations on the flux and current densities at the operating point				% deviations on objective functions at the operating point	
r_{ci}	r_{co}	h_c	l_m	r_o	t_i	t_c	t_o	t_b	h_t	A_g	A_c	J	B_m	B_j	B	P	W
1.000	0.000	0.000	-2.446	0.347	2.071	-2.129	2.553	1.726	0.341	2.744	-2.129	0.078	-1.375	-0.976	-1.344	-1.578	1.149
0.000	1.000	0.000	0.000	0.748	0.000	3.129	-0.857	0.000	0.000	0.000	3.129	-3.034	0.000	0.000	0.000	-2.457	1.680
0.000	0.000	1.000	0.000	0.000	0.000	0.000	0.000	0.000	0.639	0.000	1.000	-0.990	0.000	0.000	0.000	-0.990	0.674
1.000	1.000	0.000	-2.446	1.092	2.071	1.000	1.677	1.726	0.341	2.744	1.000	-3.022	-1.375	-0.976	-1.344	-4.062	2.837
0.000	1.000	1.000	0.000	0.748	0.000	3.129	-0.857	0.000	0.639	0.000	4.160	-3.994	0.000	0.000	0.000	-3.423	2.366
1.000	0.000	1.000	-2.446	0.347	2.071	-2.129	2.553	1.726	0.980	2.744	-1.150	-0.913	-1.375	-0.976	-1.344	-2.553	1.827
1.000	1.000	1.000	-2.446	1.092	2.071	1.000	1.677	1.726	0.980	2.744	2.010	-3.982	1.419	0.996	-1.344	-5.012	3.527

* Taken from the third row of Table 6.1 with 1% perturbation on the individual design variable

Table 6.4 Sensitivity of optimized bearing geometries of a chosen design without bias magnets (AMTB – MOGA, Chapter 5)

% deviations on design variables			% deviations on dependant variables							% deviations on cross sectional areas		% deviations on the flux and current densities at the operating point				% deviations on objective functions at the operating point	
r_{ci}	r_{co}	h_c	l_m	r_o	t_i	t_c	t_o	t_b	h_t	A_g	A_c	J	B_m	B_j	B	P	W
1.000	0.000	0.000	–	0.269	2.080	-1.368	2.606	1.735	0.436	2.752	-1.368	0.02	–	-1.348	-1.348	-0.967	0.899
0.000	1.000	0.000	–	0.805	0.000	2.368	-0.889	0.000	0.000	0.000	2.368	-2.313	–	0.000	0.000	-1.694	1.818
0.000	0.000	1.000	–	0.000	0.000	0.000	0.000	0.000	0.749	0.000	1.000	-0.990	–	0.000	0.000	-0.990	0.764
1.000	1.000	0.000	–	1.072	2.080	1.000	1.697	1.735	0.436	2.752	1.000	-2.325	–	-1.348	-1.348	-2.678	2.724
0.000	1.000	1.000	–	0.805	0.000	2.368	-0.889	0.000	0.749	0.000	3.392	-3.280	–	0.000	0.000	-2.667	2.596
1.000	0.000	1.000	–	0.269	2.080	-1.368	2.606	1.735	1.185	2.752	-0.382	-0.970	–	-1.348	-1.348	-1.948	1.666
1.000	1.000	1.000	–	1.072	2.080	1.000	1.697	1.735	1.185	2.752	2.010	-3.292	–	-1.348	-1.348	-3.642	3.506

* Taken from the sixth row of Table 6.1 with 1% perturbation on individual design variable

6.2.9 Analysis of the final population

Next, the analysis on the final optimized population is carried out for the case with bias magnets and compared to the case of without bias magnets. The *Pareto optimal design analysis* methodology implemented in Chapter 5 has been used in the present chapter. Different quantities for the case with bias magnets have been plotted with respect to the power-loss in Figure 6.5 and Figure 6.6. For the case without bias magnets, plots are given in Figure 5.10 and Figure 5.11. In the case of without bias magnets, there are two salient points observed, namely the saturation of magnetic flux in the stator-iron (i.e., point B in Figure 5.10 and Figure 5.11) and the saturation of coil current-density (i.e., point C in Figure 5.10 and Figure 5.11). In the case with bias magnets (Figure 6.5 and Figure 6.6), there are three distinct points observed namely, point A, B, and C respectively, correspond to the maximum height of the coil, the saturation of magnetic flux density in the stator-iron, and the saturation of current-density in the coil.

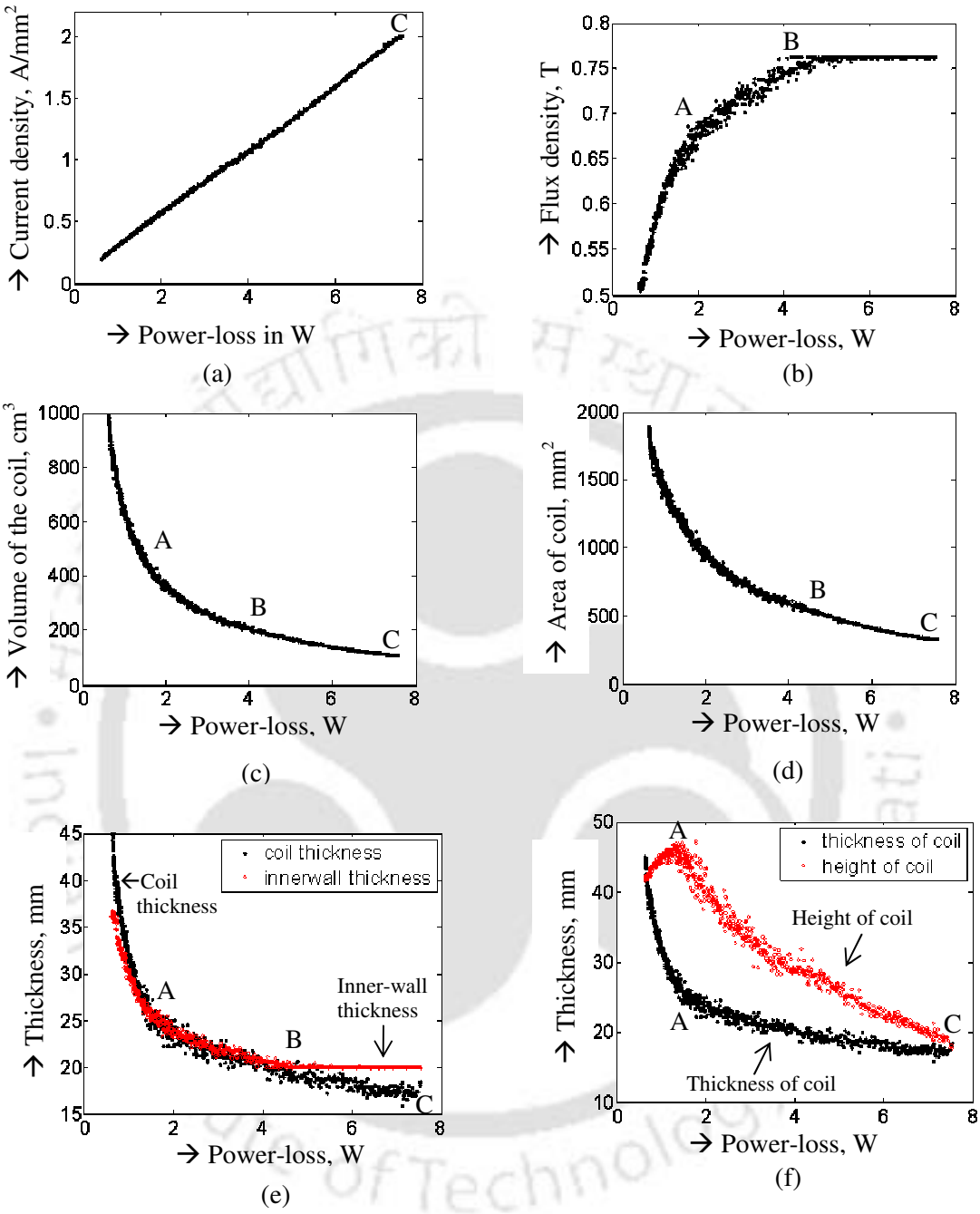

Figure 6.5 The variation of different quantities versus power-loss in the final population HMTB

(a) Current density (b) Flux density (c) area of coil

(d) Volume of the coil (e) Thickness of coil and inner wall

(f) Thickness and height of coil

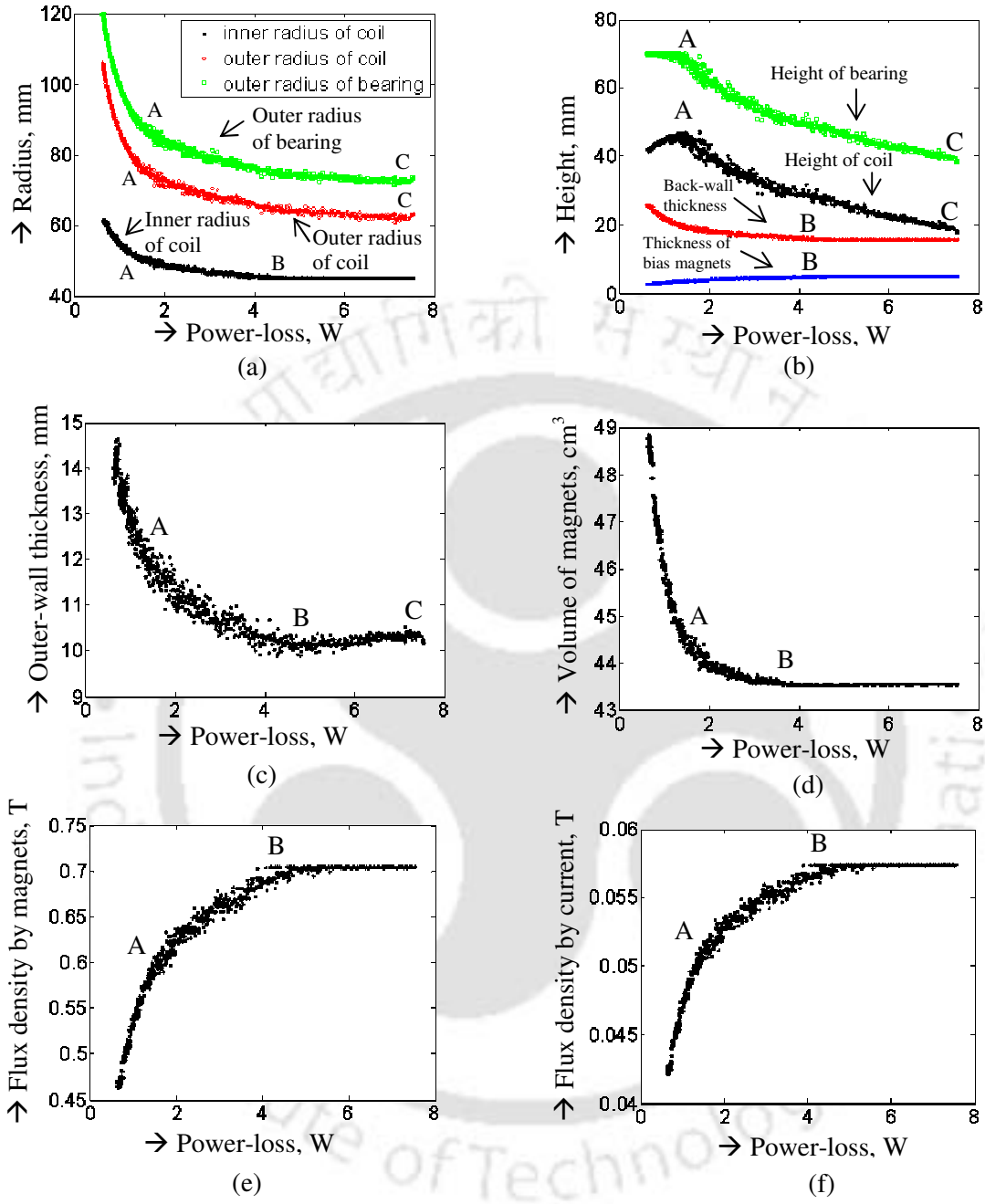

Figure 6.6 The variation of different quantities versus power-loss in the final population HMTB

(a) Inner and outer radii of the coil and outer radius of bearing

(b) Thickness of magnets, height of coil, back wall thickness and height of bearing

(c) Outer wall thickness

(d) Volume of the bias magnets

(e) Flux density by the magnets

(f) Flux density by the current

From Figure 6.5(a), it is observed that the current-density increases with the power-loss linearly till point C, where the current-density in the coil is saturated. From Figure 6.5(b) before point A, the scatter of flux-density is less than that between points A and B. Moreover, the slope of increase of flux-density with respect to the increase of power-loss is less between A and B than that before point A. At point B the magnetic flux-density gets saturated, and is constant with further increase in the power-loss. From Figure 6.5(c), it could be observed that between points B and C, the scatter of cross sectional area of the coil is reduced as compared to that of before point B, where after point B the magnetic flux-density in the stator-iron is saturated. After point C the cross-sectional area of the coil remains constant.

From Figure 6.5(d) between points A and B, the slope of decrease of volume of the coil to the increase of the power-loss is less as compared to that of before point A. Between points B and C, the scatter of points is less than before point B, and a small increase in the volume of the coil is observed after point C. This is clear from equation (4.1) that keeping the current density constant the only way of increasing the power-loss is by increasing the volume of the coil. According to Figure 6.5(e), it could be clearly observed that both the inner wall and coil thicknesses with respect to the power-loss decrease faster before point A than after point A. Between point A and point B, the scatter of points are more, and after point B the inner-wall thickness is constant, where the magnetic flux density is saturated. However, the coil thickness further decreases till the point C, where the coil current-density is saturated. After point C there is a small increase in the thickness of the coil with the increase in power-loss. From Figure 6.5(f) before point A, the height of the coil increases with the increase in the power-loss, while the thickness of coil decreases drastically with the increase in the power-loss. After point A, where the maximum height of the coil is achieved,

a further increase of the power-loss decreases the height of the coil till point C. After point C the slope of decrease of height of the coil with the increase of the power-loss is more than that of between points A and C. This is due to the fact that there is an increase in the thickness of the coil after point C with the increase in the power-loss.

Figure 6.6(a) shows that the scatter of the points of outer radius of coil before point A is less than that of after point A. The outer radius of bearing shows a similar trend as the outer radius of coil. The inner radius of coil decreases similar to the outer radius of the coil till point B and then remains constant where the flux-density is saturated. In Figure 6.6(b) the height of the bearing is constant till point A then drops with the increase in the power-loss till point C and decreases with more slope after point C. The back-wall thickness of bearing shows similar trend as the inner radius of coil since the area of the air-gap at poles A_g, is assumed to be constant throughout the magnetic circuital path according to equation

$$A_g = \pi\left(r_{ci}^{\,2} - r_i^2\right) = 2\pi r_{ci} t_b = \pi\left(r_o^{\,2} - r_{co}^2\right) \tag{6.4}$$

(The details of equations (6.4) to (6.6) have been provided in Section 2.2 of Chapter 2, at equations 2.4, 2.10 and 2.11 respectively). Hence, the back-wall thickness is a function of the inner radius of the coil only, when the inner radius of bearing fixed. The thickness of bias magnets increases with the power-loss till point B and becomes constant. According to equations

$$l_m = \frac{K_a l_g B_g}{B_r - K_f B_g} \tag{6.5}$$

and

$$F = \frac{B_g{}^2 A_g}{\mu_0} = \frac{\phi_g{}^2}{\mu_0 A_g} \quad \text{with} \quad \phi_g = B_g A_g \tag{6.6}$$

The thickness of bias magnets could be concluded as a function of the force and the inner radius of the coil, and hence the trend of the thickness of bias magnets increases with the decrease in the inner radius of coil till it becomes constant. Figure 6.6 (c) shows the trend of the outer-wall thickness with respect to the power-loss. The outer-wall thickness decreases till point B and then increases till point C after which it shows a small decrease. The scatter of points between A and B is more than before A.

Figure 6.6(d), (e) and (f), respectively, show plots of the volume of bias magnets, the magnetic flux-density supplied by bias magnets at the operating point, and the magnetic flux-density due to the current. The volume of bias magnets shows reverse trend to that of the magnetic flux-density with the increase in the power-loss (i.e., it decreases with respect to power-loss till point B and then remains constant). Magnetic flux-densities supplied by bias magnets and the current show similar trends as that of the total magnetic flux-density. It can be observed from Figure 6.6(e) and (f) that the most part of the total flux-density is supplied by bias magnets than that of the current.

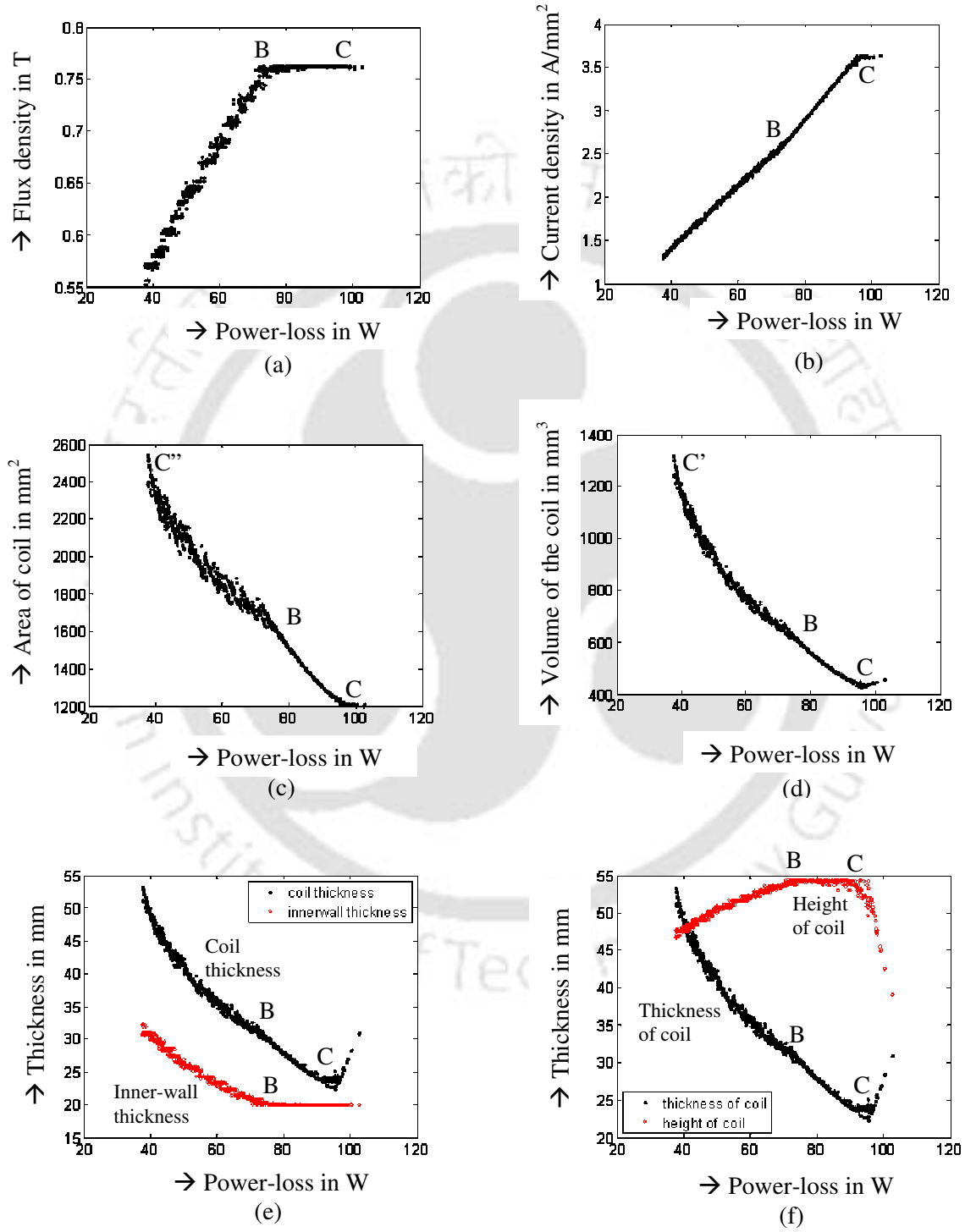

Figure 6.7 The variation of different quantities in the optimized final population at the designed load
(a) Flux density versus power-loss (b) Current density versus power-loss
(d) Area of coil versus power-loss (d) Volume of coil versus power-loss
(e) Thickness versus power-loss (f) Thickness versus power-loss

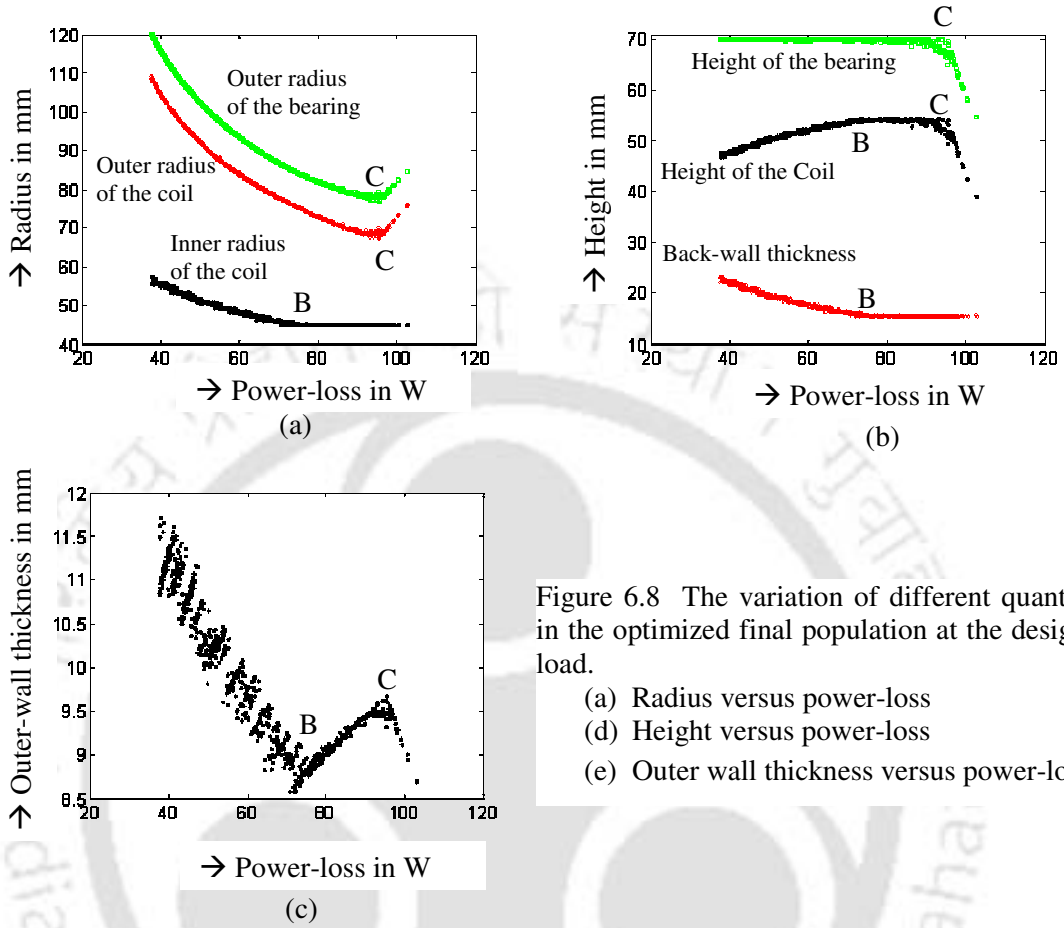

Figure 6.8 The variation of different quantities in the optimized final population at the designed load.
(a) Radius versus power-loss
(d) Height versus power-loss
(e) Outer wall thickness versus power-loss

Comparison of the case of with bias magnets and without bias magnets is summarized in this paragraph. Three salient points are observed in the case of with bias magnets, whereas it is two in the case of not using bias magnets. The slope of increase of the current-density with the power-loss after the saturation of flux-density is more in the case of without bias magnets, while it is nearly constant in the case of with bias magnets. Till the saturation of magnetic flux-density, the slope of increase of the magnetic flux-density with respect to the power-loss is constant in the case of without using bias magnets, while in the case of using bias magnets it changes after the maximum height of the coil is achieved. The increase of the power-loss after the saturation of the current-density is observed to be small in the case of using bias magnets. More power-loss due to the electrical resistance is caused in the case

of without bias magnets. Points of reaching the maximum outer radius of coil and the saturation magnetic flux-density are same in the case without bias magnets. With the increase in the power-loss, the height of the coil remains constant after reaching its maximum value till the saturation of the current-density occurs and then it drops, in the case of without bias magnets; while it drops immediately after reaching the maximum value with the increase in the power-loss in the case of with bias magnets. This discussion of comparison has been also summarized in Table 6.5.

Table 6.5 Comparison of cases with and without bias magnets

	HMTB				AMTB		
	Before A	Between A - B	Between B - C	After C	Before B	Between B - C	After C
Design Variables							
r_{ci}	↓*	↓	↔	↔	↓	↔	↔
r_{co}	↓	↓	↔	↓	↓	↓	↑
h_c	↑	↓	↓	↓	↑	↔	↓
Coil current and magnetic flux densities							
J	↑	↑	↑	↔	↑	↑	↔
B	↑	↑	↔	↔	↑	↔	↔
Other geometric parameters							
A_g	↓	↓	↔	↔	↓	↔	↔
A_c	↓	↓	↓	↔	↓	↓	↔
V_c	↓	↓	↓	↑	↓	↓	↑
r_o	↓	↓	↓	↑	↓	↓	↑
h_t	↔	↓	↓	↓	↔	↔	↓
t_c	↓	↓	↓	↑	↓	↓	↑

*↓ … decreases; ↑… increases; ↔… remains constant

6.3 Conclusions

In the present chapter, the optimal design of actuator of a *hybrid magnetic thrust bearing* (HMTB) with bias magnets using *multi objective genetic algorithms* (MOGAs) has been carried out. Two objectives have been considered namely minimizing the power loss and minimizing the weight. The method of implementation for the problem considered has been described. It is observed that the size of the bearing with bias magnets is considerably reduced as compared to the case without bias magnets for the same operating conditions in the case of objective function as the minimization of the weight. Similarly, current-densities get reduced drastically with biased magnets when the objective function is chosen as the minimization of the power-loss. Geometries of optimised bearing designs with individual objectives and multi-objectives are compared. The SOGA and MOGA results have been observed to be non-inferior to each other. Hence, it can be concluded that the end result depends upon the selection strategy also and for better convergence a hybrid selection strategy of SOGA and MOGA is suggested. For illustration, an optimum design has been chosen from the final optimized population by an '*a posteriori*' approach proposed in the present work. Sensitivities of objective functions with respect to the outer radius, the inner radius and the height of coil are observed to be approximately in the ratio 2.5:1.6:1 for both the objectives. The analysis of final optimized population has been carried out and compared with the case of without bias magnets and a few salient points are observed in the case of with bias magnets.

Till now the optimization of actuators of AMTB and HMTB has been carried at a single load in Chapters 5 and 6, respectively. How the methodology works at different loads will be seen in the next chapter (i.e. Chapter 7).

Chapter 7
Effect of the Load on the Design Optimization of Magnetic Thrust Bearings using Multi-Objective Genetic Algorithms

7.1 Introduction

In Chapter 2, the optimization problem for actuators of AMTB and HMTB has been introduced, where as in Chapter 3 the optimization tools are introduced. In Chapter 4, the single-objective optimization of actuator of an AMTB and a HMTB has been carried out using the SOGA. The actuator is optimized sequentially for the minimization of power-loss and the minimization of weight of the actuator. The multi-objective optimization of actuator of an AMTB has been carried using MOGA in Chapter 5. The minimization of power-loss and weight of the actuator are considered objectives to be optimized simultaneously. Two salient points were observed where the major changes occurred in the behaviour of different parameters of the final population. In Chapter 6, the multi-objective optimization of actuator of a HMTB has been carried out using MOGA. Three salient points are observed where the

major changes have been observed in the behaviour of different parameters of the final population.

In Chapters 4 to 6, the actuator is considered to be acted upon by a constant load of 2025N. The magnetic bearing design includes determination of geometries of the bearing and the current supplied to carry a specified load for a specified gap. However, if the operating load is changed the design may change, including the Pareto optimal front and the behavior of other parameters. Hence, it would be important and interesting to investigate the effect of the load on the Pareto frontier if the operating load is varied, and to study the behavior of design variables and other parameters in the final population with respect to the load. Moreover, the maximum load that can be supported by the AMTB and the HMTB within given constraints of material properties and the space available would be motivating to observe.

As per the discussion of previous paragraphs, in the present chapter, the effect of load on the Pareto frontier in the optimal design of thrust magnetic bearings by using multi-objective genetic algorithms (MOGAs) has been presented. Two objective functions namely the minimization of power-loss and weight of the actuator are considered. Two cases of magnetic thrust bearing actuators, without bias magnets (active magnetic thrust bearings, AMTB) and with bias magnets (i.e. hybrid magnetic thrust bearings, HMTB) have been considered for the performance comparison. Mathematical models of objective functions and associated constraints related to the geometry of the bearing, the space available, and the electrical, magnetic and thermal properties of materials of the coil and the stator-iron have been presented and discussed in Chapter 2. At a fixed load, coil dimensions namely the inner radius, the outer radius, and the height are observed to be design variables for both the AMTB and the HMTB.

The multi-objective genetic algorithm is used to generate the Pareto frontier at different loads. The *Pareto optimal design analysis methodology* that is used in Chapters 5 and 6 has been used to analyze the characteristics of Pareto frontiers, design variables and other parameters with the power-loss and are discussed comprehensively. In this work, loads are attempted to be classified based on the behavior of the current-density in the coil and the magnetic flux-density in the stator-iron. Maximum loads, which the AMTB and the HMTB could support, have been compared. Final populations have been studied independently for both the AMTB and the HMTB.

Geometries of the magnetic thrust bearing, related fundamental relations, and optimization models have been detailed in Chapter 2 and hence we go directly to the discussion of results and conclusions as detailed in following sections.

7.2 Analysis on the Pareto frontiers

As stated earlier, the main motivation of the present work is to observe the effect of load on the Pareto frontier. Hence, the load is varied from a minimum of 100 N till the maximum feasible load of the bearing beyond which there exists no feasible solution. Two objective functions are the minimization of the power-loss, P, which is given by equation

$$P = \rho \eta J^2 V_c \tag{7.1}$$

and the minimization of the weight W, which is given by equation

$$W = W_c + W_s + W_m \tag{7.2}$$

The different quantities involved in equations (7.1) and (7.2) have been detailed in sections 2.3.1.1 and 2.3.1.2, respectively. These objective functions are optimized at each operating load in the multi-objective optimization of the present problem. The Pareto optimal fronts of final populations generated at different loads for the cases of AMTB and HMTB are shown in Figure 7.1(a) and Figure 7.1(b), respectively. At each load, there could be observed a minimum and maximum power-loss corresponding to a maximum and minimum weight, in the Pareto frontier as shown in Table 7.1 and Table 7.2 for the cases of AMTB and HMTB, respectively. It can also be observed from Figure 7.1(a) and (b) that fronts are converging to a single point as the load increases. Moreover, from Table 7.1 and Table 7.2 it is observed that the difference between upper and lower bounds of objective functions and design variables of the population are very small. The maximum load where the Pareto-frontier is a single point is also called as the *feasible peak load*. Beyond this maximum load there exists no feasible design within the given constraints of space and material properties.

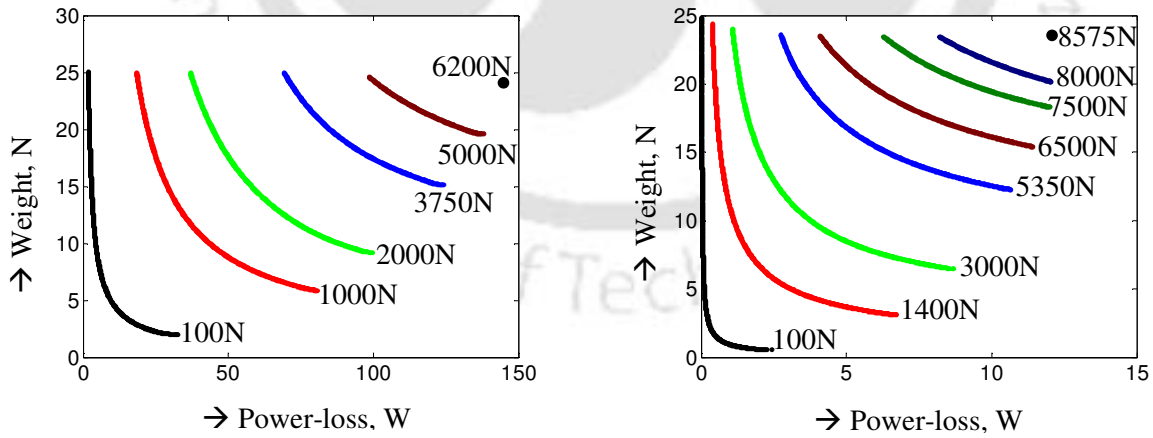

(a) Without bias magnets (AMTB) (b) With bias magnets (HMTB)

Figure 7.1 The variation of weight versus power-loss for the final populations at different loads

We can observe that for the present case, the peak load feasible for the case of without bias magnets is 6200 N and that of with bias magnets is 8575 N within the given constraints.

Hence, the peak load by using bias magnets is 138.3% of that without using bias magnets within the constraints given. This is due to the fact that the major part of the magnetic flux supplied to support the static loading is given by permanent magnets, and a small part of the magnetic flux is to support the dynamic loading, which is given by electromagnets. However, in the case of not using bias magnets the whole magnetic flux is supplied by electromagnets by the supplying electric current. Hence, in the case of using bias magnets lesser space for the coil suffices the dynamic loading and this makes more space available for the stator iron to allow more flux through it. Thus, the bearing is able to support more loads. While in the case of not using bias magnets the whole flux is generated by the electric current, and hence more space is required for the coil to supply the required current. This makes less space available for the stator iron and the load bearing capacity will be lesser than the case with bias magnets.

It can be concluded from Figure 7.1(a) and Figure 7.1(b) that by compromising in the load to be supported, we can get a wide range of design choices. Hence, it could be concluded that the load to be supported could be considered as an objective.

Table 7.1 The minimum and maximum values of the final population at different loads (AMTB)

Load(N)	100		1000		2000		3000		3750		5000		6200	
	min	max	min	max	min	max	min	max	min	max	min	max	min	max
Objective Functions														
P (W)	1.851	32.815	18.485	80.543	36.982	99.803	55.393	115.571	69.231	124.082	98.517	138.137	144.608	145.379
W (N)	1.990	25.021	5.842	24.959	9.162	24.961	12.514	25.012	15.124	24.991	19.571	24.596	24.206	24.280
Design Variables														
r_{ci} (mm)	30.00	58.03	36.23	57.47	44.72	57.17	51.84	56.81	56.60	56.96	63.73	63.74	69.91	69.91
r_{co} (mm)	46.46	109.34	57.23	108.70	67.54	108.75	77.18	108.95	83.63	108.71	92.68	104.69	100.62	100.68
h_c (mm)	28.68	60.18	46.64	58.99	43.36	54.61	37.83	50.10	37.22	47.22	34.93	43.03	39.31	39.51
Coil current and magnetic flux densities														
J (A/mm^2)	0.285	3.632	0.921	3.632	1.297	3.631	1.583	3.632	1.785	3.632	2.492	3.632	3.612	3.632
B (T)	0.012	0.381	0.386	0.762	0.550	0.762	0.679	0.762	0.757	0.763	0.762	0.762	0.762	0.762
Other geometric parameters														
A_g (mm^2)	865.5	8616.6	2162.0	8413.9	4319.9	8307.2	6479.5	8176.1	8099.4	8229.2	10799.2	10801	13391	13391.1
A_c (mm^2)	440.3	2590.3	1101.4	2476.8	1206.9	2537.7	1208.4	2506.3	1209.4	2459.6	1209.5	1762.3	1209.5	1216
V_c (mm^3)	113.5	1339.8	333.8	1281.2	428.7	1306.8	493	1300	533.7	1277.5	595.2	932.5	648.1	651.7
r_o (mm)	49.98	119.98	77.06	119.94	77.06	119.94	89.57	120.00	97.84	120.00	109.67	119.99	119.95	120.00
h_t (mm)	35.71	70.00	58.78	70.00	58.78	70.00	57.73	70.00	60.00	70.00	61.90	70.00	69.79	70.00
t_c (mm)	13.53	54.04	22.82	53.02	22.82	53.02	25.31	52.80	27.03	52.10	28.94	40.95	30.71	30.77

Table 7.2 Minimum and maximum values of final population at different loads (HMTB)

Load(N)	100		1400		3000		5350		6500		7500		8000		8575	
	min	max	min	max	min	max	min	max	min	max	min	max	min	max	min	max
Objective Functions																
P (W)	0.02	2.44	0.386	6.72	1.082	8.699	2.754	10.659	4.097	11.429	6.282	12.015	8.202	12.048	12.065	12.075
W (N)	0.55	24.83	3.072	24.356	6.469	23.986	12.275	23.549	15.402	23.49	18.281	23.456	20.147	23.448	23.441	23.449
Design Variables																
r_{ci} (mm)	28.28	58.01	39.87	60.45	51.84	63.86	65.6	65.95	71.37	71.4	76.03	76.04	78.26	78.26	80.75	80.75
r_{co} (mm)	39.49	108.55	55.41	106.9	69.13	105.48	84.61	103.47	90.65	99.65	95.96	96.14	94.32	94.34	92.22	92.22
h_c (mm)	11.69	57.32	19.25	49.38	15.57	44.53	15.13	36.98	15.59	33.7	16.28	31.11	20.35	29.88	28.5	28.52
Coil current and magnetic flux densities																
J (A/mm^2)	0.031	1.988	0.146	1.999	0.263	1.998	0.467	1.999	0.687	2	1.045	1.999	1.361	1.999	1.998	2
B (T)	0.121	0.479	0.43	0.762	0.59	0.763	0.758	0.763	0.762	0.763	0.763	0.763	0.763	0.763	0.763	0.763
Other geometric parameters																
A_g (mm^2)	548.7	8608.2	3031.1	9515.9	6479.5	10847.9	11555.2	11699.2	14039	14050.7	16198.8	16203.1	17278.8	17279.4	18520.7	18520.7
A_c (mm^2)	118.5	2418.7	319	2052.5	327.1	1756	326.9	1400.3	326.9	951.6	327	625.5	326.9	480.2	326.9	327.2
V_c (mm^3)	26.3	1248.1	97.3	1073.8	124.7	924.7	154.6	743.8	167.2	511.3	176.8	338.3	177.3	260.4	177.6	177.8
r_o (mm)	42.27	119.97	63.55	119.98	82.72	119.99	104.1	119.94	112.63	119.99	119.85	120.00	119.99	120.00	120.00	120.00
h_t (mm)	17.48	70.00	36.44	70.00	40.44	70.00	48.15	70.00	51.87	70.00	55.17	69.99	60.46	69.99	69.98	70.00
t_c (mm)	9.27	51.66	15.37	47.28	17.28	43.32	19.01	37.86	19.28	28.27	19.92	20.11	16.06	16.08	11.47	11.47
l_m (mm)	0.42	2.26	1.94	4.97	3.12	4.98	4.92	4.98	4.97	4.98	4.98	4.98	4.98	4.98	4.98	4.98

7.3 Analyses of final populations

In this section, results of multi-objective optimization are presented and analysed based on plots of different variables and parameters with the increase in load. The *Pareto optimal design analysis methodology* that is used in Chapters 5 and 6 has been used to analyze the final populations for different configurations of actuators and different loads. The case without bias magnets is presented first followed by the case with bias magnets. The scatter of values of design variables in the design space and the variation of different parameters and geometric quantities with respect to the power-loss are presented and analysed.

7.3.1 Case without bias magnets (AMTB)

For AMTB, Figure 7.2 shows plots of different quantities (i.e., the flux density, the current density, the area of the coil, the volume of the coil, the height of the bearing, the outer radius of the bearing, the inner radius of the coil, the outer radius of the coil, the height of the coil, and the thickness of the coil) versus the power-loss. Some salient points namely A′, A, B′, B, C and D have been observed and marked on these plots, however, in some cases these points are not distinct and are not shown wherever the case is. These points correspond to the load and the power-loss, and based on observations of plots these points are specified as: point A′(100N, 8.298W), point A(100N, 25.342W), point B′(2000N, 84.232W), point B(2000N, 95.623W), point C′(3750N, 69.230W), point C(3750N, 119.664W), and point D(6200N, 145.350W). Table 7.3 summarizes values of different parameters extracted from Figure 7.2 for the case of AMTB at these key points.

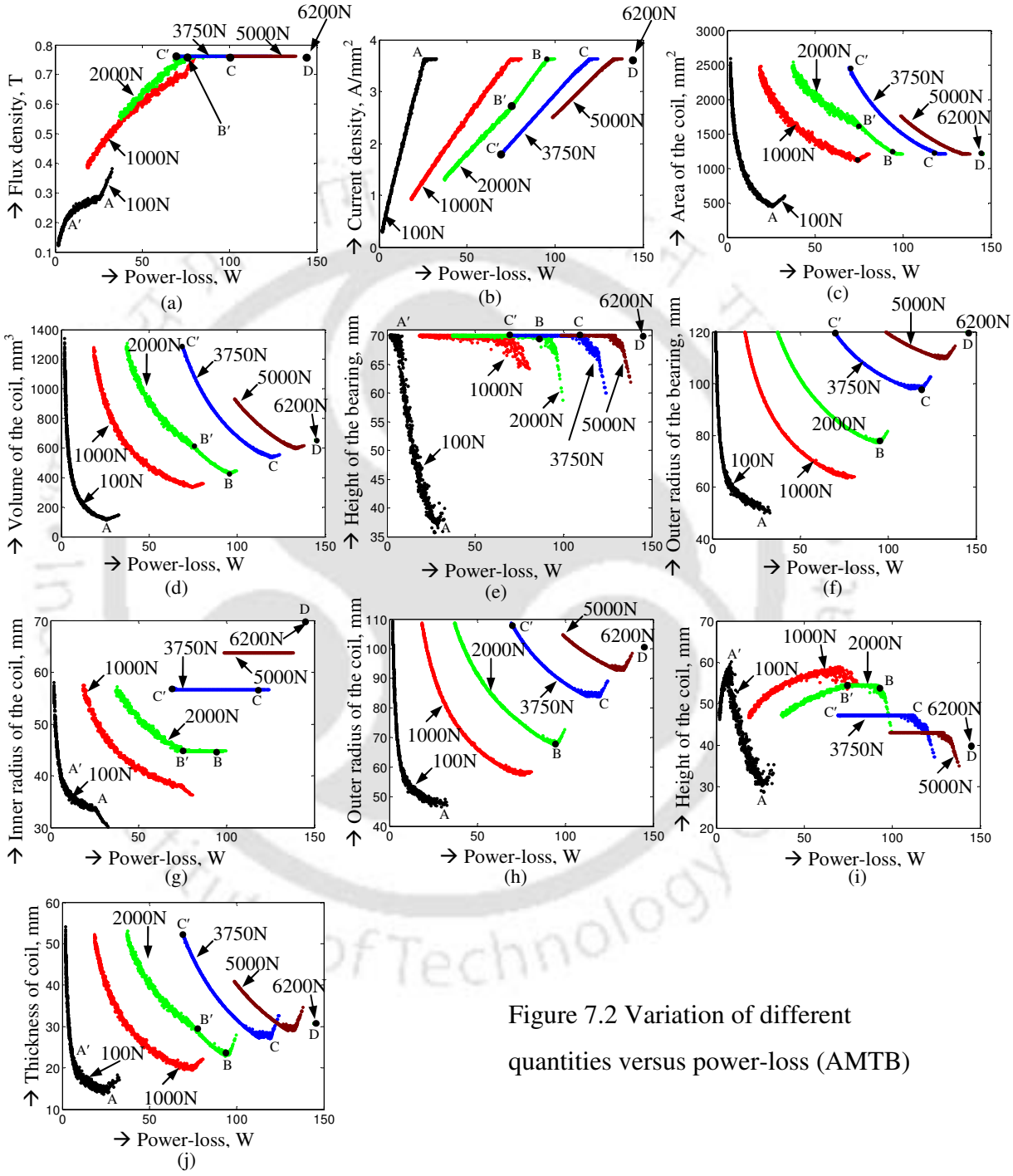

Figure 7.2 Variation of different quantities versus power-loss (AMTB)

Table 7.3 Quantities of different parameters at different points of Figure 7.2 and Figure 7.3 (AMTB)

Point	A′	A	B′	B	C′	C	D
Load(N)	100	100	2000	2000	3750	3750	6200
	Objective functions						
P (W)	8.298	25.342	84.232	95.623	69.230	119.664	145.350
W (N)	5.626	2.209	10.367	9.359	24.991	15.339	24.209
	Design Variables						
r_{ci} (mm)	36.57	33.86	44.72	44.76	56.61	56.60	69.91
r_{co} (mm)	54.76	48.22	70.57	67.9	108.71	83.84	100.64
h_c (mm)	60.19	30.65	54.58	52.36	47.21	44.40	39.36
	Coil current and magnetic flux densities						
J (A/mm2)	1.246	3.623	3.114	3.622	1.785	3.632	3.632
B (T)	0.237	0.277	0.763	0.762	0.762	0.763	0.763
	Other geometric parameters						
A_g (mm2)	2237.0	1637.4	4319.9	4330.3	8106.1	8099.8	13391
A_c (mm2)	1095.3	440.4	1410.8	1211.4	2459.6	1209.7	1209.5
V_c (mm3)	314.3	113.5	511.0	428.7	1277.5	533.7	648.1
r_o (mm)	60.92	53.35	79.72	77.38	120.00	98.02	119.96
h_t (mm)	69.92	38.35	69.96	67.75	70.00	67.18	69.84
t_c (mm)	18.20	14.37	25.85	23.14	52.10	27.25	30.73

From Figure 7.2(a), it can be observed that in the case of without using bias magnets (i.e., for AMTB) at lower loads (for example for a load of 100N), the maximum flux-density observed to be 0.381T (refer Table 7.1) while the maximum allowed magnetic flux-density is 0.763T (refer Table 4.1 in Chapter 4). This shows that the magnetic flux-density in the

stator-iron is not saturated for any design choice at the load of 100N. From Figure 7.2(b) for the load of 100N, the current-density in the coil is saturated at point A with a value of 3.632A/mm^2 (refer Table 7.1). Hence, before saturation of the current-density the flux-density increases nonlinearly with increase in power-loss till point A in Figure 7.2(a). After point A in Figure 7.2(a) the magnetic flux-density increases linearly with the increase in power-loss. After the saturation of current-density at point A in Figure 7.2(b), the power-loss increases due to the increase in volume of the coil which is justified from equation (4.1).

Above a certain load (e.g., the curve corresponds to 2000N) the flux-density increases till it gets saturated at point B′ and remains constant there after (Figure 7.2a). At this load the current-density initially increases with lesser slope with respect to power-loss till point B′ (Figure 7.2b). After point B′ the current-density increases with more slope than before point B′, till the current-density gets saturated at point B. Further increase in the load after a certain load (e.g., the curve corresponds to 3750N), the flux-density is saturated and remains constant (i.e., Point C) throughout the front (Figure 7.2a). At this load the current-density increases till it saturates (Figure 7.2b). At the peak load (i.e., point D) both the flux and current densities are saturated. Hence, from above observations various distinct load ranges could be observed (i) the unsaturated (increases) flux-density i.e., Region I, (ii) the unsaturated (increases) and saturated (remains constant) flux density, i.e. Region II, (iii) the saturated flux density (i.e. remains constant), i.e. Region III, and finally (iv) the optimised peak load, i.e. Region IV.

It can be observed from Figure 7.2(c), (i.e. the plot of the cross-sectional area of the coil versus the power-loss), that there is a minimum cross-sectional area possible at which the

current-density is saturated and it remains constant after that. In the unsaturated flux-density region (i.e. point A) the cross-sectional area of coil reduces till the current-density saturates, and then increases. In and after the unsaturated and saturated flux-density regions (i.e. point B) the cross sectional area of coil decreases till the current density saturates; then it remains constant. Moreover, at any load region till the flux density is saturated, the number of choices available are more for the same power-loss but once the flux density is saturated the number of choices for the area of cross section reduces. This is due to the fact that the inner radius of the coil and the back-wall thickness become constant and the non-dominated value is decided only by the outer radius of the coil.

From Figure 7.2(d), the variation of the volume of the coil with respect to the power-loss shows similar trend as the cross-sectional area of the coil for same reasons. One difference is that the power-loss increases linearly with increase in the volume of coil, once the current-density is saturated in all load regions. This can be justified from equation (4.1) that at the fixed current-density the power-loss is directly proportional to the volume of the coil.

By observing Figure 7.2(e) and (f), it can be observed that for least power-loss the maximum height and outer radius of the bearing are chosen for all load ranges. As the power-loss increases the height of the bearing remains constant and the outer radius of the bearing reduces to a minimum where the current-density saturates for all load ranges. After the saturation of current-density, in the unsaturated magnetic flux-density region (i.e. point A), the height of the bearing increases while the outer radius of the bearing does not show any increase. After the saturation of current-density in the unsaturated and saturated

magnetic flux-density region (i.e. after point B) the height of bearing decreases while the outer radius of bearing increases.

Figure 7.2(g-j), respectively, show the scatter of values of the inner radius of coil, the outer radius of coil, the height of coil, and the thickness of coil versus the power-loss. Since the thickness of the coil is the difference of the outer and inner radii of the coil, the behaviour of Figure 7.2(g) and (h) determine the behaviour of Figure 7.2(j). From the flux-density unsaturated region (load 100N) in Figure 7.2(i), the height of the coil increases initially till point A′ and then it decreases till point A, and subsequently it increases. In the same region, from Figure 7.2(j), it could be observed that thickness of the coil reduces till A. But the rate of decrease of thickness of the coil between points A' and A is lesser than that prior to point A′. After point A both the thickness of coil (Figure 7.2j) and the height of coil (Figure 7.2i) increase with the power-loss, while the inner radius of coil (Figure 7.2g) decreases. From Figure 7.2(g) and (i), in the flux-density unsaturated region (e.g., the curve corresponding to 100N) the decrease of the inner radius of coil after point A (Figure 7.2g) and the increase of the thickness and the height of coil (Figure 7.2i and Figure 7.2j) is due to the increase of volume of the coil (Figure 7.2d) with the power-loss as the current-density is saturated and remains constant (Figure 7.2b).

In the unsaturated and saturated flux-density region (e.g., load of 2000N) two salient points B′ and B are observed. Once the flux-density gets saturated (i.e. point B′ of Figure 7.2a) the inner radius (Figure 7.2g) and the height of the coil (Figure 7.2i) remains constant up to point B. Before point B′, the inner radius of coil (Figure 7.2g) and the thickness of coil (Figure 7.2j) decrease with the power-loss, while the height of coil increases (Figure 7.2i)

with the power-loss. After B′, the inner radius of the coil remains constant with the increase in power-loss (Figure 7.2g). The height of the coil remains constant till the current-density is saturated at point B (Figure 7.2b and Figure 7.2i), while the thickness of the coil decreases (Figure 7.2j) with the power-loss. After point B the height of the coil decreases (Figure 7.2i), while the thickness and outer radius of the coil increase (Figure 7.2h andFigure 7.2j) with the power-loss.

In the saturated flux density region (e.g., the load of 3750N) the inner radius of the coil (Figure 7.2g) remains constant throughout the front. The height of the coil remains constant till the current density is saturated at point C (Figure 7.2i), while the outer radius and the thickness of the coil (Figure 7.2h and j) decrease with the power-loss. At the peak load (i.e., 6200N) all quantities converge to a single point D, since both the magnetic flux and coil current densities are saturated at this load. Trends of different parameters with the increase in the power-loss are summarized in Table 7.4.

Table 7.4 Behavior of different variables in different load regions (AMTB)

Load region	Flux-density unsaturated (Region I)			Flux-density unsaturated – saturated (Region II)			Flux-density saturated (Region III)	
	Before A′	Between A′- A	After A	Before B′	Between B′- B	After B	Between C′- C	After C
Design Variables								
r_{ci}	↓*	↓	↓	↓	↔	↔	↔	↔
r_{co}	↓	↓	↔	↓	↓	↑	↓	↑
h_c	↑	↓	↑	↑	↔	↓	↔	↓
Coil current and magnetic flux densities								
J	↑	↑	↔	↑	↑	↔	↑	↔
B	↑	↑	↑	↑	↔	↔	↔	↔
Other geometric parameters								
A_g	↓	↓	↓	↓	↔	↔	↔	↔
A_c	↓	↓	↑	↓	↓	↔	↓	↔
V_c	↓	↓	↑	↓	↓	↑	↓	↑
r_o	↓	↓	↓	↓	↓	↑	↓	↑
h_t	↔	↓	↑	↔	↔	↓	↔	↓
t_c	↓	↓	↑	↓	↓	↑	↓	↑

*↓ - decreases, ↑ - increases, and ↔ - remains constant.

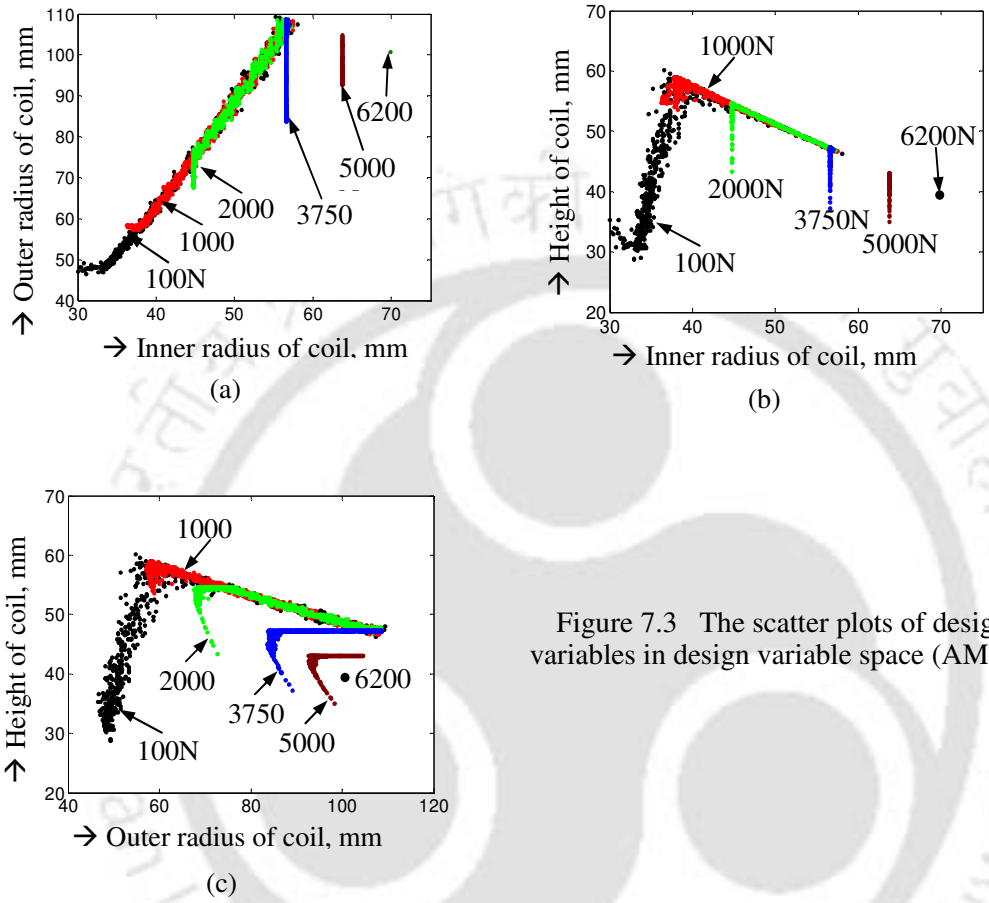

Figure 7.3 The scatter plots of design variables in design variable space (AMTB)

Figure 7.3(a – c) show the scatter of values of design variables in the design variable space without bias magnets (i.e. for the AMB). The plot of the outer radius of the coil versus the inner radius of the coil is shown in Figure 7.3(a), the height of the coil versus the inner radius of the coil is shown Figure 7.3(b), and the height of the coil versus the outer radius of the coil is shown in Figure 7.3(c). It can be observed from Figure 7.3(a) that in the unsaturated flux-density region (i.e., load of 100N), the outer radius of the coil remains constant initially and then increases with the increase in the inner radius (Figure 7.3a). In

this load region, initially the height of the coil decreases with the increase in the inner radius of the coil and then increases along with the inner radius of the coil (Figure 7.3b).

In the flux-density unsaturated and saturated region (i.e., the load of 2000N), the inner radius of the coil remains constant initially and then increases with the outer radius of the coil (Figure 7.3a). In the saturated flux-density region (i.e. the load of 3750N), the inner radius of coil remains constant and the variation takes place in the outer radius coil (Figure 7.3a) and the height of the coil (Figure 7.3b). Finally, at the peak load (i.e. the load of 6200N) the curve reduces to a single point (i.e., point D).

From Figure 7.3(b) and Figure 7.3(c) it can be observed that the maximum height that can be attained decreases with the increase in the load. This is due to the reason that with the increase in the load the requirement of inner radius of coil increases from equations (7.3) and (7.4)

$$A_g = \pi\left(r_{ci}^{\,2} - r_i^2\right) = 2\pi r_{ci} t_b = \pi\left(r_o^{\,2} - r_{co}^2\right) \tag{7.3}$$

and

$$F = \frac{B_g^{\,2} A_g}{\mu_0} = \frac{\phi_g^{\,2}}{\mu_0 A_g} \text{ with } \phi_g = B_g A_g \tag{7.4}$$

Details of equations (7.3) and (7.4) have been provided in Section 2.2 of Chapter 2, at equations (2.4) and (2.11), respectively. Similarly from equation (7.3), the requirement of back-wall thickness increases with the increase in the inner radius of the coil and correspondingly the maximum allowable height of the coil decreases.

7.3.2 Case with bias magnets (HMTB)

In this section, the case with bias magnets (i.e., HMTB) has been studied. Variations of different quantities versus the power-loss are presented in Figure 7.4(a – k). Figure 7.4(a-d) show plots of the magnetic flux-density, the coil current-density, the cross-sectional area of coil, and the volume of the coil versus the power-loss. These plots for the HMB behave similar to the corresponding plots of the AMTB in Figure 7.2(a-d). Hence, similar to the case AMTB, load ranges can be subdivided as (i) the flux-density is unsaturated (increases): Region I, (ii) the flux-density unsaturated (increases) and saturated (remains constant)): Region II, (iii) the flux-density saturated (constant)): Region III, and (iv) the peak load (both the flux and current densities are saturated)): Region IV.

The difference between the HMTB and the AMTB characteristic is in the change of quantities of the load where the load zone transition takes place. The transition from the unsaturated to unsaturated-saturated zones takes place at a load of 1400N. The transition between the unsaturated-saturated and the saturated load zones takes place at a load of 5350N. Similar to AMTB some salient points have been observed for the case of HMTB in Figure 7.4 and the corresponding values at these points have been provided in Table 7.5.

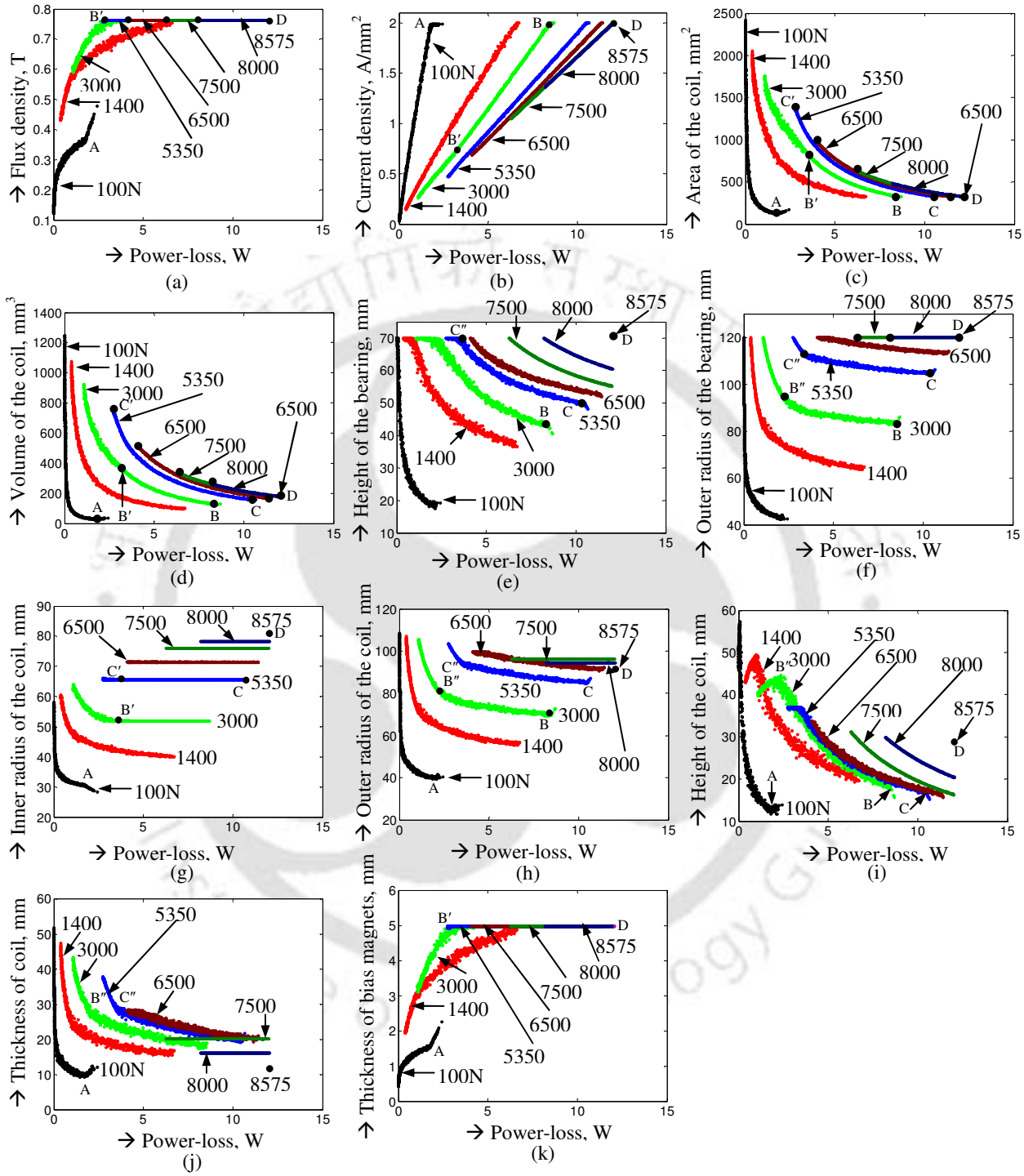

Figure 7.4 Variation of different quantities versus powerloss (HMTB)

Table 7.5 Quantities of different parameters at different points of Figure 7.4 and Figure 7.5 (HMTB)

Point	A′	A	B″	B′	B	C″	C′	C	D
Load(N)	100	100	1400	1400	1400	5350	5350	5350	8575
	Objective functions								
P (W)	0.069	1.755	1.284	4.190	8.469	3.221	7.987	10.509	12.075
W (kg)	7.313	0.609	20.795	9.369	6.502	21.212	13.653	12.302	23.441
	Design Variables								
r_{ci} (mm)	39.60	30.62	60.35	51.84	51.84	65.61	65.6	65.60	80.75
r_{co} (mm)	61.05	40.07	97.82	74.75	69.55	96.67	87.34	84.96	92.22
h_c (mm)	57.32	12.54	41.51	30.09	18.47	36.98	20.1	16.89	28.50
	Coil current and magnetic flux densities								
J (A/mm^2)	0.103	1.981	0.313	0.948	1.998	0.569	1.496	1.999	2.000
B (T)	0.206	0.358	0.631	0.763	0.763	0.763	0.763	0.763	0.763
	Other geometric parameters								
A_g (mm^2)	2962.5	982.2	9479	6479.5	6480.1	11559.6	11555.2	11555.2	18520.7
A_c (mm^2)	1229.7	118.5	1555.2	689.5	327.1	1148.8	437	327	326.9
V_c (mm^3)	388.8	26.3	772.8	274.2	124.7	585.7	210	154.6	177.6
r_o (mm)	68.34	43.8	112.19	87.47	83.07	114.13	106.33	104.39	120.00
h_t (mm)	69.99	19.15	70.00	54.96	43.34	70.00	53.11	49.90	69.98
t_c (mm)	21.45	9.45	37.47	22.91	17.71	31.06	21.74	19.36	11.47
l_m (mm)	0.77	1.51	3.49	4.98	4.98	4.98	4.98	4.98	4.98

7.3.3 Design characteristic differences of HMTB and AMTB

Though most of characteristics of the HMTB are similar to that of the AMTB below 5350N (i.e., the flux-density saturated and constant load region) some differences have been observed and are discussed in following paragraphs.

With reference to Figure 7.4(a), (b), (g) and (i); in the unsaturated and saturated flux-density region (e.g., the load of 3000N) three salient points are observed B″, B′ and B in contrast to two points in the case of AMTB (Figure 7.2g – Figure 7.2i). B″ corresponds to the point where the maximum height of coil is achieved (Figure 7.4i), B′ corresponds to the point where the inner radius of the coil becomes constant once the flux density saturates (Figure 7.4a and Figure 7.4g), and point B corresponds to the point where current density saturates (Figure 7.4b).

Above the load 6500N, the height of the bearing decreases (Figure 7.4e) till the current-density saturates without showing an initial constant trend as in the case of AMTB in Figure 7.2(e). Moreover, from Figure 7.4(g-j), it could be observed that at a load of 6500N both the outer radius and the height of the coil decrease (Figure 7.4h and Figure 7.4j), while the inner radius of coil remains constant (Figure 7.4g).

Above the load 7500N, the outer radius of the bearing remains constant (Figure 7.4f) in contrast to the AMB in Figure 7.4(f). At this load both the inner and outer radii of the coil remain constant (Figure 7.4g and Figure 7.4h), while the height of the coil decreases (Figure 7.4i).

The flux density is given by the equation

$$B_g = \frac{\mu_0 \left(K_i \vartheta_a + 2\vartheta_m \right)}{2\left(K_a l_g + K_f l_m \right)} \tag{7.5}$$

Details of equation (7.5) are given in Chapter 2 at equation (2.9). The height of bias magnet versus the power-loss (i.e. Figure 7.4k) shows the similar characteristics as the plot of flux-density (Figure 7.4a). This is because according to equation (7.5) the flux-density of bias magnets (which supports the static load applied with zero supplied current) is a function of the height of bias magnet only. Behaviours of different parameters with respect to the increase in the power-loss are summarized in Table 7.6.

Table 7.6 Behavior of different variables in different load regions (HMTB)

Load region	Flux density unsaturated (Region I)			Flux density unsaturated - saturated (Region II)			Flux density saturated (Region III)	
	Before A′	Between A′- A	After A	Before B′	Between B′- B	After B	Between C′- C	After C
Design Variables								
r_{ci}	↓	↓	↓	↓	↔	↔	↔	↔
r_{co}	↓	↓	↑	↓	↓	↑	↓	↑
h_c	↑	↓	↑	↑	↓	↓	↓	↑
Coil current and magnetic flux densities								
J	↑	↑	↔	↑	↑	↔	↑	↔
B	↑	↑	↑	↑	↔	↔	↔	↔
Other geometric parameters								
A_g	↓	↓	↓	↓	↔	↔	↔	↔
A_c	↓	↓	↑	↓	↓	↔	↓	↔
V_c	↓	↓	↑	↓	↓	↑	↓	↑
r_o	↓	↓	↓	↓	↓	↑	↓	↑
h_t	↔	↓	↓	↔	↓	↓	↔	↓
t_c	↓	↓	↑	↓	↓	↓	↓	↑
l_b	↑	↑	↑	↑	↔	↔	↔	↔

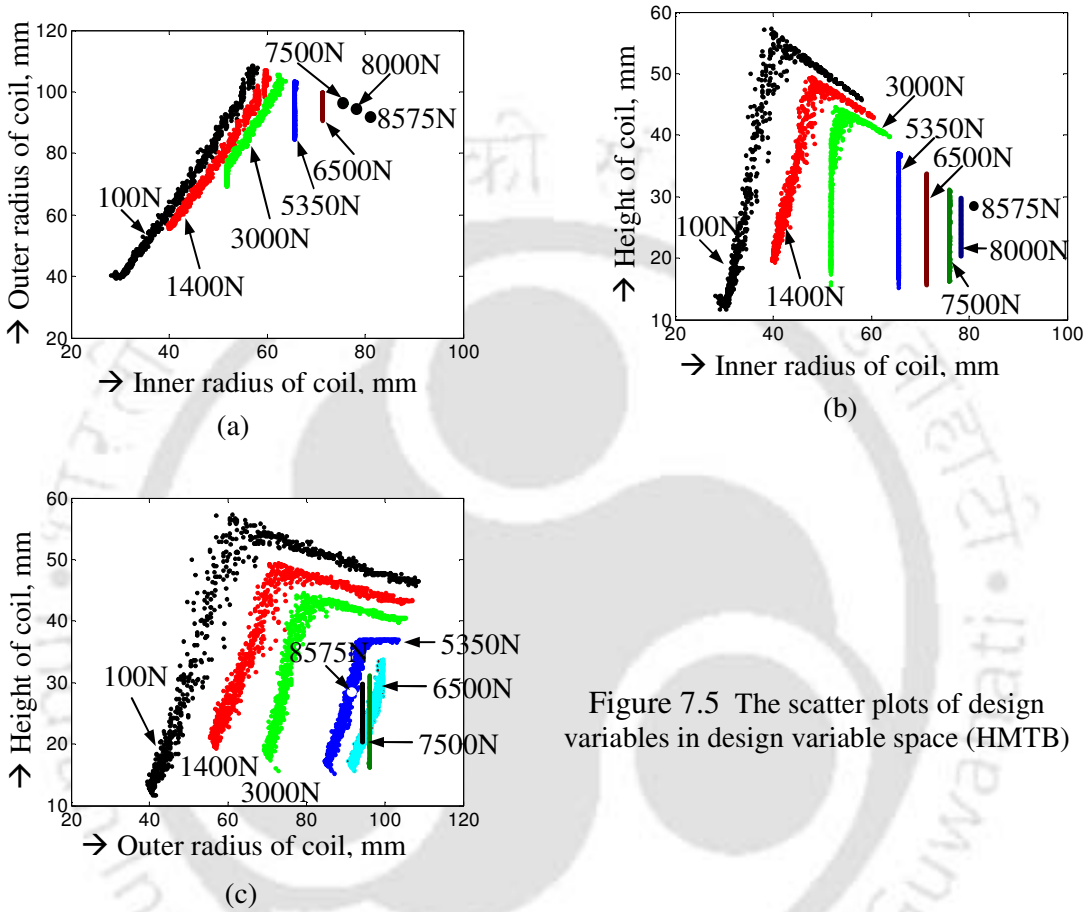

Figure 7.5 The scatter plots of design variables in design variable space (HMTB)

Characteristic differences of the design variable space are now discussed. Below the load of 7500N, the scatter of values of design variables in the design variable space for the case of HMTB (i.e. Figure 7.5a – Figure 7.5c) show similar trends as those of the AMTB. At the load of 7500N, the outer radius of the coil becomes constant in addition to the inner radius of the coil and it represents a single point (Figure 7.5a), but the height of the coil increases (Figure 7.5b and Figure 7.5c). This is due to the fact that the height of the bias magnet is a constant at 7500N (Figure 7.4k) but not the height of the coil (Figure 7.4i). Moreover, from

Figure 7.5(c) it can be observed that above the load of 7500N the outer radius of the coil decreases with the increase in the load till the height of the coil becomes constant at the peak load (i.e. 8575N) in contrast to the AMTB in Figure 7.3(c). But this decrease in the outer radius of coil is accompanied by the increase in the inner radius of the coil corresponding to the load of 7500N (Figure 7.5a and Figure 7.5b). This is due to the fact that at this load the inner radius increases to provide more area for the bias magnet, correspondingly the outer radius of the coil reduces to provide the same pole area at the outer wall as that of the inner wall according to equation (7.3). Moreover, from Figure 7.4(k), the thickness of bias magnets is constant at this load. Hence, the increase in height of the coil is to provide the space for the electric current to support the additional load.

Finally, at the peak load (i.e. 8575N) all three variables become constant at a single point and is represented by a dot of the white colour in Figure 7.5(c). The different load zones for cases of the AMTB and the HMTB are given in Table 7.7.

Table 7.7 Different load zones with respect to flux density saturation for the cases of AMB and HMB

Load zone	Unsaturated	Unsaturated-saturated	Saturated	Height decrease	Inner and outer radii of coil constant	Peak load
AMB	<1250N	1250N – 3750N	>3750N		6200N	6200N
HMB	<1400N	1400N – 5350N	>5350N	>6500N	>7500N	8575N

7.4 Conclusions

In the present Chapter, the effect of the load on the Pareto frontier has been presented in the optimal design of thrust magnetic bearings using MOGAs. The *Pareto optimal design analysis* methodology has been used to analyze the final populations for different loads and configurations. Two objective functions namely minimization of the power-loss and minimization of the weight of the bearing are considered. The results for AMTB and HMTB have been compared. As the load increases, it is observed that the Pareto frontier reduces to a single point at the peak load within the given constraints for both the cases of with and without bias magnets. Hence, the load to be supported can be considered as an objective function. The characteristics of design variables and other parameters with the power-loss have been discussed. Three distinct load zones have been observed within the given constraints namely the magnetic flux density unsaturated, the magnetic flux density unsaturated and saturated, magnetic flux density constant and saturated, and peak load. The transition load zones have been observed to be different for the cases of AMTB and HMB respectively. The peak load by using bias magnets is observed to be 138.3% of that of without using bias magnets within the constraints given.

On the whole the analysis methodology presented in the present work has an advantage of studying behavior of different parameters of Pareto optimal designs in final populations by taking a large population size. It would also be helpful in choosing proper design by the a-posteriori knowledge provided by the analysis of the final population through the proposed methodology (i.e., *Pareto optimal design analysis methodology*). This analysis can also be used to take interactive decisions during the search and guide the search at will.

Till now the optimal design of actuators of magnetic thrust bearings (i.e., AMTB and HMTB) has been studied. Integration of actuator and controller in the design optimization is the current trend in mechatronic systems. Hence in the next chapter an integrated design methodology will be implemented for the design optimization of double-acting hybrid magnetic bearing integrating the actuator and controller as a unified system.

Part - III
Integrated Design Optimization of DAHMTB

Chapter 8
Design Optimization of Double-Acting Hybrid Magnetic Thrust Bearings with Control Integration Using Multi-Objective Genetic Algorithms

8.1 Introduction

In the last few chapters the design of actuators of AMTB and HMTB has been carried using SOGA, MOGA. A novel a-posteriori design analysis methodology called *Pareto optimal design analysis* has been brought out as a methodology for the analysis of optimal designs of magnetic bearing systems. Some aspects of different design methodologies have been discussed in Section 1.4.1 of Chapter 1. Till now Chapters 2 to 7 dealt with *optimal design* of actuators of MTB. In the present chapter the *integrated-design optimization* of *double-acting hybrid magnetic thrust bearings* (DAHMTB) will be dealt.

An actuator or a controller could be independently optimized. However, when the actuator is optimized independent of the controller, the chosen actuator might not be a

feasible one when constraints of the controller are considered. This requires redesign of the actuator. Similarly, when the controller is optimized independent of the actuator, the chosen controller might not be a feasible one when constraints of the actuator (such as the current-density in the coil and the magnetic flux-density in the stator-iron, etc.) are taken into consideration. Moreover, the performance tradeoffs of the actuator and the controller, when they are optimized independently might not be the optimum when considered as a unified system. Hence, it is worthwhile to integrate the design of the actuator and the controller as a unified system and the same is investigated in the present chapter. In regard to the above discussion, the integration of geometric and control designs in conjunction with the optimization is the current trend in mechatronic products. In the present work, an optimal design methodology of *double-acting hybrid active magnetic thrust bearings* (DAHMTB) has been proposed. Double acting actuators and centralized controller are optimized as a unified system.

Conventionally, in the control of rotors in the axial direction using double-acting magnetic bearings, two identical bearings are used. However, in the present design two different bearing geometries with different operating parameters have been considered. The minimization of the power-loss, the weight, the control input and dynamic performance indices, and the maximization of the load capacity have been considered as objectives. Three objectives namely the power-loss, the weight of bearing, and the load capacity have been considered for the actuator. Whereas, two objectives namely the input and dynamic performance indices have been considered for the controller. The design considers ten geometric, two electrical, and two control design parameters. Constraints considered for the actuator are the maximum allowed current-density in the coil, maximum allowed flux-density in the stator-iron, maximum space available, and maximum power-loss allowed. The stiffness and Eigen values of characteristic equation have been considered as

constraints for the controller. Constraints are classified into three categories, namely the geometric, electrical, and control constraints.

The genetic algorithm has been implemented to carry out the constrained multi-objective optimization of the present problem. The convergence and Pareto-front spaces are studied by using populations of sizes of 100 and 200 that is run for 100 and 1000 generations. Some of the convergence criterions have been observed for actuator controller systems. Designs which are nearest to the utopia point in Pareto-front fronts are compared. Air gaps, bias currents, and lengths of permanent magnets are observed to be consistently different for individual actuators of the double-acting bearing. Performance parameters of double-acting actuators and the controller of the magnetic bearing for different choices have been presented.

The macro-geometry of double-acting actuator, actuator relations, controller relations, multi-objective optimization problem formulation for DAHMTB, and numerical results will be presented in following sections.

8.2 Macro geometry of the actuator

The macro-geometry of a DAHMTB is shown in Figure 8.1. The corresponding magnetic circuit, rotor disc displacement positions and force directions during control have been shown in Figure 8.2. Different design parameters are shown in Figure 2.11, and are described in Nomenclatures. The geometrical relations and electro-magnetic relations of single-acting actuators of MTB have been presented in section 2.2.1 and section 2.2.2

respectively. Now the corresponding electro-magnetic relations for actuators of actuators of DAHMTB will be presented in the next section.

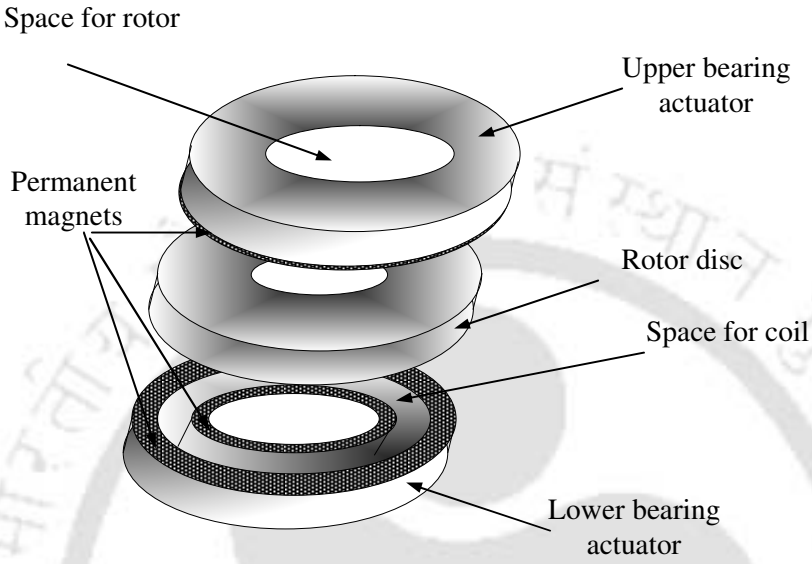

Figure 8.1 Components of magnetic thrust bearing

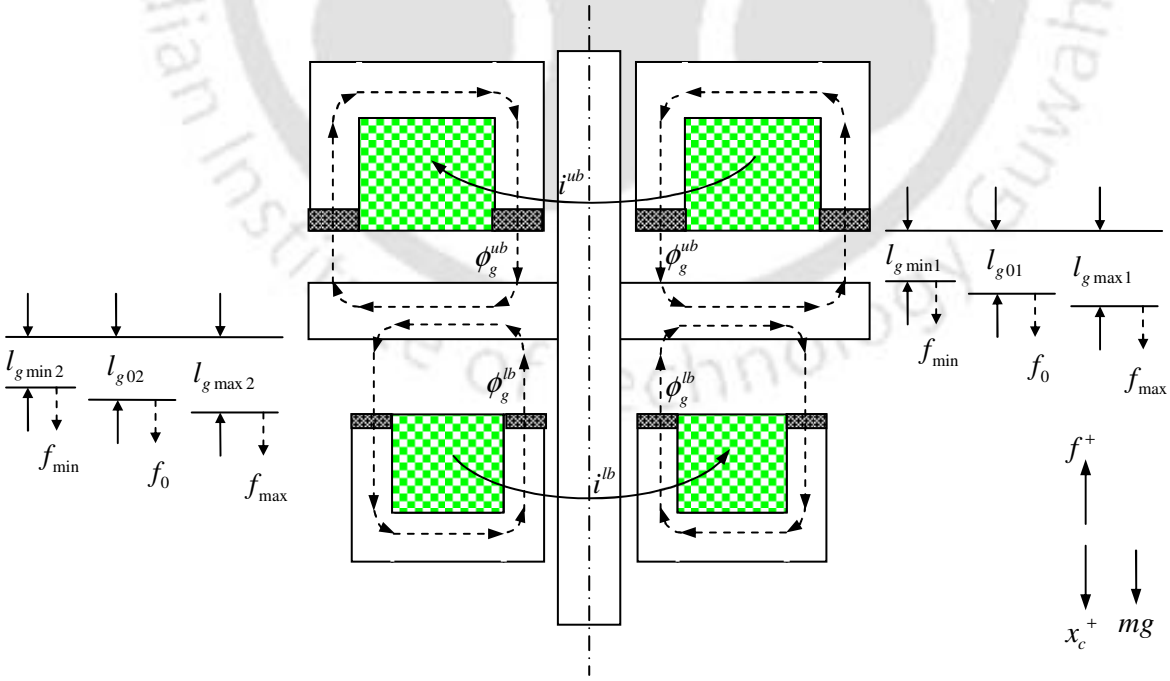

Figure 8.2 Magnetic circuit and limits of the air-gap in a double acting magnetic thrust bearing

8.3 Actuator relations

Fundamental relations related to the single-acting and double-acting HMTBs are provided in this section. These relations can be reduced for AMTBs, by ignoring parameters related to permanent magnets (i.e., ϑ_m, l_m and B_r) to zero. From the magnetic circuit theory, according to Amperes' circuital law the *magnetic flux-density* can be expressed as

$$B_g^x = \frac{\mu_0\left\{K_i\left(\vartheta_b^x + \vartheta_c^x\right) + 2\vartheta_m^x\right\}}{2\left\{K_a\left(l_{g0}^x + x_c^x\right) + K_f l_m^x\right\}} \qquad \text{with} \quad \vartheta_b = ni_b \quad \text{and} \quad \vartheta_c = ni_c \tag{8.1}$$

where i_b is the bias current, i_c is the control current, l_{g0} is the operating air-gap length, x_c is the displacement to be controlled. Superscript, x: either lb or ub, represent lower bearing or upper bearing actuator, respectively.

According the principle of virtual work, the *magnetic force* exerted by the magnetic field is obtained by differentiating the field energy with respect to the air-gap, as

$$F^x = \frac{\left(B_g^x\right)^2 A_g^x}{\mu_0} = \frac{\left(\phi_g^x\right)^2}{\mu_0 A_g^x} \qquad \text{with} \qquad \phi_g^x = B_g^x A_g^x \tag{8.2}$$

The force exerted by the double-acting bearing, F^{db} could be determined as

$$F^{db} = F^{ub} - F^{lb} \tag{8.3}$$

where F^{ub} the force is applied by the upper bearing, and F^{lb} is the force applied by the lower bearing. The *current density* in the coil, J, is related as

$$J^x = \vartheta^x / \eta^x A_c^x \tag{8.4}$$

where ni is the magneto motence, η is the coil packing-factor, and A_c is the cross-sectional area of the coil. The standard form of expression of the *power-loss* in the coil is given as

$$P^x = \rho \eta^x \left(J^x\right)^2 V_c^x \tag{8.5}$$

where ρ is the electric resistivity of the coil material and V_c is the volume of the coil. From the geometry of the thrust magnetic bearing in Fig. 2, the cross sectional area and the volume of the coil are expressed as

$$A_c^x = \left(r_{co}^x - r_{ci}^x\right) h_c^x \qquad \text{and} \qquad V_c^x = \pi \left\{ \left(r_{co}^x\right)^2 - \left(r_{ci}^x\right)^2 \right\} \left(h_c^x\right)^2 \tag{8.6}$$

For the double-acting HMTB, the total power-loss of the bearing can be defined as

$$P^{db} = P^{ub} + P^{lb} \tag{8.7}$$

where P^x is the power-loss in the coil with superscript x: *db*, *ub*, and *lb* represent double-acting bearing, upper bearing, and lower bearing; respectively. The *weight* of the bearing can be expressed as

$$W^x = W_c^x + W_s^x + W_m^x \tag{8.8}$$

where W is the overall weight of the bearing, and W_y are weights of components of bearing with the subscript y: c, s and m represent the coil, the stator, and the bias (or permanent) magnet; respectively. With reference to Figure 8.1 various components of weight of the bearing can be expressed as

$$W_c^x = \gamma_c \pi \left(r_{co}^x + r_{ci}^x\right)\left(r_{co}^x - r_{ci}^x\right) h_c^x \tag{8.9}$$

$$W_s^x = \gamma_s \pi \left\{\left(r_{ci}^x + r_i^x\right)\left(r_{ci}^x - r_i^x\right) h_c^x + \left(r_o^x + r_{co}^x\right)\left(r_o^x - r_{co}^x\right) h_c^x + \left(r_o^x + r_i^x\right)\left(r_o^x - r_i^x\right) t_b^x\right\} \tag{8.10}$$

$$W_m^x = \gamma_m \pi \left\{\left(r_{ci}^x + r_i^x\right)\left(r_{ci}^x - r_i^x\right) + \left(r_o^x + r_{co}^x\right)\left(r_o^x - r_{co}^x\right)\right\} l_m^x \tag{8.11}$$

where γ is the weight density of the corresponding material. For double-acting bearings, the overall weight of the magnetic bearing, W^{db}, could be expressed as the sum of weights of individual actuators as

$$W^{db} = W^{ub} + W^{lb} \tag{8.12}$$

In this section different relations correspond to the actuator have been presented till now, relations correspond to the controller will be presented now in the subsequent section.

8.4 Control Relations

In a double-acting bearing, two single-acting bearings are used on both sides of the disc. Control forces act on the disc in two opposite directions along the shaft as shown in Fig. 3, which also shows positive conventions of directions for the load and the displacement. When an external load acts in one direction, there will be a displacement in that direction. To bring the system back to the operating position, an additional control current should flow in the coil of the bearing which is on the opposite side of the rotor disc with respect to an operating position. In differential controller the control current is added to one bearing and the same is subtracted from the other while in uni-mode controller only one of the two coils is supplied by the control current.

Now we will summarize some of fundamental relations concerned to the controller. Using equation (8.1), the *magnetic force* generated by the double-acting bearing can be rewritten as

$$F(x_c, i_c) = \frac{\mu_0 A_g^{ub}}{4}\left\{\frac{K_i\left(\vartheta_b^{ub} + \vartheta_c^{ub}\right) + 2\vartheta_m^{ub}}{K_a\left(l_{g0}^{ub} + x_c\right) + K_f l_m^{ub}}\right\}^2 - \frac{\mu_0 A_g^{lb}}{4}\left\{\frac{K_i\left(\vartheta_b^{lb} + \vartheta_c^{lb}\right) + 2\vartheta_m^{lb}}{K_a\left(l_{g0}^{lb} - x_c\right) + K_f l_m^{lb}}\right\}^2 \tag{8.13}$$

where x_c is the displacement to be controlled, and i_c is the controlling current. Two different thicknesses of permanent magnets have been considered, which are located on either sides of the rotor disc of the thrust bearing. The magnetic *force generated by permanent magnets* can be expressed as

$$F_m = \frac{\mu_0 A_g^{ub}}{4}\left(\frac{2\vartheta_m^{ub}}{K_a l_{g0}^{ub} + K_f l_m^{ub}}\right)^2 - \frac{\mu_0 A_g^{lb}}{4}\left(\frac{2\vartheta_m^{lb}}{K_a l_{g0}^{lb} + K_f l_m^{lb}}\right)^2 \tag{8.14}$$

The s*tatic load bearing capacity* is defined as the load supported by the bearing, when the displacement and the control current are zero. This load is also called as *the bias load*. The bias magnetic flux and the bias coil-current are designed to support the static load. From equation (8.13), the static load bearing capacity is expressed as

$$F(0,0) = \frac{\mu_0 A_g^{ub}}{4}\left(\frac{K_i\vartheta_b^{ub} + 2\vartheta_m^{ub}}{K_a l_{g0}^{ub} + K_f l_m^{ub}}\right)^2 - \frac{\mu_0 A_g^{lb}}{4}\left(\frac{K_i\vartheta_b^{lb} + 2\vartheta_m^{lb}}{K_a l_{g0}^{lb} + K_f l_m^{lb}}\right)^2 \tag{8.15}$$

The *dynamic load bearing capacity* is defined as (Chang and Chung, 2002)

$$F(0, i_{c,\max}) = \frac{\mu_0 A_g^{ub}}{4}\left\{\frac{K_i\left(\vartheta_b^{ub} + \vartheta_{c,\min}^{ub}\right) + 2\vartheta_m^{ub}}{K_a l_{g0}^{ub} + K_f l_m^{ub}}\right\}^2 - \frac{\mu_0 A_g^{lb}}{4}\left\{\frac{K_i\left(\vartheta_b^{lb} + \vartheta_{c,\min}^{lb}\right) + 2\vartheta_m^{lb}}{K_a l_{g0}^{lb} + K_f l_m^{lb}}\right\}^2 \tag{8.16}$$

There are two terms used for load capacity namely, the *static load capacity* and the *dynamic load capacity*. The *static load* is due to *bias current* and/or *permanent magnets*, while the variation in the load (*dynamic load*) is due to the control current. The maximum variation in the load is compensated by the maximum current. The load expressed in equation (8.16) is instantaneous and the control current varies with a frequency according to equation (8.24). The dynamic load capacity is determined at maximum control current.

In the most of practical cases, the static load is the weight of the rotor as shown in Figure 8.2 and the dynamic load is the load due to external disturbances. Hence, bias currents can be supplied to cancel out the static load, and the control current is supplied to cancel out the disturbances.

The *overall load capacity* of the double-acting bearing is defined as

$$F(x_{c,\max}, i_{c,\max}) = \frac{\mu_0 A_g^{ub}}{4}\left\{\frac{K_i\left(\vartheta_b^{ub} + \vartheta_{c,\max}^{ub}\right) + 2\vartheta_m^{ub}}{K_a\left(l_{g0}^{ub} + x_{c,\max}\right) + K_f l_m^{ub}}\right\}^2 - \frac{\mu_0 A_g^{lb}}{4}\left\{\frac{K_i\left(\vartheta_b^{lb} + \vartheta_{c,\max}^{lb}\right) + 2\vartheta_m^{lb}}{K_a\left(l_{g0}^{lb} - x_{c,\max}\right) + K_f l_m^{lb}}\right\}^2 \tag{8.17}$$

Expanding equation (8.13) by Taylor's series and on neglecting higher order terms, it can be written as

$$F(x_c, i_c) = F(0,0) + k_x x_c + k_i i_c \tag{8.18}$$

with

$$k_x = \left.\frac{\partial F}{\partial x_c}\right|_{(0,0)}, \qquad k_i = \left.\frac{\partial F}{\partial i_c}\right|_{(0,0)} \tag{8.19}$$

where k_x and k_i are the *displacement* and *current stiffness*, respectively; which are expressed as

$$k_x = -\left.\frac{\partial F}{\partial x_c}\right|_{(0,0)} = \frac{2K_a\mu_0 A_g^{ub}}{4}\frac{\left(K_i\vartheta_b^{ub} + 2\vartheta_m^{ub}\right)^2}{\left(K_a l_{g0}^{ub} + K_f l_m^{ub}\right)^3} + \frac{2K_a\mu_0 A_g^{lb}}{4}\frac{\left(K_i\vartheta_b^{lb} + 2\vartheta_m^{lb}\right)^2}{\left(K_a l_{g0}^{lb} + K_f l_m^{lb}\right)^3} \tag{8.20}$$

and

$$k_i = \left.\frac{\partial F}{\partial i_c}\right|_{(0,0)} = \frac{2K_i\mu_0 A_g^{ub}}{4}\frac{\left(K_i\vartheta_b^{ub} + 2\vartheta_m^{ub}\right)}{\left(K_a l_{g0}^{ub} + K_f l_m^{ub}\right)^2} + \frac{2K_i\mu_0 A_g^{lb}}{4}\frac{\left(K_i\vartheta_b^{lb} + 2\vartheta_m^{lb}\right)}{\left(K_a l_{g0}^{lb} + K_f l_m^{lb}\right)^2} \tag{8.21}$$

There are different terms used for k_x and k_i by different authors which are summarized in Table 8.1. However the terms *position stiffness* for k_x and *current stiffness* for k_i have been adapted in the present work.

Table 8.1 Terminology used for k_x and k_i

Authors	k_x	k_i
Schweitzer, 1994; Chiba et. al., 2004	Force-displacement factor	Force-current factor
Knospe and Tamer, 1997; Maslen, 2000	Open-loop stiffness	Actuator gain
Antila, 1998; Zhuravlyov, 2000	Position stiffness	Current stiffness

The negative nature of the displacement stiffness in equation (8.20) denotes that the system is unstable in the absence of the control current. The equation of motion of the rotor after canceling the static load can be written as

$$m\ddot{x}_c = F_c \tag{8.22}$$

where m is the mass of the rotor, and F_c is the force generated by the magnetic bearing system after canceling the static load. From equation (8.18), it can be expressed as

$$F_c = k_x x_c + k_i i_c \tag{8.23}$$

In equation (8.23), x_c is the quantity to be controlled and i_c is the controlling input.

The controller supplies the input depending on the output of the system to be controlled. There are many kinds of controlling methods, of which PD controller is the simplest one. According to PD controller, the input control current is expressed as (Ueno and Okada, 2000)

$$i_c = -\left(k_P x_c + k_D \dot{x}_c\right) \tag{8.24}$$

where k_P is the proportional gain and k_D is the derivative gain. Non-contacting sensors can accurately determine displacements only, hence in equation (8.24) $\dot{x}_c$ is determined by differentiation of the available displacements. From equations (8.22) to (8.24), we have

$$m\ddot{x}_c + k_i k_D \dot{x}_c + \left(k_i k_P - k_x\right) x_c = 0 \tag{8.25}$$

Eigen values of equation (8.25) are

$$\lambda_{1,2} = -\frac{k_i k_D}{2m} \pm \sqrt{\left(\frac{k_i k_D}{2m}\right)^2 - \left(\frac{k_i k_P - k_x}{m}\right)} \tag{8.26}$$

For the stability of the system the real parts of all Eigen-values must be less than zero. According to Routh-Hurwitz criterion the system in equation (8.25) is stable, only if all the coefficients are greater than or equal to zero. Hence, we get following constraints

$$k_i k_D \geq 0 \qquad \text{and} \qquad k_P \geq \frac{k_x}{k_i} \tag{8.27}$$

The *performance index* of the controller is defined as (Schweitzer, 1994)

$$\chi = \int_0^{t_f} \left(x_c^2 + Q i_c^2 \right) dt \tag{8.28}$$

where χ is the performance index, Q is the weighting parameter, and t_f is the final time. To eliminate the Q-parameter in equation (8.28), two performance indexes can be defined namely, the input and output performance indexes. The input performance index of the controller is defined as

$$\chi_i = \int_0^{t_f} i_c^2 dt \tag{8.29}$$

where χ_i is the input performance index, i_c is the control current supplied to bring the system to a nominal operating position.

The *output performance index* of the controller is defined as (Sarkar and Modak, 2005)

$$\chi_o = \int_0^{t_f} x_c^2 dt \tag{8.30}$$

where χ_o is the output performance index, and x_c is the output vector of the system to bring to the nominal operating state from the disturbed state. On considering the *setting-time*, the *dynamic performance* index is defined as (Chen and Chang, 2006)

$$\chi_d = \int_0^{t_f} t x_c^2 dt \tag{8.31}$$

where t is time, and t_f is the upper-bound of the setting-time. The input and dynamic performance indexes are considered as objective functions in the present work. Different fundamental relations corresponding to the actuator and the controller have been discussed in the present section. The formulation of the multi-objective optimization problem will be discussed in the next section.

8.5 Multi-objective problem formulation

The multi-objective optimization problem consists of objective functions to be optimized by design variables while satisfying certain constraints in the process of optimization. A model of multi-objective optimization problem for the present case is provided in Table 8.2.

Table 8.2 The multi-objective optimization formulation of the problem

Minimize $f_i(\mathbf{x})$ with $i = 1,...,5$
where $\mathbf{x} = \left\{ r_{ci}^{ub}, r_{co}^{ub}, h_c^{ub}, l_{g0}^{ub}, l_m^{ub}, r_{ci}^{lb}, r_{co}^{lb}, h_c^{lb}, l_{g0}^{lb}, l_m^{lb}, i_b^{ub}, i_b^{lb}, k_P, k_D \right\}$
Subject to $g_j(\mathbf{x}) \geq 0 \quad j = 1,\ldots,14; \quad x_p^L \leq x_p \leq x_p^U \quad p = 1,\ldots,14$

Expressions for objective functions and constraints have been presented for the optimum design of double-acting hybrid magnetic thrust bearings in the following subsections.

8.5.1 Objective Functions

The load capacity of bearing should be maximized in the whole process of design. A small size of the bearing may reduce the weight but reduces the load capacity as well. Hence, the load capacity and weight are conflicting quantities. The energy utilized by the control system in stabilizing the rotor system is also important in the case of active magnetic bearings. There are two performance indexes considered in the optimization of the control energy, namely the input performance index and the dynamic performance index. The input performance index determines how much energy is utilized in stabilizing the system, and the dynamic performance index determines how fast the system is stabilized.

One of the most important factors to consider in the design of an active magnetic bearing is its power efficiency. Reducing the power consumption will reduce not only the operational costs, but also the acquisition costs. If the required power could be reduced, then smaller and therefore economical amplifiers and less power supplies could be used. The reduction of power also lessens cooling requirements of windings. While applications such as the space based systems and small pumps for medical applications have the most to gain by reducing power requirements, other typical commercial systems could also be significantly improved.

The controller can be optimized in terms of the performance index given by equation (8.28) with different optimization strategies such as the LQR (Linear Quadratic Regulator), H_2-norm, H_∞-norm, etc. An optimal LQR problem targets to control the system such that the performance index which does not include plant disturbances and the measurement noise, as given by equation (8.28), are minimal along all possible trajectories (Anderson and Moore, 1990). Including the plant disturbances and the measurement noise, the system model can

be solved for a compensator such that the steady-state mean-square error of the system, which is called as H_2-norm, is minimized (Saberi et al., 1993). When the compensator is designed for the minimization of maximum of steady-state mean-square error of the system, it is called H_∞-optimization (Kwakernaak, 1993). Optimization of the performance index by optimizing the weighting parameter Q in equation (8.28) is one method of achieving the optimized solution. The multi-objective optimization by optimizing both the H_2- and H_∞-norms as objectives was suggested by Schroder et al. (1998). Contrary to a single norm, a multi-objective approach of considering the input and output performances as separate objectives, was suggested by Sarkar and Modak (2005). The product of setting time and square of error in the output signal (the product is termed as dynamic performance index in the present study) was used as the single-objective for the control of rotor by Chen and Chang (2006). The input performance index of the controller represents the overall input given to the controller to bring an initial disturbed state to a stable operating state. Lower values of the input performance index represent the better performance. The output performance index of the controller represents the cumulative output in bringing the system to the nominal operating state from an initial disturbed state. Lower values of output performance index represent better performance. Moreover, while bringing the system to stable state, the supplied control current is directly dependant on state of the system according to equation (8.24). Hence the input and output performance indexes are interrelated. The dynamic performance index considers also the time involved in bringing the system to steady-state. The summary of different objective functions chosen for the optimization is provided in Table 8.3.

Table 8.3 Objective functions and constraints of the present multi-objective optimization problem

Objective function	Eqn. no.	Constraint	Eqn. no.	Constraint	Eqn. no.
$f_1(\mathbf{x}) = P$	(8.7)	$g_1(\mathbf{x}) = J_{\text{sat}} - \max\left(J_{\max}^{ub}, J_{\max}^{lb}\right)$	(8.32)	$g_6(\mathbf{x}) = r_{oub} - \max\left(r_o^{ub}, r_o^{lb}\right)$	(8.37)
$f_2(\mathbf{x}) = W$	(8.12)	$g_2(\mathbf{x}) = \min\left(J_{\min}^{ub}, J_{\min}^{lb}\right)$	(8.33)	$g_7(\mathbf{x}) = h_{tub} - \max\left(h_t^{ub}, h_t^{lb}\right)$	(8.38)
$f_3(\mathbf{x}) = -F$	(8.3)	$g_3(\mathbf{x}) = \alpha_{\max} B_{\text{sat}} - \max\left(B_{\max}^{ub}, B_{\max}^{lb}\right)$	(8.34)	$g_8(\mathbf{x}) = F_m^{xi}$; $g_9(\mathbf{x}) = F^{xi}$; $g_{10}(\mathbf{x}) = F^{xo}$	(8.39)
$f_4(\mathbf{x}) = \chi_i$	(8.29)	$g_4(\mathbf{x}) = \min\left(B_{\min}^{ub}, B_{\min}^{lb}\right) - \alpha_{\min} B_{\text{sat}}$	(8.35)	$g_{11}(\mathbf{x}) = k_i k_D$; $g_{12}(\mathbf{x}) = k_i k_P - k_x$	(8.27)
$f_5(\mathbf{x}) = \chi_d$	(8.31)	$g_5(\mathbf{x}) = P_{\max} - \max\left(P_{\max}^{lb}, P_{\max}^{ub}\right)$	(8.36)	$g_{13}(\mathbf{x}) = t_s - t_{slb}$; $g_{14}(\mathbf{x}) = t_{sub} - t_s$	(8.40)

8.5.2 Selection of the Design Vector

In a multi-objective optimization problem each objective function (e.g. the weight of the bearing) could be written in terms of a set of independent parameters (i.e., r_{ci}, r_{co}, h_c, l_m) and these are called design variables. All other parameters of the respective objective function (i.e., r_o, t_b, h_t) could be determined from this set of design variables. In a multi-objective optimization problem, the union of all the sets of design variables of different objectives is chosen as the design vector. In the present case, the weight of the bearing could be written in terms of the coil and bias magnet dimensions (i.e. r_{ci}, r_{co}, h_c, l_m) according to equations (8.8) ─ (8.12). The power-loss at the operating point and the load carrying capacity could be observed as functions of the bias current, i_b and the operating air-gap, l_{g0} in addition to the coil and bias magnet dimensions according to equations (8.1) ─ (8.7). Controller performance indexes are functions of gains $[k_P, k_D]$ and the actuator position and current stiffness $[k_x, k_i]$ according to equation (8.25). Moreover, according to equations (8.20) and (8.21), parameters, $[k_x, k_i]$ are functions of the bias current, the operating air-gap, and the coil and permanent magnet dimensions. Hence, the overall geometric design variables

chosen are $[r_{ci}, r_{co}, h_c, l_m]$, the operating design variables $[l_{g0}, i_b]$ and the control design variables $[k_P, k_D]$. As different design parameters have been assumed for the two actuators on opposite side of the rotor disc, the overall design vector of the system will be $[r_{ci}^{ub}, r_{co}^{ub}, h_c^{ub}, l_m^{ub}, r_{ci}^{lb}, r_{co}^{lb}, h_c^{lb}, l_m^{lb}, l_{g0}^{ub}, i_b^{ub}, l_{g0}^{lb}, i_b^{lb}, k_P, k_D]$. The dependency of different objective functions on different design variables is given in Table 8.4.

Table 8.4 Influence of design variables on various objective functions

Design Parameters	Geometric								Operating				Control	
	r_{ci}^{ub}	r_{co}^{ub}	h_c^{ub}	l_m^{ub}	r_{ci}^{lb}	r_{co}^{lb}	h_c^{lb}	l_m^{lb}	l_{g0}^{ub}	i_b^{ub}	l_{g0}^{lb}	i_b^{lb}	k_P	k_D
Weight	✓	✓	✓	✓	✓	✓	✓	✓	×	×	×	×	×	×
Load Capacity	✓	✓	✓	✓	✓	✓	✓	✓	✓	✓	✓	✓	×	×
Power-loss	✓	✓	✓	✓	✓	✓	✓	✓	✓	✓	✓	✓	×	×
Input Index	✓	✓	✓	✓	✓	✓	✓	✓	✓	✓	✓	✓	✓	✓
Dynamic Index	✓	✓	✓	✓	✓	✓	✓	✓	✓	✓	✓	✓	✓	✓

8.5.3 Constraints

The discussion on the constraints of the actuator of single-acting magnetic thrust bearings has been provided in Chapter 2. The corresponding constraints for the double-acting actuator and the constraints correspond to controller will be provided in this section.

The current density for the individual actuators of DAHMTB can be determined from equation (2.13) should not be greater than the saturation current density of the coil material or cannot be negative. Hence, constraints can be expressed as

$$J_{sat} \geq \max\left(J_{\max}^{ub}, J_{\max}^{lb}\right) \tag{8.32}$$

$$\min\left(J_{\min}^{ub}, J_{\min}^{lb}\right) \geq 0 \tag{8.33}$$

where $J_{\max}^{x}$ is the maximum density of current flowing in upper or lower bearing, $J_{\min}^{x}$ is the minimum density of current flowing in upper or lower bearing and J_{sat} is the saturation current-density of the coil.

The magnetic flux-density that flows in the stator-iron core, could be determined from equation (8.1) considering the linear range of operation with the iron saturation factor, α, the constraints correspond to upper and lower limits of magnetic flux density are expressed as

$$\alpha_{\max} B_{sat} \geq \max\left(B_{\max}^{ub}, B_{\max}^{lb}\right) \tag{8.34}$$

$$\min\left(B_{\min}^{ub}, B_{\min}^{lb}\right) \geq \alpha_{\min} B_{sat} \tag{8.35}$$

where $B_{\max}^{x}$ is the maximum magnetic flux-density flowing in upper or lower bearing, $B_{\min}^{x}$ is the minimum magnetic flux-density in the upper or lower bearing and B_{sat} is the saturation magnetic flux density of the stator iron, $\alpha_{\max}$ is the iron saturation factor corresponding to upper limit of magnetic flux-density, $\alpha_{\min}$ is the iron saturation factor corresponding to the lower limit of the magnetic flux-density.

The maximum power-loss due to the resistance of the coil material is constrained by the heat removal rate of the cooling system; hence the constraint is given by

$$P_{\max} \geq \max(P_{\max}^{lb}, P_{\max}^{ub}) \tag{8.36}$$

where $P_{\max}^{lb}$ and $P_{\max}^{ub}$ are the maximum power-loss in the lower and upper actuators respectively, and is given by equation (2.14).

The space available for the bearing is limited, and the corresponding constraints are

$$r_{oub} \geq \max\left(r_o^{ub}, r_o^{lb}\right) \tag{8.37}$$

$$h_{tub} \geq \max\left(h_t^{ub} + h_t^{lb} + l_g^{ub} + l_g^{lb} + t_d\right) \tag{8.38}$$

where r_{oub} is the upper bound of the outer radius of the bearing, h_{tub} is the upper bound of the total height of the double actuator of the bearing and t_d is the thickness of the rotor disc (thrust collar), and h_t^x can be found from equation (2.1).

The static load supported is assumed to be in the direction opposite to the upper bearing, hence the force generated by the double- acting bearing to be positive in the upper direction. Hence, forces generated due to permanent magnets including the maximum, minimum, and operating forces are to be positive. The maximum and minimum forces due to permanent magnets are determined corresponding to the maximum displacement of the rotor disc from the operating position. These maximum displacements allowed are lesser than the backup bearing clearances. The backup bearing clearances are lesser than the magnetic bearing clearances so that the magnetic material should not be spoiled by the direct contact. Hence, constraints corresponding to operating forces can be expressed as

$$F_m^{xi} \geq 0 \qquad F^{xi} \geq 0 \quad \text{and} \qquad F^{xo} \geq 0 \tag{8.39}$$

where superscripts *xi* and *xo*, respectively, represent nearest and farthest position of the rotor disc from the upper actuator. Stability conditions of the system give rise to a constraint that the real part of the eigen-value of equation (8.26) to be negative; equivalently, equation (8.27) can be used as constraints related to the stability. For a good dynamic performance, the settlement time should not be too long as well as it should not be too short and can be expressed as

$$t_{sub} \geq t_s \geq t_{slb} \tag{8.40}$$

Various constraints that are considered in the design of double-acting hybrid magnetic thrust bearings are listed in Table 8.3.

8.6 Numerical results

For the present optimisation problem, five objectives with fourteen design variables and fourteen constraints have been presented in Section 8.5. The design vector presented in Section 8.5.2 has been chosen as the chromosome. All design variables in the present problem are real in nature. Hence, the present multi-objective optimisation problem has been implemented by real-coded genetic algorithms on the basis of non-dominated sorting strategy as explained in Chapter 4.

Different input parameters chosen for the design of magnetic bearing systems, which includes both the actuator and the controller, are given in Table 8.5. Various bounds of the design vector have been summarised in Table 8.6. To avoid manufacturing infeasibilities,

the lower bound for the inner radius of coil is chosen as 27 mm, which gives a minimum 2 mm inner-wall thickness. To avoid contact between the rotor and the actuator, the lower bound of the air-gap has been chosen as 1 mm.

Table 8.5 Input parameters assumed for the DAHMTB design

Parameter	Value	Parameter	Value
Inner radius of the bearing, r_i	25.00 mm	Specific gravity of the stator-iron, γ_s	7.77 g/cm^3
Mass of the rotor, m	2.22 kg	Specific gravity of the copper, γ_c	8.91 g/cm^3
Iron saturation factors, ($\alpha_{\min}$, $\alpha_{\max}$)	(0, 0.8)	Specific gravity of the Nb-Fe-B, γ_m	7.50 g/cm^3
Variation in the air-gap, υ_x	±5%	Coil mmf loss factor, K_i	1.394
Variation in the load, υ_f	±10%	Actuator loss factor, K_a	1.072
Saturation flux density of iron, B_{sat}	1.00 T	Flux leakage factor, K_f	0.840
Remnant flux density of permanent magnets, B_r	1.2T	Maximum allowable coil volume, $V_{\max}$	820 mm^3
Saturation current density of coil, J_{sat}	4.0 A/mm^2	Maximum outer radius of bearing, r_{oub}	120 mm
Initial displacement, x_0	0.2mm	Maximum height of bearing, h_{tub}	70 mm
Initial velocity, v_0	0.0	Settling tolerance, x_s	0.01mm
Settling time upper bound, t_{fub}	1.0sec	Sampling time, τ	0.001sec
Coil packing factor, η	0.85	Settling time lower bound t_{flb}	0.1sec

Table 8.6 Initial bounds of design variables assumed for the GA

Design variables	r_{ci} (mm)	r_{co} (mm)	h_c (mm)	l_{g0} (mm)	l_m (mm)	i_b (A)	k_P	k_D
Lower limit	27.00	27.00	0.00	1.00	0.00	0.00	2000	0
Upper limit	82.99	120.0	70.00	5.00	3.00	5.00	6000	10

Population size: In a multi-objective evolutionary algorithm, a high population size increases the computational complexity while a low population size may give a poor distribution of the individuals in the Pareto frontier with a poor predictability of optimal values (Deb, 2001). Hence, results of two population sizes of 100 and 200 have been

compared. A probability of the crossover equal to 0.8 and a probability of the mutation equal to 0.07 (i.e. 1/no. of design variables) have been chosen in the present work for simulations. Values for η_c and η_m are assumed as, respectively, 5 and 10. Different GA input parameters chosen are summarized in Table 5.1.

Table 8.7 The GA parameters assumed for the implementation of MOGA

Parameter	Value
probability of crossover, p_c	0.8
probability of mutation, p_m	1/14
crossover distribution index,	5
mutation distribution index,	10
Population size	100 and 200
Number of generations	100 and 1000

Convergence criterion: The convergence criterion is a set condition where the algorithm shall be terminated. The criterion of convergence could be chosen from either the design space or objective space depending on the problem. In the present case, the mean and optimum values of objective functions from the parent population have been chosen as a convergence criterion. The algorithm is run for sufficient number of generations such that the convergence criterion is ensured. As genetic algorithms are stochastic in nature, converged solutions and number of generations that it takes to converge depend on several parameters for a particular problem such as the seed, the population size, GA operators used in the algorithm, etc. Hence, in the present work results have been compared with population sizes of 200 and 100 run for 1000 generations, and a population size of 200 run for 100 and 1000 generations. Computations have been carried on a Pentium 4(R), 2.4 GHz machine with 1.25 GB of RAM using VISUAL C++ 6.0. The maximum computational time of the algorithm for the optimization with the population size of 100 requires approximately 0.438 second per generation, with the population size of 200 it is approximately 0.905

second per generation. The computation time could be projected for higher number of generations. The computation time is mostly spent in determining the numerical integral in equations (8.29) and (8.31) with a sampling time of 0.001.

Program interactions: The computer program is written in three modules namely, the GA module, the actuator analysis module and the controller analysis module. The interaction of information of different modules of the computer program has been shown in Figure 8.3. The GA module gives the information of design variables to both the actuator analysis module and the controller analysis module. While the actuator analysis module and the controller analysis module gives objective function values and constraint violations to the GA module. Moreover, the actuator analysis module gives the displacement stiffness given in equation (8.20) and the current stiffness given in equation (8.21) to the controller analysis module, while the controller analysis module gives controlling current values given in equation (8.24) to the actuator analysis module.

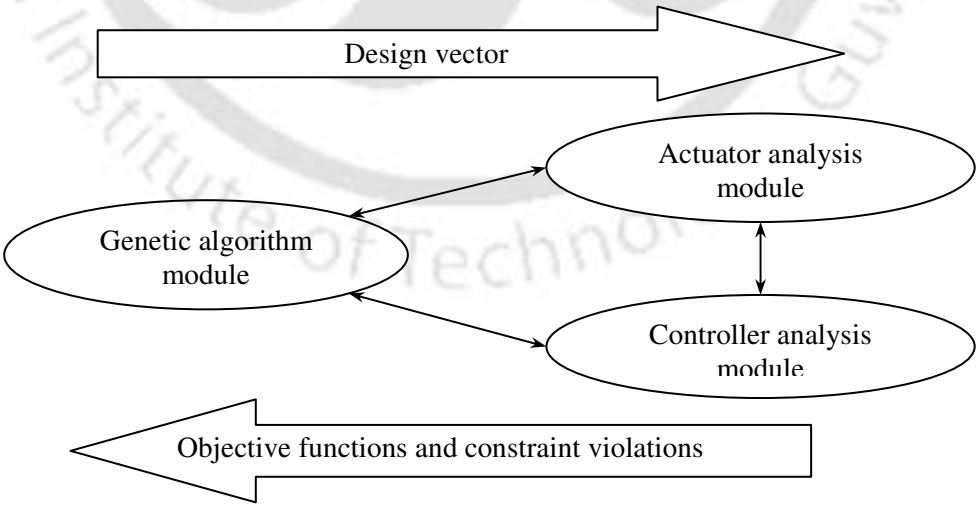

Figure 8.3 The flow of information among different modules of computer program

The number of feasible solutions in the parent population, expressed as a percentage of the population size, has been presented with the number of generations in Table 8.8. It could be observed from Table 8.8, that the infeasible solutions in the parent population of the size of 200 have been eliminated earlier than that of the population size of 100. Moreover, the rate of elimination with the generation is better in case of population size of 200 than that of 100. This shows the capability of finding a feasible solution with the higher population size.

Table 8.8 Percentage of feasible solutions in the parent population with generation

	Gen. No.	1	2	3	4	5	6	7	8	9	10	11	12
% of feasible solutions	Pop. size 100	0	0	0	0	6	12	26	56	100	100	100	100
	Pop. size 200	0	0	1	4	10.5	26.5	57	100	100	100	100	100

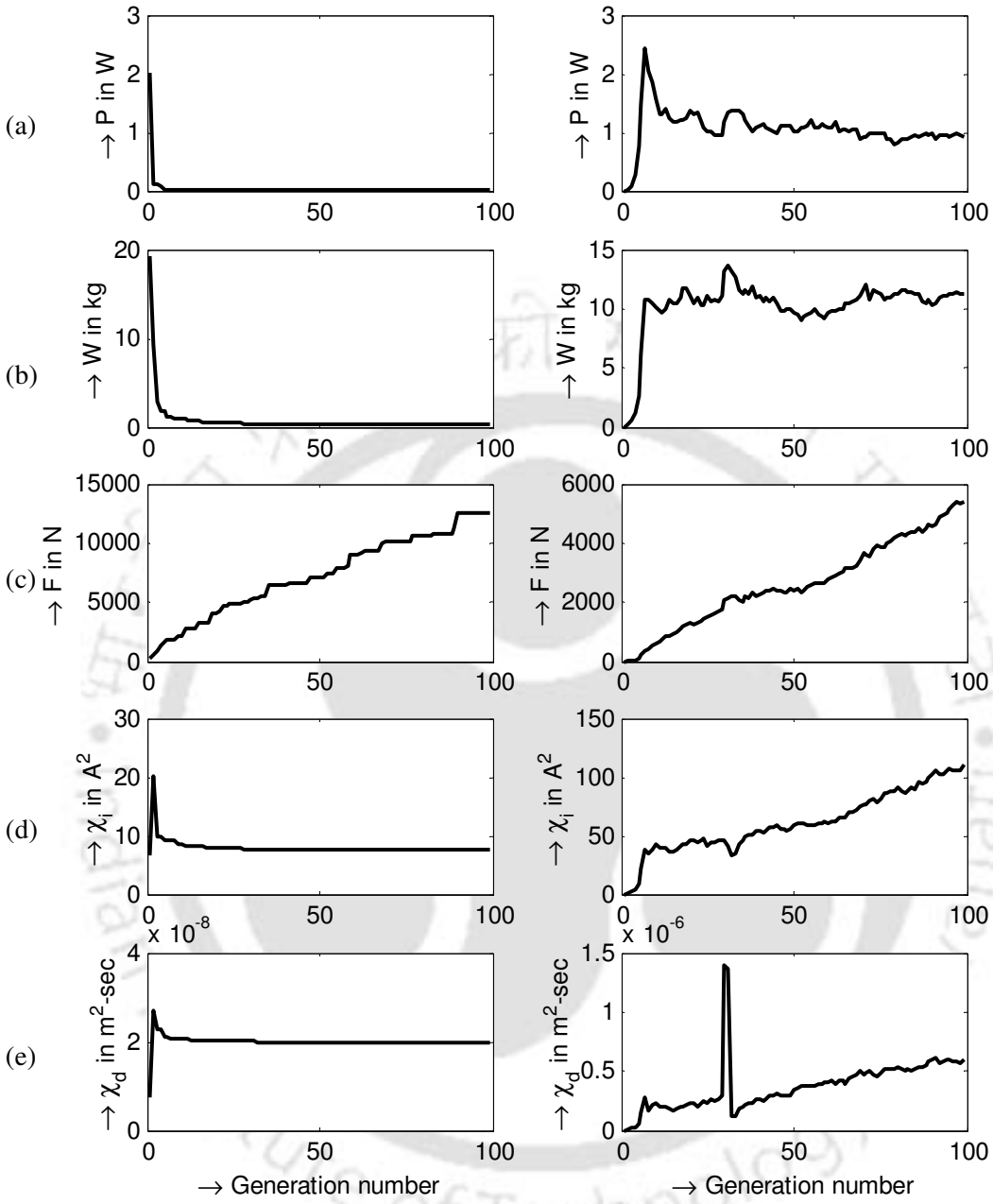

Figure 8.4 Convergence of objectives with the generation (200 population 100 generations)

(left) best value in the population (right) average value of the population

(a) Power-loss versus generation (b) Weight versus generation
(c) Load capacity versus generation (d) Input index versus generation
(e) Dynamic index versus generation

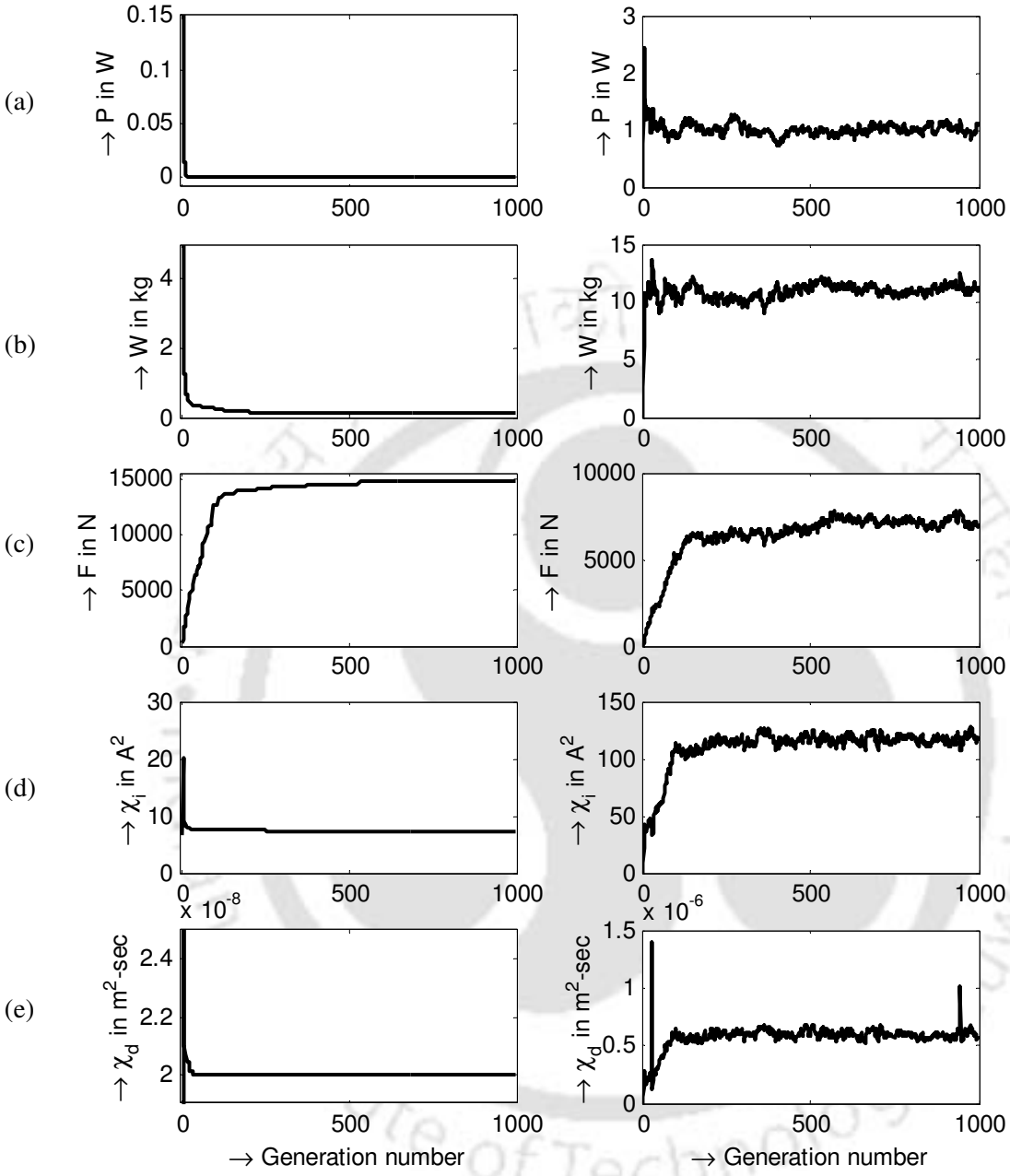

Figure 8.5 Convergence of objectives with the generation (200 population 1000 generations)
(left) best value in the population (right) average value of the population

(a) Power-loss versus generation (b) Weight versus generation
(c) Load capacity versus generation (d) Input index versus generation
(e) Dynamic index versus generation

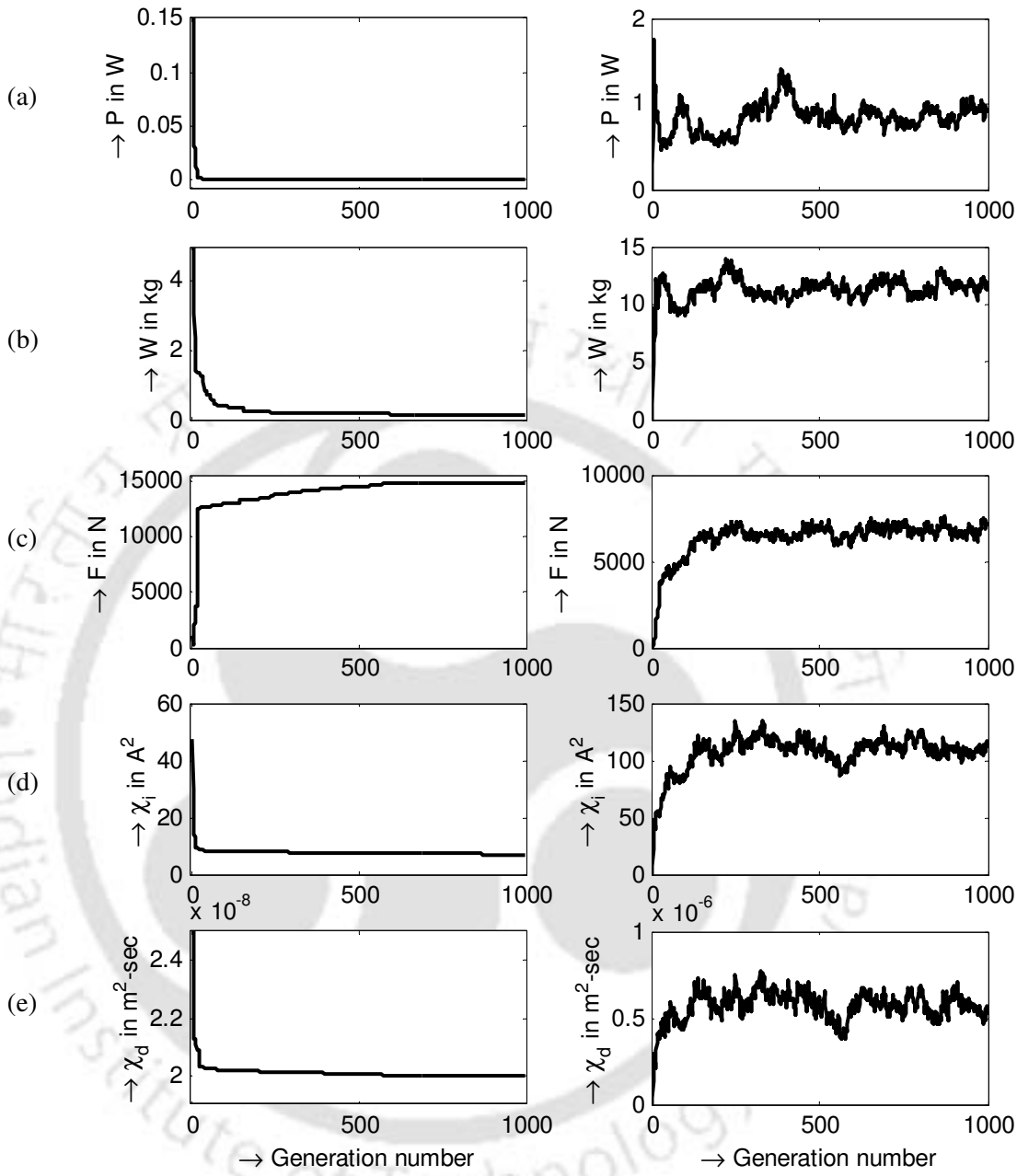

Figure 8.6 Convergence of objectives with the generation (100 population 1000 generations) (left) optimum value in the population (right) average value of the population

(a) Power-loss versus generation (b) Weight versus generation
(c) Load capacity versus generation (d) Input index versus generation
(e) Dynamic index versus generation

Convergence plots of various objective functions and their average value in the population are shown in Figure 8.4 (the population of size 200 and the generation of 100), Figure 8.5 (the population of size 200 and the generation of 1000), and Figure 8.6 (the population of size 100 and the generation of 1000). From Figure 8.4, it could be observed that though the power-loss, weight, and input and dynamic indexes have been observed to be converged, the average values of input and dynamic load capacity indexes are in increasing trend indicating the results are converged by 100 generations. From Figure 8.5 and Figure 8.6, it could be observed that after 1000 generations both the objectives and their average values are stabilized and it could be considered as one criterion of the convergence.

The optimum (i.e., the maximum for the load capacity and the minimum for rest of the objectives) and mean values of different objectives of the whole population after specified number of generations corresponding to different cases are presented in Table 8.9. The point representing these optimum objective values of Table 8.9 corresponds to the utopia point of the corresponding population in the objective space. Table 8.9 shows that the population of size 200 runs for 100 generations predicted lesser load capacity than other two cases (i.e. populations of sizes 200 and 100 run for 1000 generations). This is the result of non-convergence within 100 generations. It could also be observed from Table 8.9 that the cases of population sizes 200 and 100 with generations of 1000 approximately converged to nearer points of both the optimum and the mean, which fulfils one condition of the convergence.

Table 8.9 Optimum and mean values of the final population for different cases

		Power-loss (W)	Weight (N)	Load capacity (kN)	Input index (A^2)	Dynamic index (m^2-sec)
Pop. 200 Gen 100	Optimum	3.18e-9	0.26	12.57	7.48	2.00e-8
	Mean	0.92	11.26	5.41	110.11	6.05e-7
Pop. 200 Gen 1000	Optimum	1.67e-23	0.13	14.78	7.25	1.99e-8
	Mean	1.07	11.40	7.07	118.92	5.81e-7
Pop. 100 Gen 1000	Optimum	1.95e-16	0.14	14.83	7.07	2.00e-8
	Mean	0.96	12.01	7.29	110.78	5.13e-7

Different-cross sections of the Pareto-optimal front in two dimensions have been given in Figure 8.7, Figure 8.8, and Figure 8.9 for cases of 100 population and 1000 generations, 200 population and 1000 generations, and 200 population and 100 generations, respectively. Figure 8.7, Figure 8.8, and Figure 8.9 include data from final populations. Plots (a – d) of Figure 8.7, Figure 8.8, and Figure 8.9, show the variation of rest of objectives with respect to the load capacity. Plots (e – g) show the variation of power-loss, input and dynamic indexes with respect to the weight. Plots (h, i) show the variation of input and dynamic indexes with respect to the power-loss. Finally, plots (j) show the variation of dynamic index with respect to the input index.

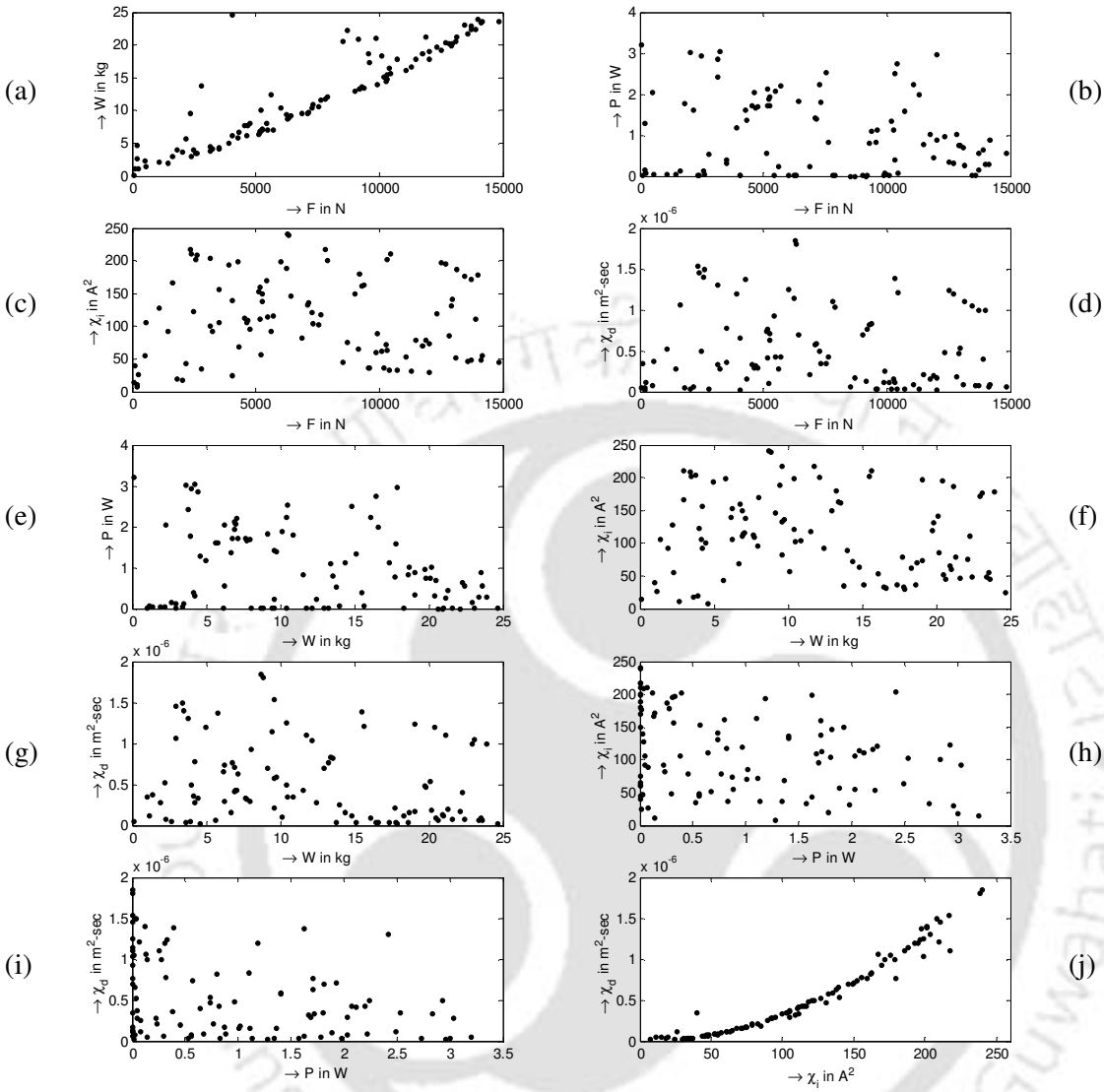

Figure 8.7 The Pareto optimal front two dimensional sections (100 population 1000 generations)

(a) Weight versus load capacity
(b) Power-loss versus load capacity
(c) Input index versus load capacity
(d) Dynamic index versus load capacity
(e) Power-loss versus weight
(f) Input index versus weight
(g) Dynamic index versus weight
(h) Input index versus power-loss
(i) Dynamic index versus power-loss
(j) Dynamic index versus input index

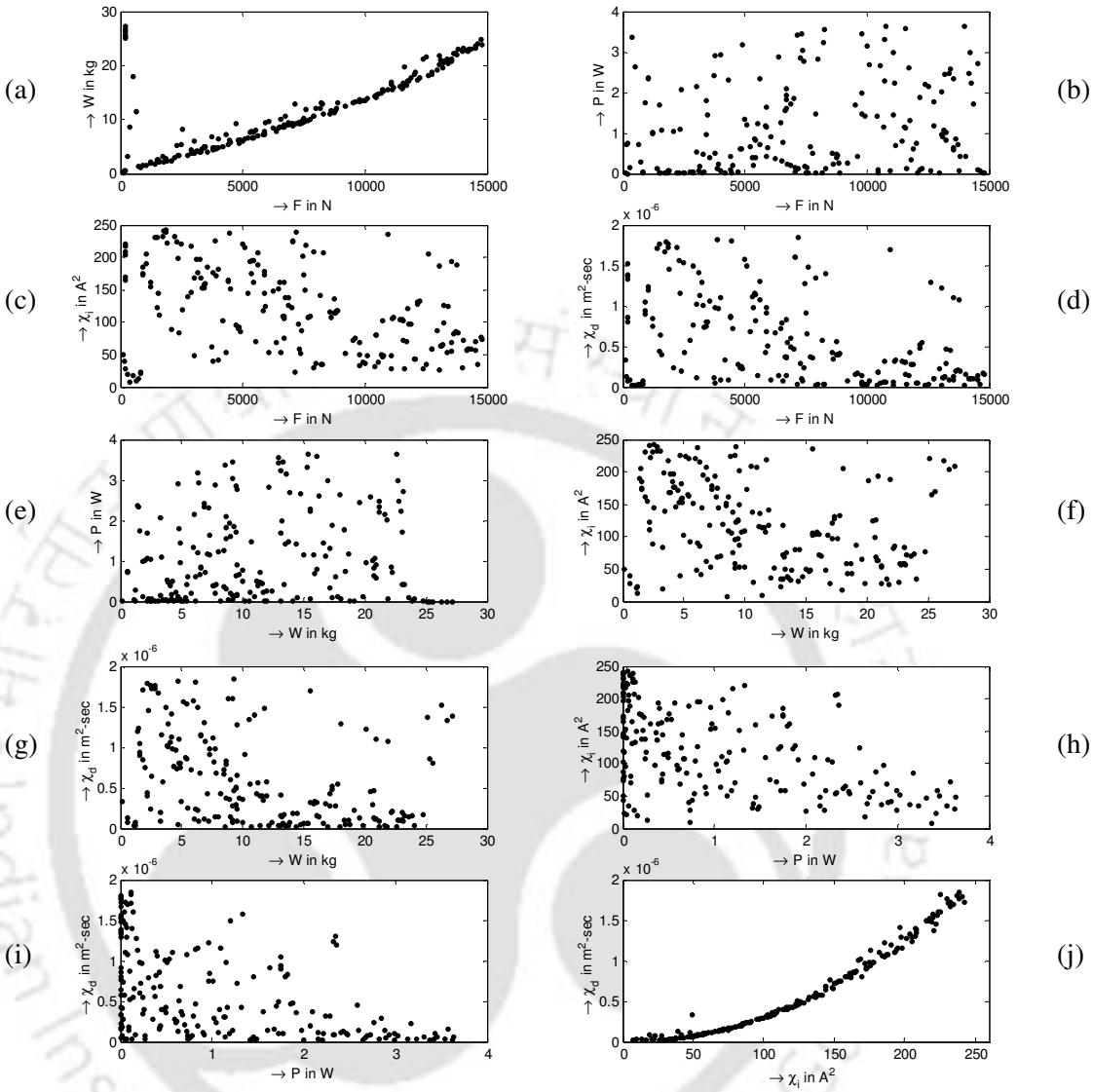

Figure 8.8 The Pareto optimal front two dimensional sections (200 population 1000 generations)

(a) Weight versus load capacity (b) Power-loss versus load capacity

(c) Input index versus load capacity (d) Dynamic index versus load capacity

(e) Power-loss versus weight (f) Input index versus weight

(g) Dynamic index versus weight (h) Input index versus power-loss

(i) Dynamic index versus power-loss (j) Dynamic index versus input index

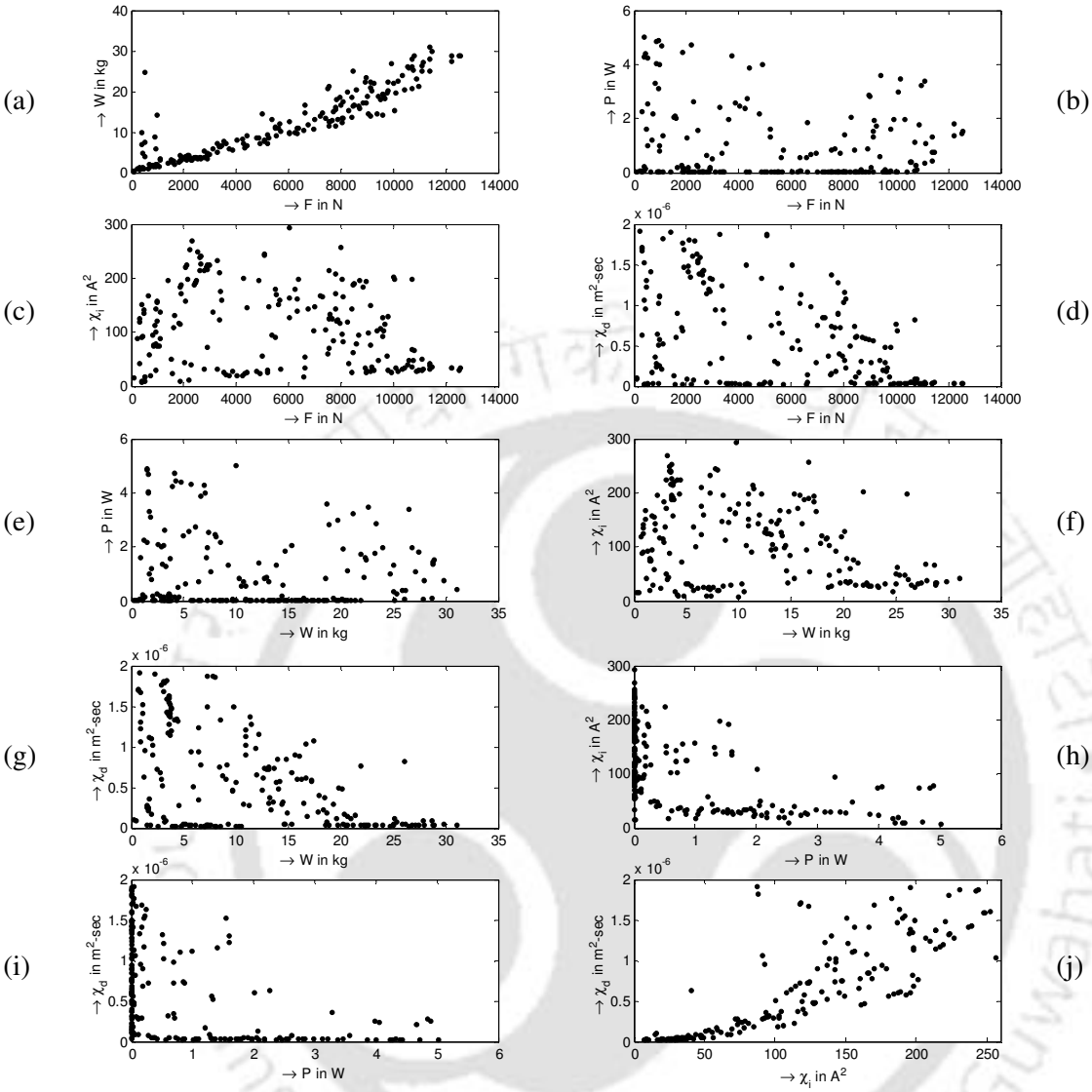

Figure 8.9 The Pareto optimal front two dimensional sections (200 population 100 generations)

(a) Weight versus load capacity

(b) Power-loss versus load capacity

(c) Input index versus load capacity

(d) Dynamic index versus load capacity

(e) Power-loss versus weight

(f) Input index versus weight

(g) Dynamic index versus weight

(h) Input index versus power-loss

(i) Dynamic index versus power-loss

(j) Dynamic index versus input index

From Figure 8.7(a) and Figure 8.8(a), it could be observed that the increase in the load capacity increases the weight. Similarly, from Figure 8.7(j) and Figure 8.8(j) it could be observed that the increase in the input index increases the dynamic index. Moreover, points in Figure 8.9(a and j) are more scattered than the respective plots of Figure 8.7 and Figure 8.8. This result provides an additional convergence criterion for the optimization of magnetic actuators and controllers. The corresponding optimized fronts of the load capacity versus the weight and the input index versus the dynamic index scattered with the narrow variation.

From Figure 8.7(e) and Figure 8.8(e), we could observe that the most of solutions fall near zero power-loss at the operating point. This is due to permanent magnets, which support the static load. Plots of Figure 8.9(b, e, h, and j) are clustered more at the zero power-loss and at the zero input and dynamic indexes than the corresponding plots of Figure 8.7 and Figure 8.8. This scatter in Figure 8.7 and Figure 8.8 indicates that the bias current, i_b deviates from zero for a better load capacity, weight, and dynamic performance of the actuator controller system.

Figure 8.7(a) and Figure 8.8(a) show that there is an optimum weight corresponding to every load. Similarly Figure 8.7(j) and Figure 8.8(j) show that there is an optimum dynamic performance index corresponding to each input performance index. However, in the case of Figure 8.7(b) (i.e., the power-loss versus the load) the points are more scattered. This shows that at each load there are different power-losses possible based on the weight chosen for the design and the algorithm chooses the best among many available. From Figure 8.7 (*b*-*i*) and from Figure 8.8 (*b*–*i*), in summary, the power-loss, input performance index and

dynamic performance index do not have proper trend of optimum design. At each force or weight value they have multiple solutions and the algorithm chooses one among them.

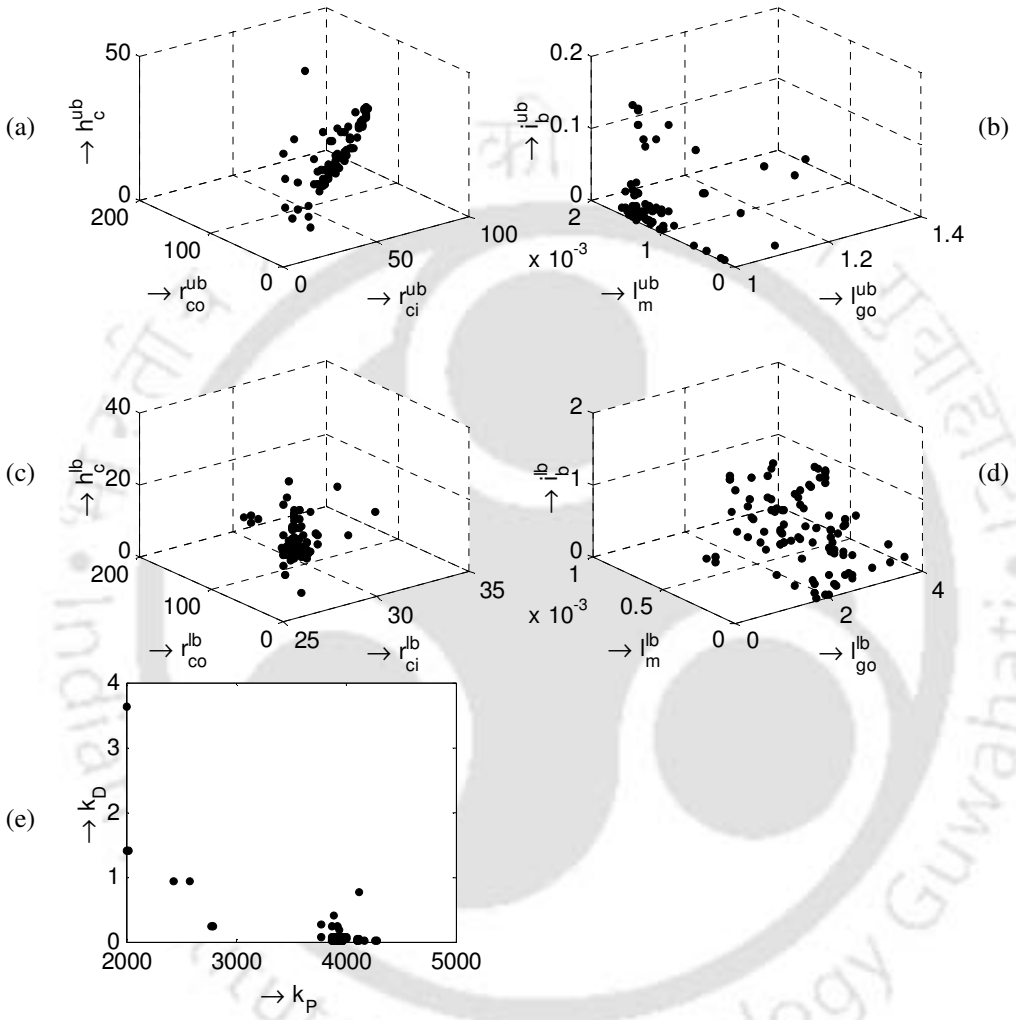

Figure 8.10 Scatter of design variables in the design variable space (100 population and 1000 generations)

(a) Inner radius versus outer radius and height (Upper bearing)

(b) Bias current versus air gap and thickness of bias magnets (Upper bearing)

(c) Inner radius versus outer radius and height (Lower bearing)

(d) Bias current versus air gap and thickness of bias magnets (Lower bearing)

(e) Derivative gain versus proportional gain (Controller)

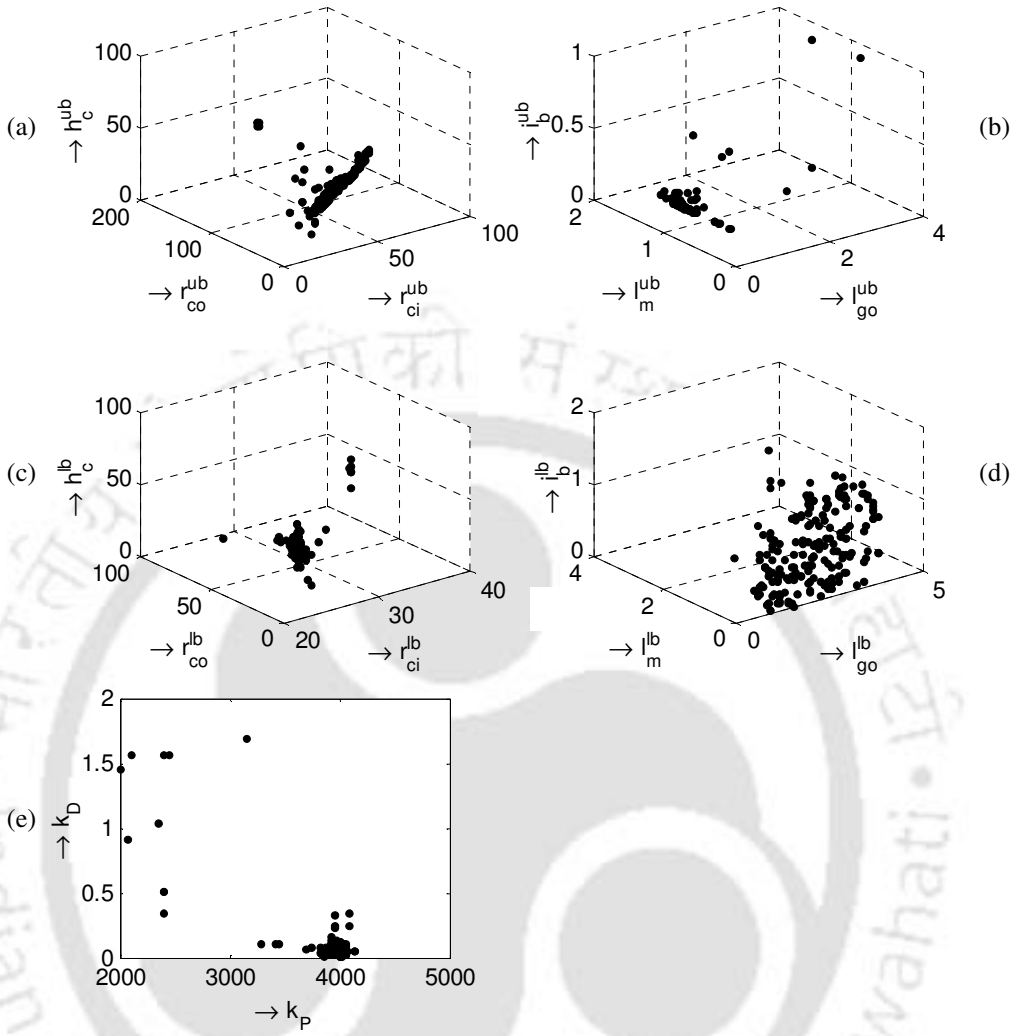

Figure 8.11 Scatter of design variables in the design variable space (200 population 1000 generations)

(a) Inner radius versus outer radius and height (Upper bearing)

(b) Bias current versus air gap and thickness of bias magnets (Upper bearing)

(c) Inner radius versus outer radius and height (Lower bearing)

(d) Bias current versus air gap and thickness of bias magnets (Lower bearing)

(e) Derivative gain versus proportional gain (Controller)

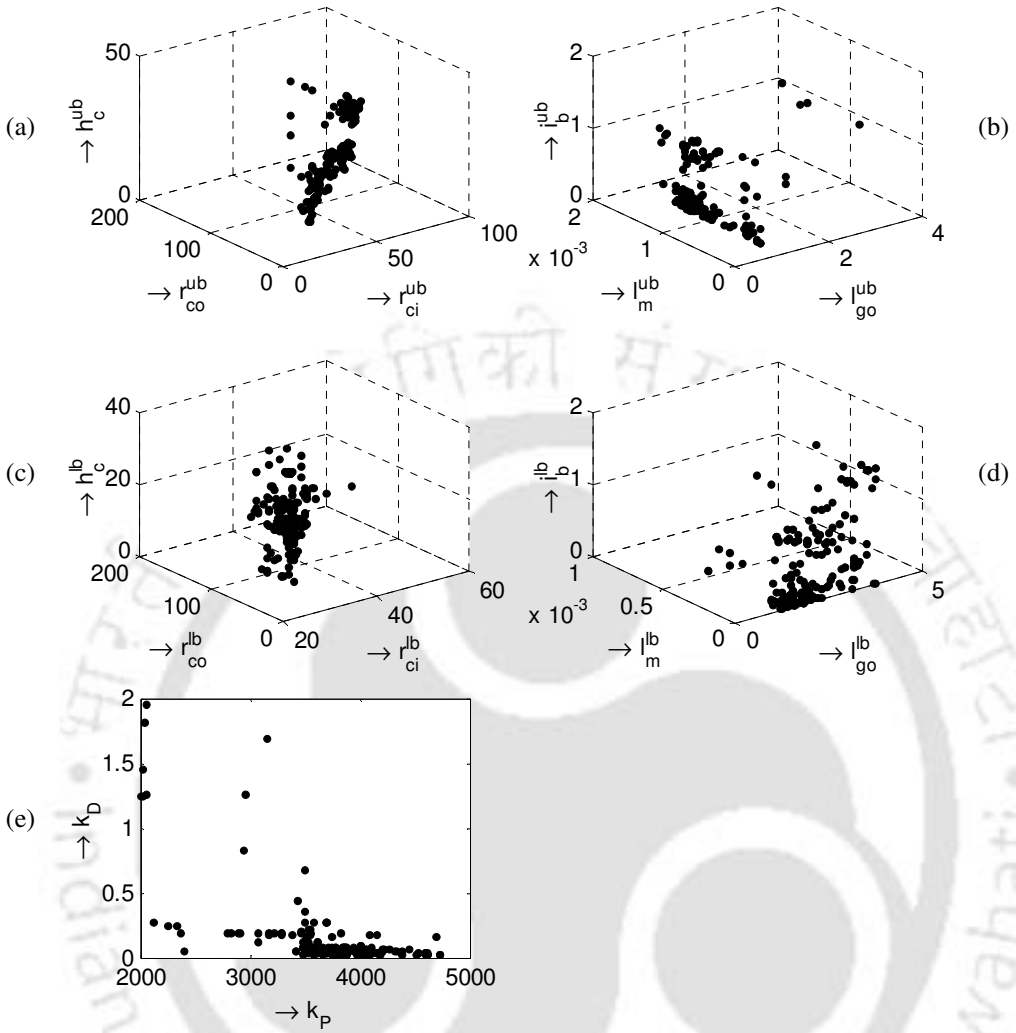

Figure 8.12 Scatter of design variables in the design variable space (200 population 100 generations)

(a) Inner radius versus outer radius and height (Upper bearing)

(b) Bias current versus air gap and thickness of bias magnets (Upper bearing)

(c) Inner radius versus outer radius and height (Lower bearing)

(d) Bias current versus air gap and thickness of bias magnets (Lower bearing)

(e) Derivative gain versus proportional gain (Controller)

The scatter of design variables for the upper and lower actuators and the controller of different cases are shown in Figure 8.10 – Figure 8.12. Plots (a) and (b) of Figure 8.10 – Figure 8.12, correspond to the upper actuator, plots (c) and (d) correspond to the lower actuator, and plot (e) corresponds to controller design variables. Bounds on design variables in final populations for different cases are summarized in Table 8.10. From Figure 8.10 and

Figure 8.11, it could be observed that the different design variables of final populations are found to be clustered in a narrow region of the design variable space. Hence, number of individuals found in the final population within chosen bounds of design variables is presented in Table 8.11. The clustered bounds on design variables are chosen by observing plots of Figure 8.11 (i.e. for the population size of 200 and number of generations of 1000). Columns 1 and 2 of Table 8.11 indicate a higher percentage of the total population converges to the specified clustered region with a population size of 200 than with a population size of 100. From columns 1 and 3, it could be observed that with the increase in number of generations, higher percentage of the population converges to the specified clustered region in the variable space. Hence, this region of variable bounds can be concluded as the optimal. From column 3 of Table 8.11, controller variables (around 31%) converge to the specified clustered region faster than the actuator variables (around 3%). Hence, the most of computational effort is taken by the convergence of actuator variables. Moreover, limits on the bias current of the clustered region for the upper bearing are nearly zero (i.e., $0.0 \le i_b^{lb} \le 0.01$), whereas that of the lower bearing are $0.0 \le i_b^{lb} \le 1.5$, it indicates though the power-loss of the upper bearing tends to be zero the power-loss of the lower bearing is not zero. This provides the reason for the scatter of points of plots (b, e, h and j) of Figure 8.7 and Figure 8.8 away from the zero power-loss at the operating point. Table 8.11 shows the tight limits on variables in the final population of size 200 with number of generations of 1000. A constraint on the derivative gain influences all geometric design variables of both the upper and lower actuators. This shows the influence of the actuator geometry on the controller choice.

Table 8.10 Bounds on design variables in the final population for different cases

Design variables		Upper actuator variables						Lower actuator variables						Controller variables	
		r_{ci} (mm)	r_{co} (mm)	h_c (mm)	l_{g0} (mm)	l_m (mm)	i_b (A)	r_{ci} (mm)	r_{co} (mm)	h_c (mm)	l_{g0} (mm)	l_m (mm)	i_b (A)	k_P	k_D
Pop 200	a	27.42	34.41	4.30	1.00	0.30	0.00	27.01	29.69	2.49	1.23	0.00	0.00	2013	0.02
Gen 100	b	76.29	109.30	47.91	3.87	1.90	1.52	47.09	103.67	38.40	4.08	0.73	1.62	4732	1.94
Pop 200	a	27.00	33.53	2.61	1.00	0.73	0.00	27.00	27.18	1.05	1.01	0.00	0.00	2001	0.01
Gen 1000	b	80.85	107.36	66.30	3.88	1.77	0.93	36.22	88.30	56.91	4.15	2.97	1.41	4133	1.69
Pop 100	a	27.00	32.90	4.50	1.00	0.15	0.00	27.00	28.23	2.59	1.00	0.00	0.00	2000	0.01
Gen 1000	b	81.01	112.41	47.36	1.38	1.73	0.16	32.42	114.57	32.54	5.00	0.64	1.22	4282	3.63

a→lower bound, b→upper bound, Pop→ Population, Gen→ Generation

Table 8.11 Number of solutions in the specified clustered region of the design variable space

*1→ $3800 \le k_P \le 4100$;
2→ $0 \le k_D \le 0.1$;
3→ $1.00 \le l_{g0}^{ub} \le 1.05$; $0.00 \le i_b^{ub} \le 0.01$; $1.00 \le l_m^{ub} \le 1.80$
4→ $35 \le r_{ci}^{ub} \le 85$; $50 \le r_{co}^{ub} \le 95$; $10 \le h_c^{ub} \le 35$;
5→ $1.0 \le l_{g0}^{lb} \le 4.2$; $0.0 \le i_b^{lb} \le 1.5$; $0.0 \le l_m^{ub} \le 1.5$;
6→ $27 \le r_{ci}^{lb} \le 28$; $30 \le r_{co}^{lb} \le 60$; $12 \le h_c^{lb} \le 40$

Bounds on the design variables	Pop 200 Gen 1000	Pop 100 Gen 1000	Pop 200 Gen 100
1*	183(91.5%)	80(80.0%)	63(31.5%)
1 and 2	160(80.0%)	75(75.0%)	61(30.5%)
1, 2, and 3	157(78.5%)	71(71.0%)	6(3.0%)
1,2,3, and 4	156(78.0%)	71(71.0%)	5(2.5%)
1,2,3,4, and 5	151(75.5%)	71(71.0%)	5(2.5%)
1,2,3,4,5, and 6	148(74.0%)	60(60.0%)	2(1.0%)

Table 8.12 Tight limits on the design variables of the final population for the case of population size 200 run for 1000 generations

Design variables		Upper actuator						Lower actuator						Controller	
		r_{ci} (mm)	r_{co} (mm)	h_c (mm)	l_{g0} (mm)	l_m (mm)	i_b (A)	r_{ci} (mm)	r_{co} (mm)	h_c (mm)	l_{g0} (mm)	l_m (mm)	i_b (A)	k_P	k_D
$3800 \le k_P \le 4100$	a	27.04	42.20	8.81	1.00	0.95	0.00	27.00	33.72	12.67	1.01	0.00	0.00	3820	0.01
	b	80.86	107.37	66.30	1.35	1.78	0.16	36.72	63.41	56.91	4.16	2.97	1.42	4089	0.34
$0 \le k_D \le 0.1$	a	35.30	51.39	8.81	1.00	0.95	0.00	27.00	33.72	12.67	1.01	0.00	0.00	3820	0.01
	b	80.86	94.27	33.00	1.32	1.78	0.11	29.93	52.54	38.46	4.16	2.97	1.42	4074	0.10
$1.00 \le l_{g0}^{ub} \le 1.05$	a	35.30	51.39	8.81	1.00	1.21	0.00	27.00	33.72	12.67	1.01	0.00	0.00	3820	0.01
$0.00 \le i_b^{ub} \le 0.01$ $1.00 \le l_m^{ub} \le 1.80$	b	80.86	94.27	33.01	1.05	1.65	0.11	29.93	52.54	38.46	4.16	2.97	1.42	4074	0.10
$35 \le r_{ci}^{ub} \le 85$	a	35.93	51.39	10.42	1.00	1.21	0.00	27.00	33.72	12.67	1.01	0.00	0.00	3820	0.01
$50 \le r_{co}^{ub} \le 95$ $10 \le h_c^{ub} \le 35$	b	80.86	94.27	33.00	1.04	1.65	0.11	29.93	52.54	38.46	4.16	2.97	1.42	4074	0.10
$1.0 \le l_{g0}^{lb} \le 4.2$	a	35.93	51.39	10.42	1.00	1.21	0.00	27.00	33.72	12.67	1.01	0.00	0.00	3820	0.01
$0.0 \le i_b^{lb} \le 1.5$ $0.0 \le l_m^{lb} \le 1.5$	b	80.86	94.27	33.00	1.04	1.64	0.11	29.92	52.54	38.46	4.16	1.32	1.42	4074	0.10
$27 \le r_{ci}^{lb} \le 28$	a	35.93	51.39	10.42	1.00	1.21	0.00	27.00	33.72	12.67	1.01	0.00	0.00	3820	0.01
$30 \le r_{co}^{lb} \le 60$ $12 \le h_c^{lb} \le 40$	b	80.86	94.27	33.01	1.05	1.65	0.11	27.91	52.54	38.46	4.16	1.32	1.41	4074	0.10

a → lower bound b → upper bound

8.7 Design choice

In Chapter 5, the minimum normalized weighted distance from the utopia point has been used as an '*a posteriori*' criterion to make a design choice in equation (5.3) for two objective functions. A generalized form of this criterion for '*p*' objectives can be expressed as

$$\zeta = \sqrt{\sum_{i=1}^{p} \left(\varepsilon_i \frac{f_i - f_{i\min}}{f_{i\max} - f_{i\min}} \right)^2} \tag{8.41}$$

where ζ is the normalized distance from the utopia point, p is the number of objectives, ε_i is the multiplicative constant correspond to i^{th} objective, f_i is the value of i^{th} objective, $f_{i\min}$ and $f_{i\max}$ respectively are the minimum and maximum values of i^{th} objective in the population. In the present case, p = 5; and i = 1, 2, ..., 5 correspond to the power-loss, the weight, the load capacity of the actuator, input performance index and dynamic performance index of the controller respectively.

Design parameters for different cases are presented in Table 8.13. The thickness of bias magnets and the bias current of the upper bearing are larger than that of the lower bearing. The nominal air-gap of the upper bearing is lesser than that of the lower bearing. This is due to the fact that the upper bearing is assumed to support the static load of the rotor. Various performance parameters at the operating point and extreme points of individual actuators of the double acting bearing are shown in Table 8.13. Performance parameters, related to both actuators and the controller, have been shown in Table 8.14 and Table 8.15 respectively.

Quantities at the minimum air-gap and the maximum air gap points are subscripted with x_o and x_i,, respectively. The maximum and minimum (i.e., the maximum on the negative side) displacements of the rotor due to controller effect are given as x_{co} and x_{ci}, respectively.

In Tables 11 and 12, case (a) (i.e. the population size of 100 with 1000 generations) and case (b) (i.e. the population size of 200 with 1000 generations) are found to match very well. Case (c) (i.e. the population size of 200 with 100 generations) is found to mismatch and this shows the non-convergence with 100 generations. From Tables 7 and 13 though the optimum values of objectives are found to match, however, other parameters are found not to match very well. It indicates that there is a need for some more study on the convergence of the population.

The design choices based on the minimum distant member from the utopia point of the final population have also been presented in Tables 11, 12, and 13 as case 6. It could be observed that these results are a compromise of all the objectives.

Controller responses for various cases are provided in Figure 8.13, Figure 8.14 and Figure 8.15. These controller responses are obtained by solving the differential equation (8.25) in time domain in closed form. An initial displacement of 0.2mm with zero initial velocity has been assumed as given in Table 8.5. Determine the Eigen values of the system according to equation (8.26), and then determine the state at each instant of time with initial conditions assumed in Table 8.5. Subsequently determine the corresponding control current for each individual actuator by using equation (8.24). It could be noted that the similar control responses of Figure 8.14 (i.e. the population size of 200 run for 1000 generations) and Figure 8.15 (i.e. the population size of 100 run for 1000 generations) could be an indication of the convergence.

Table 8.13 Bearing geometries for different cases

Design variables		Upper Bearing variables						Lower Bearing variables						Controller variables	
		r_{ci} (mm)	r_{co} (mm)	h_c (mm)	l_{g0} (mm)	l_m (mm)	i_b (A)	r_{ci} (mm)	r_{co} (mm)	h_c (mm)	l_{g0} (mm)	l_m (mm)	i_b (A)	k_P	k_D
1	a	64.88	92.82	26.11	1.03	1.56	0.00	27.68	114.57	15.6	3.46	0.18	0.00	3946	0.04
	b	27.04	107.36	66.3	1.01	1.48	0.00	36.72	63.41	47.86	3.04	0.51	0.00	3957	0.24
	c	37.18	85.98	35.88	1.02	0.3	0.00	27.53	69.97	38.4	3.81	0.01	0.00	3748	0.17
2	a	27.00	32.90	5.29	1.00	0.58	0.00	27.01	28.24	2.60	2.52	0.00	0.17	2009	3.64
	b	27.00	33.53	5.07	1.00	0.74	0.00	27.00	27.18	1.05	1.55	0.02	0.00	2108	1.56
	c	27.56	34.41	7.6	1.02	0.37	0.02	27.04	30.22	6.09	1.26	0.01	0.00	2061	1.95
3	a	81.01	91.94	30.24	1.00	1.56	0.03	27.19	38.52	15.95	3.37	0.03	0.48	3963	0.04
	b	80.86	91.80	31.31	1.00	1.50	0.02	27.01	38.77	16.51	3.25	0.03	0.04	4053	0.02
	c	75.49	91.19	31.37	1.29	1.9	0.81	40.47	91.83	21.47	3.76	0.15	0.18	3840	0.07
4	a	33.69	84.74	14.70	1.00	0.20	0.00	27.20	53.72	5.00	1.89	0.41	0.56	2000	1.41
	b	39.64	88.35	27.17	2.86	1.16	0.00	27.22	27.89	21.30	1.21	0.11	0.36	2001	1.45
	c	39.04	71.5	47.63	2.86	1.17	0.20	29.91	94.63	2.49	2.39	0.11	0.98	2017	1.45
5	a	51.36	104.33	47.36	1.33	1.73	0.00	30.37	64.33	24.40	2.63	0.07	0.15	3785	0.26
	b	45.92	95.94	45.99	3.87	0.80	0.93	27.04	88.31	5.44	3.05	0.64	0.99	3152	1.69
	c	45.92	109.31	43.63	3.87	0.80	0.93	27.04	91.7	18.26	3.05	0.64	1.01	3152	1.69
6	a	59.35	81.63	13.59	1.01	1.42	0.00	27.02	54.23	12.75	1.85	0.59	0.39	3950	0.04
	b	66.05	88.11	14.94	1.01	1.50	0.00	27.10	36.17	19.85	2.18	0.24	0.34	4020	0.06
	c	64.37	82.88	12.71	1.14	1.51	0.00	27.30	36.67	23.41	1.52	0.12	0.53	3075	0.12

1→ minimum power-loss; 2 → minimum weight; 3 → maximum load capacity; 4 → minimum input performance index; 5 → minimum dynamic performance index; 6 → minimum distant member from utopia point; a→ 100 population size and 1000 generations b→ 200 population size and 1000 generations c→ 200 population size 100 generations

Table 8.14 Parameters of upper bearing and lower bearing

Design variables		Upper bearing parameters								Lower bearing parameters							
		i_{min} (A)	i_{max} (A)	B (T)	B_{max} (T)	F (kN)	F_m (kN)	F_{xi} (kN)	F_{xo} (kN)	i_{min} (A)	i_{max} (A)	B (T)	B_{max} (T)	F (kN)	F_m (kN)	F_{xi} (kN)	F_{xo} (kN)
1	a	0.00	3.95	0.77	0.99	5.380	5.380	8.520	8.700	0.00	3.65	0.05	0.27	0.001	0.001	0.001	0.025
	b	0.00	3.96	0.76	0.99	0.155	0.155	0.254	0.257	0.00	3.76	0.17	0.38	0.049	0.049	0.067	0.261
	c	0.00	3.75	0.27	0.71	0.135	0.135	0.342	0.968	0.00	3.50	0.00	0.20	0.000	0.000	0.000	0.013
2	a	0.00	2.01	0.45	0.58	0.050	0.050	0.060	0.090	0.17	0.46	0.02	0.04	0.000	0.000	0.000	0.001
	b	0.00	2.11	0.52	0.65	0.071	0.071	0.074	0.108	0.00	0.14	0.01	0.04	0.000	0.000	0.000	0.000
	c	0.02	2.08	0.32	0.51	0.034	0.033	0.059	0.087	0.00	1.29	0.01	0.21	0.000	0.000	0.000	0.011
3	a	0.03	4.00	0.79	1.00	9.20	9.120	14.280	14.840	0.48	3.96	0.04	0.26	0.000	0.000	0.000	0.019
	b	0.02	4.08	0.77	1.00	8.836	8.776	14.501	14.781	0.05	3.92	0.01	0.26	0.000	0.000	0.000	0.018
	c	0.82	4.66	0.84	1.00	8.876	7.415	12.389	12.582	0.19	3.46	0.05	0.23	0.007	0.004	0.010	0.139
4	a	0.00	2.00	0.20	0.43	0.490	0.490	0.090	0.230	0.56	1.81	0.27	0.36	0.021	0.012	0.034	0.037
	b	0.00	2.01	0.34	0.42	0.281	0.281	0.324	0.415	0.36	1.42	0.16	0.30	0.007	0.002	0.020	0.026
	c	0.21	2.22	0.36	0.43	0.291	0.270	0.336	0.422	0.99	2.05	0.15	0.23	0.014	0.001	0.023	0.035
5	a	0.00	3.79	0.72	0.90	2.621	2.619	3.588	4.074	0.16	3.12	0.04	0.27	0.001	0.001	0.002	0.055
	b	0.93	4.09	0.25	0.38	0.230	0.145	0.269	0.532	1.00	3.15	0.27	0.38	0.019	0.010	0.026	0.039
	c	0.93	4.09	0.25	0.38	0.230	0.145	0.269	0.532	1.01	3.16	0.27	0.38	0.019	0.010	0.026	0.039
6	a	0.01	3.96	0.75	0.98	4.073	4.063	6.645	6.903	0.39	4.04	0.33	0.60	0.028	0.021	0.046	0.093
	b	0.01	4.03	0.77	0.99	5.534	5.524	8.898	9.232	0.34	4.04	0.15	0.44	0.006	0.003	0.010	0.053
	c	0.00	3.08	0.73	0.87	4.667	4.663	6.315	6.608	0.54	2.54	0.16	0.39	0.008	0.002	0.016	0.045

1→ minimum power-loss; 2 → minimum weight; 3 → maximum load capacity; 4 → minimum input performance index; 5 → minimum dynamic performance index; 6 → minimum distant member from utopia point; a→ 100 population size and 1000 generations; b→ 200 population size and 1000 generations; c→ 200 population size 100 generations

Table 8.15 Parameters of double acting bearing in the final populations

Parameters		**Double acting bearing parameters**									
		k_i (N/A)	k_x (kN/m)	P (W)	P_{xi} (W)	P_{xo} (W)	W (N)	F (kN)	F_m (kN)	F_{xi} (kN)	F_{xo} (kN)
1	a	1515.1	4781.2	0.00	9.32	22.39	22.15	5.378	5.378	8.494	8.703
	b	88.6	172.2	0.00	2.63	7.35	27.19	0.105	0.105	0.000	0.189
	c	198.1	216.2	0.00	4.88	6.57	14.20	0.135	0.135	0.329	0.968
2	a	39.7	71.1	3.20	24.89	54.94	0.14	0.051	0.051	0.056	0.088
	b	43.3	90.2	0.00	34.82	54.09	0.13	0.071	0.071	0.074	0.108
	c	40.6	52.1	0.00	32.91	34.27	0.26	0.034	0.033	0.048	0.087
3	a	2578.0	8266.7	0.56	37.98	56.17	23.58	9.204	9.119	14.264	14.837
	b	2573.4	8108.3	0.00	34.57	55.68	23.84	8.836	8.776	14.483	14.781
	c	1842.0	6083.4	1.52	11.03	48.84	28.83	8.869	7.410	12.250	12.573
4	a	121.8	101.2	1.28	13.34	5.49	4.62	0.028	0.036	0.053	0.203
	b	121.6	158.1	3.37	51.44	5.95	8.57	0.273	0.278	0.298	0.395
	c	119.9	158.8	5.02	21.68	7.35	9.98	0.277	0.268	0.301	0.400
5	a	668.4	1953.0	0.02	7.40	5.94	24.63	2.619	2.618	3.532	4.072
	b	104.1	100.3	2.64	23.19	9.14	17.94	0.210	0.135	0.230	0.505
	c	104.1	100.3	1.00	7.00	6.91	24.68	0.210	0.134	0.230	0.505
6	a	1272.4	3860.2	0.24	25.40	48.80	9.61	4.045	4.041	6.857	6.552
	b	1626.6	5085.7	0.27	38.08	50.75	12.39	5.528	5.520	8.844	9.222
	c	1368.7	4036.4	0.56	12.49	40.01	10.49	4.659	4.661	6.270	6.591

1→ minimum power-loss; 2 → minimum weight; 3 → maximum load capacity; 4 → minimum input performance index; 5 → minimum output performance index; 6 → minimum distant member from utopia point; a→ 100 population size and 1000 generations; b→ 200 population size and 1000 generations; c→ 200 population size 100 generations

Table 8.16 Parameters of controller in the final populatons

Parameters		Controller parameters							
		K_e (kN/m)	C_e (N-s/m)	t_s (sec)	x_{ci} (mm)	x_{co} (mm)	χ_i (A^2)	χ_o (mm^2)	χ_d (mm^2-sec)
1	a	1197.42	59.52	0.292	-0.462	0.500	74.61	47.93	1.74
	b	178.62	21.07	0.821	-0.474	0.500	208.26	133.06	13.87
	c	526.32	32.71	0.530	-0.465	0.500	120.96	86.16	5.76
2	a	8.65	144.37	0.125	-0.073	0.500	14.97	41.33	0.47
	b	1.19	67.81	0.259	-0.032	0.500	49.43	113.06	3.35
	c	31.67	79.06	0.217	-0.311	0.500	15.96	39.47	0.99
3	a	1951.38	101.26	0.172	-0.438	0.500	45.09	28.72	0.60
	b	2321.73	63.21	0.268	-0.477	0.500	74.20	45.18	1.54
	c	989.90	131.37	0.133	-0.427	0.500	33.18	22.54	0.36
4	a	142.43	171.79	0.102	-0.305	0.500	7.07	18.91	0.21
	b	85.35	176.10	0.100	-0.260	0.500	7.25	19.59	0.20
	c	830.55	173.37	0.101	-0.261	0.500	7.41	19.87	0.21
5	a	577.47	175.49	0.100	-0.390	0.500	24.79	17.44	0.20
	b	227.89	175.66	0.100	-0.338	0.500	17.05	18.01	0.20
	c	227.86	175.66	0.100	-0.338	0.500	17.05	18.01	0.20
6	a	1166.45	53.71	0.322	-0.460	0.500	82.63	52.97	2.14
	b	1454.33	89.84	0.191	-0.460	0.500	52.03	32.21	0.76
	c	172.56	166.08	0.104	-0.325	0.500	18.03	19.16	0.22

1→ minimum power-loss; 2 → minimum weight; 3 → maximum load capacity; 4 → minimum input performance index; 5 → minimum output performance index; 6 → minimum distant member from utopia point; a→ 100 population size and 1000 generations; b→ 200 population size and 1000 generations; c→ 200 population size 100 generations

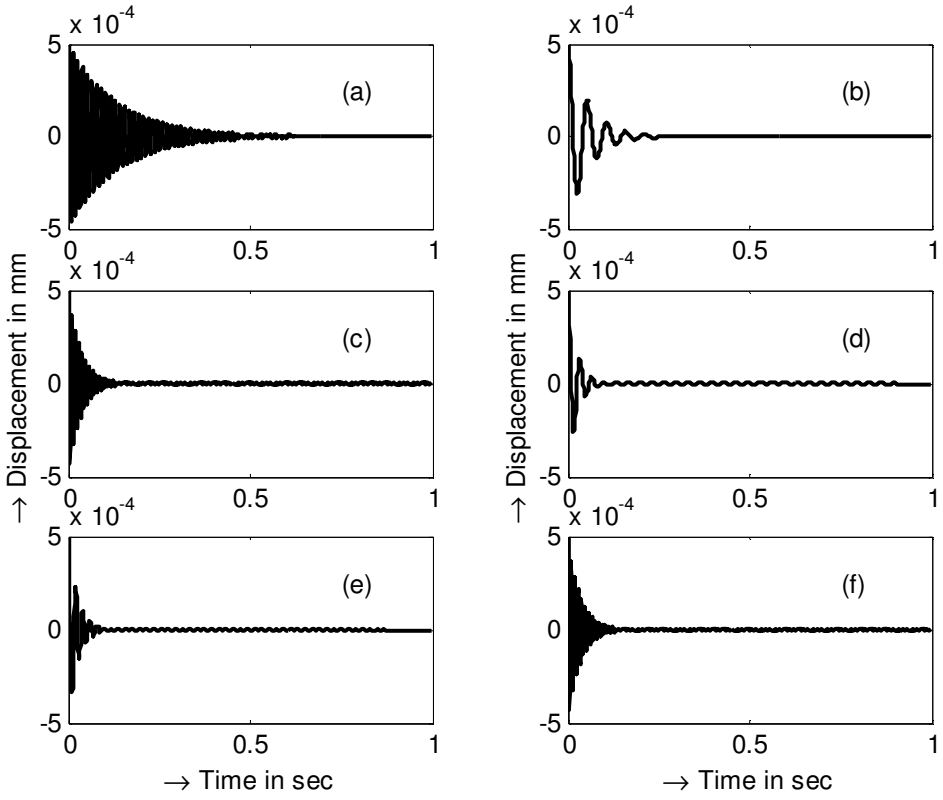

Figure 8.13 The optimal control responses for different cases (200 population and 100 generations)

(a) Minimum powerloss (b) Minimum weight

(c) Maximum load capacity (d) Minimum input index

(e) Minimum dynamic index (f) Minimum distant member (from the utopia point)

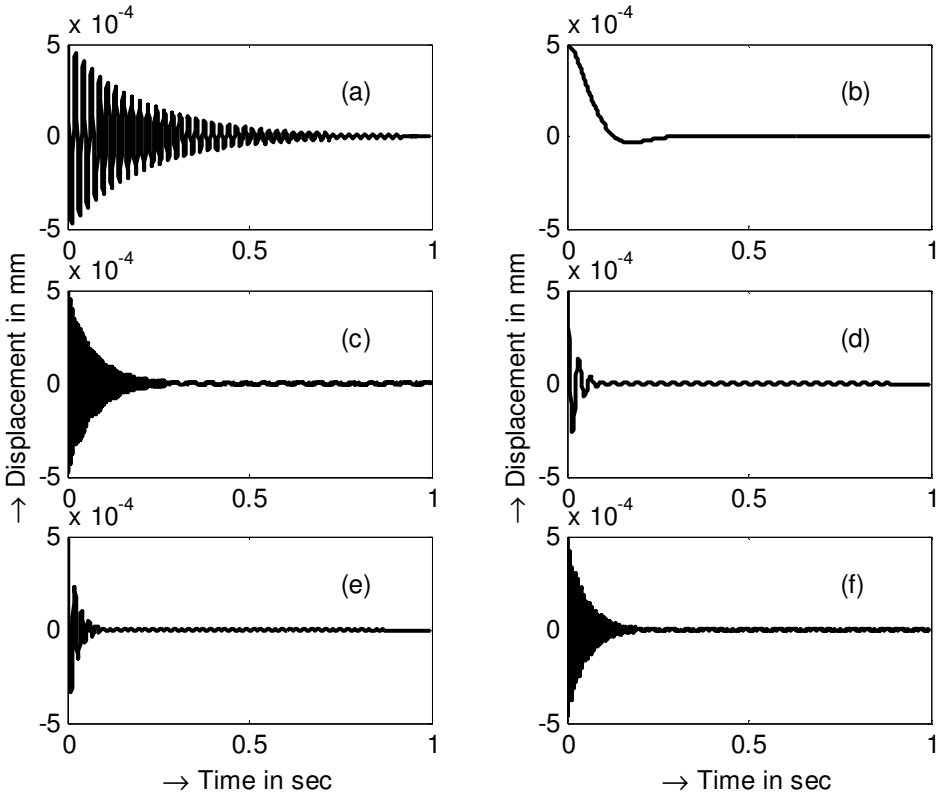

Figure 8.14 The optimal control responses for different cases (200 population and 1000 generations)

(a) Minimum powerloss (b) Minimum weight

(c) Maximum load capacity (d) Minimum input index

(e) Minimum dynamic index (f) Minimum distant member (from the utopia point)

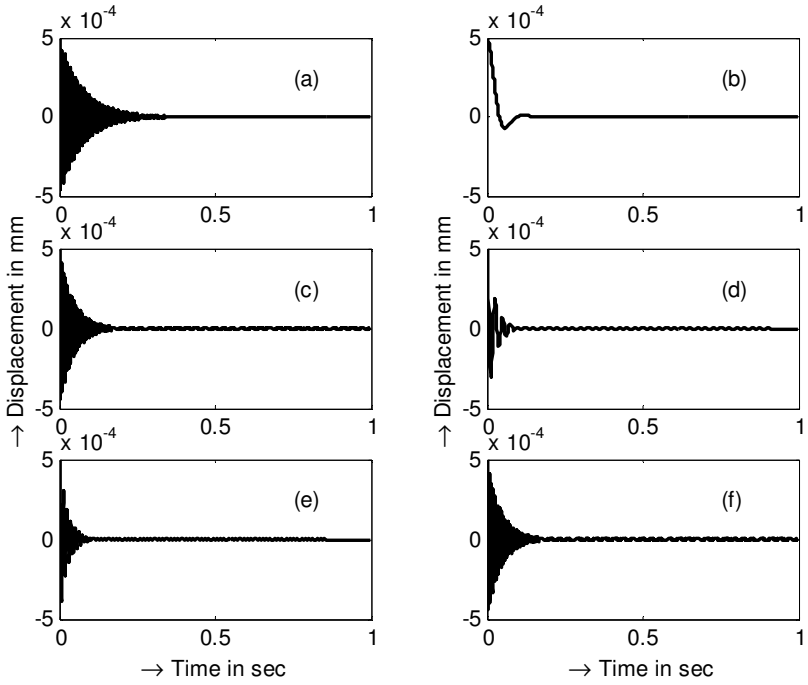

Figure 8.15 The optimal control responses for different cases (100 population and 1000 generations)

(a) Minimum power-loss (b) Minimum weight
(c) Maximum load capacity (d) Minimum input index
(e) Minimum dynamic index (f) Minimum distant member (from the utopia point)

8.8 Conclusions

In the present chapter, an optimal design of *double acting hybrid magnetic thrust bearing* (DAHMTB) has been carried out. Double acting actuators and controller are optimized as a unified system. Two different geometries have been assumed for the individual actuators of the double acting bearing. The macro-geometry of the DAHMTB has been described. The different actuator and controller relations have been presented. For the present case, the uni-mode control with a centralized controller has been assumed. The genetic algorithm has been implemented to carry out the constrained multi-objective optimization of the magnetic bearing.

Results have been compared for populations of sizes of 200 and 100 run for 1000 generations for the confirmation of convergence with the population size. Results with population of size of 200 run for 100 and 1000 generations have also been compared for the study of convergence with number of generations. Some of convergence criteria from the study on Pareto-front have been observed. Designs which are nearest to the utopia point in Pareto-front fronts are compared. Air gaps, bias currents, and lengths of permanent magnets are observed to be consistently different for individual actuators of the double acting bearing. Performance parameters of double actuators and the controller of the magnetic bearing for different choices have been presented. Depending on the actuator and controller properties, it is observed that a set of design variables influence a particular set of objectives.

In this chapter the controller is initially designed and a power amplifier that meets requirements of the controller can be procured next. Though power amplifiers can be designed with respect to designed controller requirements, sometimes it is not possible to have the required power amplifiers as a standard one, and one has to design the controller by taking constraints of the power amplifier available at hand. Though the centralization of controller requires less number of power amplifiers, but needs some complex winding schemes and control strategies. To go for a simpler winding and control strategies one may have to go for a decentralized actuator, controller and power amplifier in double-acting magnetic bearing systems. Hence, the design optimization methodology is extended to the DAHMTB with decentralized controller systems by taking consideration of constraints of the power amplifier in the next chapter.

Chapter 9
Design Optimization of Double-Acting Hybrid Magnetic Thrust Bearings with Controller and Power Amplifier Integration Using Multi-Objective Genetic Algorithms

9.1 Introduction

The actuator without considering the controller and power amplifier constraints (i.e., force, weight and power-loss as objectives) has been studied in chapters 4 -7. In chapter 8, the work is extended to the design optimization of *double-acting hybrid magnetic thrust bearings* (DAHMTBs) by integrating both the actuator and the controller as a single system and by using MOGA. The actuator-controller system with the load capacity, weight, power-loss, input-index and dynamic-index as objectives has been studied in chapter 8. The voltage limits of the power amplifier have not been considered in the previous design optimization. Without considering voltage limits on the power amplifier the controller may choose its gains in such a

way that it demand a very large voltage from the power amplifier. Hence, the main purpose in the present chapter is to study how constraints of the power amplifier affect the integrated design optimization of the actuator, controller and power amplifier system. The different procedures of design optimization have been described in following paragraphs.

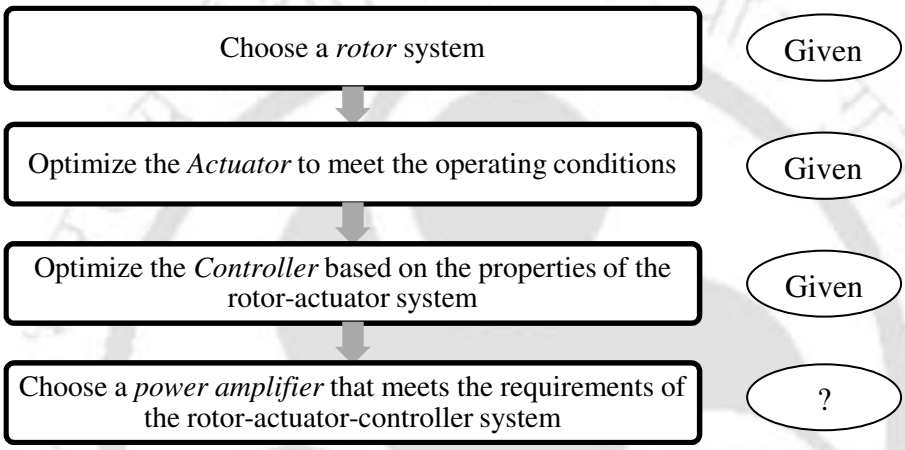

Figure 9.1 Sequential design of a power amplifier for a given rotor, actuator and controller system

A sequential design optimization procedure for magnetic bearing systems is shown in Figure 9.1. According to Figure 9.1, in the design optimization of magnetic bearing systems one can optimize the actuator irrespective of the controller and power amplifier constraints, and then optimize the controller corresponding to the chosen design of actuator. Afterwards a power amplifier can be chosen which meets the requirements of the actuator-controller system. Though power amplifiers can be designed with respect to designed controller requirements, sometimes it is not possible to have the required power amplifiers as a standard one. On the other hand designing a controller system which is compatible for a given actuator and a power amplifier is other way of achieving a practical system. This deals with the design of controller within the power rating of a given power amplifier as shown in Figure 9.2.

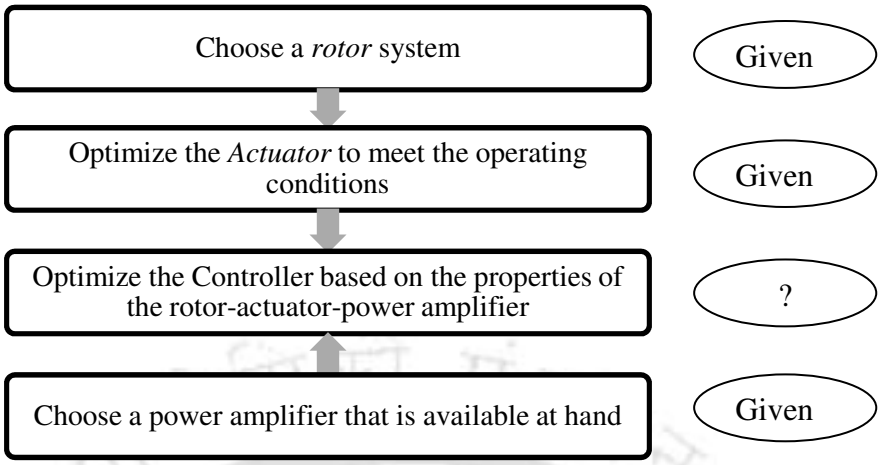

Figure 9.2 A sequential design optimization of a controller for a given rotor, actuator and power amplifier system

In the present chapter, the integrated design optimization procedure of rotor, actuator, controller and power amplifier, as shown in Figure 9.3, has been followed by using the MOGA. In the integrated design optimization, different objectives and corresponding design vector for different components of the system will be provided and different constraints on components are specified. The overall system is simultaneously optimized for the best design within the constraints provided.

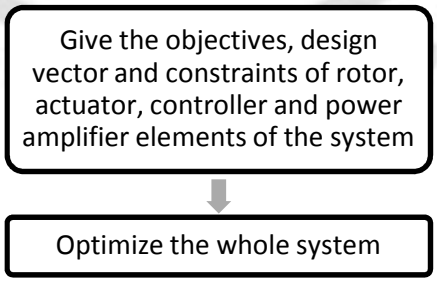

Figure 9.3 An integrated design optimization of a rotor, actuator, controller and power amplifier system

In Chapter 8, a centralized controller has been assumed for the design optimization of DAHMTB with the actuator and the controller as an integrated system. A single

PD controller with a proportional and a derivative gain for both actuators has been assumed with the uni-mode control. This requires only one power amplifier for both actuators of the DAHMTB. Though the centralization of controller requires less number of power amplifiers, it needs a complex winding scheme and control strategies. To go for a simpler winding and control strategies one might have to go for a decentralized actuator, controller and power amplifier in DAHMTB systems as shown in Figure 9.4. Hence, in the present chapter the design optimization methodology is extended to the DAHMTB with decentralized controller systems by taking consideration of constraints of the power amplifier, namely the maximum power rating, and the voltage of the power amplifier.

9.2 Macro geometry of the actuator

The macro-geometry of a double-acting hybrid magnetic thrust bearing (DAHMTB) is shown in Figure 8.2 of Chapter 8 and detailed in Section 8.2. A schematic diagram of a DAHMTB with a decentralized controller has been provided in Figure 9.4. Controllers are separately shown since the controller gains of the individual PD controllers, namely the proportional and derivative gains, are assumed to be different for each controller. Power amplifiers are also assumed to be different for each actuator supplying current to only one actuator of the system.

Different relations, corresponding to the actuator and the controller of DAHMTBs, are provided in Section 8.3. Relations correspond to the power amplifier will be presented under next sub-heading.

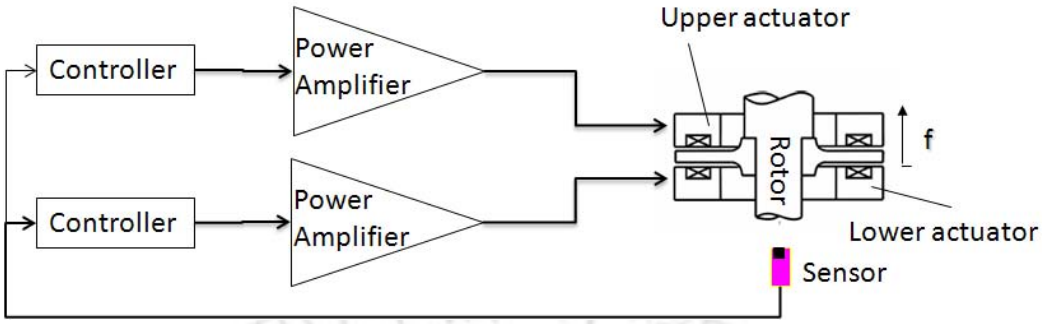

Figure 9.4 schematic diagram of a DAHMTB with decentralized controller and power amplifier

9.3 Power Amplifier Relations

The magnetic force in the system changes at a particular rate with time. This is called the *force slew rate*. The power amplifier must supply current in pace with the force change. The force slew rate is expressed as (Maslen, 2000)

$$\left.\frac{dF_c}{dt}\right|_{x_c=0} = -k_x \left.\frac{dx_c}{dt}\right|_{x_c=0} + k_i \left.\frac{di_c}{dt}\right|_{x_c=0} \tag{9.1}$$

The control current is given by

$$i_c = -\left(k_P x_c + k_D \dot{x}_c\right) \tag{9.2}$$

On substitution of equation (8.24) in equation (9.1), we get

$$\frac{dF_c}{dt} = \left(-k_x - k_i k_P\right)\dot{x}_c - k_i k_D \ddot{x}_c \tag{9.3}$$

If the effect of displacement stiffness is neglected, equation (9.1) reduces to

$$\frac{dF_c}{dt} \approx k_i \left.\frac{di_c}{dt}\right|_{x_c=0} \tag{9.4}$$

The power amplifier should be designed to supply the current at a rate equal to or more than required by the actuator. Hence, the voltage required to be supplied by the power amplifier at any point of time is given by (Meeker and Maslen, 1996)

$$v(t) = ri(t) + L\frac{di(t)}{dt} \tag{9.5}$$

where r is the electric resistance and L is the inductance of the coil wire. The inductance is given by the equation

$$L = n\frac{d\phi}{di} \tag{9.6}$$

The magnetic flux is given by the formula

$$\phi_g = B_g A_g \tag{9.7}$$

with

$$B_g = \frac{\mu_0 \left\{ K_i \left(\vartheta_b + \vartheta_c \right) + 2\vartheta_m \right\}}{2\left\{ K_a \left(l_{g0} + x_c \right) + K_f l_m \right\}} \tag{9.8}$$

For notations please refer to the Nomenclature. From equations (2.11), (8.1) and (9.6), we get

$$L = \frac{K_i n^2 A_g \mu_o}{2\left(K_a l_{g0} + K_f l_m \right)} \tag{9.9}$$

The power rating of the power amplifier is given by

$$p_{\max} = v_{\max} i_{\max} \tag{9.10}$$

From equation (9.10), the maximum current that can be supplied by the power amplifier is given by

$$i_{\max} = \frac{p_{\max}}{v_{\max}} \tag{9.11}$$

Different relations corresponding to the power amplifier have been given in the present section. The formulation of the multi-objective optimization problem of DAHMTB system including the actuator, controller and power amplifier will be discussed in the next section.

9.4 Multi Objective Problem Formulations

Different objective functions chosen for a DAHMTB with the actuator and the controller have been detailed in Section 8.4.1. The aim of the present Chapter is to optimize the actuator, controller DAHMTB system considering the constraint on the power amplifier. Hence, we consider the same objective functions as in Section 8.4.1, namely the load capacity, the power-loss and the weight of the actuator, and input and dynamic performance indexes of the controller. The load capacity, the power-loss and the weight of the double-acting actuator are given by equations (8.3), (8.7) and (8.12) , respectively.

$$F^{db} = F^{ub} - F^{lb} \tag{9.12}$$

$$P^{db} = P^{ub} + P^{lb} \tag{9.13}$$

$$W^{db} = W^{ub} + W^{lb} \tag{9.14}$$

The input and dynamic performance indexes of the controller are given by the equations (8.29) and (8.31) respectively

$$\chi_i = \int_0^{t_f} i_c^2 dt \tag{9.15}$$

and

$$\chi_d = \int_0^{t_f} t x_c^2 dt \tag{9.16}$$

Details of equations (8.3) to (8.31) have already been provided in Section 8.3.

9.4.1 Selection of the Design Vector

As the same objective functions are used in the present chapter as in Chapter 8, the design vector also consists of the coil and permanent magnet dimensions for the actuator. Hence, geometric design parameters for the actuator are chosen as $[r_{ci}, r_{co}, h_c, l_m]$, operating design parameters are $[l_g, i_b]$, and control design parameters for a simple PD controller have been chosen as $[k_P, k_D]$. However, different geometries and operating parameters have been assumed for two actuators on opposite sides of the rotor disc, with two corresponding decentralized controllers and power amplifiers, hence the overall design vector of the system will be $[r_{ci}^{ub}, r_{co}^{ub}, h_c^{ub}, l_m^{ub}, r_{ci}^{lb}, r_{co}^{lb}, h_c^{lb}, l_m^{lb}, l_{g0}^{ub}, i_b^{ub}, l_{g0}^{lb}, i_b^{lb}, k_P^{ub}, k_D^{ub}, k_P^{lb}, k_D^{lb}]$.

9.4.2 Constraints

The main operating requirements and practical limitations for the present system have been discussed in section 8.4.3. Constraints corresponding to the actuator geometry include the minimum inner wall thickness, the minimum thickness of the coil, the maximum height of the bearing, and the maximum outer radius of the bearing. Operating requirements include the load to be supported by the bearing, the maximum current-density in the coil, the saturation magnetic flux-density of the stator-iron core, and the minimum and maximum air-gaps allowed between the disc and the stator. Constraints of the controller include stability conditions of the system, the minimum and maximum setting times, and the maximum overshoot allowed. Constraints of

power amplifier include the maximum voltage that could be supplied given by equation (9.5) and the maximum power rating of the power amplifier.

The multi-objective optimization problem with various objective functions, design variables and constraints that are considered in the design optimization of DAHMTBs has been summarized in Table 9.1. In the present problem, two design variables and two constraints have been added to the problem over double-acting actuator and centralized controller system as given in Chapter 8. Hence, the optimization problem involves in the present chapter a total of five objectives, with sixteen design variables and sixteen constraints.

Table 9.1 Multi objective optimization problem

Minimize $f_i(\mathbf{x})$ with $i=1,...,5$

where $\mathbf{x}=\left\{r_{ci}^{ub}, r_{co}^{ub}, h_c^{ub}, l_{g0}^{ub}, l_m^{ub}, r_{ci}^{lb}, r_{co}^{lb}, h_c^{lb}, l_{g0}^{lb}, l_m^{lb}, i_b^{ub}, i_b^{lb}, k_P^{ub}, k_D^{ub}, k_P^{lb}, k_D^{lb}\right\}$

Subject to $g_j(\mathbf{x})\geq 0 \quad j=1,\ldots,16; \quad x_p^L \leq x_p \leq x_p^U \quad p=1,\ldots,16$

Where $f_1(\mathbf{x})=P$; $f_2(\mathbf{x})=W$; $f_3(\mathbf{x})=-F$; $f_4(\mathbf{x})=\chi_i$; and $f_5(\mathbf{x})=\chi_d$

$g_1(\mathbf{x})=J_{\text{sat}}-\max\left(J_{\max}^{ub}, J_{\max}^{lb}\right)$; $g_2(\mathbf{x})=\min\left(J_{\min}^{ub}, J_{\min}^{lb}\right)$;

$g_3(\mathbf{x})=\alpha_{\max}B_{\text{sat}}-\max\left(B_{\max}^{ub}, B_{\max}^{lb}\right)$; $g_4(\mathbf{x})=\min\left(B_{\min}^{ub}, B_{\min}^{lb}\right)-\alpha_{\min}B_{\text{sat}}$;

$g_5(\mathbf{x})=P_{\max}-\max\left(P^{ub}, P^{lb}\right)$; $g_6(\mathbf{x})=r_{oub}-\max\left(r_o^{ub}, r_o^{lb}\right)$;

$g_7(\mathbf{x})=h_{tub}-\max\left(h_t^{ub}, h_t^{lb}\right)$; $g_8(\mathbf{x})=F_{\max}$; $g_9(\mathbf{x})=F_{\text{m}}$; $g_{10}(\mathbf{x})=F_{\min}$;

$g_{11}(\mathbf{x})=k_ik_D$; $g_{12}(\mathbf{x})=k_ik_P-k_x$; $g_{13}(\mathbf{x})=t_s-t_{slb}$; $g_{14}(\mathbf{x})=t_{sub}-t_s$

$g_{15}(\mathbf{x})=v_{\max}-\max\left(v_{\max}^{ub}, v_{\max}^{lb}\right)$, $g_{16}(\mathbf{x})=p_{\max}-\max\left(p_{\max}^{ub}, p_{\max}^{lb}\right)$

9.5 Numerical Results

The optimization tool has been described in Chapter 8. The computer program involves power amplifier analysis module in addition to the GA, actuator and controller modules. Figure 9.5 and Figure 9.6 show for the DAHMTB the interaction between different modules of the computer program.

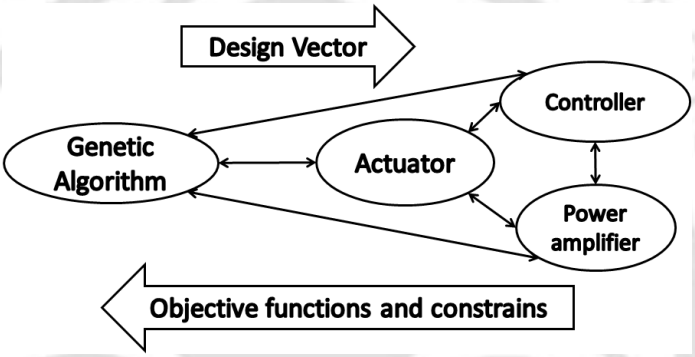

Figure 9.5 The flow of information among different modules namely the GA, actuator, controller and power amplifier modules of computer program

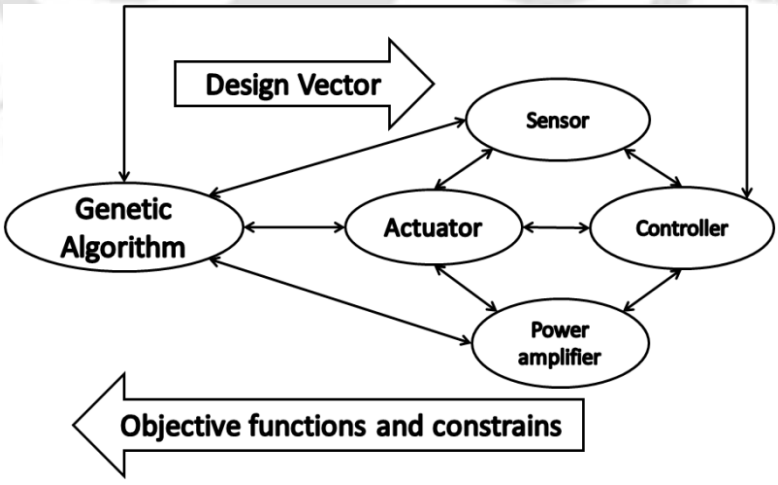

Figure 9.6 The flow of information among different modules including the GA, actuator, sensor, controller, and power amplifier modules of computer program

9.5.1 Input parameters

Table 9.2 shows different input parameters assumed for the actuator, controller and power amplifier components of the DAHMTB system. The additional input parameters include the voltage and power rating of the power amplifier. The GA input data are provided in Table 9.3. Bounds assumed on the design variables are provided in Table 9.4.

Table 9.2 The actuator, controller and power amplifier input parameters

Parameter	Value	Parameter	Value
Inner radius of the bearing, r_i	25.00 mm	Specific gravity of the stator-iron, γ_s	7.77 g/cm^3
Mass of the rotor, m	2.22 kg	Specific gravity of the copper, γ_c	8.91 g/cm^3
Iron saturation factors, ($\alpha_{\min}$, $\alpha_{\max}$)	(0, 0.8)	Specific gravity of the Nb-Fe-B, γ_m	7.50 g/cm^3
Variation in the air-gap, υ_x	±5%	Coil mmf loss factor, K_i	1.394
Variation in the load, υ_f	±10%	Actuator loss factor, K_a	1.072
Saturation flux density of iron, B_{sat}	1.00 T	Flux leakage factor, K_f	0.840
Remnant flux density of permanent magnets, B_r	1.2T	Maximum allowable coil volume, $V_{\max}$	820 mm^3
Saturation current density of coil, J_{sat}	4.0 A/mm^2	Maximum outer radius of bearing, r_{oub}	120 mm
Initial displacement, x_0	0.2mm	Maximum height of bearing, h_{tub}	70 mm
Initial velocity, v_0	0.0	Settling tolerance, x_s	0.01mm
Settling time upper bound, t_{fub}	1.0sec	Sampling time, τ	0.001sec
Coil packing factor, η	0.85	Settling time lower bound t_{flb}	0.1sec
Maximum voltage, $v_{\max}$	120V	Maximum current, $i_{\max}$	5A

Table 9.3 GA input parameters

Parameter	Value
probability of crossover, p_c	0.8
probability of mutation, p_m	1/16
crossover distribution index,	5
mutation distribution index, η_m	10
Population size	100 and 200
Number of generations	1000, 20000

Table 9.4 bounds assumed on the design vector variables

Design Variables	r_{ci} (mm)	r_{co} (mm)	h_c (mm)	l_m (mm)	l_{g0} (mm)	i_b (A)	k_P	k_D
Lower limit	27.00	27.00	0.00	0.00	0.00	0.00	0	0
Upper limit	82.99	120.0	70.00	5.00	5.00	5.00	600	10

9.5.2 Convergence issues

Population sizes of 100 and 200 are chosen for the comparison. The number of feasible solutions in the population with the generation is provided in Table 9.5. Here, the whole population size of 100 converges to the feasible region in 18 generations, while with population size of 200 the whole population converges into feasible region in 20 generations.

Table 9.5 Number of feasible solutions in the population with generation

	Gen No.	*1-8*	*9-10*	*11*	*12*	*13*	*14*	*15*	*16*	*17*	*18*	*19*	*20*
% of feasible solutions	Pop size 200	0	0.5	1.5	2.5	3.5	5.5	9	16	29	51	90.5	100
	Pop size 100	0	0	1	3	6	14	29	49	70	100	100	100

From Table 9.5, it could be seen that the process of convergence of the whole population can be divided into three stages, namely no feasible solution, at least one feasible solution, and all feasible solutions of the population. The analysis of convergence of the population into feasible region is provided in Table 9.6. With a population size of 200 it took only 9 generations to enter into feasible range from there it took 12 generations for all population to become feasible. While with the population size of 100, it took 11 generations to enter into the feasible region, however, in 8 generations the whole population became all feasible.

Table 9.6 Analysis of convergence into feasible region

	Generations with no feasible solution	*Generations with at least one feasible solution*	*Minimum generations with all feasible solutions*
Pop size 200	1-8	9-19	20
Pop size 100	1-10	11-17	18

Populations of sizes 100 and 200 have been run for 20000 generations. The convergence plots of the best and mean values of the population with the generation for the population size of 200 have been shown in Figure 8.6. We can observe that values are being converged even after 15000 generations. The reason for the high number of generations for the convergence could be attributed to the increase in

number of design variables due to the decentralization and due to constraints on parameters of the power amplifier.

There is a constraint on the power amplifier voltage. Without the constraint on the power amplifier voltage the system can take any feasible quantity for controller. Hence, finding out a feasible solution takes fewer searches. Moreover, the considered system is a decentralized system. In a centralized control system the only one controller is used, hence only one set of gains of PD controller will be the design variables for the controller. However, in the case of decentralized control there are two controllers and correspondingly two sets of gains will be the design variables for the controllers. Moreover, the decentralized controller dictates for low control gains for the stable operation (Larocca et. al., 1990). In summary, as the number of variables increased, finding a feasible solution in conjunction with constraint on the power amplifier voltage and controller gains due to decentralization requires more number of searches.

The best and mean values corresponding to the final populations after 1000 generations, 15000 generations, and 20000 generations for the population sizes chosen has been provided in Table 9.7.

Table 9.7 The best and mean values of objective functions in final populations for different cases

		Power-loss (W)	Weight (N)	Load capacity (kN)	Input index (A^2)	Dynamic index (m^2-sec)
Pop. 200 Gen 1000	Max/min	0.13	1.13	4.54	8.58e-3	4.31e-8
	Mean	2.46	7.38	2.22	1.42	1.32e-6
Pop. 200 Gen 15000	Max/min	0.05	0.76	8.75	1.06e-3	2.23e-8
	Mean	3.06	11.87	3.64	1.63	1.41e-6
Pop. 200 Gen 20000	Max/min	0.05	0.76	8.76	9.38e-4	2.23e-8
	Mean	3.13	10.83	3.55	1.35	1.55e-6
Pop. 100 Gen 1000	Max/min	0.18	0.81	5.51	3.82e-2	2.09e-8
	Mean	3.16	8.51	2.46	1.39	1.19e-6
Pop. 100 Gen 15000	Max/min	0.07	0.67	8.61	1.97e-3	2.07e-8
	Mean	3.30	12.06	3.66	1.76	1.55e-6
Pop.100 Gen 20000	Max/min	0.05	0.68	8.27	9.63e-4	2.07e-8
	Mean	3.53	12.04	3.74	1.43	1.38e-6

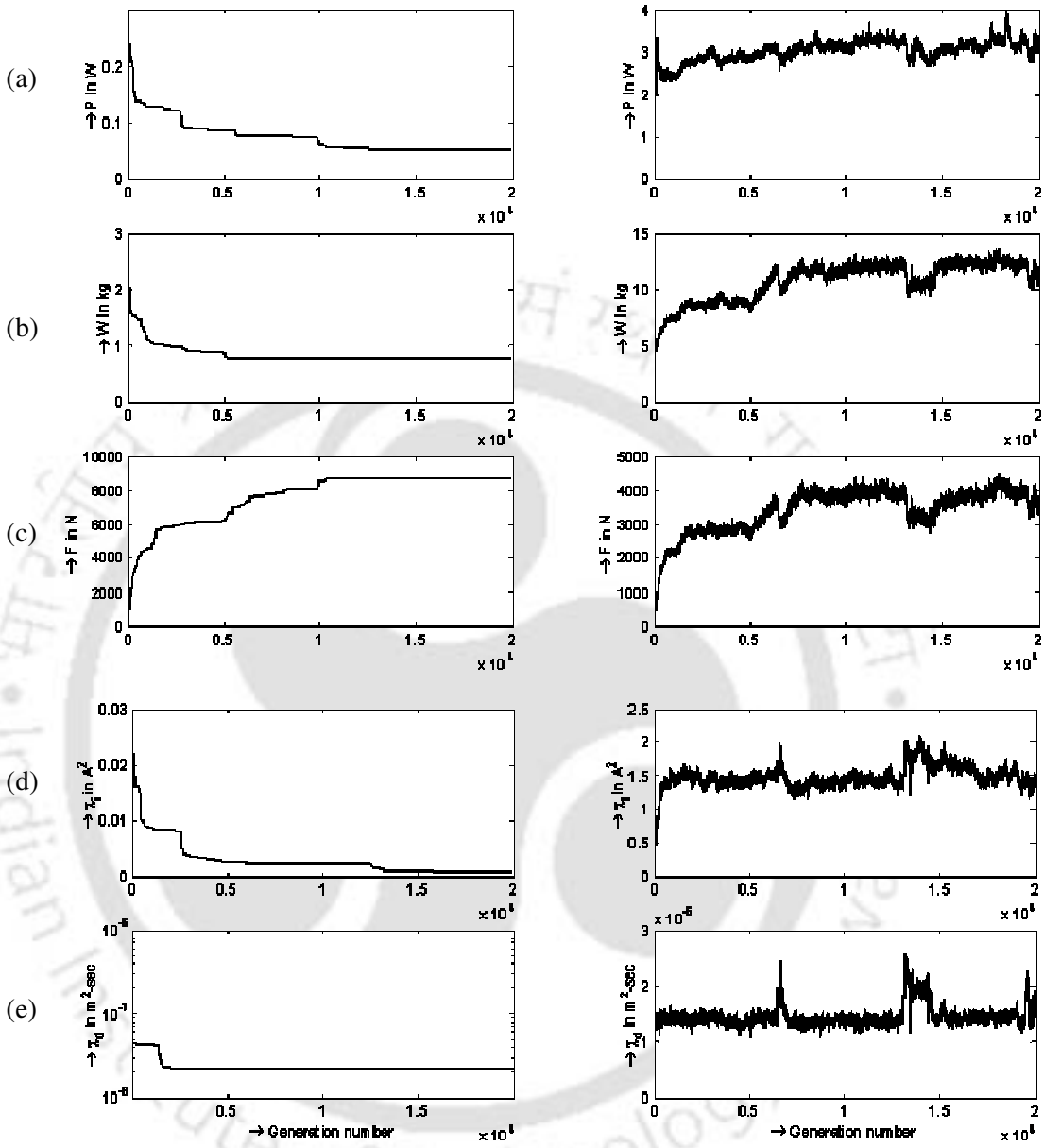

Figure 9.7 The Convergence of objectives with generation (200 population, 20000 generations)
(left) optimum value in the population (right) average value of the population

(a) Power-loss versus generation
(b) Weight versus generation
(c) Load capacity versus generation
(d) Input index versus generation
(e) Dynamic index versus generation

9.5.3 Analysis on the final population

Plots of the Pareto front in two dimensions for the final population of size 200 after 20 000 generations have been provided in Figure 9.8. From plots (a), (b) and (e) of Figure 9.8, it can be observed that both weight and power-loss increase with the increase in the load capacity. From plots (c), (d), (f), (g), (h) and (i) of Figure 9.8, we can observe that at any load, weight, and power-loss we can have different controller input and dynamic performance indexes. Hence, we have to have a proper criterion to choose a controller at any load. The plot (j) of Figure 9.8 shows that the dynamic performance index of the controller increases with the increase in the input performance index of the controller. This shows that at each input performance index there is a minimum limit for the dynamic performance index.

The scatter of different design parameters of the final population have been provided in Figure 9.9. Bounds on design variables of population size 200 after 20000 generations have been given in Table 9.8. Different values of design variables have been provided in Table 9.9. One can observe that values of controller proportional gains drastically reduced to below 300. From Table 9.4, the upper bound on the proportional gain is assumed to be 600 yet the upper bound of the controller proportional gain in the final population from Table 9.8 is below 300. Hence, it could be concluded that the constraint on the power amplifier voltage will constrain the choice of controller grains.

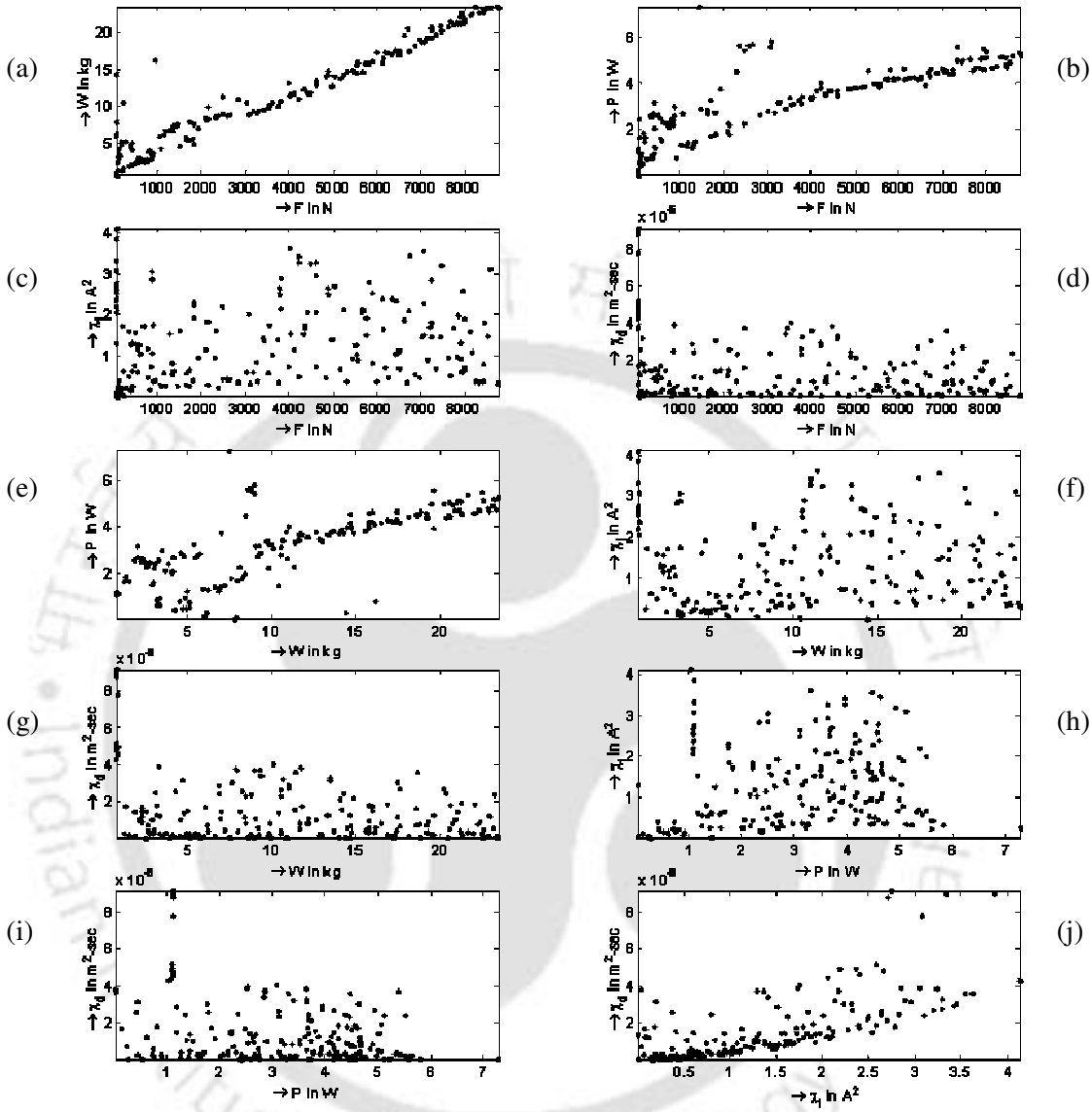

Figure 9.8 The Pareto optimal front two dimensional sections (200 population 20 000 generations)

(a) Weight versus load capacity
(b) Power-loss versus load capacity
(c) Input index versus load capacity
(d) Dynamic index versus load capacity
(e) Power-loss versus weight
(f) Input Index versus weight
(g) Dynamic index versus weight
(h) Input index versus power-loss
(i) Dynamic index versus power-loss
(j) Dynamic index versus input index

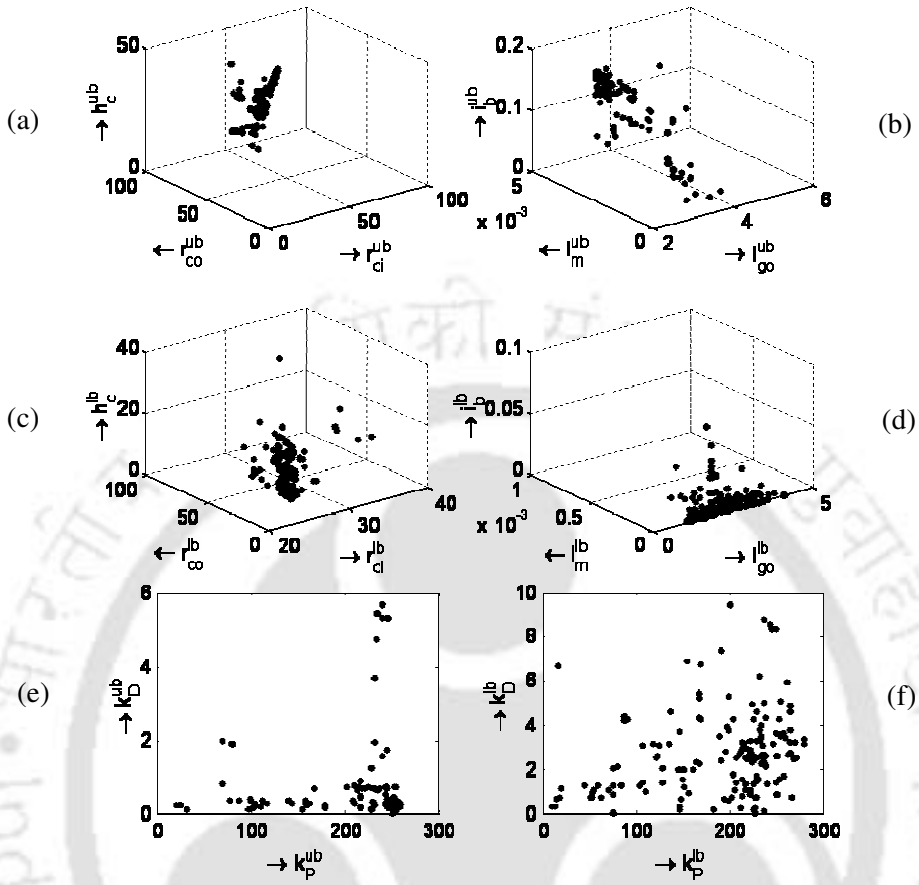

Figure 9.9 Scatter of design variables in the design variable space
(200 population 20 000 generations)

(a) Inner radius versus outer radius and height (Upper bearing)
(b) Bias current versus air gap and thickness of bias magnets (Upper bearing)
(c) Inner radius versus outer radius and height (Lower bearing)
(d) Bias current versus air gap and thickness of bias magnets (Lower bearing)
(e) Derivative gain versus proportional gain (UB Controller)
(f) Derivative gain versus proportional gain (LB Controller)

Table 9.8 bounds on the design variables in the final populations after specified number of generations for different cases

Design variables		Upper Bearing Actuator						Lower Bearing Actuator						UB Controller		LB Controller	
		r_{ci} (mm)	r_{co} (mm)	h_c (mm)	l_m (mm)	l_{g0} (mm)	i_b (A)	r_{ci} (mm)	r_{co} (mm)	h_c (mm)	l_m (mm)	l_{g0} (mm)	i_b (A)	k_P	k_D	k_P	k_D
Pop 200	a*	27.04	48.69	17.44	0.37	2.32	0.03	27.00	28.01	0.66	0.00	1.12	0.00	64.17	0.22	41.79	0.07
Gen 1000	b	59.13	70.96	48.74	4.98	4.71	0.14	39.89	62.44	46.43	0.38	4.46	0.02	273.03	4.98	269.39	6.84
Pop 200	a	27.19	43.85	14.43	0.28	2.92	0.02	27.00	27.37	0.35	0.00	1.01	0.00	20.46	0.02	10.00	0.04
Gen 20000	b	78.19	94.21	41.24	4.97	4.69	0.14	39.48	65.40	36.63	0.55	4.09	0.07	259.82	5.70	279.86	9.51
Pop 100	a	29.38	50.28	7.77	0.01	1.78	0.02	27.00	27.36	0.36	0.00	1.01	0.00	22.11	0.04	10.29	0.00
Gen 20000	b	76.23	98.53	27.33	5.00	4.88	0.14	42.22	118.39	39.60	0.34	4.16	0.05	281.81	1.13	263.52	8.61

* a → upper bound b→lower bound

Table 9.9 Values of design variables for different cases

Objective functions	GA Para-meters	Design variables															
		Upper Bearing Actuator						Lower Bearing Actuator						UB Controller		LB Controller	
		r_{ci} (mm)	r_{co} (mm)	h_c (mm)	l_m (mm)	l_{g0} (mm)	i_b (A)	r_{ci} (mm)	r_{co} (mm)	h_c (mm)	l_m (mm)	l_{g0} (mm)	i_b (A)	k_P	k_D	k_P	k_D
1*	a*	55.83	79.19	17.17	0.32	4.21	0.02	27.00	27.49	0.39	0.00	1.98	0.00	33.91	0.05	24.44	0.02
	b	53.12	68.39	29.17	0.28	3.57	0.01	27.06	27.70	0.41	0.00	1.48	0.00	32.48	0.09	15.34	0.66
	c	44.16	54.02	32.56	0.42	3.71	0.03	27.40	30.83	3.12	0.01	3.78	0.00	66.10	0.55	139.96	0.89
2	a	29.38	50.28	7.77	0.42	1.78	0.13	27.00	27.36	0.36	0.00	1.35	0.04	261.99	1.13	149.51	5.86
	b	27.20	44.16	16.96	1.51	3.38	0.12	27.00	27.37	0.35	0.00	1.19	0.01	216.67	0.18	17.89	6.68
	c	27.04	50.39	17.44	2.57	4.47	0.10	27.09	28.96	4.20	0.01	1.79	0.00	184.06	0.63	152.59	3.86
3	a	76.22	95.99	21.56	4.82	3.47	0.14	29.31	45.96	11	0.00	1.27	0.00	281.81	0.04	231.66	2.02
	b	78.19	94.16	30.01	4.87	3.53	0.13	27.71	28.48	1.92	0.00	3.07	0.00	253.95	0.11	198.19	3.93
	c	58.93	70.62	40.24	4.81	3.50	0.13	28.71	33.86	21.21	0.07	4.27	0.01	257.22	0.67	256.23	3.99
4	a	71.93	93.59	19.98	0.01	4.62	0.12	36.24	83.34	39.60	0.00	1.29	0.00	22.11	0.52	14.27	0.09
	b	39.72	82.95	41.24	0.39	3.91	0.02	31.02	63.28	36.63	0.00	1.41	0.00	20.46	0.24	10.00	0.29
	c	34.24	51.26	46.80	0.37	2.59	0.04	30.58	49.59	5.79	0.00	1.54	0.00	64.62	0.74	48.82	1.32
5	a	50.21	73.66	11.66	0.2	2.2	0.06	27.24	48.13	12.42	0.06	1.54	0.04	109.5	0.17	196.65	0.42
	b	27.34	51.14	32.05	2.53	4.35	0.10	27.03	37.63	18.74	0.00	1.76	0.03	202.88	0.72	201.73	0.71
	c	49.58	64.82	32.75	4.93	4.71	0.12	27.36	45.06	15.56	0.02	2.71	0.00	239.90	0.79	242.25	5.82
6	a	54.69	76.99	27.33	4.54	3.73	0.10	29.00	40.49	1.06	0.00	1.61	0.00	197.14	0.33	173.10	0.00
	b	55.56	73.60	29.44	4.42	3.38	0.10	27.11	28.00	1.07	0.00	2.53	0.00	230.76	0.30	213.66	1.54
	c	42.71	61.77	33.43	4.53	3.47	0.10	27.46	29.88	4.27	0.00	1.38	0.00	191.95	0.30	216.23	1.65

*1→ minimum power-loss; 2 → minimum weight; 3 → maximum load capacity; 4 → minimum input performance index; 5 → minimum output performance index; 6 → minimum distant member from utopia point; **a → 100 population, 20000 gen; b → 200 population, 20000 generations; c→200 population, 1000 generations

Table 9.10 Different geometrical and control parameters of upper and lower bearing actuators and controllers

	Upper bearing actuator						Lower bearing actuator						UB controller				LB controller			
	r_o (mm)	h_t (mm)	A_g (mm2)	A_c (mm2)	V_c (mm3)	W (N)	r_o (mm)	h_t (mm)	A_g (mm2)	A_c (mm2)	V_c (mm3)	W (N)	k_x (N/m)	k_i (N/A)	K_e (N/m)	C_e (N/A)	k_x (N/m)	k_i (N/A)	K_e (N/m)	C_e (N/A)
1a	93.62	39.81	7829.73	401.13	170.16	8.07	29.32	2.32	327.24	0.19	0.03	0.01	2.12e4	629	174	28	1.0e-7	0.00	0.00	0.00
b	82.90	50.13	6900.00	445.00	170.00	7.83	29.57	2.39	336.00	0.26	0.05	0.01	2.47e4	771	291	70	1.0e-6	0.00	0.00	0.00
c	65.15	47.99	4164.15	321.01	99.02	4.34	32.8	5.42	394.66	10.72	1.96	0.06	2.74e4	430	1003	236	6.3e-1	0.02	2.03	0.02
2a	52.60	12.25	748.72	162.35	40.63	0.66	29.2	2.28	326.73	0.13	0.02	0.01	4.20e4	163	733	184	6.0e-4	0.00	0.00	0.00
b	45.44	20.58	361.16	287.61	64.48	0.75	29.21	2.28	326.73	0.13	0.02	0.01	2.08e4	96	50	16	4.0e-6	0.00	0.00	0.00
c	51.43	21.97	332.88	407.16	99.04	1.08	30.78	6.22	341.58	7.88	1.39	0.05	1.83e4	102	501	64	7.1e0	0.06	2.93	0.25
3a	119.99	60.38	16285.8	426.16	230.55	20.12	48.44	14.99	734.55	183.26	43.33	0.67	2.19e6	7822	8211	311	1.0e-7	0.00	0.00	0.00
b	119.81	69.98	17245.6	478.96	259.34	23.37	30.88	4.49	448.04	1.48	0.26	0.03	2.28e6	9135	31366	961	1.0e-7	0.00	0.00	0.00
c	88.52	69.22	8947.91	470.35	191.44	12.20	36.68	24.76	626.81	109.04	21.43	0.46	1.20e6	4709	12827	3162	9.7e1	3.26	737	13.00
4a	115.36	51.61	14291.8	432.62	224.96	16.23	87.37	49.09	2162.26	1865.17	700.7	9.19	1.61e4	785	1238	405	1.2e4	2201	19089	202
b	88.51	53.63	2994.1	1782.92	687.15	10.17	65.89	42.06	1059.74	1181.38	349.98	4.21	2.27e4	1854	15160	450	4.1e1	53.00	498	15
c	56.34	55.16	1718.59	796.72	213.99	3.66	52.63	10.86	974.55	110.07	27.73	0.60	3.76e4	979	25676	722	2.0e0	1.00	46	1
5a	85.57	30.74	5955.78	273.44	106.41	5.13	49.33	14.63	368.18	259.29	61.39	0.71	6.80e4	932	33977	157	2.10e3	47.00	7129	20
b	52.32	36.82	385.39	762.56	188.02	1.99	39.01	20.69	332.52	198.45	40.31	0.49	2.48e4	241	24171	174	8.49e1	6.00	1240	5
c	77.68	56.17	5759.38	499.04	179.35	7.39	46.41	17.84	387.95	275.57	62.70	0.74	4.98e5	2343	70815	1859	2.5e1	4.00	1016	25
6a	91.07	53.5	7434.03	609.23	252.03	9.95	43.08	4.79	679	12.17	2.66	0.14	8.82e5	4742	52628	1578	8.4e-1	0.06	9.37	0.00
b	88.76	56.02	7734.42	531.12	215.51	9.89	29.9	3.09	344.62	0.96	0.17	0.02	1.05e6	4758	45188	1417	2.1e-3	0.00	0.02	0.00
c	70.81	52	3766.81	637.32	209.19	5.58	31.97	6.63	405.73	10.32	1.86	0.06	4.97e5	2703	21631	803	7.62e1	0.11	16.38	0.18

1→ minimum power-loss; 2 → minimum weight; 3 → maximum load capacity; 4 → minimum input performance index; 5 → minimum output performance index; 6 → minimum distant member from utopia point; a → 100 population, 20000 generations; b → 200 population, 20000 generations; c→200 population, 1000 generations

Table 9.11 Different electrical and magnetic parameters of actuators and power amplifiers

Objective functions	GA parameters	Upper bearing actuator						Lower bearing actuator						UBP amplifier		LBP amplifier	
		n (Turns)	i_{min} (A)	i_{max} (A)	B (T)	B_{min} (T)	B_{max} (T)	n (Turns)	i_{min} (A)	i_{max} (A)	B (T)	B_{min} (T)	B_{max} (T)	v_{max} (V)	va_{max} (VA)	v_{max} (V)	va_{max} (VA)
1	a	3168	0	0.02	0.09	0.09	0.09	1	0.00	0.01	0.00	0.00	0.00	3.42	0.06	0.00	0.00
	b	3526	0	0.02	0.10	0.10	0.10	1	0.00	0.01	0.00	0.00	0.00	3.11	0.05	0.00	0.00
	c	2484	0	0.03	0.13	0.13	0.13	72	0.00	0.07	0.00	0.00	0.00	3.74	0.13	0.13	0.01
2	a	1298	0.00	0.13	0.29	0.29	0.30	1	0.05	0.12	0.00	0.00	0.00	6.19	0.83	0.00	0.00
	b	2304	0.02	0.13	0.42	0.42	0.42	1	0.00	0.02	0.00	0.00	0.00	9.20	1.16	0.00	0.00
	c	3234	0.01	0.10	0.48	0.48	0.49	55	0.00	0.08	0.00	0.00	0.01	11.11	1.11	0.11	0.01
3	a	3416	0.00	0.14	0.80	0.80	0.80	1457	0.00	0.12	0.00	0.00	0.08	74.36	10.51	8.34	0.97
	b	3825	0.01	0.13	0.80	0.80	0.80	10	0.00	0.1	0.00	0.00	0.00	113.58	15.16	0.03	0.00
	c	3762	0.01	0.03	0.80	0.80	0.80	840	0.01	0.14	0.02	0.02	0.04	32.99	4.49	4.17	0.58
4	a	3416	0.11	0.12	0.08	0.08	0.08	14896	0.01	0.02	0.09	0.09	0.12	106.30	13.20	105.26	1.80
	b	14152	0.01	0.02	0.16	0.15	0.16	9373	0.00	0.01	0.01	0.00	0.03	119.91	2.31	43.26	0.27
	c	6336	0.01	0.04	0.22	0.20	0.23	848	0.00	0.03	0.00	0.00	0.01	104.11	4.49	3.01	0.09
5	a	2178	0.01	0.09	0.14	0.13	0.15	2065	0.00	0.14	0.09	0.05	0.15	62.51	5.41	13.09	1.82
	b	6030	0	0.14	0.53	0.49	0.54	1590	0.00	0.13	0.02	0.00	0.08	32.42	4.43	7.30	0.96
	c	3956	0.01	0.13	0.69	0.69	0.69	2200	0.00	0.12	0.01	0.01	0.08	118.33	14.88	53.57	6.66
6	a	4851	0.00	0.10	0.75	0.75	0.75	96	0.00	0.09	0.00	0.00	0.00	84.17	8.64	0.26	0.02
	b	4233	0.00	0.12	0.78	0.78	0.78	6	0.00	0.11	0.00	0.00	0.00	63.1	7.31	0.02	0.00
	c	5076	0.00	0.10	0.78	0.78	0.78	72	0.00	0.11	0.00	0.00	0.01	30.83	2.97	0.21	0.02

1→ minimum power-loss; 2 → minimum weight; 3 → maximum load capacity; 4 → minimum input performance index; 5 → minimum output performance index; 6 → minimum distant member from utopia point; a → 100 population, 20000 gen; b → 200 population, 20000 generations; c→200 population, 1000 generations

Table 9.12 The force and power-loss parameters of upper and lower bearing actuators

Objective functions	GA Parameters	UB Actuator							LB Actuator						
		F (kN)	F_m (kN)	F_{xi} (kN)	F_{xo} (kN)	P (W)	P_{xi} (W)	P_{xo} (W)	F (kN)	F_m (kN)	F_{xi} (kN)	F_{xo} (kN)	P (W)	P_{xi} (W)	P_{xo} (W)
1	a	50.28	39.83	50.60	50.27	0.05	0.06	0.00	0.00	0.00	0.00	0.00	0.00	0.00	0.00
	b	50.58	38.35	51.06	50.58	0.05	0.05	0.00	0.00	0.00	0.00	0.00	0.00	0.00	0.00
	c	59.76	45.37	60.31	59.76	0.13	0.13	0.00	0.00	0.00	0.00	0.00	0.00	0.01	0.00
2	a	50.86	30.05	52.75	50.86	0.83	0.83	0.00	0.00	0.00	0.00	0.00	0.00	0.00	0.00
	b	51.03	39.37	51.43	51.02	1.12	1.15	0.01	0.00	0.00	0.00	0.00	0.00	0.00	0.00
	c	62.27	52.26	62.45	62.24	1.11	1.11	0.01	0.01	0.01	0.01	0.01	0.00	0.01	0.00
3	a	8273.34	7184.12	8293.96	8273.35	5.22	5.22	0.00	0.00	0.00	3.55	0.00	0.00	0.65	0.00
	b	8760.05	5760.28	8782.03	8760.05	5.22	5.22	0.01	0.00	0.00	0.00	0.00	0.00	0.00	0.00
	c	4540.32	3909.17	4554.16	4540.32	4.01	4.01	0.01	0.22	0.18	0.68	0.22	0.00	0.45	0.00
4	a	69.99	0.15	81.72	69.99	3.87	3.87	3.21	15.34	0.00	23.34	15.34	0.08	0.23	0.08
	b	58.65	25.87	60.35	50.92	0.28	0.28	0.06	0.05	0.00	0.56	0.01	0.00	0.01	0.00
	c	66.61	27.99	69.54	52.92	0.44	0.44	0.03	0.00	0.00	0.07	0.00	0.00	0.02	0.00
5	a	98.22	42.36	105.76	80.36	0.51	0.90	0.01	2.25	0.59	6.25	0.79	0.11	1.33	0.00
	b	86.20	61.47	91.02	73.62	2.36	3.93	0.00	0.14	0.00	1.53	0.00	0.04	0.79	0.00
	c	2189.36	1899.15	2194.94	2156.10	3.18	3.18	0.01	0.04	0.03	1.83	0.04	0.00	1.09	0.00
6	a	3355.68	2877.07	3365.17	3337.20	2.99	2.99	0.00	0.00	0.00	0.01	0.00	0.00	0.02	0.00
	b	3761.88	3219.54	3773.11	3749.54	3.26	3.26	0.00	0.00	0.00	0.00	0.00	0.00	0.00	0.00
	c	1818.84	1562.76	1823.86	1812.72	2.18	2.18	0.00	0.01	0.01	0.01	0.01	0.00	0.02	0.00

1→ minimum power-loss; 2 → minimum weight; 3 → maximum load capacity; 4 → minimum input performance index; 5 → minimum output performance index; 6 → minimum distant member from utopia point; a → 100 population, 20000 generations; b → 200 population, 20000 generations; c→200 population, 1000 generations

Table 9.13 Parameters of double-acting bearing actuator and controller for different cases

Objective functions	GA Para-meters	Double acting bearing parameters										Controller parameters							
		k_i (N/A)	k_x (kN/m)	P (W)	P_{xi} (W)	P_{xo} (W)	W (N)	F (kN)	F_m (kN)	F_{xi} (kN)	F_{xo} (kN)	K_e (kN/m)	C_e (N-s/m)	t_s (sec)	x_{ci} (mm)	x_{co} (mm)	χ_i (A^2)	χ_o (mm^2)	χ_d (mm^2-sec)
1	a	629.45	2.12e4	0.05	0.06	0.00	8.09	50.29	39.83	50.28	50.60	174.79	28.53	0.67	0.018	-0.500	0.05	302.55	24.22
	b	771.68	2.47e4	0.05	0.05	0.00	7.84	50.59	38.36	50.59	51.07	291.69	70.29	0.84	0.000	-0.500	0.04	341.95	37.54
	c	430.27	2.74e4	0.13	0.13	0.01	4.40	59.76	45.36	60.31	59.76	1005	236	0.89	0.000	-0.500	0.69	306.47	34.56
2	a	163.19	4.20e4	0.83	0.83	0.00	0.68	50.87	30.05	50.87	52.75	733.9	184.8	0.95	0.000	-0.500	2.74	331.02	39.81
	b	96.48	2.08e4	1.12	1.15	0.02	0.76	51.03	39.38	51.03	51.44	50.32	16.93	0.79	0.007	-0.500	2.75	585.73	92.24
	c	102.2	1.83e4	1.11	1.11	0.01	1.13	62.27	52.26	62.24	62.45	504.54	64.98	0.37	0.000	-0.500	1.01	204.94	11.83
3	a	7822.81	2.20e6	5.23	5.23	0.41	20.8	8273.35	7184.13	8273.35	8291.52	8211.52	311.37	0.12	0.000	-0.500	0.66	57.56	0.96
	b	9135.33	2.29e6	5.22	5.22	0.01	23.41	8760.05	7560.28	8760.05	8782.03	31366.84	961.66	0.11	0.000	-0.500	0.30	42.46	0.59
	c	4712.9	1.20e6	4.02	4.01	0.41	12.66	4540.1	3908.99	4540.1	4553.52	13565.09	3175.37	0.91	0.000	-0.500	3.60	294.73	34.25
4	a	2986.63	2.84e4	3.95	3.96	3.44	25.43	54.65	0.15	50.31	62.87	20328.49	607.11		0.000	-0.500	0.00	43.15	0.57
	b	1908.33	2.28e4	0.29	0.29	0.08	14.38	58.6	25.88	50.36	60.33	15659.22	466.6	0.10	0.000	-0.500	0.00	44.44	0.58
	c	980.11	3.76e4	0.45	0.45	0.05	4.26	66.61	27.99	52.85	69.55	25722.65	723.93	0.10	0.000	-0.500	0.01	40.26	0.51
5	a	979.15	7.02e4	0.62	1.34	0.56	5.84	95.97	41.77	74.12	104.82	41107.06	177.47	0.10	0.190	-0.500	0.09	22.28	0.21
	b	248.3	2.50e4	2.41	3.93	0.70	2.5	86.06	61.47	72.09	91.01	25412.42	178.87	0.10	0.139	-0.500	0.16	25.56	0.22
	c	2347.59	4.91e5	3.18	3.18	0.17	8.13	2189.32	1899.13	2154.58	2194.89	71831.7	1884.49	0.10	0.000	-0.500	0.18	35.52	0.43
6	a	4742.23	8.82e5	2.99	2.99	0.03	10.11	3355.69	2877.08	3337.19	3365.17	52638.18	1578.04	0.11	0.000	-0.500	0.26	40.48	0.56
	b	4758.15	1.05e6	3.26	3.26	0.00	9.92	3761.89	3219.54	3749.54	3773.11	45188.2	1417.9	0.12	0.000	-0.500	0.33	42.43	0.62
	c	2703.32	4.97e5	2.18	2.18	0.02	5.65	1818.84	1562.76	1812.71	1823.86	21647.87	804.08	0.14	0.000	-0.500	0.33	51.13	0.87

1→ minimum power-loss; 2 → minimum weight; 3 → maximum load capacity; 4 → minimum input performance index; 5 → minimum output performance index;
6 → minimum distant member from utopia point; a → 100 population, 20000 gen; b → 200 population, 20000 generations; c→200 population, 1000 generations.

9.5.4 Analysis of parameters of individual actuators

Different electrical and magnetic parameters of the upper and lower bearing actuator and power amplifiers are provided in Table 9.11. The force and power-loss parameters are provided in Table 9.12. It could be observed from Table 9.12 that the upper bearing actuator and controller have non-zero values, while the lower bearing actuator, controller and power amplifier have most of them near zero values. This is due to fact that the lower bearing has no load constraint on it. The load is assumed to be acting opposite to the upper bearing and there is no minimum limit on the dynamic loading on the lower bearing. Hence, values chosen for the lower bearing are near zero corresponding to a small dynamic loading.

Table 9.14 comparison of convergence of forces for different cases with different populations

	Case 1	Case 2	Case 3	Case 4	Case 5	Case 6
Force(in N) with 100 pop	50	52	8291	64	104	3365
Force(in N) with 200pop	51	51	8782	60	91	3773
Dominating population size	200	100	200	100	100	200

Parameters of the double-acting bearing and controllers are provided in Table 9.13. By observing Table 9.13, a comparison of forces obtained for different cases have been presented in Table 9.14. From Table 9.14, it has been observed that for cases 1 (minimum power-loss) both 100 and 200 populations converged to forces, respectively, 50N and 51N; and case 2 (minimum weight) the forces are 52N and 51N respectively. However, for the case 3 (maximum load capacity) the forces have been observed to be converged to 8291N and 8782N, respectively, clearly showing the 200 population got better convergence. However, for case 4 (minimum input performance index) the respective forces are 64N amd 60N and for case 5 (minimum dynamic performance index) 104N and 91N and the population of 100 dominated, for case 6 (minimum distant member from the utopian point)

the respective forces are 3365N and 3773N and the population of 200 dominated. For different cases different population sizes resulted in better solutions. Hence, population size could be seen as one important criterion in multi-objective optimization using MOGA.

Moreover from Table 9.14, there seems to be so much variation for the 6 cases. This can be explained as follows**.** The minimum power-loss as objective ends with minimum load requirements (i.e. case 1). The minimum weight also ends with minimum load requirements (i.e. case 2). However, the maximum load capacity as objective (i.e. case 3) chooses the maximum possible space to accommodate the maximum possible load with the minimum power-loss and the minimum weight in the maximum space available. Similarly, the controller performance indexes as objectives have been chosen the corresponding loads. The case 6 is a combination of all the objectives with different tradeoffs resulted in the corresponding load.

A similar analysis for system settling time with control (extracted from Table 9.13) is given in Table 9.15.

Table 9.15 Comparison of convergence of forces for different cases with different populations

	Case 1	Case 2	Case 3	Case 4	Case 5	Case 6
Settling time(in Sec) with 100 pop	0.67	0.95	0.12	0.01	0.01	0.11
Settling time(in Sec) with 200pop	0.84	0.79	0.11	0.01	0.01	0.12
Dominating population size	100	200	200	–	–	100

Control responses of different designs have been provided in Figure 9.10 to Figure 9.15. These controller responses are obtained by solving the differential equation (8.25) in time domain in closed form. Determine the Eigen values of the system according to equation (8.26), and then determine the state at each instant of time with initial conditions assumed in

Table 9.2. Subsequently determine the corresponding control current for each individual actuator by using equation (8.24). Then by using equations (9.5) to (9.11) we can determine the inductances individual actuators, voltages of individual power amplifiers.

In all the plots from Figure 9.10 to Figure 9.15, the plots (a) show the dynamic response of rotor, plots (b) show the upper actuator and power amplifier responses, and plots (c) show the lower actuator and power amplifier responses. From these plots one can observe the responses of different components for different cases.

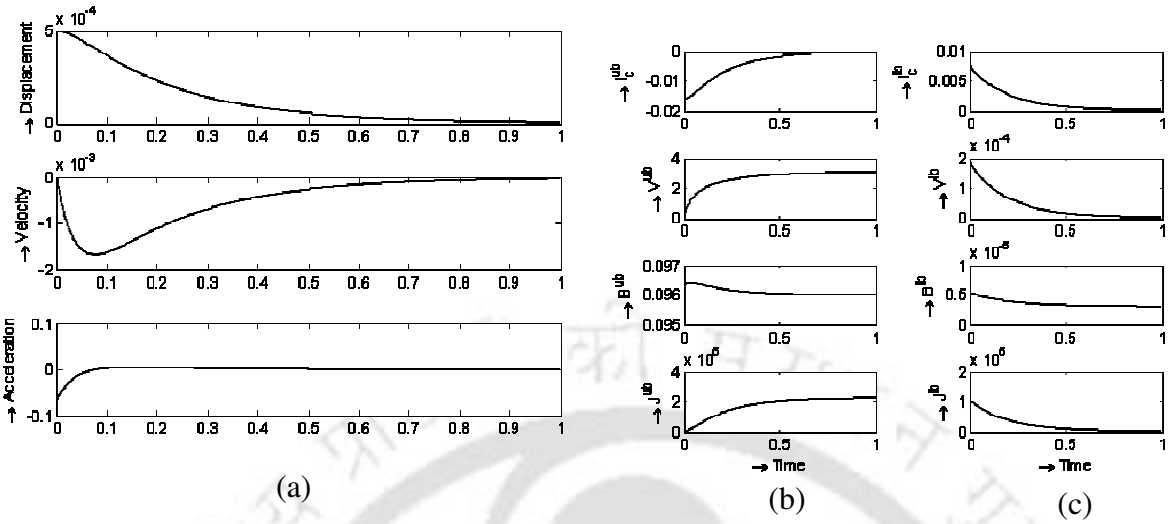

Figure 9.10 Responses of the chosen design with the minimum power-loss (units Displacement in m, velocity in m/sec, acceleration in m/sec^2, time in sec, J in A/mm^2, B in T, V in V and i_c in A)

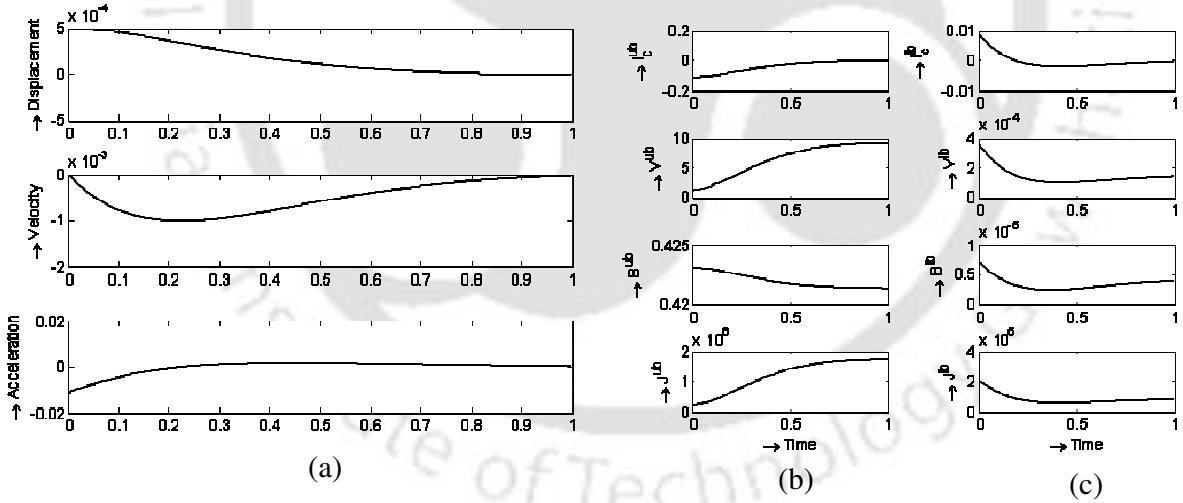

Figure 9.11 Responses of the chosen design with the minimum weight (units Displacement in m, velocity in m/sec, acceleration in m/sec^2, time in sec, J in A/mm^2, B in T, V in V and i_c in A)

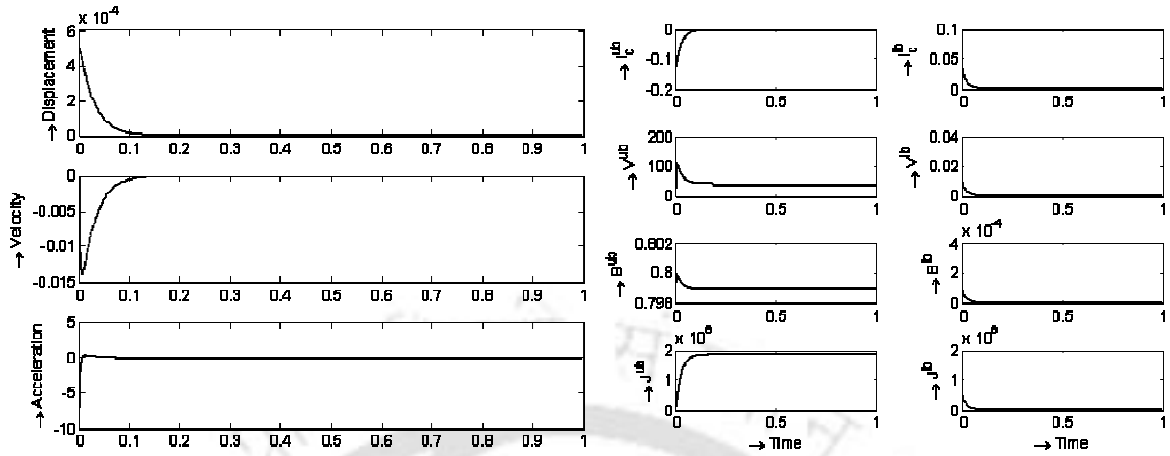

Figure 9.12 Responses of the chosen design with the maximum load capacity(units Displacement in m, velocity in m/sec, acceleration in m/sec^2, time in sec, J in A/mm^2, B in T, V in V and i_c in A)

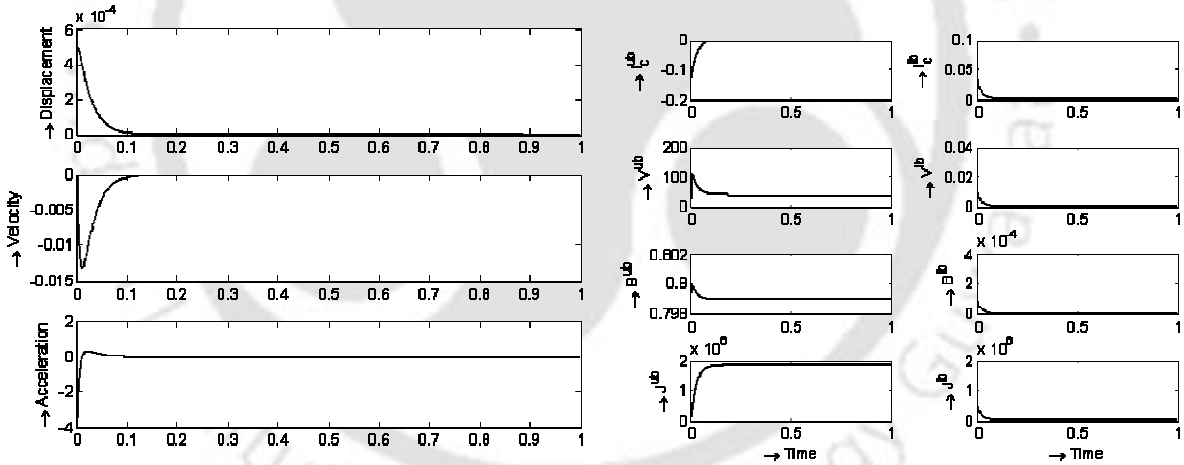

Figure 9.13 Responses of the chosen design with the minimum input performance index(units Displacement in m, velocity in m/sec, acceleration in m/sec^2, time in sec, J in A/mm^2, B in T, V in V and i_c in A)

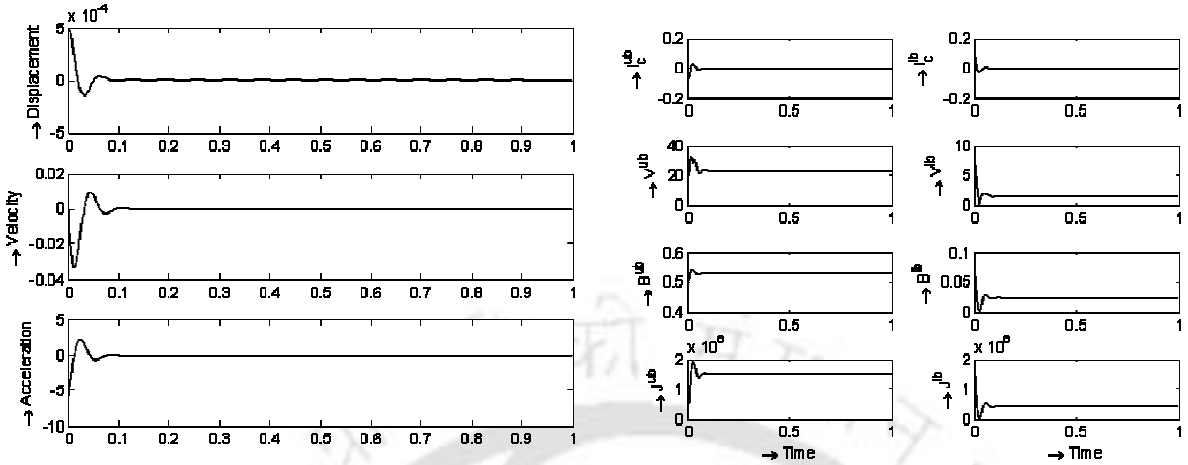

(a) (b) (c)

Figure 9.14 Responses of the chosen design with the minimum dynamic performance index (units Displacement in m, velocity in m/sec, acceleration in m/sec^2, time in sec, J in A/mm^2, B in T, V in V and i_c in A)

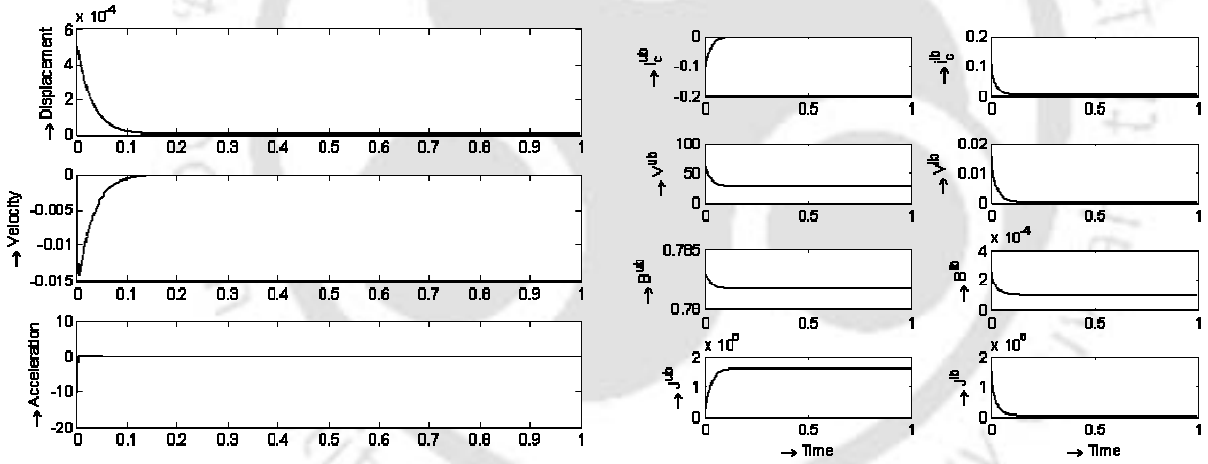

(a) (b) (c)

Figure 9.15 Responses of the chosen design with the minimum distant member from the utopian point (units Displacement in m, velocity in m/sec, acceleration in m/sec^2, time in sec, J in A/mm^2, B in T, V in V and i_c in A)

9.6 Conclusions

In the present chapter, genetic algorithms based multi-objective optimization of *double-acting hybrid magnetic thrust bearings* (DAHMTBs) by integrating the actuator, the controller and the power amplifier as a single system has been investigated. The

decentralized actuator, controller and power amplifier has been considered on both sides of the thrust disc of the rotor.

The load capacity of bearing, the weight of bearing, the power-loss in the coil, the input performance index and the dynamic performance index have been considered as objectives for the optimization. First three objectives corresponding to the actuator and remaining two objectives correspond to the controller.

Constraints considered for the actuator are the maximum allowed current-density in the coil, maximum allowed flux-density in the stator iron, maximum space available, and maximum power-loss allowed. Eigen values of characteristic equation and settling time of the system have been considered as constraints for the controller. The voltage and the power rating are considered as the power amplifier constraints.

Two different geometries are considered for the upper and lower actuators with two controllers and power amplifiers correspondingly. In the present chapter, the effect of constraints of the power amplifier has been studied.

Genetic algorithm has been implemented to carry out the constrained multi-objective optimization of the present problem. The convergence and Pareto-front spaces have been studied. The controller gains have been drastically reduced below 300 with the constraint on the power amplifier. The lower bearing, controller and power amplifier parameters have been observed to be near zero as the load is assumed to be acting opposite to upper actuator only.

Designs which are nearest to utopia point in Pareto-front fronts are compared. Similar to actuator controller integrated system, air gaps, bias currents, and lengths of permanent magnets are observed to be consistently different for individual actuators of the double acting bearing. Performance parameters of double-acting actuators and the controller of the magnetic bearing for different choices have been presented. Forces and settling times of different cases have been compared for population sizes of 100 and 200. Different population sizes have converged to better values for different choices the final population. Hence, the population size is observed to be an important criterion for multi-objective optimization using MOGA.

Control responses of different parameters of the rotor, the actuator, and the power amplifiers have been shown in plots. With such analysis one can observe how different design choices of final population respond dynamically.

Overall conclusions of the present thesis and the future scope will be provided in the next chapter.

Chapter 10
Conclusions & Future Scopes

10.1 Conclusions

In the present chapter, conclusions of the overall thesis and future scopes have been summarized. The overall thesis has three parts, namely the background, the optimal actuator design, and the optimum actuator-controller-amplifier integrated design. Part I includes the Chapters 1 to 3 which give the *background* of magnetic bearings, Part II includes the Chapters 4 to 7 which deal with the *optimal design* of actuator, and part III includes the Chapters 8 and 9 which deal with the *integrated design* of the actuator, controller, and amplifier in a magnetic bearing. Now main points of various chapters and conclusions drawn from them are summarized in the following subsection.

10.1.1 Chapter-wise observations and conclusions

Chapter 1 Introduction and Literature Review

- In the introduction some background on electromagnetism has been given. Working principle of AMB is explained. A new diverse classification of magnetic bearings has been presented.
- Advantages of AMBs with applications has been presented, and limitations of AMBs and how they are overridden over the period of time by researchers and practice engineers has been reviewed
- A classification on control system technology has been given. Different aspects of design namely modelling, analysis, design, procedure and production based on which design methodologies have been discussed in detail.
- Work on different configurations of AMBs has been reviewed. Works on magnetic thrust bearings, control systems and genetic algorithms in their design optimization have been reviewed; and found limited work in this area for MTBs. This gave motivation to pursue the present work.

Chapter 2 Formulations of Optimization Problems of Magnetic Bearings

- Some basic concepts of magnetic thrust bearing macro-geometry have been detailed. Analysis of magnetic thrust bearing has been carried out by using the magnetic circuit theory.
- The optimum design formulation for actuators of AMTB and HMTB has been provided. Objective functions namely the power-loss and the weight of the actuator

have been detailed. The importance of objectives for ground and aviation applications has been explained.

- It has been observed that the power-loss contributes towards running cost; acquisition costs of the controller, power amplifier, cooling system; and cooling costs of the coil in both ground and aviation applications. It has been also been observed that the weight of the bearing contributes towards purchasing, space occupied, and foundation strength in ground applications, while it contributes towards purchasing, transportation, space occupied, foundation strength, and dynamic stability of the structure in aviation applications.
- The coil dimensions namely the inner radius of coil, outer radius of coil, and height of coil have been observed to be influencing parameters of both the objectives (i.e., power-loss and weight). Hence, chosen as design vector in both the cases of AMTB and HMTB, and for the objective functions.
- Load capacity, maximum current density, maximum magnetic flux density, power-loss allowed in the coil, space occupied by the bearing have been considered as constraints of the optimization problem and has been discussed in detail.
- The detailed discussion on how the different design and dependant parameters influence the objectives and constraints has been presented with tables. It is observed that for given input parameters, the design parameters are chosen and the dependant parameters are found from the input and design parameters. The constraints and the objectives can be determined by using the input, design and dependant parameters.
- This chapter gives the background problem formulation for all the remaining chapters so that the results could be analyzed in the subsequent chapters.

Chapter 3 Single- and Multi-Objective Genetic Algorithms

- Different methods of the single-objective optimization both in the deterministic and stochastic approaches have been introduced. Reasons for the choice of genetic algorithms as an optimization tool for the present work have been provided.
- The details of operators involved in GA namely, the selection, the crossover, the mutation, and the elitism have been explained. At the end some key issues of the convergence, the decision making and the population size related to SOGA have been discussed.

Chapter 4 Design Optimization of Magnetic Thrust Bearing Actuators Using Single Objectiv Genetic Algorithms

- The optimal design of a thrust magnetic bearing using SOGAs has been performed for the actuator configurations namely AMTB and HMTB. SOGA has been carried with the objectives as minimization of the power-loss and minimization of the overall weight of the actuator, one at a time.
- Convergence plots of objective functions with the generation have been shown and the number of generations taken for the convergence is observed to be different for different cases. The best geometries of different cases have compared. Comparison has been done in two fold and it is specified as the comparison of objectives with the same configuration and the comparison of configuration with the same objective.
- From results, it is observed that the size of the bearing actuator of HMTB is considerably reduced as compared to the case of AMTB for the same conditions for the objective function as the maximization of load-to-weight ratio. Similarly, current-densities reduce drastically with bias magnets when the objective function is chosen as the minimization of the power-loss.

- It is also observed that objectives chosen, namely the power-loss and the weight are two conflicting quantities characterizing a decrement in one objective causes an equivalent increase in the other (i.e., reduction in the weight causes increase in the power-loss, and vice-a-versa) and to have a better design characteristic the multi-objective optimization is suggested.

Chapter 5 Optimum Design & Analysis of Magnetic Thrust Bearings Using Multi-Objective Genetic Algorithms

- The optimal design of actuators of AMTB using MOGAs has been carried out. Two objectives have been considered, namely, the minimizing the power loss and minimizing the weight of the bearing. The inner and outer radii of the coil, and the height of the coil have been proposed as design variables based on their dependency on objective functions. The method of implementation of the multi-objective genetic algorithm for the problem considered has been described.

- Geometries of designs with optimal individual objectives and a chosen design from the optimal Pareto front based on the minimum normalized distance criterion are compared. The sensitivity analysis is carried out with respect to a small perturbation of dimensions of design variables. It is observed that the effect of outer radius of coil is nearly double than the other two design variables. However, overall objective functions were insensitive for small perturbations.

- A novel *Pareto optimal design analysis* has been introduced to study the behavior of final optimized population designs of AMTB actuator systems by using large population size. By the analysis on the final population, the saturation of magnetic flux-density and coil current-density are observed to be the salient points, where the

major changes occur in the behavior of different design parameters in the final population.

- On the whole, the present work gives a direction to choose the proper design options for different applications based on the a-posteriori knowledge provided by the final population. The methodology could be implemented to the optimal design of different types of magnetic bearings with permanent magnets and with integration of differential control as well. This has been the motivation for subsequent chapters.

Chapter 6 Optimum Design & Analysis of Hybrid Magnetic Thrust Bearings Using Multi Objective Genetic Algorithms

- The optimal design of actuator of a *hybrid magnetic thrust bearing* (HMTB) with bias magnets using *multi-objective genetic algorithms* (MOGAs) has been carried out with two objectives namely the minimizing the power loss and the minimizing the weight.
- It is observed that the size of the bearing with bias magnets is considerably reduced as compared to the case of without bias magnets for the same operating conditions in the case of objective function as the minimization of the weight.
- Similarly, current-densities get reduced drastically with bias magnets when the objective function is chosen as the minimization of the power-loss. Geometries of optimized bearing designs with individual objectives and multi-objectives are compared.
- An *'a posteriori'* criterion proposed in the present work for choosing a design from the final population has been used to find different design choices and the results have been compared with SOGA. The SOGA and MOGA results have been

observed to be non-inferior to each other. Hence, it can be concluded that the end result depends upon the selection strategy also and for better convergence a *hybrid selection strategy* of SOGA and MOGA is suggested.

- Sensitivities of objective functions with respect to the outer radius, the inner radius and the height of coil are observed to be approximately in the ratio 2.5:1.6:1 for both the objectives.

- The *Pareto optimal design analysis* of the final optimized population that has been introduced in the present work has been carried out and a few salient points (i.e., a point where the height of the coil is maximum feasible, saturation of magnetic flux density, and saturation of current density) are observed in the case of with bias magnets.

Chapter 7 Effect of the Load on the Design Optimization of Magnetic thrust Bearings using Multi Objective Genetic Algorithms

- The effect of load on the Pareto frontier has been presented in the optimal design of thrust magnetic bearings using MOGAs. The *Pareto optimal design analysis* methodology has been used to analyze the final populations for different loads and configurations. Two objective functions namely minimization of the power-loss and minimization of the weight of the bearing are considered. The results for AMTB and HMTB have been compared.

- As the load increases, it is observed that the Pareto frontier reduces to a single point at the peak load within the given constraints for both the cases of with and without

bias magnets. Hence, the load to be supported can be considered as an objective function.

- The characteristics of design variables and other parameters with the power-loss have been discussed. Three distinct load zones have been observed within the given constraints namely the magnetic flux density unsaturated, the magnetic flux density unsaturated and saturated, magnetic flux density constant and saturated, and peak load. The transition load zones have been observed to be different for the cases of AMTB and HMB, respectively.

- The peak load by using bias magnets is observed to be 138.3% of that of without using bias magnets within the constraints given. On the whole the analysis methodology presented in the present work has an advantage of studying behavior of different parameters of Pareto optimal designs in final populations by taking a large population size.

- It would also be helpful in choosing proper design by the a-posteriori knowledge provided by the analysis of the final population through the proposed methodology (i.e., *Pareto optimal design analysis methodology*). This analysis can also be used to take interactive decisions during the search and guide the search at will.

Chapter 8 Design Optimization of Double-Acting Hybrid Magnetic Thrust Bearings with Controller Integration Using Multi-Objective Genetic Algorithms

- An optimal design of *double-acting hybrid magnetic thrust bearing* (DAHMTB) has been carried out. Double acting actuators and controller are optimized as a unified system. Two different geometries have been assumed for the individual actuators of the double-acting bearing. The macro-geometry of the DAHMTB has been described. The different actuator and controller relations have been presented.

- For the present case, the uni-mode control with a centralized controller has been assumed. The genetic algorithm has been implemented to carry out the constrained multi-objective optimization of the magnetic bearing. Results have been compared for populations of sizes of 200 and 100 run for 1000 generations for the confirmation of convergence with the population size. Results with population of size of 200 run for 100 and 1000 generations have also been compared for the study of convergence with number of generations.

- Some of convergence criteria from the study on Pareto-front have been observed. Designs which are nearest to the utopia point in Pareto-fronts are compared. Air gaps, bias currents, and lengths of permanent magnets are observed to be consistently different for individual actuators of the double-acting bearing.

- Performance parameters of double actuators and the controller of the magnetic bearing for different choices have been presented. Depending on the actuator and controller properties, it is observed that a set of design variables influence a particular set of objectives.

- In this chapter the controller is initially designed and a power amplifier that meets requirements of the controller can be procured next. Though power amplifiers can be designed with respect to designed controller requirements, sometimes it is not possible to have the required power amplifiers as a standard one, and one has to design the controller by taking constraints of the power amplifier available at hand. Though the centralization of controller requires less number of power amplifiers, but needs some complex winding schemes and control strategies. To go for a simpler winding and control strategies, one may have to go for a decentralized actuator,

controller and power amplifier in double-acting magnetic bearing systems. Hence, the design optimization methodology is extended to the DAHMTB with decentralized controller systems by taking consideration of constraints of the power amplifier in the final chapter.

Chapter 9 ***Design Optimization of Double-Acting Hybrid Magnetic Thrust Bearings with Controller and Power amplifier Integration Using Multi-Objective Evolutionary Algorithms***

- In the present chapter, genetic algorithms based multi-objective optimization of *double-acting hybrid magnetic thrust bearings* (DAHMTBs) by integrating the actuator, the controller and the power amplifier as a single system has been investigated. The decentralized actuator, controller and power amplifier has been considered on both sides of the thrust disc of the rotor.

- The load capacity of bearing, the weight of bearing, the power-loss in the coil, the input performance index and the dynamic performance index have been considered as objectives for the optimization. First three objectives corresponding to the actuator and remaining two objectives correspond to the controller.

- Constraints considered for the actuator are the maximum allowed current-density in the coil, maximum allowed flux-density in the stator-iron, maximum space available, and maximum power-loss allowed. Eigen values of characteristic equation and settling time of the system have been considered as constraints for the controller. The voltage and the power rating are considered as the power amplifier constraints.

- Two different geometries are considered for the upper and lower actuators with two controllers and power amplifiers correspondingly. In the present chapter, the constraints of the power amplifier have also been taken into consideration in the present integrated optimization problem.

- After implementation of the Genetic algorithm to the present constrained multi-objective optimization problem, controller gains have been drastically reduced to below 300 with the constraint on the power amplifier.

- The convergence and Pareto-front spaces have been studied. It took 20000 generations for convergence. The reason for the high number of generations for the convergence could be attributed to the increase in number of design variables due to the decentralization and due to constraints on parameters of the power amplifier.

- The lower bearing, controller and power amplifier parameters have been observed to be near zero as the load is assumed to be acting opposite to the upper actuator only.

- Designs which are nearest to utopia point in Pareto-front fronts are compared. Similar to actuator-controller integrated system, air-gaps, bias currents, and lengths of permanent magnets are observed to be consistently different for individual actuators of the double-acting bearing.

- Performance parameters of double-acting actuators and the controller of the magnetic bearing for different choices have been presented. The upper bearing actuator and controller have non-zero values, while the lower bearing actuator, controller and power amplifier have most of them near zero values. This is due to fact that the lower bearing has no load constraint on it. The load is assumed to be acting opposite to the upper bearing and there is no minimum limit on the dynamic loading on the lower bearing. Hence, values chosen for the lower bearing are near zero corresponding to a small dynamic loading.

- Comparisons of forces and controller settling-time have been done for different design choices of final population with population sizes of 100 and 200. For different cases different population sizes resulted in better solutions. Hence, population size could be seen as one important criterion in multi-objective optimization using MOGA.

- Control responses of different parameters of the rotor, the actuator, and power amplifiers have been shown in plots for different design choices of final populations. From these figures one can observe the responses of different components for different cases.

10.1.2 Overall conclusions

In the present thesis, an optimal design and an integrated design optimization of magnetic thrust bearing systems have been dealt with a background of literature, problem formulation and an optimization tool. The overall thesis targeted to optimize actuators of different configurations of magnetic thrust bearings, including AMTB, HMTB and DAHMTB. It also considers the optimization of different controllers, namely centralized and decentralized controllers. The optimization involves different objective functions including power-loss, weight of a single acting actuator, load capacity of a double acting actuator, input and dynamic performance index of a controller. Moreover, it has used different optimization tools in the namely SOGA and MOGA. However, these many complexities have been dealt in a systematic way in the present thesis.

Initially, single acting actuators of an AMTB and a HMTB have been optimized using SOGA. The power-loss and weight have been optimized independently for both the

configurations. Coil dimensions (i.e., the inner radius, the outer radius and the height of coil) have been observed to be design vector for a specified operating load. A HMTB actuator needs determination of thickness of permanent magnets. The design vector remained same for a specified operating load as of AMTB. However, when the operating load is not specified then operating parameters namely, the thickness of bias magnets, length of air-gap and bias current supplied have been added to the design vector along with coil dimensions. When the controller integrated along with the actuator, the gains of the controller have been added to the design vector along with actuator design vector. For a centralized control system one set of control gains were taken while for a decentralized system the controller gains will be different for each actuator.

The SOGA study helped in studying the performances of optimized geometries of actuators of the AMTB and the HMTB. The SOGA study inferred the superior performance of HMTB in both the power-loss and the weight for a particular operating load. An AMTB completely supplies the magnetic flux by electric current and the power-losses have been observed to be high. In a HMTB the bias magnetic flux is supplied by permanent magnets and the all the static loads can be nullified without any current supply. Hence, for an AMTB the power-loss is more than the HMTB actuator for the same operating load and constraints. Similarly, the minimum weight of the actuator of a HMTB is very low as compared to that of an AMTB due to no bias current is supplied and the corresponding volume of the copper winding is reduced.

Through SOGA study, it is observed that for a single configuration the weight and the power-loss are conflictive to each other. This result inferred an attempt of multi-objective optimization of actuators of both AMTB and HMTB with the weight and the power-loss as

objectives of optimization and at a specified operating load. Consequently, actuators of an AMTB and HMTB have been optimized by using MOGA with power-loss and weight as objectives in succession. From these two studies as compared the MOGA and SOGA resulted in non-inferior solutions to each other (i.e., the MOGA dominated in one objective while the SOGA dominated in other objective). Such results infer to go for hybrid selection criteria of the MOGA and the SOGA.

The MOGA optimization for AMTB and HMTB also lead us into a *novel analysis* which we call it as *Pareto optimal design analysis* (PODA) by which the different parameters of designs of the Pareto optimal front of the final population could be analyzed. It is a population based analysis. Generally, it is highly difficult to arrive at a closed form representation of the Pareto optimal front. Hence, it is very difficult to analyze the front by continuous mathematics. Consequently, one has to go for numerical solutions which are discrete. As the *Pareto optimal design analysis* methodology is population based and one can arrive at a close to optimal front by taking high population sizes as it is taken now.

Advantages of the methodology

- It is a useful tool in analyzing the Pareto optimal systems which are highly difficult to represent by a close form solution.
- Studying the behavior Pareto optimal systems is a novel idea which would be useful in understating the Pareto optimal behavior of systems (i.e., the behavior of different designs of a Pareto optimal front with respect to each other) .
- The methodology is also useful as a guide in a decision making.

Limitations of the methodology

- The methodology is highly dependent on the *accuracy* and the *uniform distribution* of the solutions of the Pareto optimal front obtained. A compromise in one of these issues (i.e., accuracy and distribution of the solutions) would result in a diverse understanding from the facts.

- The methodology also needs high population sizes to get *accurate* and *uniformly distributed* Pareto optimal set. Hence, it is a costly attempt with increase in the number of objectives. Moreover, the cost increases exponentially with every additional objective.

Applications of the methodology

- The methodology presented here could be utilized in generating correlations between different objectives of a Pareto optimal set.

- It is also useful in decision making interactively (during the search) by analyzing the present population and the trends of previous iterations

- It is also useful in an 'a-posteriori' decision making of proper design choices depending on the behavior of different parameters of the obtained Pareto optimal set (i.e., final population).

- More applications could be searched for such as generating standards, etc.

The *Pareto optimal design analysis* methodology has been implemented to study the behaviour of Pareto optimal fronts of AMTB and HMTB by changing load. The Pareto front reduced to a single point with increase in load and it has been concluded that the load to be supported as an objective. Moreover, by analyzing the different parameters of Pareto optimal designs at various loads, different load zones were found. This is another advantage of *Pareto optimal design analysis* methodology.

As a progression of study, a centralized controller is included with an actuator of a DAHMTB and the design optimization is carried by an *integrated design optimization* methodology. At this point the design entered from an optimal design to an integrated design optimization. This resulted in an increase in the number of design objectives, design variables and constraints with interaction between different subsystems. The number of objectives increased to 5 with number of design variables 14. From results it has been observed that not all variables influence all objectives and constraints. Hence, it is concluded that better optimization strategies can be adapted. Moreover, the necessity of incorporating the power amplifier constraints has been emphasized.

Consequently constraints of the power amplifier are considered. A decentralized controller has been considered. Design variables increased to 16 though the number of objectives remains 5. The number of constraints also increased with decentralization and power amplifier constraints. The overall problem resulted in slower convergence which went beyond 15000 generations. The gains of the controller reduced drastically with the constraint on the power amplifier. It is observed that the population size is an important factor in MOGA by the comparison of load capacity and settling times for different population sizes (i.e., 100 and 200).

The overall exercise of the optimization gives rise to a novel methodology of analysis of Pareto optimal systems called *Pareto optimal design analysis* by which one can predict the behavior of different designs in the Pareto front with respect to each other. It has also lead to a general *integrated design optimization methodology* by which one can optimize magnetic bearing systems with the actuator, controller, and amplifier as an integrated system by using the SOGA or the MOGA.

The future scope of work is presented in the following section.

10.2 Future Scopes

As the AMB technology is interdisciplinary involving mechanical, electrical, electronics, control subjects and its optimization involves artificial intelligence, with number of subsystems involved. The problem attempted in the present work raises number of applications and challenges in front. Some of the foreseen future work is summarized in the following subheadings.

10.2.1 Additional objectives

In the case of actuator, *the load capacity* has been considered as an objective in the present work. However, this load capacity can be subdivided into two components namely, the *static* and *dynamic load capacities*. Moreover, the *static* and *dynamic load capacities* are mutually conflicting (e.g., with the increase in the static load capacity causes an equivalent

decrease in the dynamic load capacity). There is a maximum load allowable for a particular design of AMB in the space available. The total load acting on the bearing is the sum of *static load* which is constant and *dynamic load* which is varying. Hence, an increase in the static load decreases the dynamic load allowable on either side of static load. Thus both the static and dynamic load capacities are mutually conflicting for a particular design of the AMB. Hence, studies can be done with these as multi-objective functions.

Specific load capacity (i.e., the ratio of load capacity to the overall weight of the bearing) can be considered as an objective of maximization type. Attempts were made to maximize the specific load capacity in a deterministic way (Imlach, 1999; Khoo et al., 2005). Hence, it can be implemented even in the optimization with MOGA.

Weight of the cooling system can also be taken as an objective. Studies have to be done how the overall weight of the system is affected after optimization including cooling system.

Tradeoffs of the power amplifier such as the *cost* and *power rating* of the amplifier can also be taken into consideration as objectives to improve the overall system performance. Moreover, the cost should be minimized while the power rating of the amplifier should be maximized; hence they are of conflicting nature.

10.2.2 A systematic integrated design optimization

There are two effects namely constraints and objectives in an optimization problem. In an integrated design methodology these two effects can be studied in a systematic way. An initial component such as actuator can be optimized with constraints and objectives. Any additional component such as controller to be considered in integration can be integrated in

constraints and/or in objectives. The study can be done as to how the controller constraints affect the optimum of an actuator. Similarly, studies on how objectives of the additional system affect the optimum of the actuator. Such studies would help in getting more detailed and in-depth understanding of the systems and their optimization.

10.2.3 Decision making

A system can be considered for a number of objectives. Each added objective in the system increases the ambiguity of decision making due to tradeoffs between different objectives of the system. Moreover, there are number of subsystems (e.g., actuator, controller, and power amplifier, etc.) involved in the present problem and each subsystem can be considered for a number of objectives. This results in further increase of complexity due to the tradeoffs between the objectives of intra-subsystem as well as inter-subsystem. Hence, as the number of objectives increases especially those are conflictive with each other, ambiguity in taking a final decision will increase. Hence, the area of *decision making* should be explored more elaborately in the selection of a proper design to the particular application. Prioritizing different objectives of the system can be one way of dealing this problem.

10.2.4 Novel algorithm

There are number of subsystems involved in the present problem. Each subsystem consists of a number of objectives, constraints and design variables. However, all the design variables do not influence all the objectives and constraints. Hence, different design

variables and corresponding objectives and constraints can be grouped as a subsystem. The overall system can be studied by a *novel algorithm* and a *convergence* criterion.

10.2.5 Applications of the methodology

Though the present methodology is *implemented* to magnetic thrust bearings, it can also be potentially implemented to other kinds of magnetic bearing systems such as magnetic radial bearings, bearing-less motors, etc. and even in *applications* of other fields.

As an application the combined radial and thrust bearings can be studied. However there are number of challenges involved and some of them are mentioned below.

The number of axes to be controlled increases to 5 in the case of combined radial and thrust bearings; whereas in the pure thrust case, it is a single axis control. Consequently, the number of actuators, controllers, and power amplifiers required increases.

In relation to optimization, the number of design variables and constraints increases corresponding to two radial bearings, controllers and power amplifiers for the four additional axes control.

In relation to control of the system, in high speed applications, the gyroscopic effects make the rotations about the axes perpendicular to axis coupled to each other. In low speed applications the rotor is considered to be rigid, the radial displacements at the two bearings in the same plane are coupled. Misalignment also causes similar coupling with the axes of the same plane (Schweitzer, 1994). This coupling requires complex control algorithms and winding schemes of the actuators.

In the case of radial bearings, the unbalance is another issue to be taken into consideration which can be nullified by generating compensating control currents (Mohamed and Vishniac, 1995).

In relation to measurements the positioning of the sensor at the center of the bearing is not possible. Hence, an offset is provided for the sensor position. This offset creates complexities in measurement and the estimation of rotor displacement at the bearing centre (Schweitzer, 1994).

The number of axes of control can be reduced by using passive magnetic bearing in the radial direction by using permanent magnetic bearings (Ueno and Okada, 2000). However, coupling between the axial and radial stiffness is another major issue to be taken into consideration if permanent magnets are used in radial bearings. In fact a radial magnetic bearing will give axial negative stiffness twice that of radial stiffness (Samantha and Hirani, 2008). The axial bearing should be designed to compensate this negative stiffness caused by radial bearings.

10.2.6 Experimentations

Experiments have to be conducted whether a given solution is feasible practically and/or nearer to the actual optimum. The objectives namely load capacity, power-loss, weight of the actuator, the dynamic performance parameters of the controller namely stiffness and damping, etc. and critical operating conditions of the system such as the saturated current density, saturated magnetic flux density, peak operating temperature and dynamic stability

of the bearing considered are of prime importance in testing the AMB systems and their compatibility. The major challenge lies is manufacturing a complete system for each trial. As different components are to be concurrently manufactured one has to check whether the different components give a compatible overall setup.

10.2.7 Concurrent production

Concurrent production of each individual component is another area of concern. In interdisciplinary systems such as AMBs the individual components should be produced one after the other. For example, the controller should be designed after knowing the practical stiffness properties of the actuator-rotor system. This consumes lot of waiting time for the controller to be designed till the actuator-rotor system is manufactured and determine its properties. On the other hand if the controller can be approximated from the numerical approximation of actuator properties, the production time would be reduced significantly which results in reduction of the production costs as well as increase in the production.

Bibliography

Bibliography

Aenis M. and Nordmann R. (1998). Active magnetic bearings for the identification of dynamic characteristics of fluid bearings. *Sixth International Symposium on Magnetic Bearings* .

Aenis M., Knopf E, and Nordmann R. (2002). Active magnetic bearings for the identification and fault diagnosis in turbomachinery. *Mechatronics , 12*, 1011–1021.

Albrecht P. R., Walowit J. A., and Pinkus O. (1982). Analytical and experimental investigation of magnetic support systems, Part II: Experimental investigation. *Transactions of ASME Journal of Lubrication Technology , 104* (3), pp. 429-437.

Allaire P. E., Mikula A., Banerjee B. B., Lewis D. W., and Imlach J. (1989). Design and Test of Magnetic Thrust Bearing. *Journal of Franklin Institute , 326* (6), 831–847.

Allaire, P. E., Hilton, E., Baloh, M., Maslen, E., Bearnson, G., Noh, D., Khanwilkar. P., and Olsen, D., (1998). Performance of a Continuous Flow Ventricular Assist Device: Magnetic Bearing Design, Construction, and Testing, Artificial Organs, 22(6): pp. 475-480.

Allaire, P. E., Humphris R. R., and Kelm, R. D. (1985). Magnetic bearings for vibration reduction and failure prevention. *Mechanical Failures Prevention Group 40th Meeting.* Gaithersburg, Maryland: National Bureau of Standards, 16-18, April.

Amiss, J. M., Jones, F. D., and Ryffel, H. H. (1988). In *Machinery's Handbook, 23 revised edition* (pp. 302-314). New York: Industrial Press Inclusives.

Anand, D. K., Kirk, J. A., and Bangham, M. L. (1986). Simulation, design and construction of a flywheel magnetic bearing. *Design Engineering Technological Conference.* Columbus, Ohio, October 5-8: ASME.

Anderson B. D. O., and Moore J. B. (1990). *Linear Optimal Control.* Englewood Cliffs, N. J.: Prentice Hall.

Antila M., Lantto E., and Arkkio A. (1998). Determination of Forces and Linearized Parameters of Radial Active Magnetic Bearings by Finite Element Technique. *IEEE Transactions on magnetics , 34* (3), 684 – 694.

Baigrie, B. S. (2006). Electricity and magnetism: a historical perspective. Westport: Greenwood Press.

Banerjee B. B. and Rao D. K. (1995). Design and Analysis of an Electromagnetic Thrust Bearing. *Third International Symposium on Magnetic Suspension Technology*, (pp. 337-348). Tallahassee, Florida, December 13-15.

Bassani R. (2007). A Stability Space of a Magnetomechanical Bearing. *Transactions of the ASME Journal of Dynamic Systems, Measurement, and Control , 129*, 178 - 181.

Beams J. W. (1937). High rotational speeds. *Journal of Applied Physics , 8*, 795-806.

Bear, C. C. et al., (1994). Development and Operation Experience with Advanced Magnetic Bearing System. Proceedings of Revolve '94, Calgary, Alberta, Canada, June 1994

Berry, M. V. (1996). The levitron: An adiabatic trap for spins. *Proceedings: Mathematical, Physical and Engineering Sciences , 452* (1948), 1207-1220.

Betschon F. and Knospe C. R., (2001). Reducing Magnetic Bearing Currents via Gain Scheduled Adaptive Control. IEEE/ASME Transactions on Mechatronics, 6(4), 437-443.

Betschon, F. (2000). *Design Principles of Integrated Magnetic Bearings.* Zurich: Swiss Federal Institute of Technology.

Bleuler, H. (1992). A survey of magnetic levitation and magnetic bearing types. *JSME International Journal , 35* (3), 335-342.

Bloodgood V.D. Jr., Groom N.J. and Britcher C.P. (2000). Further development of an optimal design approach applied to axial magnetic bearings. *NASA-2000-7ismb-vdb* .

Bloodgood, V.D. Jr. (1998). *Design Optimization of Magnetic Bearings and Magnetic Suspension Systems.* Masters Thesis, Old Dominion University, December.

Blumenstock, K. A. (2002). *Patent No. US 6,359,357 B1.* U. S.

Boldea I. and Nasar S. A. (1999). Linear Electric Actuators and Generators. *IEEE Transactions on Energy Conversion , 14* (3), 712-717.

Bornstein K. R. (1991). Dynamic Load Capabilities of Active Electromagnetic Bearings. *Transactions of ASME Journal of Tribology , 113*, 598 - 603.

Bray J. W. (2009). Superconductors in Applications; Some Practical Aspects. *IEEE Transactions on Applied Superconductivity , 19* (3), 2533-2539.

Brunet, M. (1988). Practical Applications of Active Magnetic Bearings to the Industrial World. *First International Symposium on Magnetic Bearings*, (pp. 225-244). Switzerland.

Bui L. T., Branke J., and Abbas H. A. (2005). Multiobjective Optimization for Dynamic Environments. *IEEE Paper No. 0-7803-9363-5/05* , pp. 2349-2356.

Buren T. V., Troster G., (2007): "Design and optimization of a linear vibration-driven electromagnetic micro-power generator", Sensors and Actuators, 135(2), pp. 765–775

Burrows C. R. (1987). Discussion: "Effect of Control Algorithms on Magnetic Journal Bearing Properties" (Humphris, R. R., Kelm, R. D., Lewis, D. W., and Allaire, P. E., 1986, ASME J. Eng. Gas Turbines Power, 108, pp. 624–632). *109*, 353.

Cade I. S., Sahinkaya M. N., Burrows C. R., and Keogh P. S. (2009). On the use of actively controlled auxiliary bearings in magnetic bearing systems. *Transactions of ASME, Journal of Engineering for Gas Turbines and Power , 131* (2), 022507.

Canders W.-R., and Lee W.-L. (1997). Integrated radial and axial low cost magnetic bearing. *Proceedings of MAG '97*, (pp. 303-312). Virginia, USA.

Carlson-Skalak S., Maslen E., and Teng Y. (1999). Magnetic Bearing Actuator Design using Genetic Algorithms. *Journal of Engineering Design , 10* (2), pp. 143-164(22).

Carlyle W. M., Kim B., Fowler J. W., and Gel E. S. (2001). Comparison of Multiple Objective Genetic Algorithms for Parallel Machine Scheduling Problems. *In Proceedings of the First international Conference on Evolutionary Multi-Criterion Optimization, 7-9, March.*

Cavarec P.E., Ahmed H. B., Multon B., and Prévond L. (2001). Advantage of Increasing the Number of Airgap Surfaces in Synchronous Linear Actuators. *Proceedings of International Conference Electromotion'01*, (pp. 251-256). Bologna, 19-20 June.

Chakraborthy I., Vinay K., Nair S.B., and Tiwari R. (2003). Rolling element bearing design through genetic algorithms. *Engineering Optimization , 35* (6), 649 –659.

Chang H. and Chung S. C. (2002). Integrated Design of Radial Active Magnetic Bearing Systems using Genetic Algorithms. *Mechatronics , 12* (1), 19–36.

Chen C. H., and Chang S. H. (2006). Genetic Algorithms Based Optimization Design of a PID Controller for an Active Magnetic Bearing. *IJCSNS International Journal of Computer Science and Network Security , 6* (12), 95-99.

Chen H. –C. (2008). Optimal Fuzzy Pid Controller Design Of An Active Magnetic Bearing System Based On Adaptive Genetic Algorithms . *Proceedings of the Seventh International Conference on Machine Learning and Cybernetics*, (pp. 2054 - 2060). Kunming, 12-15 July.

Chen, S. L., Hsu, C. T. (2002). Optimal Design of A Three Pole Active Magnetic Bearing. *IEEE Transactions on Magnetics , 38* (5), 3458–3466.

Chiba A., Fukao T., Ichikawa O., Oshima M., Takemoto M., and Dorrell D. G. (2005). *Magnetic Bearings & Bearingless Drives.* Newnes: Elsevier.

Chiba A., Fukao T., Ichikawa O., Oshima, M., Takemoto M. and Dorrell D.G. (2005). *Magnetic Bearings & Bearingless Drives.* Newnes, Elsevier.

Chiba A., Hanazaioa M.,Fukao T., and Rahman M. A. (1993). Effects of Magnetic Saturation on Radial Force of Bearingless Synchronous Reluctance Machines. *IEEE conference Record of the 1993 Industry Applications Society Annual Meeting*, *1*, pp. 233-239. Toronto, Ont., Canada.

Choi D.H., and Yoon K.C. (2001). A design method of an automotive wheel bearing unit with discrete design variables using genetic algorithms. *Transactions of ASME Journal of Tribology , 123* (1), pp. 181–187.

Closs M, Buhler P, Schweitzer G., (1998). Miniature active magnetic bearing for very high rotational speeds. *Proceedings of 6th international symposium on magnetic bearings*, Virginia, USA, 62–66

Coello C. A. C. (1999). A comprehensive survey of evolutionary-based multiobjective optimization techniques. *Knowledge Information Systems , 1* (3), 269-308.

Coello C. A. C. (2000). An Updated Survey of GA-Based Multiobjective Optimization Techniques. *ACM Computing Surveys , 32* (2), 109-143.

Cohon, J. L. (1985). *Multi-criteria programming: Brief review and aaplication.* (J. S. Gero, Ed.) New York: Academic press.

Davey K., Filatov A., and Thompson R. (2005). Design and Analysis of Passive Homopolar Null Flux Bearings. *IEEE Transactions on magnetics , 41* (3), 1169-1175.

Davidon W. C. (1959). *Variable metric methods for minimization.* Argonne National Labs Report, ANL-5990.

Deb K. (2001). *Multi-Objective Optimization using Evolutionary Algorithms.* Chichester: Wiley-Interscience Series in Systems and Optimization, John Wiley & Sons.

Deb K. and Agarwal R. B. (1995). Simulated Binary Cross-Over for Continuous Search Space. *Complex Systems*, *9*, pp. 115–148.

Deb K., Pratap A., Agarwal S., and Meyarivan T. (2002). A fast and elitist multiobjective genetic Algorithm: NSGA-II. *IEEE Transactions on Evolutionary Computation , 6*, 182–197.

Deb, K. (1995). *Optimization for engineering design: algorithms and examples.* New Delhi: Prentice Hall of India Private Ltd.

DeWeese R. T., Palazzolo A. B., Chinta M., and Kascak A. (1998). Magnetic Thrust Bearing Concepts: Tests and Analyses. *Journal of Intelligent Material Systems and Structures , 9* (2), 81-86.

Ding G., Zhou Z., Hu Y., and He D. (2006). FEA-based Optimal Design of the Radial Magnetic Bearings in Magnetic Suspended Hard Disk Drive. *Proceedings of the 2nd IEEE/ASME International Conference on Mechatronic and Embedded Systems and Applications*, (pp. 1-6).

Dussaux M. (1990). The industrial aplications of the active magnetic bearings technology. *proceedings of 2nd International Symposium on Magnetic Bearings* (pp. 33-38). Tokyo, Japan: Tokyo University.

Dyck D.N. and Lowther D.A. (1996). Automated Design of Magnetic Devices by Optimizing Material Distribution. *IEEE Transaction on Magnetics , 32* (3), 1188–1193.

Earnshaw S. (1842). On the nature of the molecular forces which regulate the constitution of the lumiferous ether. *Transactions of Cambridge Phillosophical Society , 7*, pp. 97-112.

Ehmann, C., Sielaff, T., Nordmann, R. (2004). Comparison of Active Magnetic Bearings with and without Permanent Magnet Bias. *The Ninth Int. Symposium on Magnetic Bearings.* Lexington, Kentucky, August.

Eisenhaure D. B., Downer J. R., Bliamptis T. E., and Hendrie S. D. (1984). A combined attitude, reference and energy storage system for satellite applications. *AIAA Aerospace Sciences Meeting.* Reno, Nevada 9912, Jan.

Fan Y-H. and Lee A-C. (1995). Decentralized Control of a rotor system supported by magnetic bearings. *International Journal of Machine Tools Manufacturing , 35* (3), 445-458.

Fedigan, S. J., (1993). *A Real-Time Operating System for a Magnetic Bearing Digital Controller*. Master of Science Thesis, University of Virginia, June

Filatov A.V. and Maslen E.H. (2001). Passive magnetic bearing for flywheel energy storage systems. *IEEE Transactions on magnetics , 37* (6), 3913-3924.

Fonseca C. M., and Fleming P. J. (1995). An overview of evolutionaxy algorithms in multi-objective optimization. *Evolutionary Computation , 3* (1), pp. 1-16.

Foster E. G., Kulle V. and Peterson R. A. (1986). The application of active magnetic bearings to a natural gas pipeline compressor. *ASME Paper 86-GT-61, Presented at International Gas Turbine Conference.* Dusseldorf, 8-12 June.

Fowler M. (1997). *Historical Beginnings of Theories of Electricity and Magnetism.* Retrieved 16th, Nov, 2009, from http://galileoandeinstein.physics.virginia.edu/more_stuff/E&M_Hist.html

Fukata, S., Yutani, K., and Kouya, Y., 1998, "Characteristics of magnetic bearings biased with permanent magnets in the stator", JSME Int J Ser C, 41(2), 206–213

Gao Y., Shi L., and Yao P. (2000). Study on Multi-Objective Genetic Algorithm. *Proceedings of 3rd World Congress On intelligent Control and Automation*, (pp. 646-650).

Ghanmi S., Guedri M., Bouazizi, M. -L., and Bouhaddi N. (2007). Use of Metamodels in the Multi-Objective Optimization of Mechanical Structures with Uncertainties. *International Journal for Computational Methods in Engineering Science and Mechanics , 8* (5), pp. 283 - 302.

Glauser M., Jiang W., Li G., Lin Z., Allaire P. E., and Olson D., (2006) Optimization of an Axial Flow Heart Pump With Active and Passive Magnetic Bearings Artificial Organs 30 (5) , pp. 400–403

Goldberg D. E. (1989). *Genetic Algorithms in Search, Optimization, and Machine Learning*. Reading, Massachussetts: Addison-Wesley.

Gray, S., Baxter, B., and Jones, G. (1990). Magnetic bearings can increase availability, reduce O&M costs. *Power engineering , 1*, 26-29.

Griffiths D. J., (2005). *Introduction to Electrodynamics*. Prentice-Hall of India Pvt. Ltd, New Delhi

Groom, N. J., Bloodgood, V. D. Jr. (2000). A Comparison of Analytical and Experimental Data for A Magnetic Actuator. *NASA/TM-2000-210328, September* .

Gruver W. A. and Sachs E. W. (1980). *Algorithmic Methods in Optimal Control.* London: Pitman.

Gupta S., Tiwari R., Nair S. B. (2007). Multi-objective design optimisation of rolling bearings using genetic algorithms. *Mechanism and Machine Theory , 42* (10), 1418-1443.

Gurnani, A., Ferguson, S., Donndelinger, J., Lewis, K. (2005). Feasibility Assessment in Preliminary Design Using Pareto Sets. *ASME Proceedings of IDETC/CIE September, 24 - 28.* Long Beach, California, USA.

Haberman H., and Brunet M. (1984). The active magnetic bearing enables optimum damping of flexible rotor. *ASME Paper No. 84-GT- 117*, ASME Gas Turbine Conference. Amsterdam, June.

Haberman H., and Liard, G. (1980). An active magnetic bearing system. *Tribology International* , 85-89, April.

Hale A. L., Dahl, W. E. (1985). Optimal simultaneous structural and control design of maneuvering flexible spacecraft. *Journal of Guidance, Control, and Dynamics , 8* (1), 86 - 93.

Han W-S., Lee C- W., and Okada Y. (2002). Design and Control of a Disk-Type Integrated Motor-Bearing System. *IEEE/ASME Transactions on Mechatronics , 7* (1), 15-22.

Hermann, P. K., (1973). A radial active magnetic bearing. *London Patent No. 1 4478 868*, 20 November

Higuchi T., Horikoshi A. and Komori T. (1990). Development of an Actuator for Super Clean Rooms and Ultra High Vacua. *Proceedings of 2nd International Symposium on Magnetic Bearings*, (pp. 115-122). Tokyo, Japan, 12-14 July.

Higuchi, T., (1984). Magnetically floating actuator having angular positioning function. *United States Patent No. 4 683 391*, March 12.

Hijikata K., Kobayashi S., Takemoto M., Tanaka Y., Chiba A., and Fukao T. (2008). Basic Characteristics of an Active Thrust Magnetic Bearing With a Cylindrical Rotor Core. *IEEE Transactions on Magnetics , 44* (11), 4167 - 4170.

Hisao I., Yusuke N., and Tsutomu D. (2006). Comparison between Single-Objective and Multi-Objective Genetic Algorithms: Performance Comparison and Performance Measures. *2006 IEEE Congress on Evolutionary Computation.* Sheraton Vancouver Wall Centre Hotel, Vancouver, BC, Canada, July 16-21.

Holmes, F. T., and Beams, J. W., (1937). Frictional Torque of an Axial Magnetic Suspension. *Nature*, 140, 30-31

Hu T., Lin Z., Jiang W., Allaire P. E. (2005). Constrained Control Design for Magnetic Bearing Systems. *Journal of Dynamic Systems, Measurement, and Control , 127* (4), 601 – 616.

Hu, X., Huang, Z., and Wang, Z. (2003). Hybridization of the Multi-Objective Evolutionary Algorithms and the Gradient-based Algorithms. *IEEE Paper No. 0-7803-7804-0 /03* , 870-877.

Humphris, R. R., Kelm, R. D., Lewis, D. W., and Allaire, P. E. (1986). Effect of Control Algorithms on Magnetic Journal Bearing Properties. *ASME Journal of Engineering Gas Turbines and Power , 108*, 624–632.

Hustak, J. F., Kirk, R. G., and Schoeneck, K. A. (1986). Analysis and test results of turbocompressors using active magnetic bearings. *American Society of Lubrication Engineers 41st Annual Meeting, Preprint No. 86-AM-lA-1.* Toronto, 12-15, May.

Ide N., Nonami K., Ueyanma H. (1996). Robust Control of Magnetic Bearing Systems Using mu-Synthesis with Discriptor Form. *Proceedings of Third International Conference on Motion and Vibration Control*, *1*, pp. 152-157. Koyo Seiko Co., September, 2.

Imlach, J. (1999). *Patent No. 5962940.* US.

Imoberdorf P., Zwyssig C., Round S. D. and Kolar J.W. (2007). Combined Radial-Axial Magnetic Bearing for a 1 kW, 500,000 rpm Permanent Magnet Machine. *Applied Power Electronics Conference, APEC 2007 - Twenty Second Annual IEEE, Feb.25 - March 1*, (pp. 1434-1440).

Jahanmir S., Heshmat H., Ren Z., Hunsberger A. Z., Heshmat C. A., Walton J. F. II, Tomaszewski M. J., (2006). Design Of A Small Centrifugal Blood Pump With Hybrid Magnetic Bearings. *ASAIO Journal*, 52(2), pp. 54A.

Jang S. -M., Lee U. -H., Choi J. -Y., and Hong J. -P. (2008). Design and analysis of thrust active magnetic bearing. *Journal of Applied Physics , 103* (7), 07F122.

Johnson D., Brown G. V., and Inman D. J. (1998). Adaptive Variable Bias Magnetic Bearing Control. *Proceedings of the American Control Conference, June*, (pp. 2217-2223). Philadelphia, Pennsylvania.

Jung K. S. and Lee S. H. (2009). Contact-less revolving stage using transverse flux induction principle. *Precision Engineering , 33*, 107–115.

Karaboga D. (2005). *An Idea Based On Honey Bee Swarm For Numerical Optimization.* Technical Report-TR06, Erciyes University, Engineering Faculty, Computer Engineering Department.

Kasarda M. E. F. (2000). An overview of active magnetic bearing technology and application. *The Shock and Vibration Digest , 32* (2), 91-99.

Kasarda M.E.F., Allaire P.E., Norris P.M., Mastrangelo C., Maslen E. H., (1999). Experimentally determined rotor power losses in homopolar and heteropolar magnetic bearings. *Journal of Engineering for Gas Turbines and Power*, *121*(4), pp. 697-702

Keith F. J., (1988). *Digital Control System Design for Active Magnetic Bearings*. Master of Science Thesis, University of Virginia, May 1988

Kemper H., (1937). Overhead suspension railway with wheelless vehicles employing magnetic suspension from iron rails. German Patent Nos. 643316 and 644302

Kennedy J. and Eberhart R. C. (1995). Particle Swarm Optimization. *IEEE Proceedings of the International Conference on Neural Networks IV* (pp. 1942-1948). Perth, Australia: IEEE Service Center, Piscataway, NJ.

Kenny A. and Palazzolo A. B. (2002). Comparison of the Dynamic Response of Radial and Tangential Magnetic Flux Thrust Bearings. *IEEE/ASME Transactions on Mechatronics , 7* (1), 61-66.

Kenny A., Palazzolo A.B., and Provenza A. . (2004). An integrated magnetic circuit model and finite element model approach to magnetic bearing design. *37th Intersociety Energy Conversion Engineering Conference, 2002. IECEC '02. 29-31 July* (pp. 181- 184). IEEE.

Khoo W.K.S., Garvey S.D., and Kalita K. (2007). The specific load capacity of radial-flux radial magnetic bearings. *IEEE Transactions on Magnetics , 43* (7), 3293-3300.

Khoo W.K.S., Kalita K., and Garvey S.D. (2005). High Specific Load Capacity Magnetic Bearings. *International Conference on Power Electronics and Drives Systems, 2005. 2*, pp. 1009- 1014. IEEE PEDS 2005.

Kim C, Lee J, and Park J-K. (2002). Optimal Design for A Heteropolar Magnetic Bearing Considering Nonlinearities. *International Journal of the Korean Society of Precision Engineering , 3* (1), 13-19.

Kim S. J., Song M. G., Park N-C., Yoo J., Park Y-P., and Park K-S. (2009). Optimal design of moving-magnet type actuators for optical disk drives considering effect of coil electromagnet. *IEEE Transactions on Magnetics , 45* (5), 2228 – 2231.

Kim H. Y. and Lee C. W. (2000). Analysis of eddy-current loss for design of small active magnetic bearings with solid core and rotor. *IEEE Transactions on Magnetics , 40* (5), 3293–3301.

Kim, H. Y., and Lee, C. W. (2006). Design and control of active magnetic bearing system with Lorentz force-type axial actuator. *Mechatronics , 16*, 13-20.

Kim S. J., Abe K., Kanebako H., Okada Y., and Lee C. W., (2002). A Lorentz force type self-bearing motor with new 4-pole winding configuration. *Proceedings of 8th International Symposium on Magnetic Bearings*, Mito, Japan, 35–40.

Kim S. J., Shimonish T., Kanebako H., and Okada Y., (2000). Design of hybrid type short-span self-bearing motor, *Proceedings of 7th international symposium on magnetic bearings*. Zurich: ETH, 359–364

Kimura T. and Negishi T. (1990). An Application of Magnetic Bearings to Titanium Powder Production. *2nd International Symposium on Magnetic Bearings*, (pp. 101-107). Tokyo, Japan, July 12-14.

Klesen, C., Nordmann, R., Schönhoff, U. (1999). Design of a Minimum Current Magnetic Bearing. *5th International Symposium On Magnetic Suspension Technology.* Santa Barbara, CA, December.

Knospe C. R. (2007). Active magnetic bearings for machining applications. *Control Engineering Practice , 15*, 307–313.

Knospe C. R. and Tamer S. M. (1997). Experiments in robust control of rotor unbalance response using magnetic bearings. *Mechatronics , 7* (3), 217-229.

Knowles J.D. and Corne D.W. (2004). Metaheuristics for Bounded Pareto Archiving: Theory and Practice. In M. S. X. Gandibleux, *In Multiobjective Optimization, Lecture Notes in Economics and Mathematical Systems* (Vol. 535). Springer.

Komori, M., Yamane, T., 2000, "Magnetic levitation system with a millimeter sized cylindrical rotor", Mechatronics, 10, 595–607

Kreyszig E. (2006). Advanced engineering mathematics. John Wiley.

Kuhn H. W. and Tucker A. W. (1951). Nonlinear programming. in: J. Neyman (Ed.), Proceedings of Second Berkeley Symposium on Mathematical Statistics and Probability. University of California Press.

Kwakernaak H. (1993). Robust control and H∞- optimization. *Automatica , 29*, 255 – 273.

L. Lin, L, H. Y. Jan, and N. C. Shieh. (2003). GA-based multiobjective PID control for a linear brushless dc motor. *IEEE Transactions on Mechatronics , 8* (1), 56-65.

Larocca P., Fermental D. and Cusson E. . (1990). Performance Comparison Between Centralized And Decentralized Control Of The Jeffcott Rotor. *Proceedings of the 2nd International Symposium on Magnetic Bearings*, (pp. 295-300). Tokyo, Japan, 12-14 July.

Lee A. C., Hsiao F. Z., and Ko D. (1994). Analysis and testing of a magnetic bearing with permanent magnets for bias. *JSME International Journal Series C , 37* (4), 774.

Lee S- Q., and Gweon D- G. (2000). A new 3-DOF Z-tilts micropositioning system using electromagnetic actuators and air bearings. *Precision Engineering , 24*, 24–31.

Lee W. -L., Canders W. -R., and Schumacher W. (2000). New Approaches for Axial Magnetic Bearings. *Seventh International Symposium on Magnetic Bearings*, (pp. 443-448). ETH Zurich, August 23-25.

Lee, A., and Hsiao, F. Z. (1994). Optimum design of the magnetic bearing-controlled rotor systems. *Proceedings of the Fourth International Symposium on Magnetic Bearings*, (pp. 139-144).

Lee, C. W., and Jeong, H. S., (1996). Dynamic modeling and optimal control of cone shaped active magnetic bearing system. *Control Engineering Practice*, *4*, 1393–1403

Levine J., Lottin J., and Ponsart J. C. (1996). A Nonlinear approach to the control of magnetic bearings. *IEEE Transactions on control system technology , 4* (5), 524-544.

Lewis, D. W., and Allaire, P. E. (1987). Control of oscillating transmitted forces in axial thrust bearings with a secondary magnetic bearing. *Tribology Transactions , 30* (1), 1-10.

Lim C. K., He S., Chen I-, Yeo S. H. (1999). A Piezo-on-Slider Type Linear Ultrasonic Motor for theApplication of Positioning Stages. *Proceedingsof the 1999IEWASME tntemationalConferenceon AdvancedIntelligentMechatmnics*, (pp. 103-108). Attanta,USA, September19-23.

Liu J., Choi H., Palazzolo A., Tucker R., Kenny A., Kang K-D., Ghandi V., and Provenza A. (2008). High Temperature Hybrid Radial Magnetic Bearing Systems Capable of Operating up to 538°C (1000°F). *Proceedings of 20th International Workshop on Rare Earth Permanent Magnets and Their Applications.* Crete, Greece, Sept. 8-10.

Locke D. H., Swanson E. S., Walton J. F., Willis J. P., and Heshmat H., (2003). Testing of a centrifugal blood pump with a high efficiency hybrid magnetic bearing. *ASAIO journal*, *49*(6), pp. 737-743.

Lösch F., and Bühler P. (2000). Identification and Automated Controller Design for Rigid Rotor AMB Systems. *Seventh International Symp. on Magnetic Bearings* , 57-63.

Malone, C. L. (1993). Power to Weight Optimization for Magnetic Bearings. *Mag '93: Magnetic Bearings, Magnetic Drives and Dry Gas Seals Conference & Exhibition.* Alexandria, Virginia, July.

Manos S., and Poladian L. (2005). Multi-objective and constrained design of fibre Bragg gratings using Evolutionary Algorithms. *Optics Express , 13* (19), pp. 7350–7364.

Martorell, S., Sánchez, A., Carlos, S., and Serradell, V. (2004). Alternatives and challenges in optimizing industrial safety using genetic algorithms. *Reliability Engineering & System Safety , 86* (1), 25-38.

Maslen E. (2006). Self–sensing for active magnetic bearings:overview and status. *Proceedings of 10th International Symposium on Magnetic Bearings (ISMB 10).* Martigny (Switzerland), August: Digest of Technical Papers.

Maslen E. H. (2000). *Magnetic Bearings Lecture notes*. (University of Virginia) Retrieved from http://people.virginia.edu/~ehm7s/courses/magnetic_bearings/mag_brgs.pdf

Maslen E.H., and Meeker D. C. (1995). Fault tolerance of magnetic bearings by generalized bias current linearization. *IEEE Transactions on Magnetics , 31*, 2304–2314.

Maslen, E. H., Allaire, P. E., Noh, M. D., and Sortore, C. K. (1996). Magnetic bearing design for reduced power consumption. *ASME Journal of Tribology , 18*, 839–846.

Maslen, E. H., Hermann, P., Scott, M. A., and Humphris, R. R. (1989). Practical Limits to the Performance of Magnetic Bearings: Peak Force, Slew Rate, and Displacement Sensitivity. *ASME Journal of Tribology , 111* (2), 331-336.

Matsumura F., Fujita M. and Oida C. (1987). Theory and Experiment of Magnetic bearing Combining Radial control and Thrust control. *IEEE Transactions on Magnetics , MAG-23* (5), 2581-2583.

Meeker D. C., Maslen E. H., and Noh M. D. (1996). An Augmented Circuit Model for Magnetic Bearings Including Eddy Currents, Fringing, and Leakage. *IEEE Transactions on Magnetics , 32* (4), pp. 3219-3227.

Meinke P., and Flachenecker G., (1974), Electromagnetic drive assembly for rotary bodies using a magnetically mounted rotor, United States Patent No. 3 988 658, July 29

Miki M., Tanaka Y., Yamaguchi Y., Ishizawa T., and Yamamura A. (1990). Single Axis Active Magnetic Bearing System with Mechanical Dampers for High Speed Rotor. *Proceedings of 2nd International Symposium on Magnetic Bearings*, (pp. 183-187). Tokyo, Japan, 12-14 July.

Mohamed, A. M., and Emad, F. P. (1992). Conical magnetic bearings with radial and thrust control. *IEEE Trans Automatactic Control , 37* (12), 1859–1868.

Mohamed, A. M., and Vishniac I. B-, (1995). Imbalance Compensation and Automation Balancing in Magnetic Bearing Systems Using the Q-Parameterization Theory. *IEEE Trans Control Systems Technology , 3* (2), 202-211.

Molenaar L., Zaaijer E. and Beek F. V. (1998). A Novel Long Stroke Planar Magnetic Bearing Actuator. *Proceedings of 4th International Conference on motion and Vibration'98, MoViC'98.* ETH-Zurich, Switzerland.

Moscato P. (1999). Memetic Algorithms : A Short Introduction. In D. M. Carne D. (Ed.), *New Ideas in Optimization.* London: McGraw-Hill.

Moser R., Sandtner J., and Bleuler H. (2006). Optimization of Repulsive Passive Magnetic Bearings. *IEEE Transactions on Magnetics , 42* (8), 2038-2042.

Mukhopadhyay, S. C., Ohji, T., Iwahara, M., and Yamada, S. (2000). Modeling and control of a new horizontal shaft hybrid type magnetic bearing. *IEEE Transactions on Industrial Electronics , 47*, 100-108, February 1.

Na U. J. (2004). Fault tolerance of homopolar magnetic bearings. *Journal of Sound and Vibration , 272*, 495–511.

Na U. J. and Palazzolo A. B. (2000). Fault Tolerance of Magnetic Bearings with Material Path Reluctances and Fringing Factors. *IEEE Transactions on Magnetics , 36* (6), 3939-3946.

Na U. J. and Palazzolo A. B. (2000). Optimized realization of fault-tolerant heteropolar magnetic bearings. *ASME Journal of vibration and acoustics , 122* (3), 209-221.

Noh M. D., Antaki J. F., Ricci M., Gardiner J., Paden D., Wu J., Prem E., Borovetz H., Paden B. E. (2008). Magnetic Design for the PediaFlow Ventricular Assist Device. *Artificial Organs , 32* (2), 127–135.

Ohji T., Ichiyamaa S., Ameia K., Sakuia M., and Yamada S. (2004). A new conveyor system based on a passive magnetic levitation unit having repulsive-type magnetic bearings. *Journal of Magnetism and Magnetic Materials* , 272–276.

Okada Y., Konish H., Kanebako H. and Lee C. W. (2000.), "Lorentz force type self-bearing motor", Proceedings of 7th international symposium on magnetic bearings, Zurich: ETH, 353–358

Onuma H., Murakami m., and Masuzawa T., (2005). Novel Maglev Pump With a Combined Magnetic Bearing. *ASAIO Journal*. 51(1), pp. 50-55

Onwubolu G. C., and Babu B.V. (2004). *New Optimization Techniques in Engineering* (Vol. 141). Berlin Heidelberg, New York: Springer-Verlag.

Ota M., Andoh S., and Inoue H. (1990). Maglev Semiconductor Wafer Transporter for Ultra-High-Vacuum Environment. *2nd International Symposium on Magnetic Bearings*, (pp. 109-114). Tokyo, Japan, 12-14 July.

Paden B., Groom N., and Antaki J. F. (2003). Design Formulas for Permanent-Magnet Bearings. *Transactions of the ASME Journal of Mechanical Design , 125*, 734 - 738.

Park J. H., and Asada H. (1994). Concurrent design optimization of mechanical structure and control for high speed robots. *ASME Transactions on Journal of Dynamic Systems, Measurement and Control , 116* (3), 344-356.

Park, Y.-J., and Chung, S.-C. (1998). A study on the optimum design of radial magnetic bearings. *KSME (A) , 22* (7), 1166-1176.

Park, Y.-J., and Chung, S.-C. (1999). A study on the integrated design of axial magnetic bearing systems. *KSME (A) , 22* (7), 1166-1176.

Polajzer, B. (2003). Design and Analysis of an Active Magnetic Bearing Experimental System. Ph. D. Thesis, University of Maribor, Slovenia.

Post R. F., and Ryutov D. D. (1998). Ambient-Temperature Passive Magnetic Bearings: Theory and Design Equations. *In Sixth International symposium on magnetic bearings*, (pp. 109-122). Cambridge, Massachusetts.

Rachmawati, L. and Srinivasan, D. (2006). A multi-objective evolutionary algorithm with weighted-sum niching for convergence on knee regions. *Proceedings of the 8th Annual Conference on Genetic and Evolutionary Computation*, (pp. 749-750). Seattle, Washington, USA, July 08 - 12.

Raghuwanshi M. M. and Kakde O. G., (2004), "Survey on multiobjective evolutionary and real coded genetic algorithms," In Proc.of the 8th Asia Pacific Symposium on Intelligent and Evolutionary Systems, pp. 150-161,

Rao S. S. (1996). *Engineering Optimization: Theory and Practice.* New York: John Wiley & Sons, Inc.

Rao, B. R., and Tiwari, R. (2007). Optimum Design of Rolling Element Bearings using Genetic Algorithms. *Mechanism and Machine Theory , 42* (2), 233-250.

Ravichandran T., Wang D., and Heppler G. (2006). Simultaneous plant-controller design optimization of a two-link planar manipulator. *Mechatronics , 16*, 233–242.

Ravindran A., Ragsdell K. M. and Reklaitis G. V. . (2006). *Engineering Optimization: Methods and Applications.* New Delhi: Wiley India Pvt. Ltd. .

Ren S., and Stephens L. S. (2005). Closed-Loop Performance of a Six Degree-of-Freedom Precision Magnetic Actuator. *IEEE/ASME Transactions on Mechatronics , 10* (6), 666-674.

Ren Z., Jahanmir S., Heshmat H., and Walton J., (2007): Hybrid Magnetic Bearings for a Centrifugal Blood Pump, Proceedings of ASME/STLE International Joint Tribology Conference, IJTC2007, San Diego, California USA, 22-24, October.

Robertson W. (2003). *Design of a non-contact magnetic spring for vibration isolation.* Audelaide, Australia: The University of Audelaide.

Romero L. A. (2003). Passive Levitation in Alternating Magnetic Fields. *SIAM Journal on Applied Mathematics , 63* (6), 2155-2175.

Romero L. A. (2003). Spin Stabilized Magnetic Levitation of Horizontal Rotors. *SIAM Journal on Applied Mathematics , 63* (6), 2176-2194.

Saberi A., Sannuti P., and Chen B. M. (1995). *H2 Optimal Control.* Englewood Cliffs, N. J., : Prentice Hall,.

Salazar A. O., Chiba A., Fukao T. (2000). A review of developments in bearingless motors. *Seventh International Symposiun on Magnetic Bearings*, (pp. 335-340). ETH Zurich, August 23-25.

Samanta P. and Hirani H. (2008). Magnetic Bearing Configurations: Theoretical and Experimental Studies. *IEEE Transactions on Magnetics , 44* (2), 292-300.

Sarkar D., and Modak J. M. (2005). Pareto-optimal solutions for multi-objective optimization of fed-batch bioreactors using nondominated sorting genetic algorithm. *Chemical Engineering Science 60* , 481 – 492.

Schaffer J. D. (1985). Multiple objective optimization with vector evaluated genetic algorithms. *In Proceedings of the First International Conference on Genetic Algorithms and Their Applications* (pp. 93-100). Hillsdale, New Jersey: Lawrence Erlbaum Associates Inc., .

Schmidt E., (2008), Parameter Evaluation of a Hybrid Magnetic Bearing by using 3D Finite Element Analyses Australasian Universities Power Engineering Conference (AUPEC'08), Paper P-105, 1-6

Schneeberger T. and Kolar J. w. (2006). Novel Integrated Bearingless Hollow-Shaft Drive. *IEEE Industry Applications Conference*, (pp. 70- 75).

Schroder P., Chipperfield A. J., Fleming P. J., and Grum N. (1997). Multi-Objective Optimization of Distributed Active Magnetic Bearing Controllers. *Genetic Algorithms in Engineering Systems: Innovations and Applications., Sept., 1997* (pp. 13-18). IEE.

Schroder P., Green B., Grum N., and Fleming P. J. (1998). On-line Genetic Auto-Tuning of Mixed H2/H∞, Optimal Magnetic Bearing Controllers. *UKACC International Conference on CONTROL '98, 1-4 September 1998.*

Schweitzer G. (2002). Active Magnetic Bearings – Chances and Limitations. *Proc. 6th International IFToMM Conf. on Rotor Dynamics.* Sydney, Sept. 30-Oct. 3.

Schweitzer G. (2005). Safety and Reliability Aspects for Active Magnetic Bearing Applications - A Survey. *Proceedings of the Institution of Mechanical Engineers, Part I: Journal of Systems and Control Engineering , 219* (6), 383-392.

Schweitzer G. and Nordmann R. (2009). Touch-down Bearings. In a. S. Maslen E. H., *Magnetic Bearings Theory, Design, and Application to Rotating Machinery* (pp. 389-406). Berlin Heidelberg: Springer.

Schweitzer G., and Maslen E. H. (2009). Magnetic Bearings: Theory, design and application to rotating machinery. New York: Springer.

Schweitzer, G., Bleuler, H., and Traxler, A. (1994). Active Magnetic Bearings: Basics, Properties and Applications of Active Magnetic Bearings. Zürich

Shiau T. N., Kuo C. P., and Hwang J. R. (1997). Multi-objective Optimization of a Flexible Rotor in Magnetic Bearings With Critical Speeds and Control Current Constraints. *Journal of Engineering Gas Turbines and Power , 119*, 186-195.

Shimada A.,Horiuchi Y., and Shamoto K. (2000). A Study on Magnetic Bearings for Machine Tool's High Speed Spindle. *Seventh International Symposium on Magnetic Bearings*, (pp. 183-188). ETH Zurich, August 23-25.

Shimizu H., and Taniguchi O. (1968). Research on the control systems of magnetic bearing. *Bull JSME , 11* (46), 699-705.

Shimizu H., and Taniguchi O. (1971). Research on the self-exciting vibration of thrust-type magnetic bearing (cylindrical mode). *Bull JSME , 14* (72), 541-549.

Smith, R. D., and Weldon, W. F. (1995). Nonlinear control of a rigid rotor magnetic bearing system: modeling and simulation with full state feedback. *IEEE Transactions on Magnetics , 3* (2), 973-980.

Song W.,Tseng K. J., and Chan W. K. (2001). Design of a bearingless BLDC motor. *Proceedings of the Australasian Universities Power Engineering Conference 2001, AUPEC'01*, (pp. 619-624). Perth, Australia, September 23-26.

Sortore, C. K., Allaire, P. E., Maslen, E. H., Humphris, R. R., and Studer, P. A., (1990), "Permanent magnet biased magnetic bearings-design, construction and testing", Proceedings of 2nd international symposium on magnetic bearings, Tokyo Japan, pp. 112–114

Srinivas N. and Deb K. (1993). *Multiobjective optimization using nondominated sorting in genetic algorithms.* Technical Report, Indian Institute of Technology Delhi, Delhi, India.

Srinivas N. and Deb K. (1994). Multi-objective optimization using non-dominated sorting in genetic algorithms. *Evolutionary Computation , 2* (3), 221-248.

Srinivasan S., Maslen E. H., and Barrett L. E. (1997). Optimization of bearing locations for rotor systems with magnetic bearings. *Journal of Engineering for Gas Turbines and Power , 119* (2), 464-468.

Stoll R. L. (1974). *The Analysis of Eddy Currents.* London: Oxford University Press.

Storn R. and Price K. (1995). Differential Evolution - A Simple and Efficient Adaptive Scheme for Global Optimization over Continuous Spaces. Technical Report, International Computer Science Institute, March.

Studer, P. A., (1977). A Practical magnetic bearing. *IEEE Transactions on Magnetics*, *13*(5), pp. 1155-1157.

Stumberger G., Dolinar D., Palmer U., and Hameyer K. (2000). Optimization of radial active magnetic bearings using the finite element technique and the differential evolution algorithm. *IEEE Transactions on Magnetics , 36* (4), 1009-1013.

Sun Y., Ho Y-S., and Yu L. (2009). Dynamic Stiffnesses of Active Magnetic Thrust Bearing Including Eddy-Current Effects. *IEEE Transactions on Magnetics , 45* (1), 139 - 149.

Taha H. A. (2005). *Operations Research – An Introduction,*. New Delhi : Prentice-Hall of India Pvt. Ltd. .

Toumi, K. Y-. (1996). Modeling, Design, and Control Integration:A Necessary Step in Mechatronics. *IEEE/ASME Transactions on Mechatronics , 1* (1), 29-38.

Ueno S., and Okada Y. (2000). Cahracteristics and control of a bidirectional axial gap combined motor – bearing. *IEEE/ASME transactions of mechatronics , 5* (3), 310-318.

Vowles, H. P. (1932). Early Evolution of Power Engineering . *Isis , 17* (2), 412–420.

Walowit, J. A., and Pinkus, O. (1982). Analytical and experimental investigation of magnetic support systems Part I: Analysis. *Transactions of ASME Journal of Lubrication Technology , 104* (3), 418-428

Wearden P. D., Morell V. O., Keller B. B., Webber S. A., Borovetz H. S., Badylak S. F., et al. (2006). The PediaFlow pediatric ventricular assist device. *Seminars in thoracic and cardiovascular surgery, Pediatric cardiac surgery annual,* , 92-98.

Wei Z., Li G. and Qi L. (2006). New quasi-Newton methods for unconstrained optimization problems. *Journal of mathematics and computation , 175*, 1156-1188.

Xu, H. X., and Kian K. X. (2008). Gyro-effect and Earnshaw's Theorem:Stable and Unstable Equilibrium for Rotary and Stationary Permanent Magnetic Levitators. *The 2nd International Conference on Bioinformatics and Biomedical Engineering, 2008. ICBBE 2008,16-18 May.* IEEE.

Yan H.- S., and Yan G.- J. (2009). Integrated control and mechanism design for the variable input-speed servo four-bar linkages. *Mechatronics , 19*, 274-285.

Yanliang X, Yueqin D, Xiuhe W, and Kong Y. (2006). Analysis of Hybrid Magnetic Bearing With a Permanent Magnet in the Rotor by FEM. *IEEE Transactions on Magnetics , 42* (4), 1363 – 1366.

Yao Y. D., Huang D. R., Hsieh C. C., Chiang D. Y., Wang S. J., and Ying T. F. . (1996). The Radial Magnetic Coupling Studies of Perpendicular Magnetic Gears. *IEEE Transactions on Magnetics , 32* (5), 5061-5063.

Yeh T. J., and Toumi K. Y. (1994). Design and control integration for magnetic bearing systems: Part 1 – modeling and performance limitations. *Dyn. Control , 2*, 939-943.

Yeh T. J., and Toumi K.Y. (1994). Design and control integration for magnetic bearing systems: Part 2 – loop-transfer-recovery-based design methodology. *Dyn. Control , 2*, 945-949.

Zeisberger M., Habisreuther T., Litzkendorf D., Surzhenko O., Muller R. and Gawalek W. (2001). Optimization of Levitation Force. *IEEE Transactions on Applied Superconductivity , 11* (1), 1141–1144.

Zhang Y. and Kobayashi N. (2006). Control for Passing Through Critical Speeds of an Energy Storage Flywheel System by Bias Current Control. *10th International Symposium on Magnetic Bearings*, (pp. 308-313). Martigny, Switzerland, 21-23, Aug.

Zhenyu Y., and Pedersen G. (2006). Automatic tuning of PID controller for a 1-D levitation system using a genetic algorithm - A real case study. *Proceedings of the IEEE Interna Symposium on Intelligent Control*, (pp. 3098-3103). Munich, Germany, Oct. 4-6.

Zhilichev Y. (2000). Analysis of a Magnetic Bearing Pair with a Permanent Magnet Excitation. *IEEE Transactions on Magnetics , 36* (5), 3690 - 3692.

Zhuravlyov Y. N. (2000). On LQ-Control of magnetic bearing. *IEEE Transactions on control systems Technology , 8* (2), 344-350

Zitzler E. and Thiele L. (1999). Multi-objective evolutionary algorithms: A comparative case study and the strength Pareto approach. *IEEE transactions on Evolutionary Computation , 3* (4), 257-271.

Zitzler E., Laumanns M. and Thiele L. (2001), SPEA2:Improving the Strength Pareto Evolutionary Algorithm, TIK-Report 103. ETH Zentrum, Gloriastrasse 35, CH-8092 Zurich, Switzerland

Zmood R. B., Pang D., Anand D. K., and Kirk J. A. (1990). Robust magnetic Bearings for Flywheel Energy Storage Systems. *2nd International Symposium on Magnetic Bearings*, (pp. 123-129). Tokyo, Japan, 12-14 July.

Zmood, R. B., Qin, L. J., Kirk, J. A., and Sun, L. (1997). A Magnetic Bearing System Design Methodology and its Application to a 50Wh Open Core Composite Flywheel. *Proceedings of the 32nd Intersociety Energy Conversion Engineering Conference, July 27 – August 1*, (pp. 2306 – 2311). Honolulu, Hawaii.

List of Publications

JOURNALS

Rao J. S., and Tiwari R. (2008). Optimum Design and Analysis of Thrust Magnetic Bearings Using Multi Objective Genetic Algorithms. *International Journal for Computational Methods in Engineering Science and Mechanics , 9* (4), 223 – 245.

Rao J. S., and Tiwari R. (2009). Design Optimization of Double-Acting Hybrid Magnetic Thrust Bearings with Control Integration Using Multi-Objective Evolutionary Algorithms. *Mechatronics , 19*, 945–964.

CONFERENCES

Rao, J. S., and Tiwari, R., (2006), "Design Optimization of Thrust Magnetic Bearings Using Genetic Algorithms", 7th IFToMM-Conference on Rotor Dynamics, Vienna, Austria, 25-28 Sept

Rao, Jagu S., and Tiwari, R., 2008, "Design Optimization of Double-Acting Hybrid Magnetic Thrust Bearings Using Genetic Algorithms", 9*th International Conference on Motion and Vibration Control, Munich, Germany,* 15-18 Sept

ARTICLES UNDER REVIEW AND IN PREPARATION

Rao, Jagu S., and Tiwari R., "Optimum Design of Axial Hybrid Magnetic Bearings Using Multi-Objective Genetic Algorithms", *International Journal for Computational Methods in Engineering Science and Mechanics* (Under Review)

Rao, Jagu S., and Tiwari R., "Effect of load on the Pareto frontier in the design of magnetic bearings using Multi Objective Genetic Algorithms", (In preparation)

Rao, Jagu S., and Tiwari R., "Multi-objective design optimization of double acting hybrid magnetic thrust bearing integrated with control considering power amplifier constraints and decentralization", (In preparation)